



University of Navarra

School of Sciences

***Characterization of cellular and molecular responses
of human glioblastoma to Transforming Growth
Factor- β signalling pathway inhibition***

Gabriel Osvaldo Gallo-Oller



University of Navarra

School of Sciences

Characterization of cellular and molecular responses of human glioblastoma to Transforming Growth Factor- β signalling pathway inhibition

Doctoral thesis presented by **Gabriel Osvaldo Gallo-Oller** to obtain the PhD degree by the University of Navarra.

The present Doctoral thesis has been carried out under our supervision, at the **Brain Tumour Biology Unit and at the Department of Biochemistry and Genetics**, and we authorize its presentation before the Commission who will judge it.

Pamplona, October 2015.

Dr. Javier Sáez Castresana

Dr. Javier Dotor

This work has been performed thanks to a predoctoral fellowship from the *Departamento de Educación del Gobierno de Navarra*. The research was supported by grants from the following agencies: Fondo de Investigación Sanitaria, Instituto de Salud Carlos III, in Madrid; and Departamento de Salud del Gobierno de Navarra, Fundación Universitaria de Navarra, and Caja Navarra, in Pamplona.

Por y para ustedes, mamá y papá

A mis hermanos

*todo
nació para ser compartido,
para ser entregado,
para multiplicarse.*

PABLO NERUDA

AGRADECIMIENTOS

Me gustaría que estas líneas sirvieran para expresar mi más profundo y sincero agradecimiento a todas aquellas personas e instituciones que han colaborado en la realización del presente trabajo.

A la Universidad de Navarra, por brindarme esta oportunidad de seguir especializándome y formándome durante estos años.

A mis directores de tesis Dr. Javier Sáez Castresana y Javier Dotor, por la orientación, el seguimiento y la supervisión continúa de la misma, pero sobre todo por la motivación y el apoyo recibido a lo largo de estos años.

Quisiera hacer extensiva mi gratitud a profesores y compañeros del Departamento de Bioquímica y Genética y, especialmente a los miembros del CIFA en donde comencé este trabajo.

A la Universidad Nacional de Río Cuarto, donde comencé mi formación científica, y en especial al Departamento de Patología Animal.

To Dr. Peter Hau and all his team, for the effort and help during my research stay in Germany.

Este trabajo no hubiera sido posible sin el amparo incondicional que me otorgaron y el cariño que inspiraron mis padres, en especial mi madre que ha entendido mis ausencias.

Un agradecimiento muy especial merece la comprensión, paciencia y el ánimo recibidos de mi familia y amigos, que a pesar de la distancia siempre estuvieron a mi lado. Las palabras nunca serán suficientes para testimoniar mi aprecio y agradecimiento.

A todos ustedes, mi mayor reconocimiento y gratitud.

INDEX

ABBREVIATIONS AND ACRONYMS	1
ABSTRACT	1
INTRODUCTION	3
1. GLIOBLASTOMA MULTIFORME	3
1.1 Incidence and prevalence.....	4
1.2 Risk factors.....	5
1.3 Aetiology of GBM.....	6
1.4 Survival after diagnosis.....	7
1.5 Histological characteristics	7
1.6 Classification.....	8
1.6.1 Histological classification.....	8
1.6.2 Molecular classification	9
1.7 GBM pathogenesis.....	12
1.7.1 Migration and Invasion.....	12
1.7.2 Hypoxia and GBM tumorigenesis.....	13
1.7.3 Apoptosis.....	14
1.7.3.1 Significance of apoptosis in GBM	15
1.7.3.2 Anoikis in cancer.....	16
2. CANCER STEM CELLS	17
2.1 Cell of origin.....	17
2.2 Neural Stem Cells.....	18
2.3 Cancer Stem Cell theory and GBM	19
2.4 Identification and isolation of CSC.....	20
2.4.1 CSC surface markers.....	21
2.4.1.1 CD133	21
2.4.1.2 CD15	22
2.4.1.3 L1CAM	22
2.4.1.4 A2B5	22
2.4.1.5 Integrin $\alpha 6$	23
2.4.1.6 CD44	23
2.4.2 Intracellular markers	23
2.4.3 Side population.....	24
2.4.4 Development of neurospheres.....	24
2.4.5 <i>In vivo</i> transplantation.....	25
2.5 Molecular CSC subtypes of GBM	25
2.6 Hypoxia and CSC	26

2.7 CSC regulatory signalling pathways.....	27
2.7.1 RTK-AKT signalling	27
2.7.2 Notch signalling	28
2.7.3 Sonic Hedgehog signalling	28
2.7.4 WNT- β -catenin signalling	29
2.7.5 STAT3 signalling	29
2.7.6 PDGF signalling	29
2.7.7 Bone morphogenetic proteins	30
3. TRANSFORMING GROWTH FACTOR BETA SIGNALLING PATHWAY	31
3.1 TGF- β signalling elements.....	31
3.1.1 Ligands.....	31
3.1.2 Receptors.....	32
3.1.3 Cytoplasmic factors	32
3.2 Activation of TGF- β signalling pathway	33
3.2.1 Canonical signalling	34
3.2.2 Non-canonical signalling.....	36
3.2.3 TGF- β signalling pathway regulation.....	36
3.3 TGF- β signalling in GBM.....	38
3.4 Escaping from the TGF- β antiproliferative control.....	39
3.5 TGF- β pathway and GBM CSC.....	41
4. TREATMENT FOR GLIOBLASTOMA MULTIFORME	43
4.1 GBM conventional treatments	43
4.1.1 Surgical resection	43
4.1.2 Chemotherapy.....	43
4.1.3 Radiotherapy	44
4.2 Hypoxia and new therapeutics treatment evaluation.....	44
4.3 Therapeutic implications of the blood-brain/tumour barrier	45
4.4 Molecular biology based treatments	47
4.5 Apoptosis as a therapeutic target in GBM.....	50
4.6 Current CSC-based therapies for the treatment of GBM	50
4.7 Therapies for GBM targeting TGF- β signalling pathway.....	52
4.8 Inhibitory peptides P17 and P144	54
HYPOTHESIS AND OBJECTIVES	57
MATERIALS AND METHODS	59
I) MATERIALS.....	59
1.1 Reagents and chemicals	59
1.2 Buffers.....	60

1.3 Oligonucleotides.....	61
1.4 Synthetic peptide.....	62
1.5 Proteins and antibodies.....	62
1.5.1 Growth factors and recombinant proteins	62
1.5.2 Antibodies.....	62
1.6 Cell lines and cell culture	65
1.6.1 Commercial Cell Lines.....	65
1.6.2 Brain Tumour Initiating Cells	65
1.7 Animals	67
II) METHODS.....	69
2.1 Quantification of cell viability/proliferation	69
2.1.1 Thiazolyl Blue Tetrazolium Bromide assay	69
2.1.2 Proliferation analysis by Trypan blue exclusion assay.....	69
2.2 Apoptosis determinations	70
2.2.1 ELISA	70
2.2.2 Conventional Acridine Orange-Ethidium Bromide (AO/EB) staining	70
2.2.3 Anoikis determination	71
2.3 Matrigel invasion assay	71
2.4 Soft agar colony-forming assay	72
2.5 Neurosphere formation assay	72
2.6 Clonogenic assay.....	73
2.7 2D Migration assays.....	74
2.7.1 Monolayer wound healing assay with mechanical disruption.....	74
2.7.2 Culture-inserts wound healing assay	74
2.7.3 Sphere formation assay.....	75
2.8 Gene expression analysis.....	76
2.8.1 RNA isolation	76
2.8.2 Reverse transcription reaction	77
2.8.3 Quantification by reverse transcription-quantitative polymerase chain reaction.....	77
2.9 Determination of protein expression	78
2.9.1 Western blot.....	78
2.9.2 Flow cytometry.....	78
2.10 <i>In vivo</i> subcutaneous tumour xenograft assay.....	79
2.10.1 Tumour xenografts samples processing for mRNA and protein isolation	79
2.10.2 Histology and immunohistochemistry analysis.....	79
2.11 Orthotopic mouse brain tumour model.....	80
2.11.1 Peptide P144 inactivation.....	80
2.11.2 Time-dependent stability analysis of peptide P144 biological activity	81

2.11.3 Biological inactivation analysis.....	81
2.11.4 Analysis of time-dependent chemical stability of peptide P144.....	81
2.11.5 Surgical intracranial tumour injection.....	82
2.11.6 Osmotic pump implantation.....	83
2.11.7 Assembly and priming of Alzet® osmotic pumps.....	84
2.11.8 Magnetic resonance imaging.....	86
2.11.9 Animal euthanasia and sample processing.....	87
2.11.10 Histology.....	87
2.12 Statistical analysis.....	87
RESULTS	89
I) <i>IN VITRO</i> FINDINGS.....	89
1. ANALYSIS OF CELLULAR RESPONSE TO P144 IN TWO GLIOBLASTOMA COMMERCIAL CELL LINES.....	89
1.1 P144 decreases proliferation.....	89
1.2 P144 induces apoptosis.....	90
1.3 P144 modifies apoptosis evolution and increases late apoptosis.....	91
1.4 P144 impairs anoikis escape in detached cell culture conditions.....	94
1.5 P144 inhibits invasiveness and migration.....	99
1.6 P144 impairs tumorigenesis phenotype.....	100
2. BRAIN TUMOUR INITIATING CELLS (BTIC) LINES RESPONSE TO P144.....	103
2.1 Morphological culture characterization of BTIC under normoxia and hypoxia.....	103
2.2 BTIC cell lines express cancer stem cell markers.....	105
2.3 P144 treatment decreases BTIC proliferation ratio.....	106
2.4 P144 treatment impairs clonogenic survival.....	110
2.5 P144 inhibits migration in 2D assays.....	111
2.6 P144 cellular type-dependent inhibition activity.....	120
2.7 P144 inhibition correlates with CSC markers expression.....	121
3. MOLECULAR ANALYSIS OF TGF- β SIGNALLING PATHWAY INHIBITION BY P144 IN GLIOBLASTOMA A172 AND U-87 MG CELLS.....	125
3.1 P144 blocks activation of the TGF- β signalling pathway and nuclear translocation of P-SMAD2.....	125
3.2 P144 regulates <i>in vitro</i> SMAD7 and SKI expression.....	134
II) <i>IN VIVO</i> FINDINGS.....	141
4. EVALUATION OF ANTITUMOUR ACTIVITY OF P144 IN A NUDE MOUSE SUBCUTANEOUS MODEL.....	141
4.1 P144 reduces growth rate and increases survival in nude mice implanted human glioblastoma xenografts.....	141
4.2 P144 regulates <i>in vivo</i> levels of SMAD7 and SKI.....	144
5. P144 EFFECT ON GLIOBLASTOMA DEVELOPMENT IN THE BRAIN ENVIRONMENT OF A NUDE MICE INTRACRANIAL MODEL.....	147

5.1 P144 presents no <i>in vitro</i> residual effect over U-87 MG cell line proliferation.....	147
5.2 P144 biological activity is lost with autoclave treatment.....	148
5.3 P144 chemical and <i>in vitro</i> activity time stability.....	152
5.4 P144 <i>in vitro</i> release from Alzet® osmotic pump system.....	156
5.5 U-87 MG cell line intracranial tumours generation.....	158
5.6 P144 affects tumour size in the intracranial <i>in vivo</i> model.....	159
DISCUSSION	165
1) Evaluation of response to P144 in A172 and U-87 MG glioblastoma cell lines	165
2) <i>In vitro</i> analysis of P144 effect over CSC subpopulation	171
3) <i>In vitro</i> characterization of TGF- β signalling pathway inhibition by P144.....	174
4) Analysis of therapeutic potential of P144 in mouse models.....	175
5) P144 modulation of SMAD7 and SKI expression (<i>in vitro</i> and <i>in vivo</i> findings)	181
CONCLUSIONS	187
REFERENCES	189
PUBLICATIONS	203

INDEX OF FIGURES

Figure 1. Worldwide incidence of brain tumours - 2012 estimation	4
Figure 2. Representative histological images of WHO gliomas grade classification.....	9
Figure 3. Molecular vs WHO grade classification of GBM	11
Figure 4. Normal CNS differentiation and tumour transformation	17
Figure 5. Anatomical localization of the NSC in SVZ and SGZ in humans and mice.....	19
Figure 6. Heterogeneity models for solid tumours.....	20
Figure 7. Expression and secretion of TGF- β isoforms.....	34
Figure 8. The canonical and non-canonical signalling pathways of TGF- β	35
Figure 9. Different degrees of BBTB in GBM.....	46
Figure 10. TGF- β signalling pathway targeting compounds.....	53
Figure 11. Schematic representation of culture-inserts handling	75
Figure 12. Experimental design schematic representation of P144 biological activity time kinetics analysis.....	81
Figure 13. Alzet [®] osmotic pumps models	84
Figure 14. Schematic representation of brain system using Alzet [®] Osmotic Pumps.....	85
Figure 15. Antiproliferative effect of P144 measured by MTT assay.....	89
Figure 16. Apoptosis determination by ELISA.....	90
Figure 17. Schematic representation of the necrotic process and states detected by AO/EB staining.....	92
Figure 18. Schematic representation of the apoptotic process and states detected by AO/EB staining.....	92
Figure 19. Apoptosis determination by AO/EB staining in A172 and U-87 MG cell lines	93
Figure 20. AO/EB staining apoptosis quantification for A172 and U-87 MG cell lines.....	94
Figure 21. A172 and U-87 MG culture development under induced anoikis by anchorage-independent cell growth conditions	96
Figure 22. Total protein quantification of A172 and U-87 MG cells under anoikis induced culture conditions.....	97
Figure 23. Apoptosis markers analysis in A172 and U-87 MG cell lines under anoikis induction.....	98
Figure 24. Matrigel invasiveness determination in commercial glioblastoma cell lines	99
Figure 25. Wound healing assay for A172 and U-87 MG cell lines	100
Figure 26. Colony-forming assay in soft agar for A172 and U-87 MG cell lines.....	101
Figure 27. Neurosphere formation inhibition by P144 in A172 and U-87 MG cell lines.....	102
Figure 28. Culture morphology of U-87 MG and BTIC cell lines.....	104
Figure 29. XTT-based proliferation assay determination.....	105
Figure 30. Proliferation analysis in U-87 MG cell line and selected BTIC lines	107
Figure 31. Proliferation analysis at different initial cell density.....	109
Figure 32. Clonogenic assay derived clones morphology	110
Figure 33. Wound healing assay in U-87 MG and BTIC lines	112
Figure 34. Quantification of wound healing assay in U-87 MG and BTIC lines.....	113
Figure 35. RAV57 cell passage number effect over P144 migration inhibition in wound healing assay.....	114
Figure 36. Spheroid assay in U-87 MG and BTIC cell lines	115
Figure 37. Migration capacity quantification by spheroid assay	116
Figure 38. RAV20 cell line migration analysis through passages under normoxia conditions in spheroid assay	118

Figure 39. RAV19 cell line migration analysis through passages under hypoxia conditions in spheroid assay.....	119
Figure 40. Correlation between CSC markers expression and P144 inhibitory percentages observed in proliferation, wound healing, and spheroid assay	122
Figure 41. Inhibition of SMAD2 phosphorylation by P144.....	126
Figure 42. Blockade of TGF- β 1 or TGF- β 2 induced SMAD2 phosphorylation by P144	127
Figure 43. Cytoplasmic and nuclear P-SMAD2/SMAD2 kinetic analysis in A172 cell line treated with TGF- β 1	129
Figure 44. Cytoplasmic and nuclear P-SMAD2/SMAD2 kinetic analysis in U-87 MG cell line treated with TGF- β 1	130
Figure 45. P-SMAD2 nuclear translocation analysis in A172 and U-87 MG cell lines	132
Figure 46. Blockade of TGF- β 1 induced P-SMAD2 nuclear translocation by P144 in A172 and U-87 MG cell lines	133
Figure 47. Gene expression kinetics of P144 treated A172 and U-87 MG cell lines.....	135
Figure 48. <i>SMAD7</i> , <i>SKI</i> and <i>SNON</i> gene expression analysis in glioblastoma cell lines	137
Figure 49. <i>SMAD7</i> and <i>SKI</i> relative expression in NHA, A172 and U-87 MG cell lines.....	138
Figure 50. Protein expression of SMAD7 and SKI in A172 and U-87 MG cell lines	139
Figure 51. Effect of P144 over U-87 MG xenograft nude mice subcutaneous model	142
Figure 52. Histological analysis of tumour samples from subcutaneous xenograft model	143
Figure 53. Tumours tissue immunohistochemical quantification of proliferation, apoptosis and angiogenesis.....	144
Figure 54. Expression levels of <i>SMAD7</i> , <i>SKI</i> and <i>SNON</i> genes in tumour samples from P144 treated mice.....	145
Figure 55. <i>In vivo</i> phosphorylation status of SMAD2 and protein level of SMAD7 and SKI.....	146
Figure 56. Analysis of potential antiproliferative residual effect of P144 on U-87 MG cell line.....	148
Figure 57. Autoclaved P144 absorbance quantification by spectrophotometry	149
Figure 58. HPLC analysis of autoclaved P144.....	149
Figure 59. Analysis of autoclaved P144 biological activity.....	150
Figure 60. Biological activity analysis of non-corrected and corrected concentrations of autoclaved P144	151
Figure 61. Analysis of P144 chemical stability by HPLC	153
Figure 62. P144 time-dependent biological stability determined by proliferation assay.....	154
Figure 63. Time-dependent P144 biological activity in Na ₂ CO ₃ as vehicle assessed by migration analysis.....	155
Figure 64. Time-dependent P144 biological activity in TRIS as vehicle assessed by migration analysis.....	156
Figure 65. P144 <i>in vitro</i> delivery determination from Alzet [®] osmotic pump system	157
Figure 66. Tumour intracranial model pre-assay	158
Figure 67. Body weight evolution	160
Figure 68. Magnetic Resonance Imaging and H&E	161
Figure 69. Intracranial tumour volume analysis	162
Figure 70. Apoptosis quantification in H&E slides	163

INDEX OF TABLES

Table 1. Classification of glioma tumours according to the WHO classification (2007)	3
Table 2. Criteria used for glioma grading according to the WHO classification (2007)	9
Table 3. Cancer stem cell markers in GBM	21
Table 4. GBM CSC subtypes according to expression profiles	26
Table 5. CSC principal signalling pathways and their roles in GBM	27
Table 6. Ongoing clinical trials using molecular based therapeutic strategies for GBM	49
Table 7. Current status of apoptosis-targeted preclinical and clinical trials in GBM.....	50
Table 8. TGF- β pathway targeting agents currently under preclinical and clinical development for GBM treatment	54
Table 9. Primer sequences used for RT-qPCR	61
Table 10. Antibodies used in western blot	64
Table 11. Classification and growth characteristics of BTIC selected cell lines	67
Table 12. Initial seeding cells density established for proliferation analysis in Trypan blue exclusion assay	70
Table 13. Initial seeding cell suspension density established for wound healing assay	75
Table 14. Initial cell seeding density and preincubation time established for spheroid assay.....	76
Table 15. Early endpoint parameters and criteria	83
Table 16. Specifications of osmotic pump models considered for intracranial model.....	86
Table 17. Expression levels of stem cell markers in U-87 MG and BTIC lines under normoxia and hypoxia conditions	106
Table 18. Clonogenic assay analysis.....	111
Table 19. Percentage of inhibition observed in proliferation, wound healing and spheroid assay in the presence of P144.....	121
Table 20. Final conditions for the intracranial mouse model	159

ABBREVIATIONS AND ACRONYMS

ABC	ATP-binding cassette	CNS	central nervous system
ABL	Abelson murine leukaemia viral oncogene homolog 1	Co-SMAD	common SMAD
ALDH1	aldehyde dehydrogenase 1	CREB/ATF	cAMP responsive element binding protein-like/ Cyclic AMP-dependent transcription factor
ALDH1A3	aldehyde dehydrogenase 1, member A3	CSC	cancer stem cells
ANG-1/2	Angiopoietin 1/2	Ct	threshold cycle
ANOVA	analysis of variance	Da	Dalton
AO/EB	acridine orange / ethidium bromide	DAB	3,3'-diaminobenzidine
AP1	activator protein 1	DMEM	Dulbecco's modified Eagle's medium
ARF	alternate reading frame protein	DNA-PK	DNA-dependent protein kinase
ASR	age standardized incidence rate	DPBS	Dulbecco's phosphate-buffered saline
BAX	BCL-2-associated X protein	Dr. rer. nat.	Doctor rerum naturalium
BBB	blood brain barrier	DTT	dithiothreitol
BBTB	blood brain tumour barrier	e.g.	for example
BCL-2	B-cell chronic lymphocytic leukaemia/lymphoma 2	EDTA	Ethylenediaminetetraacetic acid
BCR	breakpoint cluster region	EF	enrichment factor
bFGF	basic fibroblast growth factor	EGF	epidermal growth factor
BID	BCL-2 homology 3 interacting-domain death agonist	EGFR TKI	EGFR tyrosine kinase inhibition
BIT	bovine serum albumin, insulin and transferrin supplement	EGFR	epidermal growth factor receptor
BMP	bone morphogenetic proteins	EGFRvIII	EGFR variant III
BRAF	v-rapidly accelerated fibrosarcoma (Raf) murine sarcoma viral oncogene homolog B	ELISA	enzyme-linked immunosorbent assay
BTIC	brain tumour initiating cells	EPHA2	ephrin type-A receptor 2
Cat No	catalogue number	ERBB2	erb-b2 receptor tyrosine kinase 2
CBP	CREB binding protein	ERK	extracellular signal-regulated kinases
CD	cluster of differentiation	FGFR1	fibroblast growth factor receptor 1
CDK/4/6	cyclin-dependent kinase/4/6	FAK	focal adhesion kinase
CDKN1A/2A/2B	cyclin-dependent kinase inhibitor 1A/2A/2B	FLT3	FMS-like tyrosine kinase 3
CED	convection enhanced delivery	FOX/G1	forkhead box/G1
CIP1	CDK-interacting protein 1	GB	glycoprotein B
c-KIT	v-Kit Hardy-Zuckerman 4 feline sarcoma viral oncogene homolog	GBM	glioblastoma multiforme
		H&E	haematoxylin and eosin
		HCMV	human cytomegalovirus
		HDAC	histone deacetylase

Abbreviations And Acronyms

HER2	human epidermal growth factor receptor 2	ms	milliseconds
HIFs	hypoxia inducible factors	MTLA	medical-technical laboratory assistant
HOX	homeobox	mTOR/ C1	mammalian target of rapamycin/ complex 1
HPLC	high performance liquid chromatography	MTT	methyl-thiazolyldiphenyl-tetrazolium bromide (3-[4,5-Dimethyl-2-thiazolyl]-2,5-diphenyl-2H-tetrazolium bromide)
HRP	horseradish peroxidase	N	total sample size
IC ₅₀	half maximal inhibitory concentration	NF-κB	nuclear factor kappa-light-chain-enhancer of activated B cells
ICV	intracerebrovascular	NHA	normal human astrocytes
IDH 1/2	isocitrate dehydrogenase 1/2	No	number
IE1	immediate-early protein 1	ns	non-significant
IHC	immunohistochemistry	NSC	neural stem cells
INK4	inhibitor of CDK4	O/N	overnight
IP	intraperitoneal	OLIG2	oligodendrocyte lineage transcription factor 2
I-SMAD	inhibitory SMAD	p	statistical probability
IV	intravenous	PB	phosphate buffer
JNK	JUN-N terminal kinase	PBS	phosphate buffered saline
kDa	kilo Dalton	PDGF	platelet-derived growth factor
kPa	kilopascal	PDGFA/B	platelet-derived growth factor A/B (ligand)
L1CAM	Line-1 cell adhesion molecule	PDGFR α/β	PDGF receptor/alpha/beta
LAP	latency associated peptide	PE	plate efficiency
LIF	leukaemia inhibitory factor	PFA	paraformaldehyde
LLC	large latent complex	PI3K	phosphatidylinositol 3-kinase
LOH	loss of heterozygosity	PIGF	phosphatidylinositol-glycan biosynthesis class F protein
LTBP	latent TGF-β binding protein	PKC-β	Protein kinase C beta
M	Molar	PMSF	phenylmethylsulfonyl fluoride
μg	microgram	PS	phosphatidylserine
μL	microliter	PTEN	phosphatase and tensin homolog
μm	micrometre	R	multivariate correlation coefficient
μM	micromolar	RET	receptor tyrosine kinase
MAPK	mitogen-activated protein kinases	ROS	reactive oxygen species
MET	mesenchymal-epithelial transition factor	rpm	revolutions per minute
MGMT	O6 methylguanine DNA methyltransferase	RPMI	Roswell park memorial institute medium
min	minutes		
mL	millilitres		
mm ^{2/3}	millimetre, square millimetre, cubic millimetre		
mM	milimolar		
MRI	magnetic resonance imaging		

R-SMAD	receptor regulated SMAD	SV40	simian vacuolating virus 40
RT	room temperature	SVZ	subventricular zone
RTK-AKT	receptor tyrosine kinase-AKT	TBS	tris-buffered saline
RT-qPCR	reverse transcription quantitative polymerase chain reaction	TCGA	the cancer genome atlas research network
s	seconds	TERT	telomerase reverse transcriptase
SARA	SMAD anchor for receptor activation	TGF- β	transforming growth factor beta
SC	subcutaneous	TIE-2	Tyrosine kinase with immunoglobulin-like and EGF-like domains 2
SCR	v-src avian sarcoma (Schmidt-Ruppin A-2) viral oncogene homolog	Tm	melting temperature
SD	standard deviation of a sample	TMZ	temozolamide
SDS	sodium dodecyl sulphate	TNF	tumour necrosis factor
SDS-PAGE	sodium dodecyl sulphate polyacrylamide gel electrophoresis	TP53	tumour protein p53
SF	survival fraction	RUNX	runt-related transcription factor
SGZ	subgranular zone	T β 1Ab	antibody anti TGF- β 1
SHH	sonic hedgehog	T β R1/II/III	transforming growth factor beta receptor type I/II/III
SKI	Sloan Kettering Institute	U	unit
SLC	small latent complex	US28	unique short (US) genome region 28
SMAD	similar to mothers against decapentaplegic	v/v	volume per volume
SMURF1/2	SMAD ubiquitination regulatory factor 1/2	VEGF	vascular endothelial growth factor
SMURFs	SMAD ubiquitination regulatory factors	TRAIL	TNF-related apoptosis-inducing ligand
SNON	SKI-related novel gene N protein	VEGFR	vascular endothelial growth factor receptor
SOX2	sex determining region (SR) Y-box 2	vs	versus
SP	side population	WHO	world health organization
STAT3	signal transducer and activator of transcription 3	wk	week
		WNT	wingless/int
		XIAP	X-linked inhibitor of apoptosis protein

ABSTRACT

ABSTRACT

Glioblastoma Multiforme (GBM) is the most prevalent malignant brain tumour accounting for 60-70% of all gliomas. Improvements in survival over the past 100 years can be measured only in weeks, and current achieved median survival ranges only 12-15 months. A hallmark of this malignancy is the intrinsic resistance to current therapies. Numerous efforts using molecularly targeted therapeutics have not significantly changed the near uniform lethality of this disease. The TGF- β signalling pathway plays a key role in GBM. It is implicated in progression, infiltration, and chemo/radioresistance as well as in the maintenance of stem-like phenotype of GBM CSC. Several inhibitors of different elements and regulators of the TGF- β pathway have entered to clinical trials. Among them, P17 and P144 inhibitory peptides of the TGF- β pathway have been tested for the treatment of different diseases including tumours. We decided to analyse the therapeutic potential of P144 for the treatment of GBM. We found that P144 impaired *in vitro* cellular processes as proliferation, migration, invasiveness and tumorigenicity. Apoptosis and anoikis were significantly increased by P144. Additionally, P144 blocked the TGF- β protective effect against apoptosis. The inhibition of TGF- β signalling by P144 affected the self-renewal capacity of a putative CSC subpopulation *in vitro*. These results were confirmed by the analysis on Brain Tumour Initiating Cells (BTIC) isolated from human GBM biopsies. P144 decreased *in vitro* proliferation, migration, and self-renewal capacity of this subpopulation. The effect of P144 was impaired by hypoxia. However, the precise underlying mechanism of hypoxia on P144 must be elucidated. We confirm the inhibition of TGF- β signalling by P144 through SMAD2 phosphorylation blockade, the pivotal initiation event of the pathway, which was translated to a reduction of P-SMAD2 nuclear translocation. Both results suggested an *in vitro* regulation on the transcriptional target genes of the TGF- β pathway in GBM cell lines. Furthermore, we confirmed *in vitro* and *in vivo*, the upregulation of SMAD7 and the downregulation of SKI by P144 at transcriptional and translational levels. This observation strongly suggests the implication of these factors in the molecular mechanism triggered by P144. The therapeutic potential of P144 was analysed in a mouse subcutaneous tumour model. Despite that P144 impaired tumour growth and led to an increase in survival, negative contradictory results were obtained in the *in vivo* intracranial model. We can conclude that the therapeutic potential of P144 as a treatment of GBM is clear. However, previous to potential clinical development, further studies are required in order to confirm P144 effect over GBM in the brain environment, as well as to explore P144 therapeutic potential in combination with current (TMZ and/or radiation) and emerging molecular based therapies.

INTRODUCTION

INTRODUCTION

1. GLIOBLASTOMA MULTIFORME

Malignant gliomas are the most common type of primary brain tumours [1]. Bailey and Cushing in 1926 proposed the first glioma classification on the basis of more than 400 specimens from surgical clinics of the Johns Hopkins and Peter Bent Brigham Hospitals [2]. The classification of the World Health Organization (WHO) is currently in use and divides gliomas into four groups: astrocytomas, oligodendrogliomas, oligo-astrocytomas (or mixed gliomas) and ependymomas (Table 1) [1, 3].

	I	II	III	IV		I	II	III	IV
Astrocytic tumours					Oligodendroglial tumours				
Subependymal giant cell astrocytoma		•			Oligodendroglioma		•		
Pylocytic astrocytoma	•				Anaplastic Oligodendroglioma			•	
Pilomyxoid astrocytoma		•			Oligoastrocytic tumours				
Diffuse astrocytoma		•			Oligoastrocytoma		•		
Pleomorphic Xanthoastrocytoma		•			Anaplastic Oligoastrocytoma			•	
Anaplastic astrocytoma			•		Ependymal tumours				
Glioblastoma *				•	Subependymoma		•		
Giant cell glioblastoma				•	Myxopapillary ependymoma		•		
Gliosarcoma				•	Ependymoma			•	
					Anaplastic ependymoma				•

Roman numerals indicate the WHO grading system. Modified from Louis *et al* (2007) [3]. Grade I: benign, slow growth; Grade II: absence of mitosis, angiogenesis and necrosis; Grade III: mitosis, absence of angiogenesis and necrosis; Grade IV: high mitosis rate, angiogenesis, and necrosis.

* Also designated as Glioblastoma Multiforme.

Glioblastoma Multiforme (GBM) accounts for 60-70% of all gliomas, anaplastic astrocytomas for 10-15%, anaplastic oligodendrogliomas and anaplastic oligoastrocytomas for 10%, and the remaining 5-20% belong to less common tumour types, such as anaplastic ependymomas and anaplastic gangliogliomas [4]. GBM correspond to the most malignant form of glioma and was first identified in 1863 by Dr. Rudolf Virchow as a tumour with glial cell origin using macroscopic and microscopic techniques [5]. The term “multiforme” reflects the heterogeneity of this type of

tumour regarding clinical presentation, pathology, genetic signature, and response to treatment [1].

GBM may be primary, arising *de novo*, usually in patients aged >50 years, or secondary if arising from a lower-grade tumour, more commonly in younger patients, presenting a tendency to progress to GBM in a few years [1].

1.1 Incidence and prevalence

Brain tumours amount less than 2% of all malignant neoplasm establishing a small fraction of the overall human cancer burden. However, a significant number of central nervous system (CNS) neoplasms affect children (including retinoblastomas and peripheral neuroblastomas) and rank second in incidence after leukaemia. In fact, after leukaemia, brain tumours are the leading cause of cancer mortality in children [6]. Worldwide, the incidence of brain tumours is estimated to be around 1.8% of all cancer cases and constitutes the 17th most common cancer type with more than 256,000 new cases diagnosed in 2012. Variations between countries may reflect different prevalence of risk factors, screening, and diagnostic methods (Fig. 1) [7].

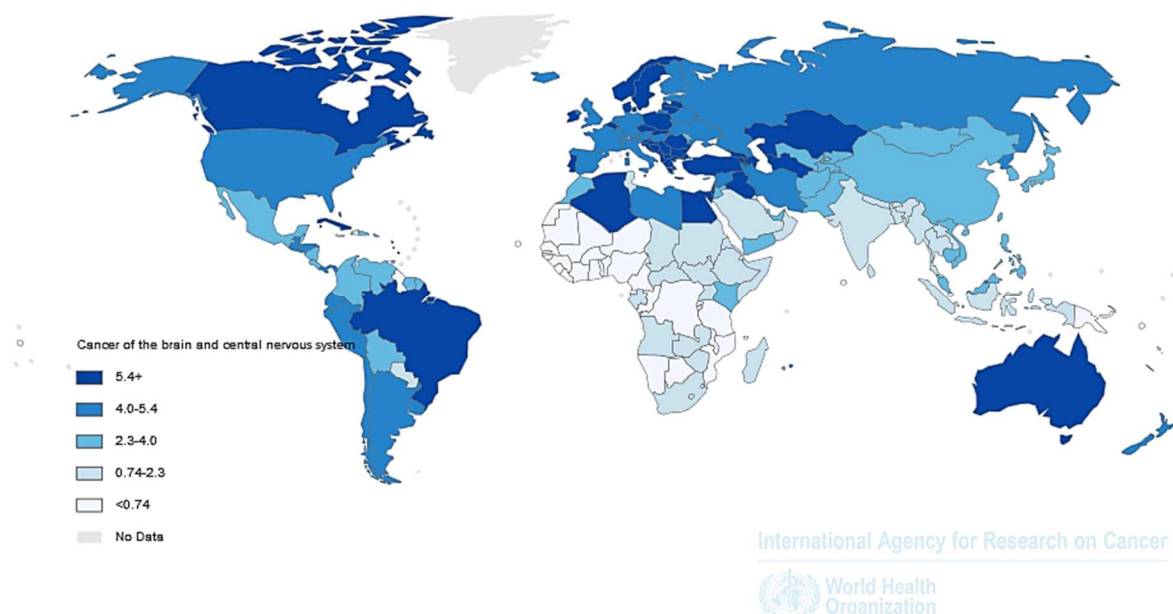


Figure 1. Worldwide incidence of brain tumours - 2012 estimation. Values indicate the age-standardized incidence rate (ASR) per 100,000 people. Image taken from GLOBOCAN [8].

Brain cancer incidence presents a significant geographic variation. Incidence is higher in Europe and North America, with ASR between 4.9 and 8 per 100,000 people and 5.3 per 100,000 people, respectively [8]. It is difficult to determine whether geographic differences are due to

variation in data collection technique and/or coverage of surveillance methods, or are objective differences in incidence [9].

Glioma is the most common primary brain tumour, accounting for 32% of CNS tumours and 80% of malignant CNS tumours. In these tumours, astrocytoma represent about 76% of all glioma cases. GBM is the most common, malignant, and lethal astrocytoma, accounting for around 60-70% of all astrocytic tumours. New cases are diagnosed especially in the elderly, being median patient age at diagnosis time approximately 64 years [4, 5]. The incidence rates vary over time per registry and by gender, where males have higher incidence rates as compared to females in a ratio that fluctuates between 1.26:1 to 1.58:1 [5, 10]. This tumour is twice as common in Caucasians, especially in those living in industrial areas. Cases of GBM in children and neonates are also reported. It is estimated that GBM incidence is 1.1 to 3.6 per 100,000 infants with a male to female children ratio of 3.3:1. There are no morphological differences between GBM occurring in children and adults. Reported differences are related only to the proliferative activity of glioma cells, being the proliferation index (Ki-67 index) higher in children [10].

1.2 Risk factors

Malignant glioma is a disease of the elderly, as previously described. At present, due to population ageing and diagnostic imaging improvement in developed countries, the incidence of glioblastoma is likely to increase [4, 5, 11]. Besides, no clear underlying cause has been identified for the majority of malignant gliomas. But several inherited, monogenic Mendelian cancer syndromes are associated with increased incidence of specific glioma subtypes such as GBM [5, 9]. These monogenic disorders account for only a very small amount of glioma cases (< 5%). Approximately 5-10% of patients with malignant gliomas have a family history of gliomas. First degree relatives of patients with glioma have a twofold increased risk of developing a brain tumour, especially when the patient developed the tumour at a younger age [9].

In the absence of a clear pattern of risk variants, segregation analysis has determined that genetic risk factors for glioma are best explained using a polygenic model. Single-nucleotide polymorphisms (SNPs) at seven loci that increased glioma risk were identified: telomerase reverse transcriptase (*TERT*, rs2736100), epidermal growth factor receptor (*EGFR*, rs2252586, and rs11979158), coiled-coil domain containing 26 (*CCDC26*, rs55705857), cyclin-dependent kinase inhibitor 2B (*CDKN2B*, rs1412829), pleckstrin homology-like domain, family B, member 1 (*PHLDB1*, rs498872), tumour protein p53 (*TP53*, rs78378222), and regulator of telomere elongation helicase (*RTEL1*, rs6010620). *TERT*, *RTEL1*, *EGFR*, and *TP53* increase risk of all types of glioma, while only *CDKN2B* is associated with astrocytic tumours (WHO grades II to IV) [9, 12].

Exposure to therapeutic as highdose ionizing radiation is the most firmly established environmental risk factor for glioma, and the genetic factors influence the extent of risk from these exposures. Gliomas may present as early as 7-9 years after irradiation and may be particularly relevant in children, whose brains are still under developing processes at the time of exposure. Extensive research has been performed since 1990s to address the correlation between the use of mobile phones and glioma risk. The scientific evidence included in the 2011 International Agency for Research on Cancer (IARC) report, as well as the scientific evidence reported since its publication do not support a significant association between the use of cellular phones and risk of gliomas [9, 13].

Allergies have been reported to be protective against multiple cancer types, including gliomas. Although the majority of reports have found an association between allergies and atopic disease (e.g. psoriasis, asthma) with reduced glioma risk, some studies have reported the opposite effect. It has been suggested that the observed protective effect may be due to increased surveillance by the innate immune system for those with allergies, but this potential mechanism has not been definitively proven [9, 13].

1.3 Aetiology of GBM

The aetiology of GBM has not been fully elucidated. GBM is believed to be a spontaneous tumour, despite the fact that medical histories describe the development of glioma in relatives of the patients. The familial form of GBM is described in only 1% of cases. However, the genetic background for development of this type of glioblastoma is different for those arising spontaneously. GBM may also occur in the course of genetic diseases as tuberous sclerosis, Turcot syndrome, multiple endocrine neoplasia type IIA, and neurofibromatosis type I. In addition, acquired head injuries, which occurred as a result of a brain contusion, may predispose to the onset of glioblastoma [4, 10].

Viruses, such as human cytomegalovirus (HCMV) and human polyoma viruses, as John Cunningham (JC) virus and SV40, are also believed to be among the aetiological agents for glioma development. HCMV induces congenital encephalitis and multi-organ changes in immunocompromised adults and shows tropism for glial cells. The virus encodes proteins (such as IE1, US28, GB), which activate intracellular signalling pathways involved in mitogenesis, mutagenesis, apoptosis, inflammation, and angiogenesis. Products of these genes cause dysregulation of key GBM signalling pathways as platelet-derived growth factor receptor (PDGFR), AKT, and signal transducer and activator of transcription 3 (STAT3), but also cause disturbances in monocyte and glial cell functions [10]. The absence of correlation between HCMV's seroprevalence (80%) and low prevalence of GBM in general population ($5 \times 10^{-5}\%$) supports the

non-association between the HCMV infection and glioma aetiology. The potential role of HCMV in glioma genesis has not yet been elucidated. However, it has been suggested that HCMV could modulate the malignant phenotype in glioblastomas. Growing evidence indicates that infection by HCMV is associated with a more aggressive phenotype of glioblastoma, promoting invasion and angiogenesis [14, 15].

1.4 Survival after diagnosis

The most conclusive prognostic factors for glioblastoma are extent of tumour resection, age at diagnosis, and Karnofsky performance status, a scoring to determine and quantify cancer patients' general well-being and activities of daily life [13, 16]. Survival varies significantly by grade across all glioma subtypes. GBM has the poorest prognosis among glioma types, with a five year survival rate of only 0.05% to 4.7%. Age is significantly associated with poor survival for all gliomas, but the effect is more pronounced for GBM [13].

Despite optimal treatment, the median survival for GBM is 12-15 months after diagnosis, even with maximal surgical resection, adjuvant radiotherapy, and chemotherapy [4]. Recurrent GBM has a worse prognosis, with a median patient survival of 3-6 months [1]. Improvements in survival over the past 100 years can be measured only in weeks [17].

1.5 Histological characteristics

Morphologically, GBM consists of small cells, characterized by pleomorphism, anaplasia, and significant anisokaryosis. GBM cells are polygonal to spindle-shaped with acidophilic cytoplasm and indistinct cellular borders, with oval or elongated nuclei and roughly clumped hyperchromatic chromatin with multiple distinct nucleoli with central or pericentral location. Binuclear and multinucleated cells, as well as lymphocytes, neutrophils, macrophages, and necrotic cells, can also be present. Additionally, GBM is highly vascularized. Endothelial cells from newly developed vessels are phenotypically different from normal endothelial cells, focally overlapped, hyperplastic, and heterogeneous in size and shape. GBM shows vascular thrombi leading to endothelial cell damage and proliferation, leading to an extravasation of blood cells [6, 10, 18].

Necrotic foci are one of the most characteristic features of GBM [10, 19]. Two types of histological necrosis are typically encountered, depending on the localization and size of the necrotic area. The first one consists of large areas of necrosis within the central area of the tumour, resulting from insufficient blood supply in all primary glioblastomas. The other type contains small, irregularly shaped necrotic foci surrounded by pseudopalisading areas created by radially oriented glial cells observed in both primary and secondary glioblastomas. The pseudopalisading cell

population could represent: (i) rapidly proliferating neoplastic cells that have “outgrown their blood supply” and undergone central necrosis; (ii) a population resistant to apoptosis, which has accumulated because of increased cell survival; (iii) a mixed population of tumour and inflammatory cells adjacent to necrosis; or (iv) a population of cells migrating to or from a central focus. Cell density of pseudopalisades is almost twice as high, but proliferation activity is from 5 to 50% lower than in other tumour zones. The pseudopalisading areas show the presence of multiple apoptotic cells as well [10, 18].

1.6 Classification

1.6.1 Histological classification

Multiple classification schemes have been designed to organize the heterogeneity of gliomas. The first grading system by Bailey and Cushing [2] was followed by the Kernohan [20], St. Anne-Mayo [21], and WHO [3, 22] grading systems. Gliomas are currently classified under the WHO system, a modification of the St. Anne-Mayo grading scheme [19]. Since the increased malignancy of these tumours is accompanied by an increase of atypia degree, nuclear hyperchromatosis, increased mitotic index, presence of necrotic areas and atypical blood vessels [10], grades are based on four key histomorphological features including (i) nuclear atypia, (ii) mitotic figures, (iii) microvascular proliferation, and (iv) necrosis. Lesions with 3-4 variables are grade IV tumours, those with two variables are grade III tumours, and those with one characteristic are grade II tumours [19]. Histological characteristics are shown in Fig. 2, and the histological characteristics of each grade are summarized in Table 2.

Although higher WHO grade correlate with poor prognosis, multivariate analysis of these tumour grades shows significant variability in prognosis within each tumour grade, supporting the use of additional molecular markers to allow better risk stratification [19].

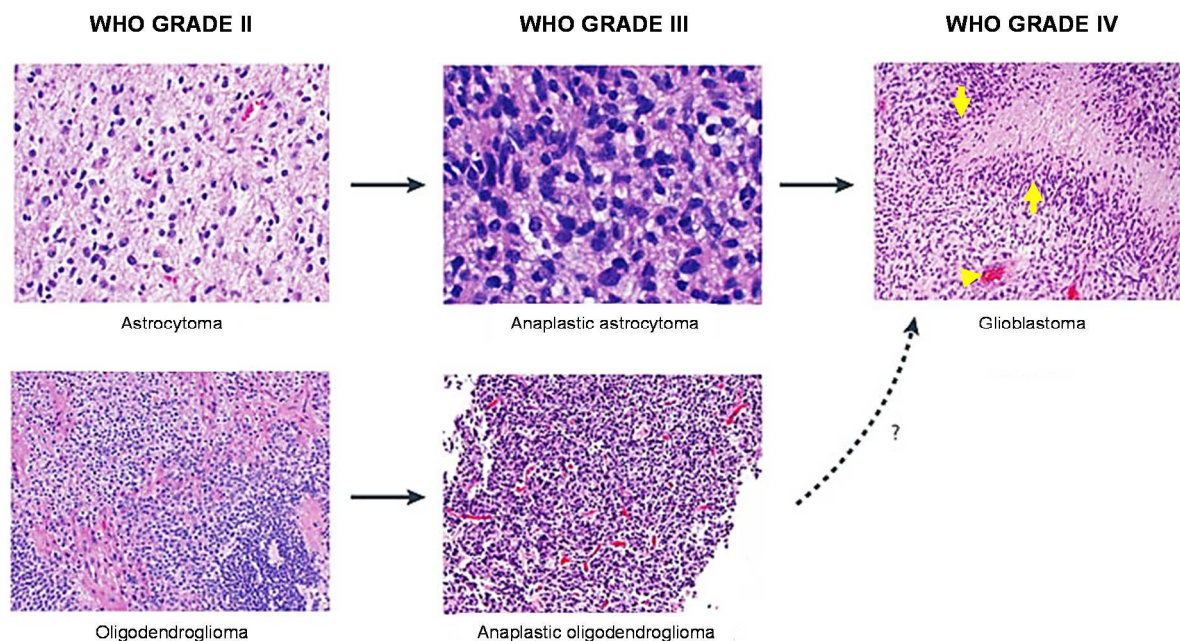


Figure 2. Representative histological images of WHO gliomas grade classification. Arrows indicate the possible progression from WHO low-grade gliomas to GBM. For GBM, microvascular proliferation (yellow arrowhead) and pseudopalisading necrosis (yellow arrows) are indicated. Modified from Huse and Holland [23].

Table 2. Criteria used for glioma grading according to the WHO classification (2007).

	Histological characteristics	Example
Grade I	No malignant histological characteristics	Pilocytic astrocytoma
Grade II	Tumour composed primarily of astrocytes (fibrillary, protoplasmic, gemistocytic, giant cells, and combinations thereof); evident atypia, but no mitoses	Astrocytoma
Grade III	Tumour showing mitotic activity and areas of anaplastic transformation; such tumours are not difficult to distinguish from glioblastoma	Anaplastic astrocytoma
Grade IV	Anaplastic tumour, usually astrocytic, with high cellularity, endothelial proliferation, or necrosis with pseudopalisading	Glioblastoma

1.6.2 Molecular classification

Over the past few years, genomic and proteomic characterization have confirmed the molecular heterogeneity of GBM [5]. Traditionally, GBM has been classified into primary or secondary subtypes on the basis of clinical presentation and features (such as response to therapy), although both subtypes are indistinguishable at the morphological level. Approximately, 95% of GBM emerge as *de novo* primary tumours. Secondary GBM arise and progress from lower grade astrocytomas and are quite rare. It is now known that both subtypes constitute distinct diseases with specific genetic profiles. Primary GBM are characterized by *EGFR* gene amplification

and mutation; loss of heterozygosity (LOH) of chromosome 10q containing phosphatase and tensin homolog (*PTEN*) gene; overexpression of mouse double minute 2 (*MDM2*); and deletion of p16. The hallmarks of secondary GBM include mutations of *TP53* and *retinoblastoma (RB)* gene; overexpression of *PDGF factor A (PDGFA)* and *PDGFR alpha (PDGFR α)*; and LOH of 19q [5, 24].

Two decades of molecular studies have identified important genetic events in newly diagnosed GBM, which was the first cancer studied by The Cancer Genome Atlas (TCGA) [25, 26]. This integrated genomic analysis using hierarchical clustering of 840 gene signature, determined an expression-based molecular classification of GBM into at least four molecular subtypes: pro-neural, neural, classical, and mesenchymal subtypes, characterized by aberrations and gene expression alterations on *EGFR*, *NF1*, *PDGFR α* , and *erb-b2 receptor tyrosine kinase 2 (ERBB2)*, respectively. Each subtype is enriched for different mutation, genomic, and transcript alterations [5, 26, 27].

The pro-neural subgroup is enriched for mutations in *isocitrate dehydrogenase 1 and 2 (IDH1/2)* genes, mutation in *TP53* gene, and amplification of *PDGFRA*, *CDK6*, *CDK4*, and *MET* genes, displaying an oligodendrocytic cell expression profile. Additionally, this group contained the highest percentage of young patients, likely due to *IDH1* enrichment associated with younger age [5, 28]. The neural subtype has elevated levels of neural markers such as *neurofilament light polypeptide (NEFL)* but has no specific genetic alterations when compared to the other subtypes of GBM, although elevated rates of *ERBB2* mutation were observed in this subtype. It is characterized by a normal brain tissue gene expression profile. The classical subtype is characterized by *EGFR* amplification and deletion of *PTEN*. It also harbours the mutant *EGFR* variant III (*EGFRvIII*), which is constitutively active and with in-frame deletions of exons 2-7, and it usually presents an astrocytic cell expression pattern and loss of chromosome 10 [5, 28]. Last, the mesenchymal subtype is associated with a poor overall survival and presents *NF1* mutations, *MET* amplifications, and loss of *TP53* and *CDKN2A*. This GBM subclass displays increased angiogenesis, hypoxia, inflammatory infiltrates, and inflammatory signalling pathways, including NF- κ B, STAT3, and TGF- β [5, 29]. Fig. 3 summarizes the four subclasses of GBM and their relation with WHO classification.

In current clinical practice, standard histopathology is complemented by molecular testing generally performed on single tumour biopsies. The four GBM subtypes defined by the TCGA have been increasingly applied in the clinic due to their prognostic ability and ease of testing for a single typical molecular alteration: *IDH1/2* mutation (pro-neural), *EGFR* amplification (classical), or *NF1* loss (mesenchymal) [27]. While there is a significant correlation between traditional pathological grouping and newer molecular subtypes, overlap is incomplete [13].

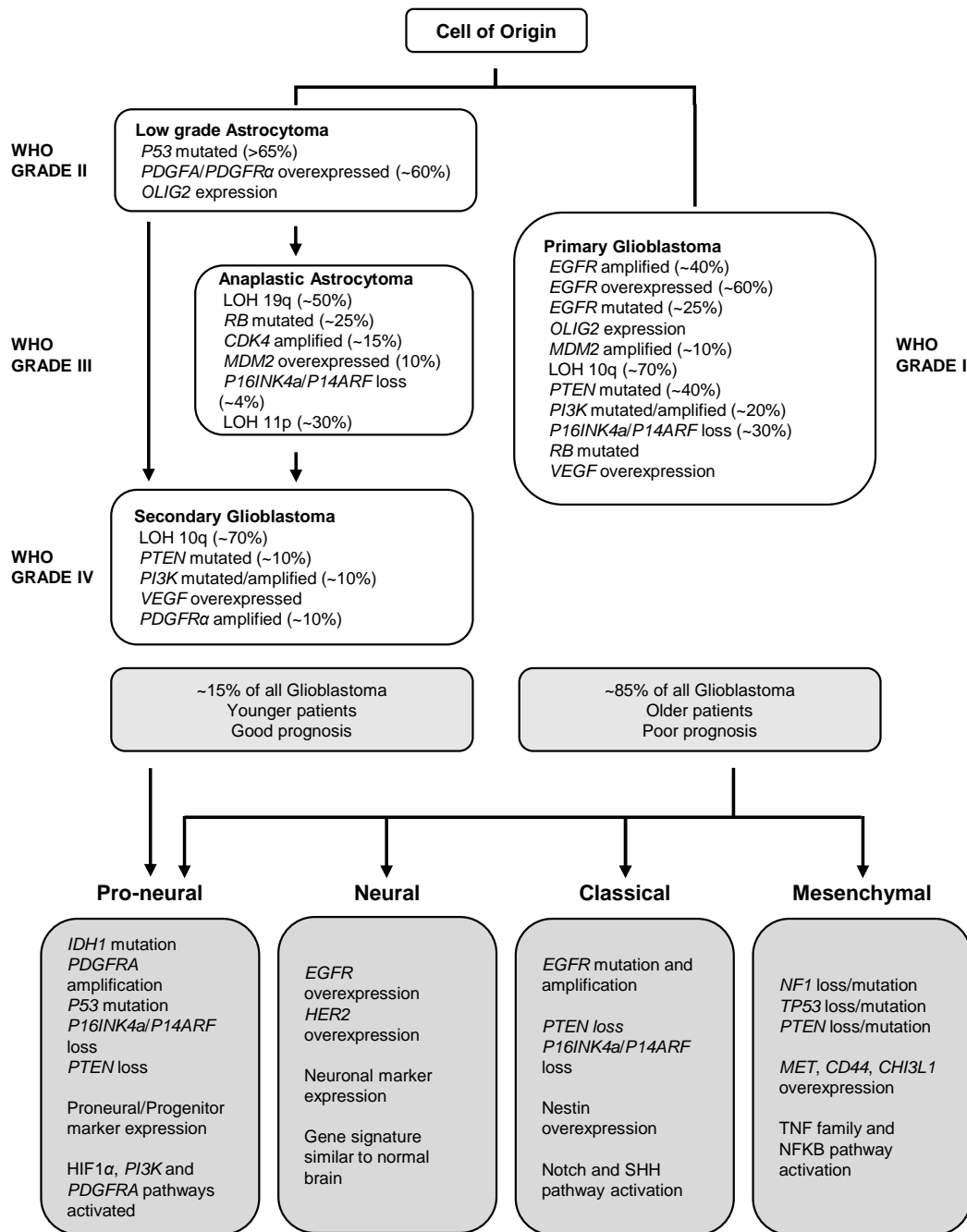


Figure 3. Molecular vs WHO grade classification of GBM. The related chromosomal/genetic alterations for each group as well as the relation between WHO and molecular classification with primary and secondary GBM are described. Modified from Agnihotri *et al* [5].

In addition, the established transcriptional profile between subtypes of GBM correlates not only with the classical histological classification for GBM but also with differences in clinical outcome [23]. For instance, secondary GBM are pro-neural virtually in all occasions. On the contrary, primary GBM can be classified in any of the above mentioned subtypes [29], although some evidence indicates that its expression pattern could be more related to the mesenchymal subtype [30]. A recent study showed that classical GBM displays an effective response to radiation

and chemotherapy [19]. Patients with pro-neural GBM subtypes demonstrate improved survival over the proliferative or mesenchymal subtype [31]. These transcriptional profiles suggest that, despite the genomic heterogeneity, GBM with similar expression profiles are fundamentally driven by alterations in the same basic signalling pathways and may therefore be susceptible to the same class of targeted therapeutics [23]. A more detailed molecular understanding of these tumours is crucial for an improved classification, for outcome prediction, and for tailoring specific treatments to individual tumour types or patients [32].

1.7 GBM pathogenesis

GBM develops mainly in the brain. This tumour is located in the hemispheres or subtentorially in the brain stem and cerebellum. It is characterized by an infiltrative growth pattern; therefore the tumour mass is not clearly distinguishable from normal tissue. The growing tumour causes an increase of intracranial pressure, oedema, and sometimes leads to hydrocephaly. Brain functions (sensory, motor, and cognitive) affectation by GBM is highly diverse and directly depends on tumour location leading to progressive degeneration, clinical complications and death. Metastases of GBM by cerebrospinal fluid or blood are rare and target the spleen, pleura, lungs, lymph nodes, liver, bones, pancreas, and small intestine. It has been hypothesized that the low metastatic potential of GBM results from the barrier created by cerebral meninges, but also from the rapid tumour growth and short course of this disease [10].

1.7.1 Migration and Invasion

During GBM growth, migration, and progression, the tumour cells closely interact with the extracellular matrix (ECM). The brain is considered as a largely free of a well-defined ECM organ. A well-defined ECM exists in the form of a true basement membrane only around all cerebral blood vessels. This particular characteristic of the brain ECM suggests a unique invasive mechanism of these tumours, which explains that despite the highly invasive behaviour, they remain poorly metastatic. The dissemination of tumour cells is a function of two phenotypes: migration and invasion. Both terms could be used interchangeably, but there are clear functional differences. Classically, migration refers to the capacity of cell locomotion. In contrast, invasion involves migration and also the degradation of ECM barriers by proteases that allow tumour cells translocation through ECM barriers. Tumour cell growth and invasion within the CNS imply complex interactions between malignant, glial, neural, and endothelial cells involving different elements as growth factors, proteases, ECM components, and specific cell surface receptors. A better understanding of the complex regulation and the signalling molecules involved in glioma invasion is still needed in order to design new and effective treatment modalities against invasive tumour cells [33].

1.7.2 Hypoxia and GBM tumorigenesis

Clear evidences show that hypoxia is involved in the malignant transformation of cells and subsequent tumour growth [34, 35]. GBM is a highly vascularized human tumour, but its microcirculation is functionally very inefficient compared with that of normal brain tissue. Intratumoural necrosis, the hallmark of GBM, is found in both small and large tumours, suggesting that necrosis derives from inadequate vascular supply but also from intrinsic molecular and/or genetic changes within the tumour [34]. Additionally, the degree of necrosis within GBM correlates inversely with patient outcome and survival. These poor vascularization produce the formation of hypoxic areas that lead to the formation of necrotic foci. It has been hypothesized that in the progress from low-grade astrocytoma to GBM, small areas of hypoxia within the tumour mass induce the clonal selection of cells that best react against this hypoxic stress. These cells present high proliferation potential, induce angiogenesis, and display resistance to therapy [34-36].

The necrotic foci above described are typically surrounded by pseudopalisading cells, a configuration that is relatively unique to GBM and other malignant gliomas (Fig. 2). A tumour progression model may explain the development of pseudopalisades and its relation with angiogenesis and aggressive clinical behaviour. The model hypothesizes a sequence that begins with an infiltrating astrocytoma, continues with (i) vascular occlusion within the tumour; (ii) hypoxia in regions surrounding vascular pathology; (iii) outward migration of tumour cells away from hypoxia, creating a peripherally moving wave (pseudopalisades) and central necrosis; (iv) secretion of hypoxia-inducible proangiogenic factors by pseudopalisading cells; (v) an exuberant angiogenic response creating microvascular proliferation in regions adjacent to central hypoxia; and (vi) accelerated outward expansion of tumour cells toward a new vasculature. All these microscopic processes result in a peripherally expanding tumour with a large degree of central necrosis [35].

Hypoxia generates several adverse effects in the treatment of GBM due to direct (as on radiation therapy) or indirect effects. Under normoxia, radiation reacts with intracellular water and molecular oxygen generating reactive oxygen species (ROS), which cause severe DNA damage. In addition, the radiation conditions required to achieve the same effect is three times higher than under normoxia and DNA damage is repaired faster. Indirect effects include the activation of hypoxia inducible factors (HIFs) that operate as key transcription factors for regulating hypoxia responsive genes (such as VEGF, ABC transporters and elements of the PI3K/AKT/mTOR signalling pathway). Therefore, tumour hypoxia with deregulated expression of HIFs in GBM leads to recurrence, deficient response to treatment and poor prognosis for patients. The factors regulated

by HIFs act together to produce a high radio- and chemoresistance under hypoxia conditions [37, 38].

Other factors influencing the hypoxia-induced resistance are:

- (i) the distance between drug supplying blood vessels and tumour cells (diffusion barrier);
- (ii) the lower growth rate of hypoxic cells compared to well oxygenized tumour cells (affecting the antiproliferative effect of cytotoxic drugs); and
- (iii) the hypoxia-induced expression of ATP binding cassette (ABC) transporters on endothelial and tumour cells.

ABC transporter proteins actively (driven by ATP hydrolysis) efflux cytotoxic drugs from the cell, maintaining drug level below a cell-killing threshold. The expression of ABC transporters and the development of a drug-resistant phenotype could be activated by HIFs [37, 38].

1.7.3 Apoptosis

The term apoptosis was first proposed in 1972 to describe a morphologically distinct form of cell death or necrosis. Apoptosis has been recognized and accepted as a distinctive and important mode of “programmed” cell death, which involves the genetically determined elimination of cells. This process occurs during development and aging as a homeostatic mechanism to maintain a correct balance of cell populations in tissues. Apoptosis is also a defence mechanism during immune reactions or when cells are extremely damaged. Although a wide variety of stimuli and conditions, both physiological and pathological, can activate apoptosis, not all cells will finally die in response to the same stimulus [39].

Apoptosis is morphologically distinct from necrosis, which refers to the degradative process that occurs after nonprogrammed cell death. Apoptosis usually manifests with pseudopodia retraction, detachment from the substrate, shrinkage (pyknosis), chromatin condensation, nuclear fragmentation (karyorrhexis), and shedding of apoptotic bodies. By contrast, cells undergoing necrosis display none of these morphological features nor cytoplasmic vacuolization [39, 40]. However, during the past two decades, dozens of neologisms have been emerged to define new supposed cell death modalities, but only few truly reflect new cell death modalities biochemically and morphologically distinct from apoptosis and necrosis. Thus, although terms including mitotic catastrophe, entosis, pyroptosis, parthanatos, and anoikis are being used, most of them refer to cell death pathways that are executed (at least in part) by the molecular machinery of apoptosis or necrosis [40].

Apoptosis is an energy-dependent, highly complex and sophisticated mechanism involving different molecular events. To date, there are two well-defined apoptotic pathways: the extrinsic or death receptor pathway, and the intrinsic or mitochondrial pathway. However, both pathways are linked through molecules with cross-active capacity [39]. The extrinsic apoptosis is induced by extracellular stress signals mediated by specific transmembrane receptors. In contrast, the intrinsic apoptosis requires a diverse array of intracellular signals (nonreceptor mediated stimuli) that directly activate targets within the cell and are mitochondrial-initiated events [39, 41].

The caspase family of aspartate proteases are the central executors of apoptotic cell death. Caspases are cytosolic latent proteins activated by proteolytic cleavage. They are subdivided in two categories, initiators and effectors. Effector caspases (3, 6, and 7) cleave multiple cellular substrates during the death process. Activation of initiator caspases requires adaptor proteins that lead to their dimerization and auto-activation. Caspases activation is induced either by ligation of death ligands to specific cell surface receptors (extrinsic pathway) or after the release of pro-apoptotic factors from mitochondria (intrinsic pathway). Numerous studies substantiate the existence of alternative and caspase-independent forms of programmed cell death [42].

Other important effectors in the apoptotic cascade are lamins. Lamins, the major component of nuclear cytoskeleton, are implicated in various nuclear functions including maintenance of chromatin organization, apoptosis, and replication. Lamin A and Lamin C, in particular, are substrates of proteases and caspase-6-mediated proteolysis. The cleavage of Lamin A is crucial for nuclear apoptotic events such as shrinkage, disassembly of nuclear membrane, and formation of apoptotic bodies [43].

The precise regulated programme of apoptotic cells under physiological conditions is compromised in glioblastoma, leading to a survival advantage of the tumour cells. Nevertheless, key players of the apoptotic cascades are present in glioblastoma cells and therefore prone to therapeutic interventions [44].

1.7.3.1 Significance of apoptosis in GBM

Cancer is a clear example of dysfunctional mechanisms of the cell cycle, with either cell overproliferation and/or cell removal decrease. In fact, apoptosis suppression during carcinogenesis is thought to play a pivotal role in the development and progression of some cancers [39]. Indeed, a high resistance against classical, caspase-dependent apoptosis is an established hallmark of malignant gliomas [42].

In GBM cells, several key regulatory elements of cell homeostasis and apoptosis are altered at the levels of LOH, inactivating mutations, methylation, or altered expression, including the

TP53, the B-cell chronic lymphocytic leukaemia/lymphoma 2 (BCL-2) protein family, the inhibitor of apoptosis proteins (IAPs) or receptor tyrosine kinases like the EGFR and their down-stream signalling cascade. Currently, efforts are focused on the detection of specific alterations in apoptosis pathways in GBM. These alterations are the first-line targets for therapeutic interventions and constitute new approaches in treatment of GBM, such as the inhibition of BCL-2 [44].

1.7.3.2 Anoikis in cancer

Literally meaning “the state of being homeless”, this ancient Greek term was introduced to describe the apoptotic response of adherent cells due to the absence of cell-to-matrix interactions. Anoikis may currently be defined as an adherent cell-restricted lethal cascade that is initiated by detachment from the matrix. It should be noted that in most, if not all, situations, the cell death programme induced by anoikis is executed by the molecular machinery for intrinsic apoptosis [41].

Anoikis prevents detached cells’ re-adhesion to new matrices or tissues in incorrect locations and their dysplastic growth, ensuring normal development and tissue homeostasis. Then, anoikis programme failure could induce cells surviving under nonadherent conditions or proliferation at ectopic sites. Thus, the anoikis process is emerging as a hallmark in cancer cells that contributes to metastases in distant organs [45]. The initiation and execution of anoikis is mediated by intrinsic and extrinsic apoptosis pathways, which terminally converge into the activation of caspases and downstream molecular pathways, culminating in the activation of endonucleases, DNA fragmentation, and cell death [45]. The anoikis programme is induced through proteins of the BCL-2 family that include the multi-domain pro-apoptotic proteins as BCL-2-associated X protein (BAX) [45]. Activation of BAX is the major initiator of the intrinsic pathway of apoptosis and plays a crucial role in anoikis conditions, particularly *in vitro* [46].

Resistance to anoikis in epithelial cancer cells sustains invasiveness and metastatic potential. Thus, the characterization of related molecular cascades has a pivotal therapeutic relevance [41]. To date, anoikis resistance has been established as a clear target against tumour progression. An identification of the hierarchy of the elements involved in this cellular response may be of high clinical significance. Identification of successful approaches to block anoikis resistance could allow the control of metastatic process [45].

2. CANCER STEM CELLS

2.1 Cell of origin

The cell of origin could be defined as the initial cell or group of cells that generate the formation of a tumour due to the acquisition of neoplastic lesions [5, 47]. It has been hypothesized that the putative cell of origin of GBM can be developed by three different process: (i) dedifferentiation of mature glia to unregulated stem-like cells through mutations or epigenetic lesions; (ii) increase of the limited self-renewal potential of neural progenitors by the acquisition of mutations which lead to unregulated stem like cells properties; and (iii) transformation to a tumorigenic phenotype of adult neural stem cells (NSC) (which normally have tight regulation over their proliferative and differentiation potential) through mutations (Fig. 4) [5].

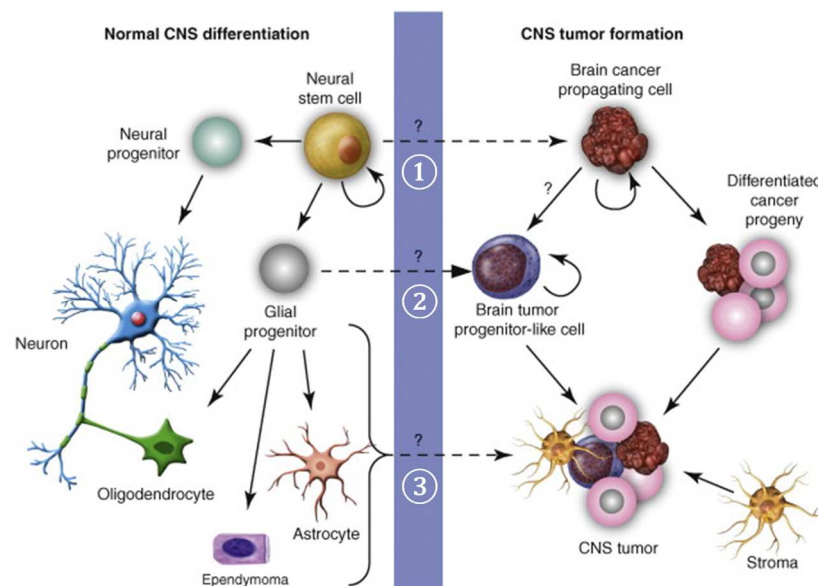


Figure 4. Normal CNS differentiation and tumour transformation. NSC differentiate to neural and glial progenitors that then give rise to neurons, oligodendrocytes, and astrocytes. GBM might originates from NSC ①, from neural progenitors ②, or from differentiated cells through mutations acquisition ③. Local or systemic stroma cells recruitment can be essential for tumour maintenance, progression, and recurrence. Curved arrow represents self-renewal ability. Image was taken from Hadjipanayis and Van Meir [48].

The high heterogeneity of GBM at the time of diagnosis makes any retrospective analysis of clinical specimens unsuitable for a correct identification of a cell of origin [49]. It is unknown if more than one cell of origin may generate a single type of tumour. Current data indicate that several cell types are capable of transformation into cells of origin according to the mutations acquired. For instance, different mouse models allowed the analysis of the mutation accumulation

process in different cell types of brain. The use of these models confirmed the potential of NSC to act as cell of origin. However, NSC lineage and cells outside of the neurogenic niches (as neurons) also display tumour-initiating potential. Furthermore, the cells of origin of each genetic subtypes of GBM are still unexplored and under discussion [47, 49].

2.2 Neural Stem Cells

Neurogenesis in adults is responsible for neurons and glial cell replacement for cell replenishment, remodelling, and response to injury. Since its discovery, Neural Stem Cells (NSC) and their progeny became the most possible cell of origin for GBM [47]. There has been intense speculation concerning progenitor generation and its role in adult brain. NSC present self-renewal capacity, pluripotency, and a complex pattern of genetic expression. NSC are able to generate new neurons, and are involved in neurogenesis within specialized brain regions (e.g. olfactory bulb, hippocampus, and central canal of the spinal cord) [1, 50]. Active neurogenesis in adult humans and mice suggests that a decline or a defect in the process may play a role in neurodegenerative disorders or glioma formation, respectively [47].

It is established that multipotent cells could be isolated and cultured from the human or mice subventricular zone (SVZ) and subgranular zone (SGZ) of the dentate gyrus (Fig. 5). Such cultures were extremely heterogeneous, but they were shown to be capable of direct *in vitro* differentiation to both glia and neurons, indicating that they contained either undifferentiated precursors and NSC [47]. Besides these brain regions, NSC were described in striatum, frontal, and temporal cortex, as well as the subcortical white matter. However, the SVZ constitutes the largest reservoir of NSC in both the adult rodent and human brain. A substantial amount of clinical and basic research suggests the potential role of NSC and/or progenitor cells of the SVZ as cells of origin [17].

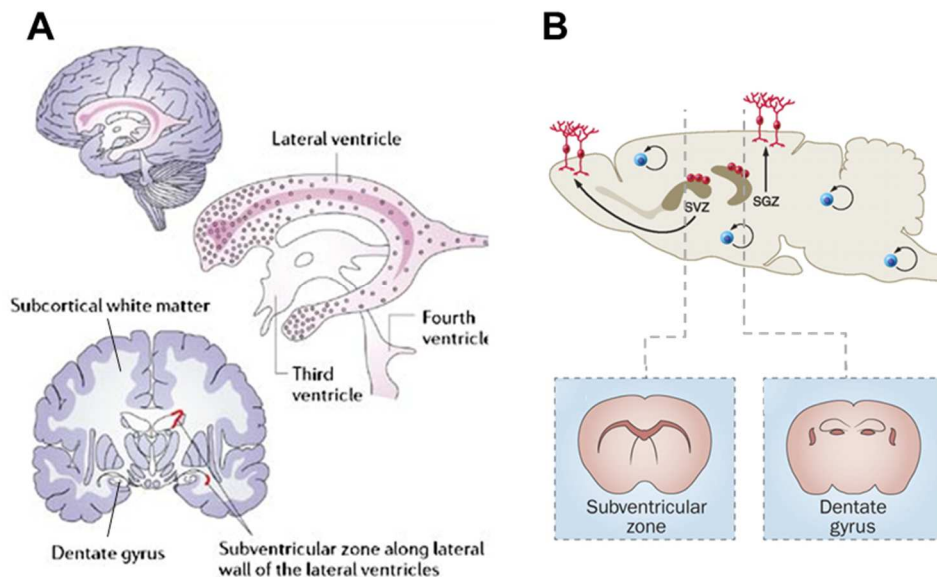


Figure 5. Anatomical localization of the NSC in SVZ and SGZ in humans and mice. (A) In the adult human brain, a population of SVZ astrocytes has been identified as comprising NSC. (B) The SVZ and dentate gyrus within the adult brain mouse. Neurogenesis from NSC (red cells) to neurons is represented. Parenchymal progenitors are graphed as blue cells. Neurogenesis in this region (SGZ) has been demonstrated to take place in adult mammals. The figure was generated from Vescovi *et al* [51], Martino *et al* [52], and Ziegler *et al* [53].

2.3 Cancer Stem Cell theory and GBM

Over the last decade, biological basic research has demonstrated that stem cells have a critical role in the generation and maintenance of multicellular organisms and in the development, growth, and recurrence of tumours [54]. The relevant similarities between cancer and normal stem cells have sustained the CSC Theory proposed by Reya *et al* [55]. This theory consists in an alternative to the stochastic model for solid tumours that proposes that each cell present in the tumour mass has the potential to originate a new tumour. The proposed CSC theory or hierarchical model implies that only a small subpopulation, the CSC subset, can proliferate extensively and sustain the growth and progression of a neoplastic clone and form a new tumour (Fig. 6) [55].

Characteristics of CSC are directly related with stem cells properties. These shared characteristics include (i) *self-renewal*: the process of cell division that maintain an undifferentiated state, sustaining the CSC pool within the tumour mass; and (ii) *multilineage differentiation*: capacity to generate a heterogeneous population of cancer cells, leading to a cell hierarchy within the tumours. Additionally, a unique feature for CSC was postulated, the tumorigenicity. The CSC are the only cancer cells able to initiate and recapitulate the original malignancy when xenotransplanted in animal models. For that reason, they are also referred to as Tumour Initiating Cells, or BTIC in the case of CNS tumours [26, 56].

It is relevant to point out the difference between the GBM CSC (or BTIC) and the cell of origin. GBM CSC are defined as the cell subpopulation that sustains the tumour and is present in the differentiated tumour mass, whereas the cell of origin is the cell (or group of cells) that initially gives rise to the tumour but is not present in the differentiated tumour mass. Although the GBM CSC and the cell of origin shared the tumorigenic ability, they are not identical entities [5, 49]. Indeed, the cell of origin has no intrinsic ability of self-renewal and might only have potential for a single-lineage differentiation, and are not part of the tumour [49].

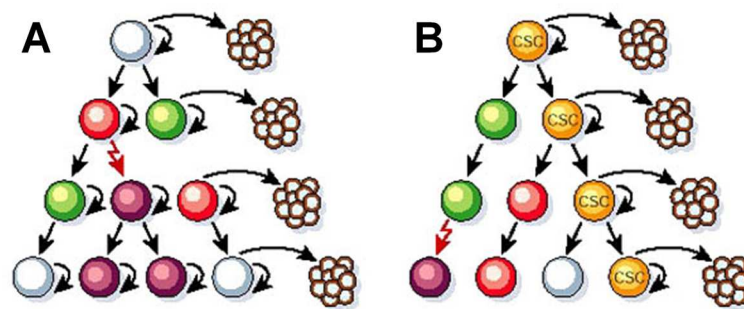


Figure 6. Heterogeneity models for solid tumours. The stochastic model (A) established that most of the cells present in the tumour have the potential to proliferate to give rise to a new tumour. Conversely, in the hierarchical model (B) most cancer cells have limited proliferative potential and only CSC (yellow) have the ability to proliferate extensively and form new tumours. Image modified from Reya *et al* [55].

Subsequent to the discovery of NSC in the adult CNS, CSC subpopulations were isolated from GBM tissues [17, 57, 58]. These isolated GBM CSC were able to reinitiate tumours when seeded into new mice brains with higher efficiency than their non-stem counterparts in the tumour. Current evidence suggests that GBM CSC may derive from NSC or lineage-restricted progenitors [47]. Indeed, GBM CSC share a crucial feature with NSC: the expression of distinctive stem/precursor markers that can be helpful to distinguish them from non-CSC population [56].

2.4 Identification and isolation of CSC

The study of CSC involves a general work-flow: (i) stem-cell isolation from relevant tissues using specific markers, (ii) development of neurospheres, (iii) *in vitro* differentiation of neurospheres into neurons, astrocytes, and oligodendrocytes, and (iv) tumour formation when injecting tumour-derived neurospheres into immune-compromised mice [59]. Correct sorting, identification, and isolation of CSC has emerged as a priority in GBM [60]. However, this identification and isolation constitutes a difficult and controversial issue since different methods and criteria had been used and no standardized protocol is available [51].

2.4.1 CSC surface markers

Several molecules have been classified as cell surface markers of GBM CSC. Although no single marker has been demonstrated to efficiently isolate GBM CSC, probably due to the heterogeneity of the disease [61]. The identification of additional markers for GBM CSC enrichment and isolation is critical. However, markers that have been shown to be successful for NSC as well as other cancer stem cell systems, must be considered and evaluated for GBM CSC [61, 62]. A summary of the currently surface markers used to the isolation of GBM CSC are presented in Table 3, and a brief explanation of their nature and function will follow.

Table 3. Cancer stem cell markers in GBM.

Marker	Type	Normal function	CSC regulation	CSC systems
CD133	Surface glycoprotein	Unknown	Positivity associated with more aggressive tumours	Colon, leukaemia, liver, lung, breast, prostate
CD15	Cell surface glycan	Cell adhesion and migration	Enrichment marker of stem cells in CD133- tumours	Medulloblastoma, gliomas
L1CAM	Adhesion molecule	Nervous system development	Neuronal cell adhesion molecule required for maintaining the growth and survival of CD133+ glioma cells with stem-like properties	Gliomas, colorectal
A2B5	Surface Glycoside	Astrocytes differentiation	Mixed evidence of association with more aggressive tumours	Gliomas
Integrin $\alpha 6$	Transmembrane receptor	Cell adhesion, laminin receptor	Regulates self-renewal, proliferation and tumour formation by interacting with ECM	Breast ($\beta 3$ and $\beta 1$), colon ($\beta 1$), prostate ($\alpha 2\beta 1$ and $\alpha 6$)
CD44	Cell surface glycoprotein	Hyaluronic acid receptor, cell-cell interactions, cell adhesion and migration	Positivity associated with more aggressive tumours; localized in the endothelial stem cell niche	Bladder, breast, colon, gastric, head and neck, ovarian, prostate

Modified from Lathia *et al* [62] and Jhanwar-Uniyal *et al* [54].

2.4.1.1 CD133

CD133 (= PROMININ-1) is a pentaspan membrane protein with relatively unknown function since it is related with a photoreceptor defect phenotype. CD133 has previously been shown to be a marker of normal embryonic neural and hematopoietic stem cells, constituting a useful marker of GBM CSC and other cancers [62]. The potential of CD133 as GBM CSC marker was first described by Galli *et al* [57]. Singh *et al* [63] proved the potential of this CD133-positive cells to

generate tumours *in vivo*. One hundred CD133-positive cells were enough to generate tumours in immunodeficient mice, whereas the injection of 1×10^5 CD133-negative cells lacked this capacity. Despite this first evidence, CD133 is not consistently expressed in all GBM, and CD133-negative cells were capable of originating tumours in further studies. When present, CD133 expression can be used for the isolation of GBM CSC, however the low expression in some tumour samples suggest the need of additional markers [61]. The utility of CD133 as GBM CSC surface marker has been controversial and context-dependent. However, a functional role for CD133 as a regulator of the PI3K-AKT pathway has been elucidated in GBM CSC [62, 64].

2.4.1.2 CD15

Recently, CD15 (= SSEA-1 or Lewis^x antigen) has been explored as an enrichment marker of GBM CSC [61, 65-67]. CD15 is a glycan motif linked to glycoproteins, proteoglycans or lipids on the cell surface [68]. This cell surface glycan (3-fucosyl-N-acetyl-lactosamine) is detected in embryonic and adult NSC and has been linked to bFGF responses. CD15 enriches GBM CSC when CD133 is either absent or limited to a small fraction of cells. However, there is low knowledge about CD15 biological activity in GBM CSC. The function of CD15 has been thoroughly investigated in the immune system and in the context of cancer cell migration. However, the functional relevance of CD15 in the CNS is far less well understood [68]. It has been suggested that probably constitutes a cell cycle-dependent marker linked to proliferation [62].

2.4.1.3 L1CAM

Line-1 cell adhesion molecule (L1CAM), a neural cell adhesion molecule overexpressed in GBM, also allows for the enrichment of CSC. L1CAM is a glycoprotein belonging to the immunoglobulin superfamily, and its structure comprised of an intracellular domain, a transmembrane region and an extracellular domain that interacts with another L1CAM molecule, growth factor receptors, and ECM proteins such as $\alpha 5 \beta 1$ and $\alpha \nu \beta 3$ integrins [69, 70]. Interestingly, while its biological function in normal brain has not been fully elucidated, targeting L1CAM in GBM stem cells showed therapeutic benefits *in vitro* and *in vivo* [62]. L1CAM has been suggested to mediate the interplay between different cell subpopulations within the tumour. However, the use of L1CAM to identify CSC or glioma grade has not been validated yet [71].

2.4.1.4 A2B5

Anti-A2B5, an antibody against polysialogangliosides (a commonly used glial/white matter progenitor cell marker), has also been explored as a potential CSC marker in GBM. A large percentage of brain tumours and GBM cells present positivity for A2B5 [62]. The A2B5 reactivity and its relationship with CD133 expression and tumorigenicity was investigated [72]. Moreover,

both A2B5+/CD133+ and A2B5+/CD133- populations maintained tumorigenicity in transplantation mouse models. It is suggested that A2B5 could be used to enrich CD133- GBM CSC in isolation strategies [62].

2.4.1.5 Integrin α 6

Integrins are a family of transmembrane cell surface molecules that constitute the principal adhesion receptors for the ECM. In vertebrates, 24 different integrin heterodimers exist with differing substrate specificity and tissue expression [73]. Integrin α 6 is one of the subunits of this family and forms heterodimers with integrin β 1 or β 4. It also interacts with the laminin family of ECM proteins [62, 73, 74]. Integrin α 6 was identified as a stemness marker in embryonic, hematopoietic, and NSC. Recently, the perivascular microenvironment examination of GBM surgical biopsy specimens, a region enriched in GBM stem cells, identified integrin α 6 as an additional GBM stem cell marker with a potential therapeutic application [74]. The use of Integrin α 6 as a GBM CSC marker [75, 76] highlights the importance of evaluating the microenvironment in order to identify additional GBM enrichment markers and pathways as potential therapeutic targets [62].

2.4.1.6 CD44

In addition to the previously mentioned markers, studies demonstrate that subpopulations of glioma cells may be distinguished by the high expression of the CD44 adhesion molecule. CD44 is a class I transmembrane glycoprotein involved in many cellular processes such as growth, survival, differentiation and motility, and constitutes the major receptor for hyaluronic acid [77]. It is commonly expressed in numerous malignancies as breast and pancreatic cancer, and highly expressed in mesenchymal CSC derived from GBM. Additionally, CD44 was found to co-express with CD133 in GBM neurospheres [71] and is being considered a GBM CSC marker [26, 78].

2.4.2 Intracellular markers

Comparative gene expression analysis led to the identification of additional potential CSC markers in GBM, including inhibitor of DNA binding 1 (ID-1), octamer-binding transcription factor 4 (OCT4), MUSASHI-1, NANOG, and ALDH1. Some of these markers are expressed in embryonic stem cells, suggesting that CSC overlap not only with NSC but also with even less differentiated stem cells. Wide evidence suggests the correlation of these factors with the histopathological grade in glioma patients and therapy resistance. These proteins can be used to develop new prognosis tools, therapeutic targets as well as intracellular markers for GBM CSC [71, 79-81].

2.4.3 Side population

Purification of CSC in malignant gliomas can also be achieved based on their ability to efflux the Hoechst dye 33342, a technique called Side Population (SP). SP cells expressed various ABC transporters, explaining negative staining with the Hoechst dye, but more importantly conferring drug resistance due to an active transport system that efflux drugs outside the cells. The SP technique is controversial since the assay can be detrimental to non-dye excluding cells [48].

2.4.4 Development of neurospheres

An interesting feature of CSC or BTIC is their capacity of easy and extensive expandability when cultured with appropriate growth factors, such as epidermal growth factor (EGF) or basic fibroblast growth factor (bFGF). This culture condition allows CSC isolation, since proliferation and *in vitro* generation of multipotent cell clones (neurospheres) is feasible [51]. Neurosphere assays were initially used by Reynolds and Weiss in 1992 to isolate NSC from the mouse striatum [82], and were subsequently used to successfully enrich BTIC from brain tumours. This assay represents a *bona fide* method of isolating and enriching CSC and, most importantly, *in vivo* studies have shown that neurosphere formation capacity is a significant predictor of clinical outcome in glioma patients [83].

During neurospheres formation, the serum-free and selective culture system, induces that the majority of or totally differentiated tumour cells rapidly die. On the contrary, CSC respond to mitogens, divide, and form neurospheres that can be dissociated and replated to generate secondary spheres [83]. This process can be repeated by serial sub-culturing, which results in an exponential increase in the total number of cells and neurospheres that are generated [51]. The appearance of spheres after initial seeding and its maintenance in further passages are now widely accepted as indicators of a CSC phenotype and self-renewal [80].

Despite its wide use, the neurospheres assay present some limitations that must be considered. For instance, neurospheres may arise as an artefactual result from the experimental conditions rather than reflect *in vivo* related events [83], and also constitute complex, heterogeneous cell clusters that consist of stem cells, progenitor cells, and more differentiated cells [84].

Currently, there is no standardized protocol to compare results from different studies. In fact, it was proved that differences in culture conditions could affect the enrichment and isolation of CSC subpopulations [85]. The use of mitogens further confounds the results, as combinations of EGF, bFGF, PDGF, leukaemia inhibitory factor (LIF), and even neural survival factor have been used in different studies. The use of hormones is also inconsistent: whereas some studies use

progesterone and/or insulin, other studies use neither of them. Other additives that are notably different include serum-free supplements such as bovine serum albumin, insulin and transferrin supplement (BIT), N2, B27, antibiotics, and antimycotics. This wide variation in media components used among laboratories significantly complicates data interpretation and limits the comparison among studies [83].

2.4.5 In vivo transplantation

The utility of the neurosphere assay, CD133 and other CSC markers immunophenotyping, and of the SP assay in GBM CSC research has been widely proved. Nevertheless, several limitations for each assay must be considered [83, 86]. The transplantation of prospective CSC into mouse models to determine tumour formation is the most reliable characteristic to identify this subpopulation. These techniques in mouse models are considered as the standard for CSC activity evaluation. In addition, these methods have evolved to isolate CSC from human primary tumours and early passages xenografts, for CSC *in vivo* characterization [80]. For this characterization, tumour cells are transplanted into immunocompromised mice, monitoring the tumor growth at different time points; then, xenograft tumours or primary human tumours must be isolated from the mice and implanted into other immunocompromised mice to show self-renewal and tumour formation capacities [87, 88]. Xenotransplantation of CSC of a human tumour into mice with a compromised immune system do not accurately reflect factors critical for carcinogenesis such as the microenvironment and the immune response. However, new genetic modified mouse models improved the limitations of the xenograft model [89].

2.5 Molecular CSC subtypes of GBM

Two mutually excluding distinct types of GBM CSC were identified: pro-neural and mesenchymal [26, 90, 91]. These two GBM CSC subtypes were identified by genome-wide profiling and possess unique properties directly linked to therapeutic resistance of the individual GBM CSC subtypes (Table 4). The observed CSC genetic profile does not necessarily coincide with the GBM molecular classification (Fig. 3) from which CSC were isolated [90]. This discrepancy between GBM and CSC subtypes is unsolved and could be explained by technical limitations or biological mechanisms [92].

Phenotypically, these two CSC subtypes present differences. Mesenchymal CSC are more aggressive, angiogenic, and resistant to radiation treatment than pro-neural CSC both *in vitro* and *in vivo*. In addition, mesenchymal CSC are predominantly derived from primary GBM, whereas pro-neural reside in both primary and secondary GBM [90-92].

Table 4. GBM CSC subtypes according to expression profiles.

	CSC subtypes	
	Pro-neural	Mesenchymal
Frequency	60-65%	35-40%
Original tumour grade	Grade III, GBM	Mostly GBM, some Grade III
Stem cell marker	CD133, CD15	ALDH1A3, CD44
Potential cell of origin	Embryonic-neonatal neural stem cell	Adult neural stem cell-differentiated astrocyte

Modified from Nakano [92].

CSC might acquire mutations that induce immortality, self-renewal, and variable progenitor's differentiation [26, 59]. The GBM recurrence after standard therapy failure is generally accompanied with a phenotype adaptation in CSC subtypes regarding its expression pattern and tumorigenic ability. These changes can be maintained in further progenies [92]. This phenotypic plasticity in CSC and non-CSC subpopulations may explain barriers in defining a single marker or a set of markers that provides a definitive identity. If the mechanism of phenotype interconversion is widespread, this will explain the complex identification of robust CSC markers as well as the role of definitive identification on the use of functional definitions [26, 60].

2.6 Hypoxia and CSC

In the brain, oxygen sensing is integrated into physiological signalling pathways controlling NSC proliferation and cell fate determination in their niche. This control may be disrupted in gliomas and other brain cancers. Presence of small foci of hypoxic necrosis is a key risk factor of GBM, often associated with surrounding microvessel proliferation. A relation between hypoxia conditions and increased tumorigenicity in GBM CSC has been reported. The expression of CSC markers, signalling pathways, and resistance to therapy are modulated under hypoxia conditions [93].

GBM CSC are enriched in functional niches (perivascular space and hypoxic regions). These niches stimulate CSC survival and stem-cell phenotype, supporting the hypothesis that hypoxia is pivotal for initiation, progression, and maintenance of the stemness. The association of hypoxia with tumour invasion, chemo- and radioresistance, and low survival rate of GBM patients could be explained by CSC. Additionally, HIFs highly expressed by GBM CSC upregulate expression of CSC markers and maintenance of the CSC pool [38].

Hypoxia and HIFs play an important role in the initiation, progression, recurrence of GBM and the CSC phenotype [38, 93]. CSC eradication through HIFs and hypoxia inhibition is a research area of great interest that may open new GBM therapeutic opportunities [94-98].

2.7 CSC regulatory signalling pathways

Induction and maintenance of stemness are related with several signalling pathways (Table 5). These molecular pathways are clear targets for new improved strategies to treat GBM, but also could explain the functional differences between GBM CSC and NSC [59, 99].

Table 5. CSC principal signalling pathways and their roles in GBM.

Signalling pathway	Function
Self-renewal	
Notch	Maintenance of CSC Neurosphere formation Tumorigenesis Asymmetric division
TGF- β	Regulation of self-renewal Maintenance of perivascular CSC
Sonic Hedgehog	Promotion of self-renewal and migration Upregulation of stem cell related genes Tumorigenesis
WNT/ β -catenin	Self-renewal and maintenance of CSC Tumorigenesis Associated with bad prognosis
PI3K/AKT	Promotion of CSC self-renewal <i>in vitro</i> Proliferation and survival of CSC Tumorigenesis
MAPK	Proliferation and survival of CSC
Differentiation	
BMP	Inhibition of asymmetric division Differentiation and proliferation block
Notch	Tumour endothelium trans-differentiation
TGF- β	Trans-differentiation to vascular pericytes

Taken from Bayin *et al* [79].

2.7.1 RTK-AKT signalling

Receptor tyrosine kinases (RTK) transduce signalling of multiple oncogenic growth factors as EGF and bFGF that support the *in vitro* growth of both NSC and CSC. The EGFR-mediated growth signalling through the activation of the PI3/AKT/mTOR pathway is one of the most relevant and best characterized pathways in GBM. GBM frequently display EGFR amplification and/or

expression of the constitutively active variant EGFRvIII that increases EGFR-AKT signalling in cancer cells. Additionally, AKT signalling correlates with poor prognosis in GBM patients. EGFR activity is required for maintenance of GBM CSC, since EGFR kinase inhibitors attenuates CSC *in vitro* proliferation, neurospheres formation, and induces apoptosis. Targeting the EGFR/PI3/AKT signalling pathway may have specific effects on GBM CSC to reduce tumorigenic potential. Nevertheless, some clinical trials have been disappointing, suggesting that this target is an insufficient therapeutic option that requires a greater focus on PI3 inhibitors [59, 99].

2.7.2 Notch signalling

Notch proteins (Notch 1-4) are transmembrane receptors that mediate short-range cellular communication between neighbouring cells that are in physical contact. After the interaction with ligands (Jagged-1, -2, and Delta-like-1, -3, and -4), Notch receptors dissociate from the cell membrane, translocate to the nucleus and promote transcriptional responses including: differentiation, proliferation, apoptosis, and maintenance of CSC. Notch signalling contributes to cellular processes, including embryogenesis and angiogenesis. Furthermore, Notch promotes the proliferation of NSC, and Notch aberrant activation has been found in GBM and in its CSC subpopulation. Notch signalling has been linked to radioresistance of CSC, suggesting that inhibition of Notch may not only disrupt the maintenance of CSC but also reduce the radioresistance of CSC. Although blocking Notch signalling constitutes a good strategy targeting CSC, inhibitors are still in early clinical phase [59, 80, 99].

2.7.3 Sonic Hedgehog signalling

The Sonic Hedgehog (SHH) signalling is one of the key regulatory pathways during embryogenesis and is critical for the maintenance of several types of adult stem cells, including NSC. SHH pathway involves different soluble ligands: Sonic-Hedgehog (SHH), Desert-Hedgehog (DHH) and Indian-Hedgehog (IHH). Two transmembrane proteins act on the receiving cell: Patched (PTCH) which binds the ligands, and Smoothed (SMO) which acts as a signal transducer. Aberrant activation of SHH pathway was found in GBM, and correlates with tumour grade and malignancy. Inhibition of SHH signalling suppresses self-renewal and proliferation, while increasing apoptosis. Cyclopamine is one of the most studied inhibitors of SHH and enhances the efficacy of temozolamide (TMZ). SHH is critical for CSC maintenance and targeting this pathway with pharmacologic inhibitors may suppress CSC growth and improve the efficacy of conventional therapies against GBM. Currently, multiple candidates of upstream and downstream pharmacologic inhibitors of SHH are under development, although the side effects of these inhibitors need to be carefully evaluated [59, 80, 99].

2.7.4 WNT- β -catenin signalling

The canonical wingless/int (WNT) cascade is one of the critical regulators in embryonic and adult stem cells. WNT signalling usually begins with WNT ligand binding one of the Frizzled family membrane receptors. The signal reaches the cytoplasm, where the unphosphorylated β -catenin accumulates and travels to the nucleus, inducing a cellular response via gene transduction. In brain, WNT signalling regulates development as well as proliferation and self-renewal of NSC. WNT- β -catenin signalling has been related with the contribution to radioresistance in GBM and maintenance of CSC in this tumour. WNT could be a therapeutic target for GBM CSC and in brain tumours, as this pathway is supporting motility/invasiveness of GBM. Currently, there are multiple trials involving WNT inhibitors in conjunction with current therapies in other tumours as gastric, liver, pancreatic, ovarian, and colorectal. However, its therapeutic potential in GBM is under evaluation [59, 80, 99].

2.7.5 STAT3 signalling

The signal transducer and activator of transcription 3 (STAT3) is a critical transcriptional regulator involved in a wide range of cellular activities including immune response, CNS development, stem cell maintenance, and tumorigenesis. The embryonic stem cell decision between self-renewal and differentiation depends on the interactions of STAT3 with other pathways. Genetic knockdown of STAT3 or inhibition with specific inhibitors disrupts proliferation and maintenance of GBM CSC. STAT3 inhibitors are undergoing clinical development. However, as STAT3 is also important for the maintenance of NSC and required for critical immune responses and other normal cellular activities, targeting STAT3 may display significant side effects and is unlikely to be specific for GBM CSC [59, 80, 99].

2.7.6 PDGF signalling

GBM express all PDGF ligands (PDGFA-D) and their specific receptors (PDGFR α and β). PDGFR α is present in low-grade gliomas and enhanced by amplification in GBM. Imatinib is an inhibitor of PDGFR α , indicated for the treatment for myeloid and gastrointestinal tumours. Unfortunately Imatinib did not show clinically meaningful antitumour activity in a phase II clinical trial with recurrent GBM. GBM CSC express PDGFR β and its activation promotes glioma stem cell self-renewal, suggesting that targeting of this receptor can be beneficial in treatment of GBM patients [59, 100].

2.7.7 Bone morphogenetic proteins

The bone morphogenetic proteins (BMPs), as part of transforming growth factor beta (TGF- β) superfamily, regulate a large number of cellular processes during development and injury responses. The BMPs instruct cell fate during neural development. The role of BMPs in GBM, and specially in CSC subpopulation became more detailed after the discovery that CSC can epigenetically regulate BMPs receptors to shift towards a foetal phenotype to escape from the pro-differentiation effects of BMPs. BMPs exert a negative action in GBM CSC preventing tumour growth and mortality in mice. Overall, mimicking events induced by members of BMPs and identifying genes induced and repressed in this condition might lead to new targets of therapy [59, 99].

3. TRANSFORMING GROWTH FACTOR BETA SIGNALLING PATHWAY

In the early 1980s, it had become apparent that cell growth is controlled by many polypeptides and hormones. A new hypothesis of “autocrine secretion” was postulated, which suggested that polypeptide growth factors are able to cause malignant transformation of cells. Among these polypeptides, the Transforming Growth Factor beta (TGF- β) was described as a secreted polypeptide capable of inducing anchorage independent fibroblast proliferation and collagen production [101].

The TGF- β superfamily of secreted factors includes over 30 members comprising activins, nodals, BMPs, and growth and differentiation factors. Members of the family are found in both vertebrates and invertebrates groups [102, 103]. TGF- β superfamily signalling provides animal cells with tightly controlled developmental programmes and cell behaviour, producing effects on proliferation, morphogenesis, tissue homeostasis, and regeneration. Consistent with its ubiquitous activity, aberrant TGF- β signalling is associated with a wide range of human pathologies including autoimmune, cardiovascular, and fibrotic diseases, as well as cancer [101-103]. TGF- β members are subdivided into two functional subgroups, TGF- β -like and the BMPs-like subgroup [102].

3.1 TGF- β signalling elements

3.1.1 Ligands

TGF- β -type subfamily growth factors are homodimeric or heterodimeric polypeptides with multiple regulatory properties depending on cell type, growth conditions and presence of other polypeptide growth factors. Its expression is controlled by distinct promoters and their secretion is temporal, tissue specific, and as a latent precursor [101].

TGF- β protein sequence is highly conserved among species, with 99% homology between corresponding isoforms in human and murine proteins. There are three known isoforms of TGF- β encoded by genes located in different chromosomes. All genes have a length of more than 100 kb and contain seven exons. They are expressed in mammalian tissues and contain highly conserved regions. TGF- β 1 (chromosome 19q13) is the most abundant and ubiquitously expressed isoform. It has been localized in cartilage, membrane bone, and skin, suggesting a role in growth and differentiation of these tissues. TGF- β 2 (chromosome 1q41) was first described in human glioblastoma cells and is expressed by neurons and astroglial cells in the embryonic nervous system. It is also important in tumour growth enhancing cell proliferation in an autocrine way and/or reducing immune-surveillance of tumour development. TGF- β 1 and TGF- β 2 share 71% sequence similarity. TGF- β 3 (chromosome 14q24) was isolated from a rhabdomyosarcoma cell

line and it shares 80% of amino acid sequence with TGF- β 1 and TGF- β 2. It is essential for the epithelial-mesenchymal interaction and is expressed in lung adenocarcinoma and kidney carcinoma as well as in the umbilical cord at high levels [101].

3.1.2 Receptors

In most cells, three types of cell surface proteins mediate TGF- β signalling: TGF- β receptor I (T β RI), II (T β RII), and III (T β RIII), and are encoded by different genes: *TGFBR1* (chromosome 9q22), *TGFBR2* (chromosome 3p22) and *TGFBR3* (chromosome 1p33-p32). T β RI and T β RII mediate signal transduction. Both receptors are transmembrane serine/threonine kinases, which associate in a homo- or heteromeric complex and act as tetramers. Type II range from 85 to 100 kDa, while type I receptor is smaller and ranges from 65 to 70 kDa. T β RI contains a characteristic, highly conserved 30 amino acids domain in the cytoplasmic part, which needs to be phosphorylated to fully activate T β RI. Out of these three receptors, T β RIII, also called betaglycan, is a membrane-anchored proteoglycan. It is the largest (250-350 kDa) and most abundant binding molecule from the three TGF- β receptors [101].

Another protein, the endoglin (CD105) was shown to act in other cell types as T β RIII for TGF- β . Although T β RIII and endoglin are co-receptors not directly involved in intracellular TGF- β signalling due to lack of the kinase domain, they can control access of TGF- β to its receptors and consequently modulate intracellular TGF- β activity. T β RIII binds all three isoforms of TGF- β , with higher affinity for TGF- β 2; however, endoglin binds TGF- β 1 and TGF- β 3 with constant affinity and has only weak affinity for TGF- β 2 [101, 102].

3.1.3 Cytoplasmic factors

The TGF- β pathway directly transduce extracellular stimuli from the cell-surface transmembrane receptors to the nucleus through intracellular mediators, the SMAD proteins [101, 102]. SMAD proteins consist in two globular Mad-homology domains (termed MH1 and MH2 domains) coupled by an unstructured linker. The amino-terminal MH1 domain contains a hairpin structure with DNA-binding ability. The MH2 domain has a series of hydrophobic surface patches for versatile interactions with cytoplasmic adaptor proteins, receptors, DNA-binding cofactors, coactivators, and corepressors [103]. SMAD proteins can be classified into three groups based on their function: the receptor-regulated SMAD (R-SMAD), SMAD1, 2, 3, 5, and 8; the common SMAD (Co-SMAD), SMAD4; and the inhibitory SMAD (I-SMAD), SMAD6 and 7. The R-SMAD can be further subdivided into BMPs-activated SMAD (SMAD1, 5, and 8) or TGF- β -activated SMAD (SMAD2 and 3), according the receptor involved. I-SMAD function as intracellular antagonists of R-SMAD. Through stable interactions with activated serine/threonine receptor complex, they inhibit TGF- β

family signalling by preventing the activation of R- and Co-SMAD. Whereas SMAD6 appears to preferentially inhibit BMP signalling, SMAD7 acts as a general inhibitor of TGF- β family signalling [101, 102].

3.2 Activation of TGF- β signalling pathway

The mature dimeric form of TGF- β , composed of two monomers stabilized by hydrophobic interactions and disulphide bridges, initiates intracellular signalling. The three isoforms of TGF- β are synthesized as pro-proteins with a large amino-terminal pro-domain called the latency associated peptide (LAP), which is required for proper folding and dimerization of the mature isoform. This complex is called small latent complex (SLC). After folding and dimerization, TGF- β dimer is cleaved from its pro-peptides in trans-Golgi but it remains associated with them through noncovalent interactions, creating the large latent complex (LLC). Most cultured cell types release latent TGF- β into ECM as LLC which includes a 120-140 kDa glycoprotein called latent TGF- β binding protein (LTBP). The LTBP participates in the regulation of latent TGF- β bioavailability by addressing it to the ECM. Non-active TGF- β stays in ECM and its further activation is a critical step in the regulation of its activity (Fig. 7) [101]. A variety of molecules and factors are involved in TGF- β activation, including proteases (such as plasmin), proteins of the ECM, ROS, and pH, indicating the importance of the cell and tissue microenvironment in the activation and regulation of the TGF- β isoforms [101, 104].

The dimeric structure of bioactive forms of TGF- β suggests that they function by bringing together pairs of type I and II receptors, forming a heterotetrameric receptor complexes. Binding of TGF- β to extracellular domains of both receptors induces the functional conformation of the intracellular kinase domains. These receptors are subject to reversible post-translational modifications that regulate stability and availability of receptors. Receptor phosphorylation activates TGF- β signalling pathway [101]. First, the ligand binds to T β RII (that is signal-propagating), followed by subsequent phosphorylation of the regulatory region within T β RI (that acts as activator) [101, 103]. This leads to incorporation of T β RI and formation of a large ligand-receptor complex: dimeric TGF- β ligand and two pairs of T β RI and T β RII. TGF- β 1 and TGF- β 3 bind to T β RII without participation of type I receptor, whereas TGF- β 2 interacts only with combination of both receptors. Although ligand binding may induce auto-phosphorylation of T β RII cytoplasmic domain, signalling in the absence of T β RI has not been reported. T β RIII betaglycan promotes binding of TGF- β 2 to T β RII, since the affinity of TGF- β 2 to T β RII is low in the absence of betaglycan. Endoglin (that can act as an alternative T β RIII) binds TGF- β 1, TGF- β 3 but not TGF- β 2 in the presence of the T β RI and T β RII [101].

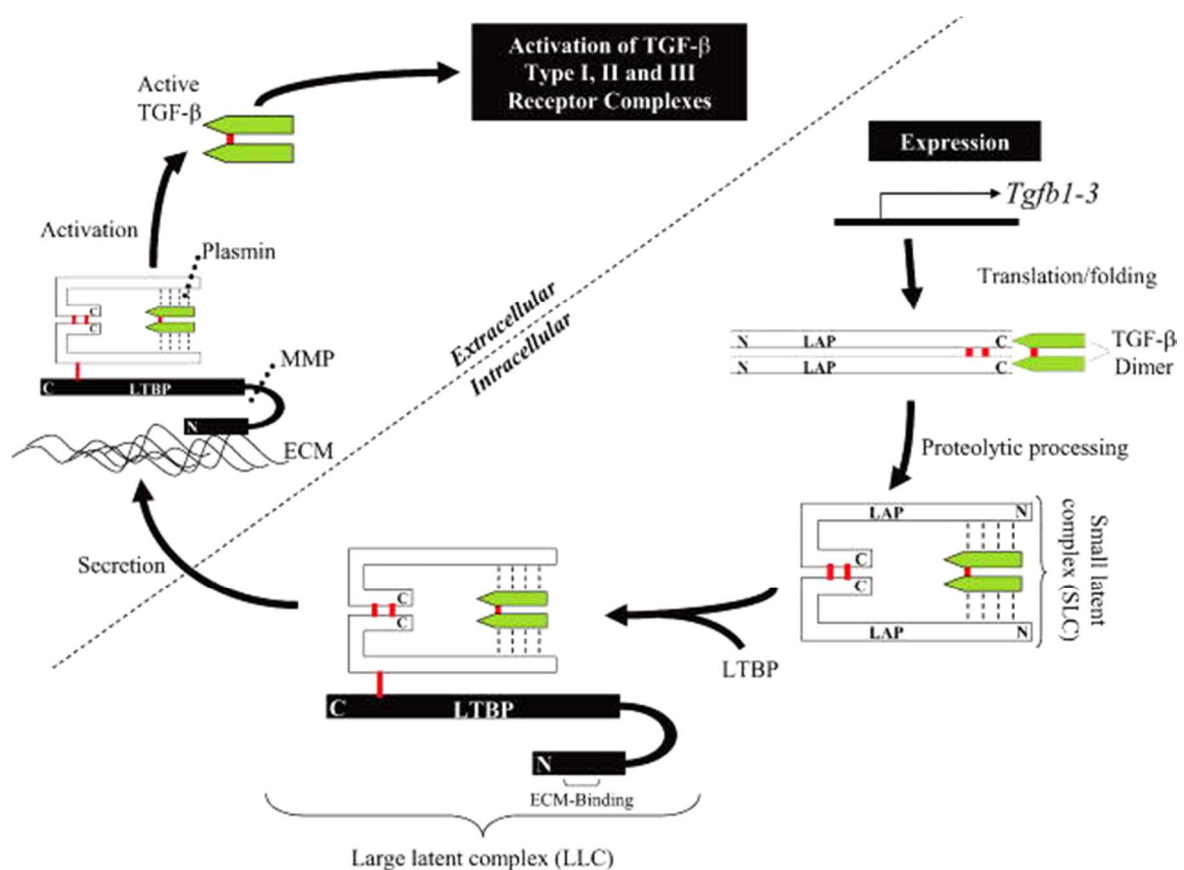


Figure 7. Expression and secretion of TGF- β isoforms. TGF- β is secreted as part of a latent complex, then activated through proteolysis or conformational changes. TGF- β may be released through proteolytic cleavage (dashed line) of the LTBP by matrix metalloproteinase (MMP) or LAP (by plasmin) or conformational change. Image taken from Stover *et al* [104].

3.2.1 Canonical signalling

The SMAD pathway is the canonical signalling pathway that is activated directly by the TGF- β cytokines (Fig. 8). T β RI recognizes and phosphorylates R-SMAD, a pivotal event in the initiation of TGF- β signal, followed by other steps of signal transduction, subjected to both positive and negative regulation [101].

After ligand recognition, R-SMAD binding to the T β RI is mediated by the protein SMAD Anchor for Receptor Activation (SARA). SARA regulates the subcellular localization of R-SMAD and recruits non-activated R-SMAD to the activated TGF- β receptor complex. The phosphorylation of SMAD2 decreases its affinity to SARA and further dissociation. Afterwards, phosphorylated complex of SMAD2/3 forms a higher-order complex with SMAD4 and moves to the nucleus [101, 102]. The SMAD2/3-4 complex is retained in the nucleus by interactions with additional protein binding partners and DNA. Dephosphorylation and dissociation with transcriptional complexes are thought to end this retention, allowing export of R-SMAD out of the nucleus [101].

Different protein binding partners regulate the SMAD activity. Each SMAD-partner combination targets a particular subset of genes and recruits either transcriptional coactivators or corepressors, in a cell type and context-dependent manner. Members of many DNA-binding protein families participate as SMAD cofactors, such as FOX, HOX, RUNX, E2F, AP1, CREB/ATF, Zinc-finger, and other proteins. Thus, SMAD reach target gene specificity. Stimulation of various cells by TGF- β leads to rapid activation or repression of a few hundred genes [101]. Several studies revealed that TGF- β pathway influence gene transcription through interaction of SMAD with transcription factors and coactivators as CREB binding protein (CBP) and p300. CBP and p300 interact with SMAD1, 2, 3, and 4 *in vitro* and *in vivo*, interactions that are stimulated by TGF- β [76-79].

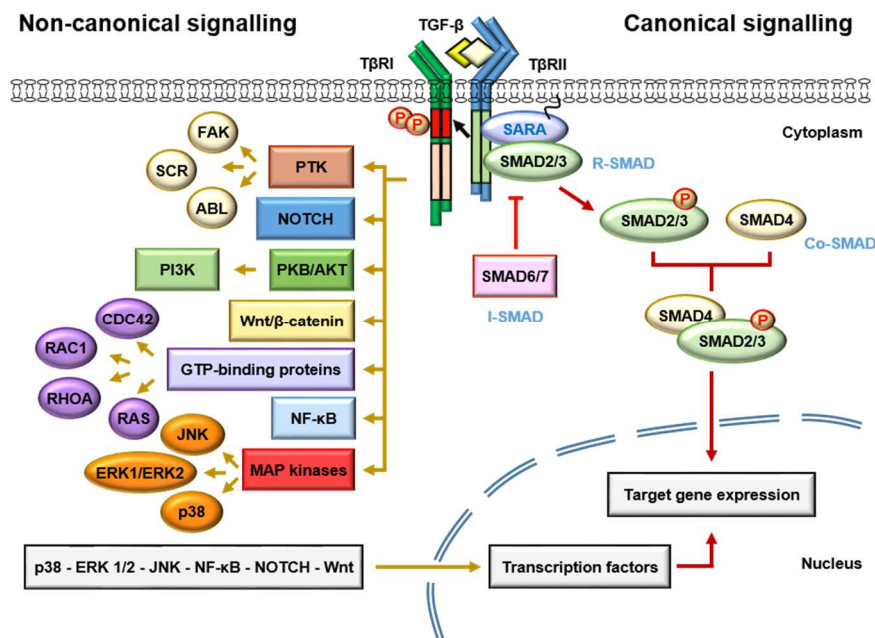


Figure 8. The canonical and non-canonical signalling pathways of TGF- β . In the canonical pathway (right), after ligand binding, TGF- β receptors dimerize and phosphorylate intracellular SMAD proteins. Complex of SMAD2/3-4 is subsequently transported into the nucleus where it binds with specific transcription factors. In the non-canonical signalling pathway (left), after ligand binding, several different branching signalling pathways can be activated. Image was created with information and images taken from Kaminska *et al* [105], Kubiczkova *et al* [101], and Massagué [103].

Once in the nucleus, SMAD complexes target specific promoters to regulate gene expression patterns. Co-SMAD and R-SMAD can directly bind to DNA but with low affinity and specificity. Given this weak DNA binding, SMAD are generally dependent on direct interaction with specific, high affinity DNA binding proteins for recruitment to appropriate target genes. Once bound to DNA in partnership with specific transcription factors, SMAD recruit coregulators to promote or

inhibit initiation of transcription, including coactivators such as basic chromatin remodelling complexes and histone-modifying acetyltransferases (HAT), or corepressors such as Histone deacetylases (HDAC). These transcriptional partners and coregulators, many of which are tissue-specific, play a fundamental role in determining the outcome of the signalling and provide one explanation for how SMAD proteins can elicit such diverse transcriptional responses in different cells [102].

3.2.2 Non-canonical signalling

The ability of TGF- β to activate SMAD independent signalling pathways is collectively referred to as “non-canonical” TGF- β signalling (Fig. 8) [101, 103]. These signalling processes operate in a context-dependent manner and contribute to cell-specific biological responses [102]. TGF- β induces activation of these non-canonical pathways through interactions of signalling mediators with the T β RI or T β RII, either directly or through adaptor proteins. Depending on the cell context, the non-canonical pathway can also be activated indirectly as a consequence of SMAD-mediated gene expression regulation [106].

TGF- β can directly (by canonical signalling) or indirectly participates in apoptosis, epithelial to mesenchymal transition, migration, proliferation, differentiation and matrix formation. It activates different proteins of mitogen-activated protein kinases (MAPK) pathway, such as extracellular signal-regulated kinases 1 and 2 (ERK1/ERK2), Jun-N terminal kinase (JNK), and p38 and PI3K kinases. Other pathways and modulators influenced by TGF- β are the growth and survival promoting pathway AKT, the small GTP-binding proteins RAS, RAS homolog family member A (RHOA), ras-related C3 botulinum toxin substrate 1 (RAC1) as well as cell division cycle 42 (CDC42) and mammalian target of rapamycin (mTOR). TGF- β participates in mediating activation of protein tyrosine kinases, particularly in mesenchymal or dedifferentiated epithelial cells and also influences NF- κ B signalling and WNT/ β -catenin pathway. The contribution of crosstalk between TGF- β and other pathways is reiterated throughout developmental and homeostatic processes and greatly impacts the diversity and complexity of biological responses to TGF- β signalling pathway [101, 102, 106].

3.2.3 TGF- β signalling pathway regulation

The TGF- β pathway is tightly regulated at different levels of ECM, membrane, cytoplasm and nucleus to ensure a fine control in duration and strength of the response.

(i) Regulation of TGF- β receptors. Once activated, TGF- β receptors are internalized via clathrin-coated pits to early endosomes that promote signalling, or alternatively, through Caveolin-1 positive lipid rafts in which receptors are ubiquitinated and then targeted to lysosomal

degradation [102]. Besides ubiquitination and degradation, receptor inactivation can also occur by phosphatases that dephosphorylate and inactivate the receptor [101, 102].

(ii) Regulation of R-SMAD and nuclear translocation. Irrespective of the presence or absence of ligand, SMAD proteins are constantly shuttle between the cytoplasm and the nucleus. However, they are too large to enter the nucleus by simple diffusion. Different transport mechanisms have been suggested for SMAD proteins, including interaction with karyopherins (as importins and exportins), as well as nucleoporins. The nuclear accumulation of SMAD complexes in response to TGF- β signalling has been proposed to be the result of alterations in the rates of SMAD import and export and the effect of cytoplasmic and nuclear retention factors, some of which preferentially bind unphosphorylated or phosphorylated SMAD, respectively [102]. Once in the nucleus, R-SMAD can be degraded by ubiquitination for their inactivation [101, 102]. Co-SMAD (such as SMAD4) are also regulated by ubiquitination, controlling its stability and the association with R-SMAD [107].

(iii) Regulation by I-SMAD. The I-SMAD are induced by TGF- β signalling and act as negative regulators of the pathway by binding to T β RI, thus competing with R-SMAD and blocking phosphorylation. I-SMAD also play a key role in degradation of receptors recruiting ubiquitin ligases SMURF1 and SMURF2 to T β RI. Further, SMURF1 and SMURF2 facilitate the inhibitory effect of I-SMAD [101, 102].

(iv) Regulation by SMAD7. SMAD7 is the principal negative regulator of TGF- β signalling. Besides its control of the TGF- β signalling pathway by ubiquitination, SMAD7 is induced by TGF- β stimulation and then acts in a negative feedback mechanism, by competing with R-SMAD for receptor binding (thus inhibiting their phosphorylation), and by interfering with the binding of SMAD complexes to DNA. However, SMAD7 also constitutes a transcriptional regulator in the nucleus and mediates the crosstalk between TGF- β and other signalling pathways [100, 105, 108].

(v) Other negative regulators. In addition, other TGF- β target genes are involved in feedback mechanisms. SKI and SNON, after induction by TGF- β , bind to SMAD and repress their transcriptional activity by disrupting functional SMAD complexes, recruiting transcription corepressor complexes and blocking the binding of transcriptional coactivators to SMAD proteins. As a result, the inhibition of basal expression of TGF- β -responsive genes such as SMAD7 is produced. Furthermore, SKI is able to interact with T β RI and to interfere with the nuclear translocation of SMAD complexes [105, 107].

(v) Other regulatory mechanisms. Numerous post-translational modifications in SMAD proteins have been described. These modifications include dephosphorylation by phosphatases to terminate SMAD activity, degradation by SMURFs of binding partners, sumoylation, acetylation, ADP-ribosylation, and linker-domain phosphorylation [102, 103, 107]. Furthermore, numerous

microRNAs target members of the TGF- β pathway and thereby regulate the production of ligands, receptors, and SMAD proteins. It was demonstrated that SMAD proteins can also directly promote the processing of a specific set of microRNAs [102, 103].

3.3 TGF- β signalling in GBM

In tumours, TGF- β can be either a proto-oncogenic or a tumour suppressor factor, depending on cell context and tumour stage. Cancer cells often evade growth inhibition effects of TGF- β , while leaving intact TGF- β -mediated cellular responses that promote tumour progression [101, 103]. This dichotomy may seem paradoxical, but it has its logic. TGF- β has cytostatic effects that are important in tissue regeneration and homeostasis. When cells incur oncogenic mutations and reach a premalignant state, TGF- β -mediated suppressive effects become more dramatic. In some tumour types, this pressure selects for mutations that eliminate TGF- β signalling partially or completely, and/or produce the aberrant activation of the pathway [103]. This paradox is reflected in clinic, where in early stage cancers, levels of TGF- β are positively associated with a favourable prognosis. Yet in advanced tumours, levels of TGF- β in the tumour microenvironment are positively associated with tumour size, invasiveness, and dedifferentiation, making TGF- β a useful prognostic biomarker and predictor of recurrence after initial or failed therapy [109].

In GBM, as in other tumours, cancer cell clones that prevail in GBM retain an intact SMAD signalling machinery [110], but lose the TGF- β tumour suppressive responses. In this way, cancer cells can maintain the SMAD pathway to their advantage and promote tumour growth and development. Many SMAD-dependent pro-tumour effects have been identified in different tumours and in GBM, such as enhancing of stemness and metastasis, seeding and extravasation of circulating tumour cells, angiogenesis, and suppression of the immune system [103, 107, 108]. These effects are explained by the overexpression of TGF- β isoforms and the acquisition of mutations in the TGF- β signalling pathway genes.

High expression levels of TGF- β isoforms in GBM indicate that TGF- β is able to induce its own expression and thereby create a malignant autocrine loop and control glioma-cell proliferation [101]. TGF- β , and in particular the isoform 2, is considered a key factor in GBM progression [28]. A positive correlation between levels of TGF- β 2 in patients' plasma, and their advanced in high-grade glioma and poor prognosis have been reported. Although correlation of TGF- β 2 levels with therapeutic response is contradictory. The expression and levels of TGF- β 1 isoform are not clearly correlated with prognosis and treatment outcome. Despite these findings, expression of both TGF- β 1 and TGF- β 2 was found to be higher in GBM compared to healthy brain tissue [111]. Apparently, while TGF- β 1 suppresses growth of normal neural precursor cells and low-grade gliomas, it can either stimulate or has no effect on high-grade gliomas. TGF- β 2 has

been shown to stimulate proliferation of both low- and high-grade tumours [110]. Additionally, TGF- β 2 has been shown to generate an autocrine loop, inducing its own expression, thus enabling oncogenic activity. A hyperactive TGF- β pathway in gliomas might therefore provide a selective growth advantage [110].

The effects of TGF- β 1 on mobility and migration are associated with changes in ECM components. TGF- β 2 has been shown to upregulate components of the ECM and enzymatic degradation to modulate glioma migration and motility [105, 110]. In GBM, TGF- β 1 may act as an angiogenic factor promoting neovascularization. TGF- β 1 signalling stimulates production of vascular endothelial growth factor (VEGF), expression that can be synergized by hypoxia conditions. TGF- β plays a crucial role in the escape of gliomas from host immunity. The antitumour response in patients with GBM may be ineffective due to the loss of a specific tumour antigen and professional antigen presenting cells in the brain. TGF- β not only enhances this effect by inhibition of the Major Histocompatibility Complex class II expression on glioma cells, macrophages, and microglia, but also exerts an immune-suppressive general effect on all the immune system cells [105]. The expression of downstream components of TGF- β signalling has been evaluated in GBM showing alterations in many components of this pathway. Some alterations registered are: the homozygous deletion of the *p15INK4B* (=CDKN2B) gene, lower protein expression of SMAD2, 3, and 4 as well as the elevated protein levels of SKI and SNON [105]. Moreover, the inability of p21CIP1 (=CDKN1A), p15INK4B, CDK4, and cyclin D1 (CCND1) to respond to TGF- β in GBM samples, suggests dysfunction of TGF- β -induced growth inhibitory signal which may explain, in part, the selective loss of growth inhibition by TGF- β in GBM [110, 112].

3.4 Escaping from the TGF- β antiproliferative control

Tumour cells tend to escape from the TGF- β antiproliferative effect by either acquiring mutations in the components of the TGF- β signalling transduction pathway, or by selectively disrupting the TGF- β antiproliferative response. In the last decades, many of the TGF- β molecular mechanisms that allow a tumour cell evade from the tumour suppressive effect of TGF- β were discovered. These mechanisms are involved in the oncogenic switch of the TGF- β response [113]. The switching from tumour suppression to tumour promotion involves different mechanisms as mutations of the tumour suppressor *TP53* and loss of SMAD4 function by different mechanisms. Epigenetic events may also mediate the TGF- β switch, as the hypo-methylation of the *PDGF β* gene that enables TGF- β to promote GBM proliferation. Undoubtedly, the expression levels of other endogenous factors play a key role in switching the tumour regulating response of TGF- β [114].

In normal epithelial cells, TGF- β SMAD signalling induces the expression of several genes promoting cell cycle arrest, including two cyclin-dependent kinase (CDK) inhibitors (to avoid

confusion in terms, from now CDKN1A and CDKN2B will be referred to as p21CIP1 and p15INK4B, respectively), and downregulates transcription factors involved in proliferation and inhibition of differentiation (TGF- β cytostatic genes programme). In the majority of tissues, TGF- β induces growth suppression associated with the increased expression or activities of p21CIP1 and p15INK4B among other CDK inhibitors [113, 115]. The TGF- β cytostatic programme is often lost in cancer due to the disruption of TGF- β signalling caused by somatic mutations or by selectively inhibiting its antiproliferative response [113]. In gliomas, the expression of the forkhead transcription factor FOXG1, selectively prevents the induction of p21CIP1 by TGF- β . Consequently, FOXG1 in gliomas allows tumour cells to escape from the p21CIP1-mediated cell cycle arrest induced by TGF- β [113].

SMAD7 has been implicated in the repression of the antiproliferative function of TGF- β . As previously mentioned, SMAD7 is an I-SMAD that is induced by TGF- β and represses TGF- β signalling, generating a negative feedback loop. Aberrant expression of SMAD7 and disruption of the feedback regulation results in an inactivation of the canonical TGF- β pathway and impairs TGF- β -mediated inhibition of proliferation. Some tumours evade the TGF- β antitumorigenic response through the acquisition of abnormally high levels of SMAD7 [109, 113]. But indeed, SMAD7 can have both pro- and antitumour actions depending on the cancer type and the cell context [116].

As previously mentioned, SKI and SNON are two negative regulators of the TGF- β signalling. They are transcriptional corepressors that when overexpressed block TGF- β -mediated cell cycle arrest [113, 116]. SKI was first identified as a viral oncogene (*v-ski*) from the avian Sloan-Kettering retrovirus (SKV) that transforms chicken embryo fibroblasts [117]. The implication of SKI in the regulation of TGF- β signalling was later described [118]. After identification of SKI, SNON was identified in a screen for genes modulating the regulation of the oncogene *c-ski* [119]. Subsequently it was proven that SNON acts as a regulator of the cellular growth state both in the context of cancer biology and neurobiology, exerting effects on a number of different cell types (such as neurons and epithelial cells) [120]. SKI and SNON can interact with SMAD2, 3, and 4 to be recruited to the SMAD-binding element of the TGF- β -responsive promoters. Moreover, SKI and SNON are able to recruit corepressor complexes and repress the ability of SMAD to activate their target genes. Binding to SKI or SNON interferes with the interaction of SMAD4 and R-SMAD disrupting the SMAD2/3-4 complex. Among other TGF- β responses, SKI prevents the induction of *p21CIP1* by TGF- β . Many human tumours express high levels of *SKI* and/or *SNON* indicating that some tumours can escape from the TGF- β tumour-suppressive function due to overexpression of these two factors [113]. Emerging evidence also suggests a tumour suppressor activity for SKI

and/or SNON, which could depend on the capacity of these proteins to modulate additional intracellular pathways involved in cancer cell growth [116].

3.5 TGF- β pathway and GBM CSC

Autocrine TGF- β signalling plays an essential role in maintenance of stem-like phenotype of GBM CSC, which acts via different downstream pathways. TGF- β induces expression of *sex determining region (SR) Y-box 2 (SOX2)*, a stemness gene, and this induction is mediated by *SOX4*, a direct TGF- β target gene [121]. Also TGF- β , increases the expression of CD44, a CSC marker described in GBM, through the expression of different transcriptional regulators [105, 111]. There is evidence that in the particular case of TGF- β 2, in addition to its central role in other oncogenic processes in GBM, it also promotes self-renewal of GBM CSC. This phenotype promotion is probably mediated by LIF, a cytokine extensively studied as an inducer of mouse embryonic stem cell-renewal. LIF is induced by the three TGF- β isoforms in GBM, and the SMAD2/3-4 complex directly regulates the expression of LIF. LIF is highly expressed in GBM with high levels of TGF- β 2, suggesting that TGF- β 2 is responsible for the induction of LIF in human GBM [110, 122]. However, not all GBM CSC potently respond to TGF- β and this can be explained by the heterogeneous genetic background of GBM in different patients [111, 122].

Several studies have revealed critical roles of TGF- β family signalling in CSC maintenance and differentiation in several tumour types. These roles are surprisingly similar to those in normal somatic stem cell maintenance and differentiation [106]. Furthermore, the signalling pathways that control CSC functions (previously described) coincide with those pathways that are regulated by the non-canonical TGF- β pathway. This observation support many studies that directly linked TGF- β to DNA damage responses and radiosensitivity due to the presence of CSC subpopulation that probably helps to mediate resistance. Both, DNA damage responses and radioresistance, are regulated in CSC by pathways that interact with TGF- β as JNK, AKT, Notch, and WNT- β -catenin among others [106, 123, 124]. This strong relation between TGF- β signalling, CSC, and resistance to therapy suggests that the combination of radio- or chemotherapy with inhibition of TGF- β signalling may be a therapeutic strategy for GBM [106].

4. TREATMENT FOR GLIOBLASTOMA MULTIFORME

4.1 GBM conventional treatments

Anticancer treatment should lead to tumour regression and provide as long as possible disease-free or controlled survival. The treatment of GBM currently involves surgery followed by external radiation and concomitant TMZ chemotherapy followed by additional cycles of TMZ administration [1, 10]. Surgical resection alone results in a median survival of approximately six months. Combined, surgical resection plus radiotherapy extend median survival to 12.1 months. Addition of TMZ further extends the median survival to 14.6 months [125, 126]. The best therapeutic target is to pursue a more individualized perspective. Thus, treatment depends on several factors such as time of diagnosis, new onset or recurrence, performance status, and patient age [28].

4.1.1 Surgical resection

Surgery remains an important component in the treatment of GBM. It allows for a histological confirmation of the diagnosis and may also serve as a therapeutic strategy by reducing the intracranial pressure, and depending on the location of the tumour, occasionally leads to recovery of some neurological function. The principal contraindications related with surgery are poor performance status, advanced age, eloquent localization or extensive bihemispheric involvement [4, 126].

The goal of surgery is to achieve gross total resection of the contrast enhancing component of the tumour, without compromising neurological function. Gross total resection may not be possible based on anatomic structures invaded by the tumour. Since GBM infiltrates surrounding tissues, its complete resection is impossible [10]. Advances in surgical imaging techniques, such as intraoperative magnetic resonance imaging (MRI), diffusion tensor imaging, awake craniotomy, cortical mapping, stereotactic guidance, and fluorescent-guided resection, have facilitated delineation of tumour borders and can help to optimize maximal safe surgical resection. Although maximal surgical resection remains important, GBM does not have yet a complete surgical “answer” [126].

4.1.2 Chemotherapy

TMZ, an oral alkylating chemotherapeutic agent, causes DNA damage and triggers a cascade of events leading to tumour cell apoptosis. In the last years, TMZ was added to the standard care for GBM treatment. Previously, chemotherapy had no demonstrable clinic benefits, and radiotherapy alone remained the standard of care after surgical resection [126]. In 2005, a clinical

trial demonstrated that concurrent radiotherapy and TMZ followed by adjuvant TMZ significantly prolonged the median survival more than that of radiation alone: 14.6 months versus 12.1 months and a 2-year survival ratio of 26.5%. At the 5-years analysis of this study, more patients treated with TMZ survive (9.8% versus 1.9%). The best results are obtained when radiotherapy is performed after surgery [10]. These findings established the therapeutic benefit of TMZ in combination with radiotherapy, establishing the so-called “Stupp regimen” standard of care for GBM treatment [28, 125]. Despite these advances, the median progression-free survival time is only 7 months [126].

A recognized predictor for tumour response to TMZ is the epigenetic silencing of the O⁶-methylguanine-DNA-methyltransferase (MGMT) gene promoter by methylation. The ubiquitous DNA repair protein MGMT counteracts chemotherapy-induced DNA damage by restoring the structural integrity of O⁶-alkylated bases. Around half of all GBM patients harbour an unmethylated MGMT promoter, and these seem to respond poorly to TMZ chemotherapy. To date there is no alternative treatment for this group [127].

Other chemotherapy options include carboplatin, irinotecan, carmustine, and etoposide; and procarbazine, lomustine and vincristine combination, especially for recurrent GBM. Although, results of these compounds in survival extension ratio are low or have not shown significant differences [28]. For instance, carmustine has a low therapeutic activity, increasing the median survival by only eight weeks in patients with recurrent GBM [4].

4.1.3 Radiotherapy

The combination of radiotherapy plus TMZ is the most efficacious adjuvant therapy to prolong survival after primary resection. Treatment following surgery includes six weeks of radiotherapy to the surgical cavity and TMZ, followed by six adjuvant cycles of TMZ [126].

The current standard of care for radiotherapy in GBM is focal, fractionated external beam radiation therapy. Ionization radiation induces single-strand and double-strand breaks in the DNA of proliferating cells. Other modes of delivering radiotherapy have been investigated, including brachytherapy, but none have been proven more effective than the current standard approach [126].

4.2 Hypoxia and new therapeutics treatment evaluation

Resistance toward chemotherapy, primary or acquired, represents a major obstacle in clinical oncology. Three basic categories underlie most cases of chemotherapy failure: (i) inadequate pharmacokinetic properties of the drug such as fast hepatic drug metabolism, (ii) tumour cell intrinsic factors such as the expression of drug extracting pumps, and (iii) tumour cell

extrinsic conditions present in the tumour microenvironment, characterized by hostile conditions such as hypoxia, acidosis, nutrient starvation, and increased interstitial pressure [128].

Tumour hypoxia has been known to negatively affect therapy outcome for decades, the first description of its effect on radiotherapy efficacy was made by Gray *et al* in 1953 [128, 129]. The negative effect of hypoxia on the efficacy of radio- and chemotherapy is explained by the principal molecular mediators of this adaptation or HIFs [128] and other factors.

The several decades of long search for anticancer compounds produced an enormous list of substances that worked well *in vitro*, but failed dramatically *in vivo*. When searching for the underlying explanation, researchers should have in mind that the standard *in vitro* toxicity screening is performed under normoxia in buffered solutions with nutrient affluence, completely neglecting the influence of tumour microenvironmental factors. It is now widely accepted that the unique microenvironmental conditions of solid tumours, as hypoxia, are largely responsible for insufficient *in vivo* efficacy of *in vitro* identified compounds [128].

4.3 Therapeutic implications of the blood-brain/tumour barrier

The options for the treatment of GBM are limited due to the blood-brain barrier (BBB), which prevents molecules >500 Da from entering the brain. The BBB has a protective role: it mediates the removal of brain metabolic compounds, maintains the ionic concentrations, and it separates the pools of the neurotransmitters that act centrally and peripherally maintaining the homeostasis of the CNS. The BBB is a selective physical barrier, as the tight junctions between the adjacent endothelial cells do not allow for the normal paracellular transport, forcing molecules into a transcellular transport. Small molecules, such as O₂, CO₂, and small organic molecules may diffuse freely through membranes. Specific transport systems on the membrane surface enable nutrients to enter the brain, but prevent potentially toxic substances from harming the CNS. Large molecules, such as long peptides and proteins, are not able to enter the brain, unless there is a strictly regulated receptor-mediated or adsorption-mediated transcytosis [1].

The blood-brain tumour barrier (BBTB) encompasses existing and newly formed blood vessels that contribute to the delivery of nutrients and oxygen to the tumour and facilitate glioma cell migration to other parts of the brain [130] (Fig. 9). The high metabolic demands of GBM create hypoxic areas that promote the angiogenesis process, leading to the formation of dysfunctional vessels and a BBTB. As consequence, the BBB and the BBTB constitute a major obstacle in brain tumour therapy by preventing the delivery of sufficient quantities of potentially effective therapeutic agents. During the last decades numerous strategies to improve the delivery of agents to brain tumours have been under investigation. Unfortunately, these strategies have not yet matured and the most promising approaches have failed in clinical trials [130]. Considering the

limited penetration in the brain, alternative drug-delivery strategies are required for the more effective treatment of gliomas [1].

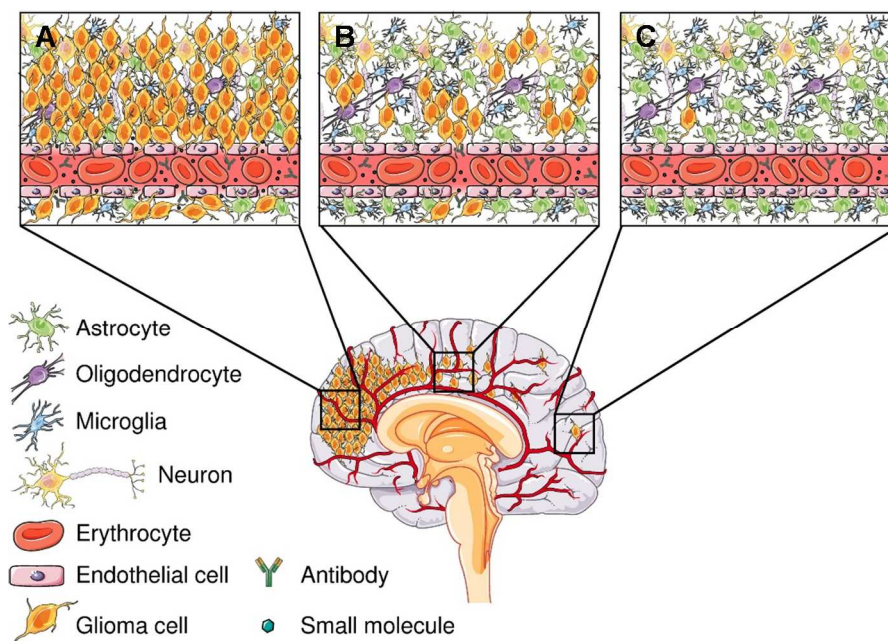


Figure 9. Different degrees of BBTB in GBM. BBTB integrity varies from completely compromised in bulky tumour areas (A) to slightly leaky in more invasive peripheral regions (B), or completely intact in sparsely invaded regions distant from the tumour bulk (C). Where the BBTB is compromised, macromolecules and compounds usually efficiently restricted from the brain can extravasate and engage glioma cells. An intact BBTB protects isolated invaded tumour cells against efficient delivery of therapeutics. The figure was taken from van Tellingen *et al* [130].

Currently, a few strategies based in the BBB/BBTB physiology have been shown to have some clinical potential. These approaches are based in exploiting the “receptor mediated transport system”, a shuttling factor coupled to a drug that targets a receptor at the BBB. An example is the GRN1005 (formerly ANG1005) a paclitaxel–Angiopep-2 conjugate administrated with Bevacizumab (an inhibitor of VEGF-A), allowing the cross of the BBB by transcytosis [130]. A phase II clinical trial for the evaluation of this strategy in recurrent high-grade gliomas is ongoing [130, 131]. Another clinically advanced candidate is the use of 2B3-101, which is a PEGylated liposome conjugated with glutathione. A phase I/II clinical trial was completed in patients with solid tumours and brain metastases or recurrent malignant glioma treated with 2B3-101 plus Trastuzumab (that blocks the epidermal growth factor receptor type 2 (HER2)). Preliminary results are also encouraging, but similar to GRN1005, it is too early to draw any conclusion [130, 131].

An apparently straightforward approach to overcome the BBTB is the delivery of therapeutic agents directly into the brain (tumour) parenchyma or into the resection cavity of glioma patients. Intracavitary drug injection, with the use of an intraventricular/intracavitary system, allows for

such direct delivery of chemotherapeutic agents to the tumour cavity. The distribution of the drug is determined by the rate and duration of the injection and by diffusion. However, insufficient drug delivery, infections, neurotoxicity, and catheter obstruction has prevented successful application of this method in a routine setting. A more promising system is the use of convection enhanced delivery (CED). CED involves the direct and continuous injection of a therapeutic agent under positive pressure using stereotactically placed intraparenchymal microcatheters, thereby allowing the passage of molecules, regardless of charge and size, into any section of the brain. Despite the advantages in terms of drug distribution throughout the brain, CED remains experimental and several practical challenges need to be resolved, including determining optimal infusion rate and volume, anatomical prerequisites for the infusion site, and problems related to the backflow along the tract [130]. Several clinical trials for the evaluation of the delivery of some known chemotherapeutics for GBM are been tested with the CED system. However, it is unlikely that by current CED approaches all infiltrative glioblastoma cells will be reached [130, 131].

Recently, a lymphatic system in the CNS was described [132], in contradiction to decades accepting that absence of a classical lymphatic drainage system was one of the intrinsic characteristic of the CNS. Although it is now accepted that the CNS undergoes constant immune surveillance, the mechanism governing the entrance and exit of immune cells from the CNS remains poorly understood. This new finding indicates the presence of a gateway able to carry both lymph and immune cells from the cerebrospinal fluid. The presence of a functional and classical lymphatic system in the CNS suggests that current dogmas regarding brain tolerance and the immune privilege of the brain should be revisited [132].

Despite the highly invasive nature of GBM rarely leads to extracranial metastasis (only 0.4% of cases), tumour circulating cells were found in bloodstream of patients with GBM diagnostic. These circulating cells are not related with BBB disruption after surgical procedures since they were also detected in GBM preoperative patients. The new lymphatic system described could explain the presence of circulating brain tumour cells and their bloodstream dissemination [132, 133].

Although this discovery may be significant in neurological disorders as sclerosis or Alzheimer's disease, it must also be considered in the development of new strategies and delivery systems for chemotherapeutics in GBM treatment. As a catchphrase in GBM therapy: "no matter how well the target is selected, there is no benefit if it is not reached" [130, 132].

4.4 Molecular biology based treatments

The limitations of current therapies for the treatment of GBM, can be solved by the use of molecular-based treatments. Since the TCGA project, there has been a growing influx of data

describing genomic alterations and expression patterns in GBM that allow for the identification of some already described and other new signalling pathways involved in the maintenance and development of CSC subpopulations. As a result, several molecular targets in GBM has been tested and new ones are under development (Table 6) [134]. Furthermore, molecular markers and predictors that initially defined GBM subtypes and are used as prognosis markers, have been later shown therapeutic potential based in their capacity to regulate tumorigenic mechanisms in GBM and in CSC subpopulations. These prognostic markers may provide an overall indication of the natural history of a tumour in a specific patient, leading to the idea of treatment individualization for GBM [32, 135]. Recently, the Ivy Foundation Early Phase Clinical Trials Consortium (USA) developed a protocol designed to define an individualized patient treatment for GBM [136]. As in other studies, the use of an extensive molecular profiling could constitutes an informed treatment decision based upon individual patient genotypes [136-138]. A more detailed knowledge of the molecular alterations associated with treatment resistance would set the stage for the next generation of trials for therapy, incorporating both molecular inclusion criteria and hypothesis-based targeted therapies. Future therapeutic trends for the treatment of GBM will have to: (i) include the new molecular classification of GBM; (ii) incorporate more efficient drug delivery systems to overcome BBB restraints; and (iii) redirect the therapeutic choices to each patient, considering the specific molecular alterations of each tumour [32, 135].

Another therapeutic approach for GBM is immunotherapy. GBM makes use of the immune system to induce a state of chronic antigen exposure, which culminates in lymphocytic exhaustion or anergy. Emerging methods of harnessing the immune system in the treatment of GBM include preventing the tumour from evading the immune system and/or exposing the immune system to antigens expressed by the tumour, thus stimulating it to attack the tumour [139].

A growing set of clinical trials based in immunotherapeutics are being evaluated, including autologous vaccines that rely on *ex vivo* modification of the patient's immune system or of the tumour itself, followed by reintroduction of altered cells. In a phase I/IIa trial, this methodology increased significantly the survival of patients [139, 140]. Another *ex vivo* approach is the use of dendritic-cell-based vaccines which, at the moment, presents the most promising results [139, 141]. This process involves obtaining dendritic cells from a patient and pulsing them with glioma antigens derived from resection. A major advantage is that multiple antigens may thus be presented. In a phase I clinical trial, the dendritic-cell-based vaccine DCVax-L[®], presents an overall survival of 31.4 months. Currently, a randomized phase III trial is ongoing [131, 139].

Table 6. Ongoing clinical trials using molecular based therapeutic strategies for GBM.

Agent	Target	Clinical phase	Agent	Target	Clinical phase
PI3K and mTOR			EGFR		
Rapamycin	mTOR	I-II	Erlotinib	EGFR TKI	I-II
Temsirolimus	mTOR	I-II	Gefitinib	EGFR TKI	I-II
Everolimus	mTOR	I-II	Cetuximab	Chimeric EGFR mAb	I-II
BKM-120	PI3K	I-II	Vandetanib	VEGFR-2, EGFR, RET	I-II
XL-147	PI3K	I	Lapatinib	HER2 and EGFR TKI	I-II
XL-765	PI3K, mTOR	I	Afatinib	HER2 and EGFR TKI	I-II
AZD8055	mTORC1, mTORC2	I	Dacomitinib	Pan-Her irreversible TKI	II
Perifosine	AKT inhibitor	I-II	Nimotuzumab	Humanized EGFR MAb	II-III
INK128	mTORC1, mTORC2	I	TP53		
CC-115	mTOR, DNA-PK	I	Ad5CMV-TP53 gene	Recombinant adenovirus containing TP53	I
VEGF			TP53 SCH-58500	Recombinant adenovirus containing TP53	I
Bevacizumab	VEGF-A	I-III	PD 0332991	CDK4/CDK6 inhibitor	II
Aflibercept	VEGF-A, VEGF-B, PIGF	I-II	SGT-53	TfRscFv-Liposome-TP53 Complex	II
Vandetanib	VEGFR-2, EGFR, RET	I-II	PDGFR		
Cediranib	VEGFR-1, VEGFR-2, VEGFR-3, c-KIT, PDGFR α - β , FGFR-1,	I-III	Sorafenib	VEGFR-2, VEGFR-3, PDGFR α , PDGFR β , BRAF, c-KIT, RAS	I-II
Cilengitide	α v β 3, α v β 5 integrins	I-III	Imatinib	PDGFR α , PDGFR β , c-KIT, BCR-ABL	I-III
Sunitinib	VEGFR-2, PDGFR β , c-KIT, RET, FLT3	I-II	Tandutinib	PDGFR α , PDGFR β , c-KIT, FLT3	I-III
Enzastaurin	PKC- β , AKT	I-III	Dasatinib	PDGFR α , PDGFR β , SRC, BCR-ABL, c-KIT, EPHA2	I-II
Sorafenib	VEGFR-2, VEGFR-3, PDGFR α , c-KIT, PDGFR β , BRAF, RAS	I-II	MGMT		
Cabozantinib	VEGFR-2, MET, RET, c-KIT, FLT3, TIE-2	I-II	O ⁶ -benzylguanine	MGMT	I-III
AMG386	ANG-1, ANG-2	I-II			
IDH					
R132H (AGI5198)	IDH1	I			
R140Q (AGI6780)	IDH2	PC			

Adapted from Bastien *et al* [134] and from the U.S. National Institutes of Health (last access June 2015) [131].
PC: Preclinical.

4.5 Apoptosis as a therapeutic target in GBM

Although much is known about the diverse genotypes causing the heterogeneous histological phenotypes of GBM and how they impact on survival, there is still no therapy that induces tumour cell apoptosis beyond that of the standard treatment. Thus, the ability to exploit apoptosis to design more effective and nontoxic therapies for GBM is under development [127].

Human glioma cell lines express both pro- and antiapoptotic factors. Manipulation of these has been shown to affect the cells ability to undergo apoptosis and some are being tested in clinical trials (Table 7). However, much of the knowledge on apoptosis deregulation in GBM relies on studies using *in vitro* cell cultures that do not represent the heterogeneous nature of the disease. In addition, GBM *in vivo* are subjected to different selection pressures compared to cells in culture that alter cell genotypes and phenotypes. Nevertheless, the increasing knowledge on apoptosis signalling might provide new strategies to improve treatment of GBM [127].

Table 7. Current status of apoptosis-targeted preclinical and clinical trials in GBM.

Well characterized apoptotic targets			Poor characterized apoptotic targets		
Agent	Target	Clinical phase	Agent	Target	Clinical phase
Gossypol	BCL-2	I-II	Vorinostat	HDAC	I-II
ABT-737	BCL-2	PC	Panobinostat	HDAC	II
HA 14-1	BCL-2, BID	PC	Marizomib	Proteasome	I
Recombinant human TRAIL (hrTRAIL)	TRAIL	PC	Disulfiram	Proteasome	I
Antagonist Ab TRA-8	TRAIL	PC	Nelfinavir	Proteasome	I
LCL161	XIAP and IAP1/2	PC			
Birinapant (TL32711)	XIAP and IAP1/2	PC			

Data were collected from Eisele and Weller [44], Krakstad and Chekenya [127], and from the U.S. National Institutes of Health (last access June 2015) [131]. **PC:** Preclinical.

4.6 Current CSC-based therapies for the treatment of GBM

Only a few years ago, the GBM CSC hypothesis was postulated and immediately accompanied by findings that identified these cells as responsible of the increased resistance to radiochemotherapy and recurrence after treatment in GBM. The therapies, focused in the

eradication of this subpopulation, are promising and different therapeutic targets have been proposed. The most promising approach is concentrate on signalling pathways which are specifically overactivated in CSC [42]. Different clinical trials evaluating CSC as specific target in GBM are being evaluated [131].

Several novel compounds and old drugs have been shown to possess selective GBM CSC-inhibitory activity, and they appear to be particularly promising for a clinical validation. Among these, metformin (widely used for the treatment of diabetes) effectively affects GBM CSC proliferation and survival through the inhibition of PI3/AKT pathway [56, 142]. Currently, two clinical trials in phase I are ongoing for the evaluation of metformin in combination with radiation and with other compounds [131]. Sorafenib, is an oral multikinase inhibitor that appears to be a promising anticancer agent. It presents antitumour activity in GBM and it preferentially affects GBM CSC through inhibition of MAPK and PI3/AKT pathways [56, 143]. Clinical trials in phase I and II are ongoing or completed to verify safety, tolerability and efficacy in combination with TMZ or radiotherapy [56, 131]. Disulfiram is an inhibitor of the ALDH enzyme family, widely and safely used for alcoholism treatment. It has been recently observed that this compound reduces cell growth and self-renewal of TMZ-resistant GBM CSC [56]. A phase II clinical trial to evaluate GBM treatment with disulfiram in combination with TMZ or radiotherapy is ongoing [131].

Several preclinical studies have been conducted to investigate immunotherapy against GBM CSC management, such as treatment of CSC with interferon gamma, EGFR-specific T-cells, and dendritic cells that specifically target CSC. The EGFRvIII peptide was recently used as a mono-antigenic vaccine to induce anti-GBM immune response. In a phase II multicentre study with a very small number of enrolled patients (N = 18), a surprising overall survival of 26 months was achieved after standard treatment combined with vaccination of EGFRvIII [144]. In line with these promising results, CSC overexpressed EGFRvIII suggesting a CSC specific effect of the vaccination [145].

Virotherapy is defined as the delivery of oncolytic viruses that selectively replicate in and kill tumour cells, while gene therapy describes the delivery of cytotoxic transgenes to the tumour cells. Both techniques have been investigated in GBM CSC in preclinical models [146, 147]. The most intensive studied cytotoxic transgene is the thymidine kinase from Herpes Simplex Virus Type 1, converting the prodrug Ganciclovir into toxic desoxyguanosine triphosphate [124]. In 2009, a phase III multicentre clinical trial using sitimagene ceradenovec, a thymidine kinase-encoding adenoviral vector, showed the first encouraging results increasing time to reintervention or decease, but with serious undesired side effects (such as seizures and hyponatremia) [148].

4.7 Therapies for GBM targeting TGF- β signalling pathway

The TGF- β signalling pathway is an attractive target for therapy in a number of diseases, including fibrotic diseases or cancer. Depending on the specific disease, the therapeutic approach may involve the inhibition of the pathway or, sometimes, its enhancement [149]. As the signalling pathway deregulations are responsible for cancer initiation and progression, interrupting the tumour promoter properties of TGF- β signalling constitutes an attractive therapeutic strategy, without altering physiologic tumour suppressor functions exhibited in early stages of tumorigenesis [101].

TGF- β inhibitory treatments include ligand traps, such as ligand-specific neutralizing antibodies, soluble ligand receptors, antisense-dependent silencing of mRNA ligands, and chemical inhibitors that block kinase activity of TGF- β family member receptors [149]. Each compound acts in a specific site and target different elements of the TGF- β signalling pathway (Fig. 10). An increasing number of clinical trials using these compounds are ongoing for its evaluation in the treatment of diverse diseases and malignancies [149]. Strategies such as the use of monoclonal TGF- β -neutralizing antibodies, large molecule ligand traps, reducing translational efficiency of TGF- β ligands using antisense technology and antagonizing T β RI/II kinase function by small molecule inhibitors are the most prominent methods being explored today [101]. Inhibitors of the TGF- β pathway developed and those that have entered to clinical trials for the treatment of GBM comprise several classes and are summarized in Table 8.

Initially, the TGF- β 2 antisense compound AP12009 (Trabedersen, Antisense Pharma) showed a promising therapeutic potential. In comparison with standard chemotherapy, the treatment with AP12009 resulted in prolonged survival of patients at 24 months, and showed a high survival rate after 14 months, compared with anaplastic glioma [149]. This compound is delivered into the brain through an implanted CED system (Introduction, section 4.3). Overall, Trabedersen proved a feasible treatment approach in these clinical studies, as no dose-limiting toxicities were reported despite an 113-fold dose escalation and multiple drug courses. The promising results obtained in phase I and IIb clinical trials set the basis for the phase III SAPPHERE study to generate data for the regulatory approval of Trabedersen in the treatment of recurrent or refractory anaplastic astrocytoma or secondary glioblastoma [110]. However, the study was terminated due to the failure in patient recruitment [131]. In 2013, Antisense Pharma (now Isarna Therapeutics) announced a revision of the development path for Trabedersen due to a poor benefit/risk ratio derived from serious adverse events related with the administration route [150].

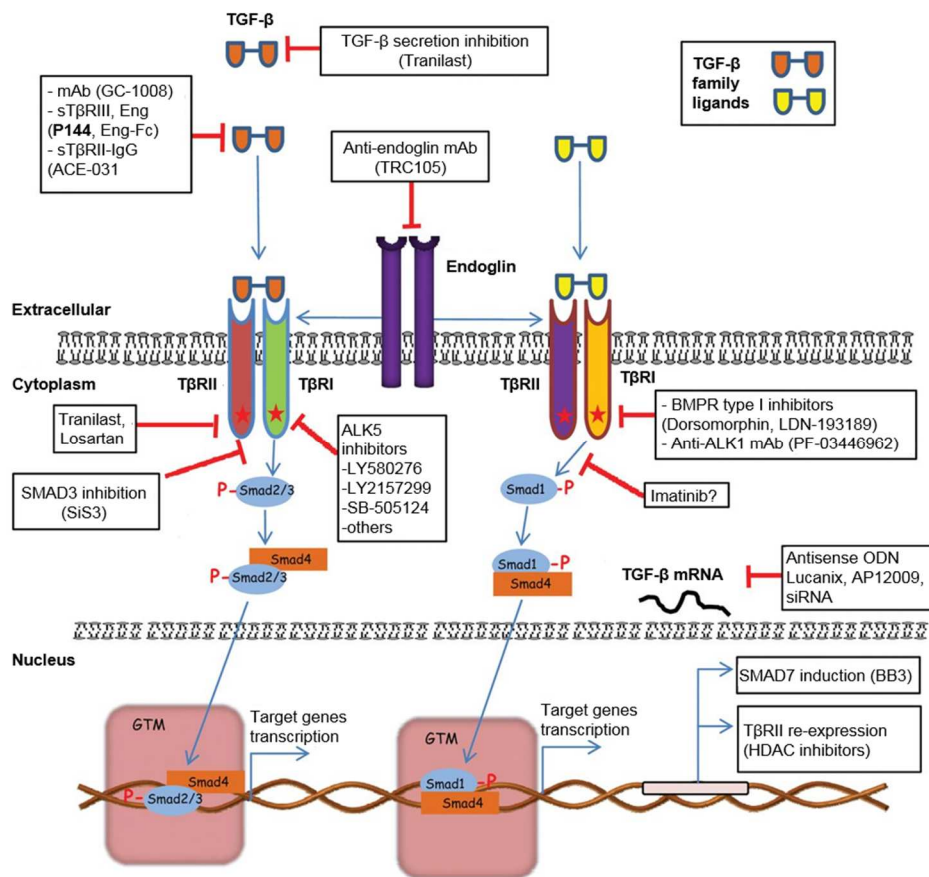


Figure 10. TGF- β signalling pathway targeting compounds. Different strategies include inhibition and enhancement of different regulatory elements of the TGF- β signalling. **GTM:** general transcription machinery. Image taken from Santibañez *et al.* [149].

Specifically for GBM, several preclinical studies have demonstrated the potential benefits of targeting the TGF- β signalling pathway in glioma, but data from clinical trials are not consistently encouraging. The reason could be that inhibition of either the TGF- β receptor binding or kinase activity may also result in alternative compensatory pathways mediated by other activators of the SMAD pathway or SMAD independent factors. Thus, in addition to targeting the TGF- β signalling pathway alone, a synergist response may be achieved by simultaneously targeting other aberrant signalling pathways. Indeed, in preclinical studies in pancreatic tumours, targeting the EGFR and TGF- β pathways concurrently shows better efficacy than targeting each signalling pathway alone [151].

Table 8. TGF- β pathway targeting agents currently under preclinical and clinical development for GBM treatment.

Agent	Type	Target	Clinical phase and status
Lerdelimumb (CAT-152)	Neutralizing antibody	TGF- β 2	Discontinued Phase III study for glaucoma
Metelimumab (CAT-192)	Neutralizing antibody	TGF- β 1	Discontinued Phase II study for scleroderma
Fresolimumab (GC-1008)	Neutralizing antibody	TGF- β 1/2/3 isoforms	II (completed)
1D11	Neutralizing antibody	TGF- β 1/2/3 isoforms	PC
Bevacizumab*	Neutralizing antibody	TGF- β 2 secretion	I, I/II and III (144 studies related with gliomas currently in develop)
AP-12009	Antisense oligonucleotide	TGF- β 2	III (terminated)
AP-11014	Antisense oligonucleotide	TGF- β 2	PC
LY550410	Small molecule inhibitor	T β RI	PC
Galunisertib (LY2157299)	Small molecule inhibitor	T β RI	I and I/II (Active, not recruiting)
LY580276	Small molecule inhibitor	T β RI	PC
LY2109761	Small molecule dual inhibitor	T β RI and T β RII	PC
SB-505124	Small molecule inhibitor	T β RI	PC
SB-431542	Small molecule inhibitor	T β RI	PC
SD-208	Small molecule inhibitor	T β RI	PC
A8301	Small molecule inhibitor	T β RI	PC

Data were collected from Flavell *et al* [152], Santibañez *et al* [149], Joseph *et al* [108], Kaminska *et al* [105], Nuezillet *et al* [153], Han *et al* [151], and from the U.S. National Institutes of Health (last access June 2015) [131]. (*) Bevacizumab was initially described as a VEGF-A inhibitor, however, has been described its potential to inhibit the TGF- β 2 secretion [154, 155]. **PC:** Preclinical.

In preclinical models, a potent antitumour activity of TGF- β inhibition in combination with radiochemotherapy was demonstrated. This finding has promoted the development and testing of TGF- β targeting agents in combinations with other therapies in patients with GBM. Initial studies showed good tolerability and safety of TGF- β targeting compounds. Which particularly strategy and combination will be the most potent, remains to be demonstrated. In this regard, the administration route of these compounds (intratumoural, intravenous or oral) may also be of importance anticipating reduced drug penetration caused by limitations in passing the BBB. Currently running and future clinical studies will need to reveal the efficacy of TGF- β targeting therapy for the treatment of GBM [108].

4.8 Inhibitory peptides P17 and P144

Continuing with the approach to inhibit the TGF- β pathway, two inhibitors peptides of TGF- β pathway have been design to directly bind TGF- β 1 and blocks its biological functions [156, 157].

P17 (KRIWFIPRSSWYERA) is a soluble hydrophilic peptide identified using a random phage display peptide library [158], whereas P144 (TSLDASIIWAMMQN) is a hydrophobic peptide derived from the extracellular sequence of human T β RIII (Betaglycan, amino acids 730–743) [159]. P17 inhibits TGF- β with a relative binding affinity of 100% for TGF- β 1, 80% for TGF- β 2 and 30% for TGF- β 3 in surface plasmon resonance assays. Similar affinity is expected for P144 [160] but its hydrophobicity is an unaffordable limiting factor to quantify potential chemical interactions with any other molecule in aqueous solutions.

Despite both peptides were initially designed for the regulation and treatment of liver fibrosis [158, 159], both peptides were evaluated for the regulation and treatment for several diseases and biological processes as early choroidal neovascularization (producing a reduction in the progression of lesions by targeting different mediators) [160], dialysate-induced damage in peritoneal membrane related with renal disease (displaying a protective effect inducing the mesothelial-to-mesenchymal transition) [157], angiogenesis (inhibiting this process *in vitro* and *in vivo* in human microvascular endothelial cells) [161], and even showing a protection of the noise-induced hearing loss in an *in vivo* model [162]. Currently, P17 is in preclinical development for different indications. P144 has been tested *in vitro* and *in vivo* in different models for fibrosis [158, 163-165]. Due to hydrophobic characteristic of the inhibitory peptide P144 (from now briefly referred to as P144) a topical application for the treatment of skin fibrosis was assessed [166]. In fact, a phase IIa study to evaluate the efficacy and safety of P144 to treat skin fibrosis in systemic sclerosis has been completed [131]. In this study, more than 80% of patients showed an improvement in the treated skin and were no reports of severe adverse events [167].

The possible therapeutic potential of both peptides in the treatment of several tumours or related process has been investigated. A study proved that P17 as well as P144 can enhance the efficacy of antitumour immunotherapy in thymoma and melanoma cell lines *in vitro* and *in vivo* [156]. Furthermore, it has been proposed that P17 and P144 can act as immunomodulators in the cellular response to tumours. P17 was able to inhibit regulatory T cells of the immune system in order to enhance the immune cellular response to the tumour [168], and P144 induced the production of cytokines in melanoma that redirect the cellular response against tumours [169]. Other tumour models, where these peptides have been evaluated, include the regulation of angiogenesis in breast carcinoma [170], liver tumour metastasis [171], and metastasis in lung cancer [172, 173].

Zubeldia *et al* [174] hypothesised that the treatment with P17 and/or P144 could constitute a therapeutic approach to inhibit metastasis in colorectal cancer throughout abrogation of epithelial to mesenchymal transition and CSC phenotype. Interestingly, the administration of P17

and P144 not only reduced liver metastasis *in vivo*, but also the presence of P17 diminished the expression of CSC markers as CD44 and SOX2 *in vitro*. This last finding suggests the potential of these inhibitory peptides to target the CSC subpopulations present in tumours [174].

HYPOTHESIS AND OBJECTIVES

HYPOTHESIS AND OBJECTIVES

Glioblastoma Multiforme (GBM) is the most prevalent malignant brain tumour accounting for 60-70% of all gliomas. Despite its low incidence in comparison to other tumours, it presents a low median survival of 12-15 months. In spite of numerous efforts using molecularly targeted therapeutics, the improvements in survival over the past 100 years can be measured only in weeks.

The TGF- β signalling pathway plays a key role in GBM progression, infiltration and chemo- and radioresistance. Thus, it is emerging as an attractive and promising therapeutic approach for the treatment of GBM. The TGF- β pathway acts on the maintenance of the stem like phenotype of GBM CSC. The CSC subpopulation has been proposed as responsible for the resistance to treatment and recurrence in GBM, therapies focused on eradicating CSC are under active development.

Several inhibitors of different TGF- β pathway elements have entered into preclinical development and clinical trials in GBM. P144, a TGF- β pathway inhibitory peptide, emerged as a potential therapeutic for the treatment of GBM.

Therefore, we decided to analyse the therapeutic potential of P144 for the treatment of GBM. Our hypothesis is that inhibition of TGF- β signalling pathway by P144 will affect several biological processes including cell proliferation, apoptosis, invasiveness, migration and stemness phenotype in GBM. The generated changes could counteract different characteristics and hallmarks of GBM development and progression to help the achievement of an effective treatment capable of GBM further elimination.

In an attempt to prove this hypothesis, the following objectives were determined:

1) Characterization of the therapeutic P144 effect in commercial glioblastoma cell lines over different processes related with the biology of GBM, including proliferation, apoptosis and invasiveness/migration.

2) *In vitro* determination of potential P144 effect over tumorigenicity aspects of GBM cell lines. In particular stem like cell phenotype, brain tumour initiating cells and further determination of P144 capacity to target these GBM subpopulations.

3) Identification of established and potential molecular modulators involved in the P144 mechanism of action and its effects at different levels:

- Determination of SMAD signalling pathway implication, including SMAD2 phosphorylation and consequent nuclear translocation after TGF- β stimulus, and evaluation of P144 effect over this pathway.
- Identification of expression changes on modulator elements of TGF- β signalling pathway that can participate in the regulation of P144 effect.

4) *In vivo* evaluation of the potential antitumour activity of P144 on GBM in immunodeficient mice, through xenograft and orthotopic GBM models.

MATERIALS AND METHODS

MATERIALS AND METHODS

I) MATERIALS

1.1 Reagents and chemicals

Listed below different reagents and chemical compounds used in the present work:

(i) 2-methylbutane was obtained from SIGMA (Cat No M32631, SIGMA, Saint Louis, MO, USA).

(ii) Camptothecin (Cat No C9911) was obtained from SIGMA (Saint Louis, MO, USA) and used as pro-apoptotic agent.

(iii) Dimethylsulfoxide (DMSO) (Cat No D8418, SIGMA, Saint Louis, MO, USA) was used for cell lysis and solubilisation of formazan salt derived from the reduction of tetrazolium formed in the MTT assay.

(iv) Dulbecco's phosphate buffered saline (DPBS) solution were purchase from GIBCO (Cat No 14190-094, GIBCO, Paisley, UK) and SIGMA (Cat No D8537, SIGMA, Saint Louis, MO, USA).

(v) EDTA (Cat No E5134, SIGMA, Saint Louis, MO, USA) was include in some solutions and buffers.

(vi) HCl solution at 1 M used to adjust the pH of solutions and buffers was obtained from PANREAC (Cat No 131020.1611, PANREAC, Castellar del Vallés, Barcelona, Spain) or Fluka Chemika (Cat No 71763, Fluka, Munich, Germany).

(vii) Isoflurane was used for inhaled anaesthesia and obtained from ABBOTT S.A. (Cat No 05260-05, Isoflo[®], Madrid, Spain) or alternatively from B.Braun (Cat No 469860, Melsungen, Germany).

(viii) Laminin solution derived from Engelbreth-Holm-Swarm mouse tumour (Cat No 354232, BD Biosciences, Bedford, MA, USA) was used to increase cells attachment when required in different assays.

(ix) Matrigel[™] (Cat No 356230, BD Biosciences, Bedford, MA, USA) was used as substrate for cell invasiveness determination.

(x) Sodium Carbonate (Na₂CO₃) (Cat No 10314471, Riedel-de Haën[®], Seelze, Germany) were dissolved in distilled water at a final concentration of 100 mM solution adjusted at pH 9.5 with HCl 1 M (Fluka) and sterilized by filtration using Steritop[®] Bottle Top Filter Units (Cat No SCGPS02RE. Merck Millipore, Darmstadt, Germany).

(xi) Thiazolyl blue tetrazolium bromide (3-[4,5-Dimethyl-2-thiazolyl]-2,5-diphenyl-2H-tetrazolium bromide) for MTT assay was obtained from SIGMA (Cat No M5655, SIGMA, Saint Louis, MO, USA).

(xii) TRIS base (Cat No T1503, SIGMA, Saint Louis, MO, USA) were used at 50 mM solution adjusted at pH 9.5 with HCl 1 M (Fluka) and sterilized by filtration with Steritop® Bottle Top Filter Units (Merck Millipore).

Dyes and chemicals used for cell staining include:

- (i) Acridine Orange (Cat No A3568, Life Technologies, Carlsbad, CA, USA).
- (ii) Crystal Violet (Cat No 252532, PANREAC, Castellar del Vallés, Barcelona, Spain).
- (iii) Ethidium Bromide (Cat No 17-1328-01, PlusOne®, GE Healthcare, Buckinghamshire, UK).
- (iv) Trypan Blue solution (0.4%) (Cat No T8154, SIGMA, Saint Louis, MO, USA).

1.2 Buffers

Buffers used in the present work include:

(i) Paraformaldehyde (3.7-4.0%) buffered to pH 7.0: obtained from PANREAC (Cat No 252931, PANREAC, Castellar del Vallés, Barcelona, Spain).

(ii) Phosphate buffer (PB): 10 mM Na₂HPO₄ (Cat No 431478, Sigma Aldrich, Saint Louis, MO, USA) and 1.4 mM KH₂PO₄ (Cat No 104873, Merck Millipore, Darmstadt, Germany). HCl 1 M (Fluka) was utilised to adjust the pH at 7.4. PB was supplemented with 4% paraformaldehyde (PFA) (Cat No 158127, Sigma Aldrich, Saint Louis, MO, USA).

(iii) Radioimmunoprecipitation assay buffer or RIPA buffer: 50 mM TRIS (Cat No 161-0719, BIO-RAD, Hercules, CA, USA), 150 mM NaCl (Cat No 131659.1211, PANREAC, Castellar del Vallés, Barcelona, Spain), 0.5% Triton® X-100 (Cat No 23.472-9, Sigma Aldrich, Saint Louis, MO, USA) and 0.5% sodium deoxycholate (Cat No D-6750, Sigma Aldrich, Saint Louis, MO, USA). Solution of TRIS and NaCl was adjusted to pH 8.0 with HCl 1 M (PANREAC) prior addition of other compounds. The buffer was supplemented with PMSF 1 mM (Cat No P7626, Sigma Aldrich, Saint Louis, MO, USA), DTT at 10 mM final concentration (Cat No y00147, Invitrogen, Carlsbad, CA, USA) and 1× Halt™ Protease and Phosphatase Inhibitor Cocktail (Cat No 78440, Thermo Scientific, Rockford, IL, USA). PMSF was prior dissolved in Isopropanol (141090.1211, PANREAC, Castellar del Vallés, Barcelona, Spain) to obtain 100 mM stock solution.

(iv) SDS-PAGE electrophoresis running buffer: for resolving SDS-PAGE under reducing conditions, the buffer composition was: 25 mM TRIS (Cat No 161-0719, BIO-RAD, Hercules, CA,

USA), 192 mM Glycine (Cat No 141340.1211, PANREAC, Castellar del Vallés, Barcelona, Spain) and 0.1% sodium dodecyl sulphate (SDS) (Cat No L4390, Sigma Aldrich, Saint Louis, MO, USA).

(v) Transfer buffer: to transfer proteins onto nitrocellulose membrane the buffer used was composed by: 25 mM TRIS (Cat No 161-0719, BIO-RAD, Hercules, CA, USA), 192 mM Glycine (Cat No 141340.1211, PANREAC, Castellar del Vallés, Barcelona, Spain) and 20% Methanol (Cat No 141091.1211, PANREAC, Castellar del Vallés, Barcelona, Spain).

(vi) Tris-buffered saline (TBS) buffer: 10 mM TRIS (Cat No 161-0719, BIO-RAD, Hercules, CA, USA) adjusted to pH 7.6-7.8 with HCl 1 M (PANREAC), 150 mM NaCl (Cat No 131659.1211, PANREAC, Castellar del Vallés, Barcelona, Spain). TBS buffer was used with or without 0.1% Tween 20 (Cat No P1379, Sigma Aldrich, Saint Louis, MO, USA).

1.3 Oligonucleotides

All oligonucleotides were obtain from SIGMA (Saint Louis, MO, USA). Specifications related to sequence, melting temperature designation and product size that enable final PCR product obtaining, are listed in Table 9.

Table 9. Primer sequences used for RT-qPCR.

Gene	Primer sequence (5' - 3')	Ref Seq Acc. #	Tm (°C)	Product (bp)
<i>SMAD7</i>	F: CCAACTGCAGACTGTCCAGATGCT R: ATGCCACCACGCACCAAGTGT	NM_005904.3	58	136
<i>SKI</i>	F: AACAAAGTACAAGCGGCGGGT R: ACACAGCCCAGGCTCTTATTGGA	NM_003036.3	58	167
<i>SNON</i>	F: GGCTGAATATGCAGGACAGTTGGC R: ACTTCTGTCTTGCTTCCCGTTCCT	NM_005414.3	58	113
<i>p21CIP1</i>	F: AAAACGGCGGCAGACCAGCA R: AGGCAGAAGATGTAGAGCGGGC	NM_000389.3	60	145
<i>p15INK4B</i>	F: CGGAATGCGCGAGGAGAACA R: GCCCATCATCATGACCTGGATCG	NM_004936.3	60	175
<i>FOXG1</i>	F: CGTTCAGCTACAACGCGCTCAT R: CAGATTGTGGCGGATGGAGTTC	NM_005249.3	60	152
<i>HPRT1</i>	F: TGACACTGGCAAAACAATGCA R: GGTCCTTTTACCAGCAAGCT	NM_000194.2	60	94

F: forward primer; **R:** reverse primer; **Ref Seq Acc. #:** reference sequences accession number; **Tm:** optimal melting temperature in Celsius scale (°C); **bp:** base pairs.

1.4 Synthetic peptide

Peptide P144 (amino acid sequence: TSLDASIIWAMMQN, MW: 1580.8 Da) was previously developed by *in silico* predictions software designed by the Department of Internal Medicine from the University of Navarra [159]. The software predicts peptides from human TGF- β 1 type III receptor with high propensity of interaction to human TGF- β 1 and assigns potential interactive regions based on the hydrophilicity/hydrophobicity, net charge and size of the amino acid chains between two sequences. After *in silico* screening, selected peptide was synthesized and biologically tested to determine the affinity and *in vitro/in vivo* activity grade.

In the present work, P144 peptide was manufactured by PolyPeptide Group (Strasbourg, France) and kindly provided by Digna Biotech Ltd. (Madrid, Spain). Chemical synthesis was performed using the solid phase method and the F-moc alternative [175]. The final product is a lyophilized acetate salt peptide with a purity above 95% (determined by high-performance liquid chromatography and mass spectrometry). P144 was resuspended in corresponding culture medium at high concentration (1-3 mg/mL) and sonicated during 3 min at RT in an ultrasonic bath at maximum power (Fungilab S.A., Barcelona, Spain) in order to reduce the particle size and increase solubility due to P144 hydrophobic profile. After sonication, additional medium was added to obtain the final peptide required concentration in each assay. In some assays, P144 was dissolved in Na₂CO₃ or TRIS solution as described below.

1.5 Proteins and antibodies

1.5.1 Growth factors and recombinant proteins

Several growth factors were added to supplement cell culture medium. Epidermal growth factor (EGF) was purchased from SIGMA (Cat No E9644, Saint Louis, MO, USA) or R&D Systems (Cat No 236-EG, Minneapolis, USA). Basic fibroblast growth factor (bFGF) was obtained from SIGMA (Cat No F0291, Saint Louis, MO, USA) or Peprotech (Cat No 100-18B, Hamburg, Germany). Both growth factors were used at 20 ng/mL. B-27 supplement 50 \times was purchased from GIBCO (Cat No 17504, Paisley, UK).

Recombinant human TGF- β 1 (Cat No 240-B) and TGF- β 2 (Cat No 302-B2) were purchased from R&D Systems (Abingdon, UK).

1.5.2 Antibodies

Specific proteins western blotting quantification were carried out through different antibodies. Antibodies name, catalogue reference, origin and handling conditions are summarized

in Table 10. Neutralizing antibody anti TGF- β 1 (from now referred in the text as T β 1Ab) (Cat No AB 101 NA) was purchased from R&D Systems (Abingdon, UK).

For flow cytometry anti-CD133/1-phycoerythrin (PE) antibody (Cat No 130-080-801, Miltenyi Biotec, Auburn, CA, USA) and anti-CD15-Allophycocyanin (APS) antibody (Cat No 130-091-371, Miltenyi Biotec, Auburn, CA, USA) were used to detect expression of CD133 and CD15, respectively. Mouse IgG1 (Cat No 130-092-212, Miltenyi Biotec, Auburn, CA, USA) and mouse IgM (Cat No 130-093-176, Miltenyi Biotec, Auburn, CA, USA) were utilised as isotype controls for CD133 and CD15 antibodies, respectively.

Immunohistochemistry detection for specific proteins were performed using Ki-67 rabbit monoclonal antibody, clone SP6 (Cat No #RM-9106-R7, NeoMarkers, Fremont, CA, USA), cleaved caspase-3 rabbit polyclonal antibody (Cat No #9661, Cell Signaling, Danvers, MA, USA) and CD-31 rat anti-mouse antibody (Cat No DIA-310, Dianova, Hamburg, Germany). Rabbit anti-rat antibody (Cat No P0450, Dako, Sant Just Desvern, Barcelona, Spain) was used as secondary antibody.

Table 10. Antibodies used in western blot.

Antibody	Size (kDa)	Manufacturer	Cat No	Specie	Dilution	Incubation	Type
anti-Smad2 (86F7)	60	Cell Signaling (Danvers, MA, USA)	#3122	Rabbit (mAb)	1:4,000	O/N (4 °C)	Primary
anti-Phospho-Smad2 (Ser465/467) (138D4)	60	Cell Signaling (Danvers, MA, USA)	#3108	Rabbit (mAb)	1:2,000	O/N (4 °C)	Primary
anti-SMAD7 (P-20)	46	Santa Cruz Biotechnology (Santa Cruz, CA, USA)	sc-9183	Goat (pAb)	1:2,000	O/N (4 °C)	Primary
anti-Ski (H-329)	≈ 95	Santa Cruz Biotechnology (Santa Cruz, CA, USA)	sc-9140	Rabbit (pAb)	1:1,000	O/N (4 °C)	Primary
anti-BAX	20	Cell Signaling (Danvers, MA, USA)	#2772	Rabbit (pAb)	1:2,000	O/N (4 °C)	Primary
anti-Lamin A/C	69/62	Santa Cruz Biotechnology (Santa Cruz, CA, USA)	sc-6215	Goat (pAb)	1:500	1 h (RT)	Primary
anti-β-Actin	42	SIGMA (Saint Louis, MO, USA)	A5441	Mouse (mAb)	1:20,000	1 h (RT)	Primary
anti-GAPDH (6C5)	37	Santa Cruz Biotechnology (Santa Cruz, CA, USA)	sc-32233	Mouse (mAb)	1:20,000	1 h (RT)	Primary
anti-Rabbit IgG-H&L (HRP)	-	Abcam (Cambridge, UK)	ab6721	Goat (pAb)	1:10,000 ^(a) 1:3,000 ^(b)	1 h (RT)	Secondary
anti-Goat IgG - H&L (HRP)	-	Abcam (Cambridge, UK)	ab6741	Rabbit (pAb)	1:10,000 ^(c)	1 h (RT)	Secondary
anti-Rabbit IgG-HRP	-	Santa Cruz Biotechnology (Santa Cruz, CA, USA)	sc-2004	Goat (pAb)	1:5,000 ^(d)	1 h (RT)	Secondary
anti-Goat IgG-HRP	-	Santa Cruz Biotechnology (Santa Cruz, CA, USA)	sc-2020	Donkey (pAb)	1:5,000 ^(e)	1 h (RT)	Secondary
anti-Mouse IgG-HRP	-	Santa Cruz Biotechnology (Santa Cruz, CA, USA)	sc-2005	Goat (pAb)	1:40,000 ^(f)	1 h (RT)	Secondary

All antibodies were diluted in TBS-Tween 0.1% with 5% powder non-fat milk. Size refers the molecular weight of Ab protein target. **mAb**: monoclonal antibody, **pAb**: polyclonal antibody. Secondary Ab dilution **(a)** for SMAD2 and PSMAD2, **(b)** for BAX, **(c)** for SMAD7, **(d)** for Ski, **(e)** for Lamin A and Lamin C, and **(f)** for β-Actin and GAPDH. **O/N**: overnight. **RT**: room temperature.

1.6 Cell lines and cell culture

1.6.1 Commercial Cell Lines

(i) **A-172** [A172] (ATCC® CRL-1620™): cell line derived from human grade IV astrocytoma and provided by the American Type Culture Collection (ATCC, Manassas, VA, USA). A172 was grown in RPMI/GlutaMAX™ medium (Cat No 61870-010) supplemented with heat-inactivated 10% Foetal Bovine Serum (Cat No 10270-106, GIBCO, Paisley, UK) and 1% penicillin/streptomycin (Cat No 15140-122, GIBCO, Paisley, UK). A172 was isolated from a human primary glioblastoma histologically classified as grade IV GBM according to WHO (World Health Organization) classification.

(ii) **U-87 MG** (ATCC® HTB-14™): cell line derived from human grade IV glioblastoma and provided by the American Type Culture Collection (ATCC, Manassas, VA, USA). U-87 MG was grown in DMEM/GlutaMAX™ (Cat No 61965-026, GIBCO, Paisley, UK), and supplemented as A172 plus 1% non-essential amino acids (Cat No BE13-114E, Lonza, Verviers, Belgium). As well as A172, U-87 MG cell line derived from a human primary glioblastoma classified as grade IV GBM (WHO classification).

(iii) **Normal Human Astrocytes** (NHA) Clonetics® (Cat No CC-2565): NHA were cultured in AGM™ BulletKit® medium (Cat No CC-3186). Both NHA cell line and AGM™ BulletKit® medium were purchased from Lonza (Walkersville, MD, USA).

All cell lines were grown as monolayer cultures in 75 cm² flasks (Cat No 156499, NUNC™, Roskilde, Denmark) to 80-90% of confluence and at 37 °C in a humidified atmosphere (5% CO₂, 95% air). Modifications in culture medium as well as culture conditions according protocol indications or assay performance are indicated in further sections.

1.6.2 Brain Tumour Initiating Cells

Brain Tumour Initiating Cells Lines (BTIC lines) were previously established at the Neuro-Oncology Department of the University Clinic at the University of Regensburg by Birgit Jachnik (MTLA) and Ina Weig-Meckl (MTLA). The BTIC were obtained through surgical resection of native glioma tissue samples obtained from patients at the Department of Neurosurgery. The patients presented a WHO grade III or IV diagnosis of high-grade glioma. After resection, the histological classification was carried out by the Department of Neuropathology following criteria of 2007 WHO CNS tumours classification. All patients gave written informed consent, and the further use of the samples was specifically approved by the ethics committee of the University of Regensburg (Protocol No 11-103-0182). The primary cell culture and establishment of BTIC cultures were prior described by Moeckel *et al* [176]. Briefly, tissue samples were kept in DPBS at

4°C and processed within 24 h after surgery. Using scalpel and followed by aspiration through a Pasteur pipette, samples were mechanically dissociated. The dissociation was helped with enzymatic dissociation with 1× Trypsin/EDTA (Cat No T3924, SIGMA, Saint Louis, MO, USA) at 37 °C for 5 min maximum in those cases where cells did not dissociate spontaneously. Cells were washed with DPBS and, in order to obtain a single cell suspension, the cell homogenate was filtered through a 30 µm pore size cell strainer (Merck Millipore, Darmstadt, Germany). The tumour cells obtained were cultured in RHB-A® medium (Cat No SCS-SF-NB-01, STEMCELLS, Cambridge, UK) supplemented with 20 ng/mL EGF (R&D Systems), 20 ng/mL bFGF (Peprotech) and 1% penicillin/streptomycin (Cat No P11-010, PAA Laboratories GmbH, Cölbe, Germany). Cultures were subcultured once a week and replaced with recently prepared supplemented medium twice a week. To analyse tumour-initiating isolation, stem cell marker expression was assessed by immunohistochemical staining of NESTIN and SOX2 expression, and flow cytometry analysis of CD133 and CD15 expression. BTIC cultures were classified as pro-neural or mesenchymal according the expression pattern. *In vitro* BTIC cultures grew as spheres, as adherent cells or exhibited a mixed growth type.

In the present work, four BTIC cell lines were selected. Histological classification, growth characteristics and denomination are summarized in Table 11. Cultures were incubated with RHB-A® supplemented medium and maintained as described above. Detachment of cells for subcultures was carried out with cell scrapers and, instead of trypsin, Cell Dissociation Solution Non-enzymatic 1× (Cat No C5914, SIGMA, Saint Louis, MO, USA) was added to obtain a single cell suspension. For all assays, BTIC cultures were used between passages 2 and 10 after thawing the cryopreserved stock. Cultures were grown under two conditions: normoxia (5% CO₂, 21% O₂) and hypoxia (5% CO₂, 3% O₂).

In all assays and conditions analysed on BTIC, a control culture of U-87 MG was included. For this purpose, the U-87 MG cell line was cultured with DMEM-Low Glucose (Cat No D6046, SIGMA, Saint Louis, MO, USA) supplemented with 10% Foetal Bovine Serum GOLD (Cat No A11-151), 1× MEM Non-essential Amino Acids (Cat No M11-003), 1× MEM Vitamins (Cat No N11-002) and 1× Penicillin/Streptomycin (Cat No P11-010). All supplements were purchased from PAA Laboratories GmbH (Cölbe, Germany).

Table 11. Classification and growth characteristics of BTIC selected cell lines.

BTIC ID	Histology Classification	WHO-Grade (I-IV)	Growth type		Molecular Classification
			Normoxia	Hypoxia	
RAV20	Primary GBM	IV	Mixed	Mixed	Mesenchymal
RAV28	Primary GBM	IV	Adherent	Adherent	Mesenchymal
RAV19	Primary GBM	IV	Spheres	Spheres	Pro-neural
RAV57	Primary GBM	IV	Adherent	Mixed	Pro-neural

Histology and WHO classification was carried out in the original tumours by independent neuropathologists.

GBM: Glioblastoma Multiforme.

1.7 Animals

In vivo experiments were performed with nude mice. For subcutaneous human tumour xenograft model, 6-8 weeks old female nude mice (Hsd: AthymicNude Foxn1nu) weighting between 19-22 gr were purchased from Harlan Laboratories Models (Harlan Italy, S. Pietro al Natisone, Italy). For intracranial human tumour orthotopic model, 8 weeks old male mice (NMRI nu/nu) weighting between 30-32 g were obtained from Charles River (Sulzfeld, Germany).

II) METHODS

2.1 Quantification of cell viability/proliferation

2.1.1 Thiazolyl Blue Tetrazolium Bromide assay

To evaluate cell proliferation in A172 and U-87 MG cells, Thiazolyl Blue Tetrazolium Bromide (MTT) assay was performed consecutively after 24 and 48 h with different P144 concentrations. Cells were seeded at 7×10^3 cells/well in a 96-well flat-bottom plate (Cat No 92096, Techno Plastic Products, TPP[®], Trasadingen, Switzerland) and grown for 24 h. P144 was resuspended in the corresponding culture medium, sonicated and then added to wells at different concentrations. After 24 and 48 h, thiazolyl blue tetrazolium bromide was added to each well at a final concentration of 5 mg/mL. Plate was incubated at 37 °C for 3 h under dark conditions. After medium removal, 150 µL of DMSO was added. The absorbance was monitored at 540 nm wavelength using Multiskan EX (Thermo Electron Corporation, Rockford, IL, USA). Assay was run in sextuplicates for each experimental condition.

2.1.2 Proliferation analysis by Trypan blue exclusion assay

The determination of P144 effect on BTIC proliferation was carried out on exponentially growing cell cultures. The RAV20, RAV28, RAV19 and RAV57 BTIC lines as well as U-87 MG were seeded in 6-well plates (Cat No 92006, Techno Plastic Products, TPP[®], Trasadingen, Switzerland) at an initial density that allows exponential growth across all the experimental assay period (Table 12). After 24 h of incubation, P144 previously dissolved in 100 mM Na₂CO₃ or 50 mM TRIS was added at a final concentration of 150 µg/mL. At different time points, cells were detached with cell scraper (Cat No 90020, Laboglob, Gottmadingen, Germany) and resuspended in DPBS (SIGMA). Trypan blue solution (0.4%) was added and the number of total cells was assessed by light microscopy in a Leica Leitz Fluovert inverted microscope (Leica Microsystem, Wetzlar, Germany) using a haemocytometer (SIGMA, Saint Louis, MO, USA). As a negative control, medium with the corresponding volume of 100 mM Na₂CO₃ or 50 mM TRIS was included for each analysed condition. This control was included in the assays where P144 was dissolved in Na₂CO₃ or TRIS as a vehicle control group, and will be merely referred hereinafter as Na₂CO₃ or TRIS. Cell proliferation was expressed as the mean of the triplicates representing the total number of viable cells in the culture that exclude the dye from the cytosol.

Table 12. Initial seeding cells density established for proliferation analysis in Trypan blue exclusion assay.

U-87 MG *		Mesenchymal				Pro-neural			
		RAV20		RAV28		RAV19		RAV57	
N	H	N	H	N	H	N	H	N	H
3×10 ⁴ cells		1×10 ³ cells		1.5×10 ³ cells		2.5×10 ³ cells		2.5×10 ³ cells	

* U-87 MG cell line generally express mesenchymal phenotype related genes [30] but its expression could vary according passage number and culture conditions. U-87 MG specific cell type designation was not indicated based on the absence of pattern expression determination of U-87 MG cells used in this work.

N: Normoxia, H: Hypoxia.

2.2 Apoptosis determinations

2.2.1 ELISA

The apoptotic rate in A172 and U-87 MG cell lines was measured at 24 and 48 h by Cell Death Detection ELISA^{Plus} (Cat No 11 920 685 001, Roche Diagnostics, Mannheim, Germany) in accordance with the manufacturer's instructions. Briefly, 1.5×10⁵ cells were seeded in 6-well plates (Cat No 3506, Corning, Tewksbury, MA, USA) plates and after an O/N incubation at 37 °C, the different treatments were added. After 24 or 48 h, the attached cells were harvested and lysed, and after a centrifugation step the final samples were obtained. 20 µL of each sample was analysed by ELISA together with positive and negative controls in each determination. Camptothecin-treated cells were used as apoptosis positive control at every measurement time point. P144 was added, in the corresponding culture medium previous sonication in the same medium, to obtain a final concentration of 100 µg/mL. The results were presented as an Enrichment Factor (EF) calculated according to the manufacturer's specifications. The EF value indicates the presence of mono- and oligonucleosomes in the cytoplasmic fraction of cell lysates produced during the apoptotic process.

2.2.2 Conventional Acridine Orange-Ethidium Bromide (AO/EB) staining

To investigate how P144 affects different steps of the apoptotic process, AO/EB staining was carried out as described by Ribble *et al* [177]. Briefly, 7.5×10⁴ cells of A172 or U-87 MG cell lines were cultured in 6-well plates (Corning) O/N and then treated with 100 µg/mL of P144. To avoid interferences of peptide particles on images uptake, P144 was resuspended in cell culture medium

and added onto the upper face of 24 mm transwells with 0.4 μm pore polycarbonate membrane insert (Cat No 3412, Corning, Tewksbury, MA, USA) allowing its uptake. At each analysed time point, adherent cells were detached with a scrapper (Cat No 3008, Corning, New York, NY, USA) and harvested with the supernatant in 15 ml tubes (Cat No 430791, Corning, New York, NY, USA). Cells were pelleted at 1,500 rpm for 5 min in an Allegra™ X-12R Centrifuge (Beckman Coulter, Pasadena, CA, USA) and washed with 1 ml of cold DPBS (Cat No 14190-094, GIBCO, Paisley, UK). Pellets were resuspended in 25-100 μL of cold DPBS to obtain a cell suspension with a density of 1×10^6 cells/mL. Acridine Orange and Ethidium Bromide were added to the cells suspension at a final concentration of 8 and 6 $\mu\text{g}/\text{mL}$, respectively. Cells were visualized, classified, counted and photographed using a Nikon Eclipse 80i microscope (NIKON Instruments Inc., Tokyo, Japan) with green (Cat No B-2E/C [FITC], Chroma Technology Corporation, Bellows Falls, VT, USA) and red (Cat No G-2E/C [TRITC], also from Chroma Technology Corporation) fluorescence filters and the Isis FISH imaging system software (MetaSystems, Altussheim, Germany). Three independent assays with triplicates for each cell line and time points were performed and in each experimental group replicate 300 cells were counted and classified.

2.2.3 Anoikis determination

In order to analyse anoikis programmed cell death escape in A172 and U-87 MG cell lines, 5×10^4 cells were resuspended in 1.5 mL of medium and seeded into 6-well plates with Ultra-Low Attachment surface (Cat No 3471, Corning, Amsterdam, Netherlands). After O/N incubation, 1.5 mL of fresh medium with 100 $\mu\text{g}/\text{mL}$ of P144 was added. As well as in AO/EB staining assay, to avoid P144 particles interferences on images uptake, 24 mm transwells with 0.4 μm pore polycarbonate membrane insert (Corning) were used. At different time points, cells were photographed with a NIKON D3200 camera (NIKON Instruments Inc., Melville, NY, USA) coupled to an inverted microscope NIKON Eclipse TS100 (NIKON Instruments Inc., Melville, NY, USA) and then harvest, centrifuged and stored at -20°C for further analysis. A negative control without P144 was included at each time point analysed. An indirect measurement of anoikis was performed by quantification of total protein extracted by cell lysis in RIPA buffer followed by protein quantification by BCA Protein Assay Kit (Cat No 23227, Thermo Scientific, Rockford, IL, USA). Confirmation of anoikis was carried out by measuring the cleavage of Lamin A and Lamin C, and protein levels of BAX by western blot. The conditions and antibodies used for anoikis determination are described in Table 10.

2.3 Matrigel invasion assay

Commercial glioblastoma cell lines, A172 and U-87 MG, invasiveness in matrigel was determined as previously described in Gallo-Oller *et al* [178]. Briefly, cells were resuspended in

cell culture medium with 0.5% FBS and added onto the upper face of 24-Millicell Culture Plate Filter Inserts (Cat No PIEP12L04, Millipore, Billerica, MA, USA) covered by Matrigel™. The lower reservoirs contained medium supplemented with 10% FBS. Inserts without P144 (only medium) were included as control. Sonicated P144 at a final concentration of 100 µg/mL in cell culture medium was added onto the upper face of inserts for the treated group. After 24 h of incubation, cells on the upper surface of the membranes were removed and cells on the lower surface of the membranes were fixed for 20 min with 70% ethanol solution. Then, cells were stained with 0.5% crystal violet solution during 10 min. After inserts washing with DPBS and allowed drying, 10 to 15 images (100× magnification) of each filter's insert were acquired with an inverted light microscope NIKON ECLIPSE TS100 with Digital SGHT DS-LS camera (NIKON, Melville, NY, USA). Quantification of area of stained cells were carried out with ImageJ Software (NIH, Bethesda, USA) [179]. Three independent experiments for each condition were performed.

2.4 Soft agar colony-forming assay

The colony formation capacity in soft agar was tested for commercial glioblastoma cell lines by plating 3×10^3 cells in 2 mL of DMEM-high glucose (Cat No D5648, SIGMA, Saint Louis, MO, USA) with 10% FBS, 1% penicillin/streptomycin, 0.1% amphotericin B and 0.4% of low electroendosmosis (EEO) agarose (Cat No 8016, PRONADISA, Laboratorios CONDA, Torrejón de Ardoz, Madrid, Spain) in 6-well plates (Corning) coated with 2 mL of DMEM high glucose with 1% of agarose. P144 (100 µg/mL) was added in 2 mL of medium on the upper face of half of wells per plate. As control, medium without P144 was added to the rest of wells. Cell medium was replaced every 2-3 days until macroscopic visualization of colonies was possible. Then, the colonies were stained with 0.05% Crystal Violet, photographed and counted. Three independent experiments with triplicates for each condition were performed. The data were represented as the average of the number of colonies formed in each replicate from the three independent experiments.

2.5 Neurosphere formation assay

In order to obtain neurospheres cultures from A172 and U-87 MG, conventional cell culture were digested with trypsin-EDTA (Cat No 25300-054, GIBCO, Paisley, UK) for 5 min at 37 °C. Cell culture medium with FBS 10% was added for trypsin inactivation and obtained cells were resuspended and centrifuged at RT for 5 min at 1500 rpm in an Allegra™ X-12R Centrifuge. Then, cells were washed twice with DPBS and completely dissociated by pipetting. 4×10^4 cells/mL were resuspended in neurosphere culture medium: Dulbecco's modified Eagle's medium/F-12 + GlutaMAX™ (Cat No 31331-028, GIBCO, Paisley, UK) supplemented with 20 ng/mL EGF (SIGMA), 20 ng/mL bFGF (SIGMA) and 1× B-27 supplement and incubated vertically in 25 cm² flasks (Cat No 430639, Corning, Tewksbury, MA, USA). Incubation in the presence or absence of

P144 at 100 µg/mL was performed at 37 °C (5% CO₂, 95% air) until neurospheres were generated. Then, total number of primary spheres formed were counted. The assay was repeated in three subsequent passages in three independent experiments with the corresponding triplicates.

2.6 Clonogenic assay

The clonogenic assay is commonly used to investigate cell survival after *in vitro* irradiation. However, this assay is also useful to test the reduction in clonogenic survival of tumour cells by other physicochemical agents. The survival determination was performed following indications from a previously published protocol [180]. Selected four BTIC lines and U-87 MG cell line were tested for the capacity to form colonies under anchorage-dependent conditions in flat-bottom 96-well plates (Techno Plastic Products) using limiting dilutions analysis. Cells were maintained in logarithmic growth with regular passages, harvested by trypsin or cell scraper for U-87 MG and BTIC, respectively. Dilutions were made in the corresponding culture medium and in order to control cell density interfering over plating efficiency, cells were seeded at two different initial densities: 1 cell/well and 5 cells/well. Treatments were performed after 24 h in order to allow proper cells attachment. Controls included addition of equivalent volume of medium or 100 mM Na₂CO₃ solution as vehicle control. For each condition, treatment and dilution, a complete 96-well plate of cells was performed. Plates were incubated under normoxia and hypoxia conditions and monitored until clones were observed (1-3 weeks). A clone was defined as a cluster of at least 40 cells and the quantification was carried out by inverted microscopy. Plate efficiency (PE) and surviving fraction (SF) were calculated as follows:

$$PE = \frac{N^{\circ} \text{ of colonies formed}}{N^{\circ} \text{ of cells seeded}} \times 100\%$$

$$SF = \frac{N^{\circ} \text{ of colonies formed after treatment}}{N^{\circ} \text{ of cells seeded} \times PE}$$

Were **PE** is the ratio of the number of colonies with respect the number of cells seeded, and **SF** is the number of colonies that arise after treatment of cells, expressed in terms of PE.

2.7 2D Migration assays

To investigate if cells migration characteristics were affected in the presence of P144, different assays were carried out in commercial glioblastoma cell lines (A172 and U-87 MG) and in selected BTIC lines.

2.7.1 Monolayer wound healing assay with mechanical disruption

In vitro cell line migration capacity for A172 and U-87 MG glioblastoma cell lines was measured by monolayer scratching wound assay. Cells were cultured in a 6-well plates (Corning) and allowed to reach confluence. Then, a linear mechanical disruption of confluent adherent cell culture (wound) was made by scratching the monolayer with a sterile pipette tip. After the scratching, cells were washed and replaced with fresh cell culture medium with (treatment) or without (control) 100 µg/mL of P144 until total cover of the wound cell culture scratching was observed in control cells. Wounds photographs were taken at different time points with an inverted light microscope NIKON ECLIPSE TS100 coupled with a Digital SGHT DS-LS camera at 100× magnification. Three independent assays with triplicates for each group were performed.

2.7.2 Culture-inserts wound healing assay

For determination of wound healing migration process in U-87 MG and RAV20, RAV19 and RAV57 BTIC lines, culture-inserts (Cat No 80209, IBIDI GmbH, Planegg, Bayern, Germany) were used. The inserts allowed a well-defined cell seeding area since the inserts bottom side present a special sticky and biocompatible surface that avoids leaking. The cell suspension was placed in wells allowing cell growth only in the designated areas. For wound healing assay, inserts were placed in the bottom surface of 12-well plates (Cat No 92012, Techno Plastic Products, TPP®, Trasadingen, Switzerland) using sterile tweezers. Then, 75 µL of cell suspension (Table 13) were seeded in each insert's well. For each cell line analysed, the number of cells was determined in previous assays allowing (after O/N incubation) a total cover of the exposed area. Then, inserts were removed with sterile tweezers (Fig. 11) leaving a cell-free gap of approximately 500 µm. A volume of 500 µL of corresponding medium was added carefully to each well plate. P144 was diluted in 100 mM Na₂CO₃ solution and added to the medium to reach a final concentration of 150 µg/mL. A control of medium as well as a vehicle control (medium plus equivalent volume of 100 mM Na₂CO₃ solution) were included. The assay was carried out by duplicates and three independent experiments with consecutive cell line subcultures were performed. Plates were observed with Leica Leitz Fluovert Inverted Microscope coupled to a ProgRes® camera (JENOPTIK AG, Jena, Germany) and pictures were taken with CapturePro 2.6 software (JENOPTIK AG, Jena, Germany). Each replicate was photographed to obtain two or three representative areas. Results

were represented as the wound area covered by cells normalized to the initial cell-free area covered through time until the area in the control cells was completely covered.

In BTIC lines that present a spheres or mixed growth type, Laminin precoated plates were used to allow cell attachment and wound covering. To obtain Laminin precoated plates, a DPBS 20.5 µg/mL Laminin solution was added in a sufficient volume to cover all the well surface. The plates were incubated at 37 °C for at least 2 h. Following incubation, the solution was removed by aspiration and two washes with sterile DPBS were performed. Plates were dried O/N in sterile conditions and then used for the intended assay.

Table 13. Initial seeding cell suspension density established for wound healing assay.

U-87 MG		Mesenchymal		Pro-neural			
		RAV20		RAV19		RAV57	
N	H	N	H	N	H	N	H
3.5×10 ⁵ cells/mL		3×10 ⁵ cells/mL		2×10 ⁵ cells/mL		3×10 ⁵ cells/mL	
Laminin (-)		Laminin (+)		Laminin (+)		Laminin (+)	

N: Normoxia, H: Hypoxia.

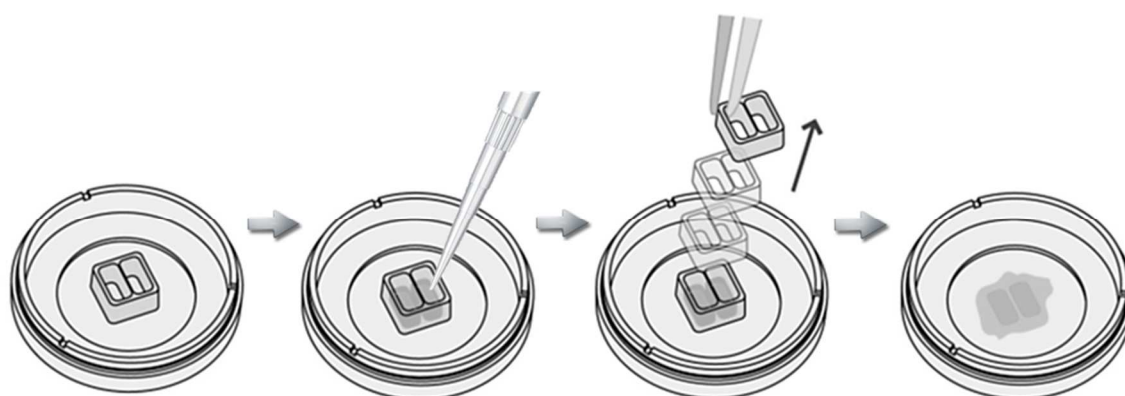


Figure 11. Schematic representation of culture-inserts handling [181].

2.7.3 Sphere formation assay

Migration ability of U-87 MG and selected four BTIC was determined through multicellular tumour spheroids generation capacity. BTIC lines suspended in 100 µL of medium (Table 14) were

seeded on a 1% agar-coated wells. After incubation for 24-48 h, mature spheroids were obtained and transferred to round-bottom 96-well plates (Cat No 92097, Techno Plastic Products, TPP®, Trasadingen, Switzerland) containing different groups with the corresponding cell medium: treatment group (P144 at 150 µg/mL), control group (cell medium) and vehicle group (corresponding volume of Na₂CO₃ or TRIS solution). Transferred spheroids were monitored using a light microscope (Leica Leitz Fluovert Inverted Microscope) and photographed (ProgRes® camera and CapturePro 2.6 software) at different time points. Spheroids and spreading surface were measured with ImageJ Software [179]. The migrated area was calculated as total area minus core area. Three independent experiments with consecutive cell passages were carried out by triplicate. For RAV19, RAV57 and RAV20 cell lines, plate wells were precoated with Laminin as described above.

Table 14. Initial cell seeding density and preincubation time established for spheroid assay.

	U-87 MG		Mesenchymal				Pro-neural			
			RAV20		RAV28		RAV19		RAV57	
	N	H	N	H	N	H	N	H	N	H
N° cells/well	2×10 ³		2.5×10 ²		2.5×10 ³		1×10 ³		7.5×10 ²	
Incubation	24 h		48 h		24 h		48 h		48 h	
Laminin	(-)		(+))		(-)		(+))		(+))	

Incubation indicates the required time to obtain mature spheres from cells, incubated over 1% agarose, to be transferred to round-bottom 96-well plates.

N: Normoxia, **H:** Hypoxia.

2.8 Gene expression analysis

2.8.1 RNA isolation

For RNA isolation, cultures were synchronized with serum starvation during 12 h before initiating each treatment. Starvation, as well as different treatments, were carried out in medium with 0.5% FBS. Total RNA was extracted with Illustra RNAspin Mini RNA Isolation Kit (Cat No 25-0500, GE Healthcare, Buckinghamshire, UK) following manufacturer's instructions.

2.8.2 Reverse transcription reaction

Reverse transcription was carried out starting with 2 µg of total RNA in a mixture containing 250 ng of random primers (Cat No P/N 58875) and 0.5 mM of each dNTPs (Cat No 10297-018). Following denaturalization at 65 °C for 5 min, DTT at 10 mM final concentration (Cat No y00147) and 5× First-Strand buffer (Cat No P/N y02321) were added. After incubation at 42 °C, 200 U of SuperScript™ II Reverse Transcriptase (Cat No 100004925) were included in the mix. The total reaction was incubated 10 min at 25 °C and inactivated by heating at 70 °C for 15 min. The reaction was performed on a Biometra® thermocycler (T3, Biometra, Göttingen, Germany). The enzyme and all reagents for the reverse transcriptase reaction were obtained from Invitrogen (Carlsbad, CA, USA).

2.8.3 Quantification by reverse transcription-quantitative polymerase chain reaction

Gene expression was assessed by reverse transcription quantitative polymerase chain reaction (RT-qPCR). The design and analysis of each pair of primers were performed with Primer3 software (<http://primer3.sourceforge.net/>) and Primer Blast (<http://www.ncbi.nlm.nih.gov/tools/primer-blast/>) in order to obtain product length, %GC, T_m, self-complementarity and/or possible products on unintended templates. Primers were selected and aligned with the mRNA and DNA sequences obtained from RefSeq (<http://www.ncbi.nlm.nih.gov/RefSeq/>) and UCSC Genome Browser (<http://genome.ucsc.edu/>). The genes selected for the analysis included: *SMAD7*, *SKI*, *SNON*, *p21CIP1*, *p15INK4B* and *FOXG1*. The housekeeping gene *HPRT1* was used as internal control of expression in all assays. The amplification step and melting curves were carried out in an IQ5 Multicolor real-time PCR detection system (BIO-RAD, Hercules, CA, USA). The reaction mix contained 12.5 µL of 2× IQ™ SYBR® Green Supermix (Cat No #170-8882, Bio-Rad, CA, USA) and 100 nM of forward and reverse primers (Table 9) in a final volume of 25 µL. An initial denaturation step at 95 °C for 10 min was followed by 40 cycles of amplification alternating between 95 °C for 15 s, the corresponding annealing temperature for each gene for 30 s and 72 °C for 30 s. After the amplification step, the melting curve analysis was carried out as follows: from 70 °C to 90 °C, 30 s at every increase of 0.5 °C. For the relative quantification, an efficiency corrected quantification model was applied in assays without control group. The derivative ratio values describe the relative expression change of the target gene related to the *HPRT1* reference gene expression. When a control was included in the experimental design, the gene expression was normalized using the levels of the *HPRT1* gene and the $2^{-\Delta\Delta Ct}$ method. All samples were run in triplicate and three independent experiments were carried out.

2.9 Determination of protein expression

2.9.1 Western blot

Western blot analysis was assessed in order to quantify protein expression of SMAD2 (phosphorylated and unphosphorylated states), SMAD7 and SKI. Total proteins were extracted from cell culture or tumour tissues using RIPA buffer. The obtained suspension was incubated at 4 °C for 10 min with 2-3 times of vortexing, and then centrifuged for 20 min at 14,000 rpm in an Eppendorf 5415 R centrifuge (Eppendorf, Hamburg, Germany). The cytoplasmic and nuclear fractions were obtained with NE-PER™ Nuclear and Cytoplasmic Extraction Reagents (Cat No 78833, Thermo Scientific, Rockford, IL, USA) according to manufacturer's instructions. Supernatant protein concentration was determined with the BCA Protein Assay Kit. 30 µg of total protein from the total lysates and 20 µg from each fraction (cytoplasmic and nuclear) were resolved by SDS-PAGE under reducing conditions and transferred onto a nitrocellulose membrane (Cat No 10600006, Amersham™ Protran™ 0.2 µm, GE Healthcare, Buckinghamshire, UK). Membranes were blocked in TBS and 5% non-fat milk for 1 h. Blots were washed with TBS-Tween 0.1% and incubated with primary antibody. Incubation with the secondary antibody was performed after three washes with TBS-Tween 0.1%. Antibodies and conditions used are summarized in Table 10. Finally, chemiluminescence and autoradiography of secondary antibody binding detection was performed using Amersham™ ECL™ Prime Western Blotting Detection Reagent (Cat No RPN2232) and Amersham Hyperfilm™ ECL™ (Cat No 10600006 and RPN203D), both purchased from GE Healthcare (Buckinghamshire, UK). Bands density was quantified using ImageJ software [179]. The obtained densitometry values were normalized to the corresponding value of GAPDH or β-Actin as loading controls. GAPDH and Lamin A/Lamin C protein levels were used to assess the purity of the cytoplasmic and nuclear fraction, respectively.

2.9.2 Flow cytometry

CD133 and CD15 expression in U-87 MG cell line, under normoxia and hypoxia, were determined through labelling of 2×10^5 cells with anti-CD133/1-phycoerythrin (PE) antibody or anti-CD15-Allophycocyanin (APC) antibody, according to manufacturer's instructions. Briefly, 2×10^5 cells were harvested and washed once with DPBS and then resuspended in labelling buffer: DPBS supplemented with 0.5% bovine serum albumin (BSA) (Cat No A2153, SIGMA, Saint Louis, MO, USA) and 2 mM EDTA. The FcR blocking reagent (Cat No 120-00-442, Miltenyi Biotec, Auburn, CA, USA) was added at 1:200 (v/v) dilution and then, specific antibodies were added at 1:50 (v/v) dilution. All positive fractions were gated using respective isotype controls, mouse IgG1 for CD133/1-PE and mouse IgM for CD15-APC. All steps were performed on ice and centrifugations at 4 °C. Fluorescence-activated cell sorting (FACS)-analyses was performed using a FACSCalibur flow

cytometer (Model FL4 Upgrade, Becton Dickinson, San Jose, CA, USA). Post-processing data analysis was performed with BD Cell Quest Pro software (Becton Dickinson, San Jose, CA, USA). A Forward Scatter vs Side Scatter dot plot was used to gate viable/nucleated cells. At least 20,000 events per sample were acquired.

2.10 In vivo subcutaneous tumour xenograft assay

For this *in vivo* assay, 20 female nude mice (Harlan, Italy) were subcutaneously injected in the right flank with 3.5×10^6 U-87 MG cells. Cells were resuspended in 200 μ L of DPBS, placed on ice, and injected into 6-wk-old animals that were anesthetized with inhaled 3-4% isoflurane (ABBOTT S.A.) in 100% Oxygen. Tumours were allowed to grow up to 500 mm³ and then mice were randomized into individual treatment groups of 10 animals: control group receiving DPBS (200 μ L/animal) and treated group receiving 200 μ g of P144 resuspended in DPBS (200 μ L/animal) every 24 h through intraperitoneal (IP) administration. In order to determine the tumour volume, the greatest longitudinal diameter (length) and the greatest transverse diameter (width) were determined every 24h with a Vernier precision calliper. Tumour volume based on calliper measurements was calculated by the modified ellipsoidal formula (tumour volume = $1/2(\text{length} \times \text{width})^2$). The end point was determined when the tumour reached 1.7 cm average diameter or at day 40 of treatment. At this point, the animals were sacrificed in a CO₂ chamber and tumour mass was surgically extracted. Afterwards, a tumour growth curve and survival curve were constructed. Statistical analysis was performed using non parametric repeated-measures (Wilcoxon matched-pairs signed rank test) and Kaplan-Meier analysis. All animals were maintained in pathogen-free conditions and treated in accordance with animal care guidelines of our institution, after study protocol approval by the ethic committee for animal experimentation of the University of Navarra (study No E31-11-008-10).

2.10.1 Tumour xenografts samples processing for mRNA and protein isolation

After tumour extraction, a sample from each tumour was directly frozen and stored at -80 °C until processing. For RNA isolation, 30 mg frozen tumour samples were homogenized through cell disruption with a pellet mixer (Cat No 47747-370, VWR, Leighton Buzzard, UK) and processed with Illustra RNAspin Mini RNA Isolation Kit following manufacturer's instructions. To obtain total proteins content of tumour samples, 30-40 mg of tissue was homogenized in RIPA buffer with a pellet mixer and then processed as previously described in this section.

2.10.2 Histology and immunohistochemistry analysis

A tissue sample from each tumour derived from the xenograft tumour implant *in vivo* assay was fixed in 3.7-4.0% paraformaldehyde buffered to pH 7.0, embedded in paraffin and sectioned

(3 µm thick) with a microtome. Paraffin sections were dewaxed and hydrated for subsequent staining. Haematoxylin and eosin (H&E) staining was performed to assess the histopathological condition of the tissues. Immunohistochemical staining for Ki-67 (with rabbit monoclonal antibody, 1:100 dilution) and cleaved caspase-3 (with rabbit polyclonal, 1:100 dilution) was performed using the EnVision™+ System-HRP (DAB) (Cat No K4011, Dako, Glostrup, Denmark) according to the manufacture's recommendations. Antigen retrieval was performed at 95 °C for 30 min in 0.01 M TRIS-1 mM EDTA buffer (pH 9.0) in Pascal pressure chamber S2800 (Dako, Sant Just Desvern, Barcelona, Spain). Slides were allowed to cool for 20 min, then endogenous peroxidase was blocked with 3% H₂O₂ (Cat No 95321, SIGMA, Saint Louis, MO, USA) in deionized water for 12 min and sections were washed in TBS-Tween buffer. Incubations with primary antibodies were performed O/N at 4 °C at their optimal dilution. In the case of CD31, sections were first incubated with rabbit anti-rat secondary antibody at a dilution of 1:200 for 30 min. After rinsing in TBS-Tween, the sections were incubated with goat anti-rabbit labelled polymer for 30 min at RT. Peroxidase activity was revealed using Liquid DAB+ Substrate Chromogen System (Cat No K3468, Dako, Sant Just Desvern, Barcelona, Spain) and sections were lightly counterstained with Harris Haematoxylin (Cat No HHS32, SIGMA, Saint Louis, MO, USA). Finally, slides were dehydrated in graded series of ethanol, cleared in xylene and mounted in DPX Mounting medium. Paraffin sections and further processing of samples for immunohistochemistry (IHC) were carried out by the Morphology Core Facility of the Center of Applied Medical Research (CIMA, Pamplona, Spain). The image analysis was carried out through ImageJ software [179].

2.11 Orthotopic mouse brain tumour model

For the development of orthotopic mouse brain tumour model, several previous determinations were carried out.

2.11.1 Peptide P144 inactivation

Peptide P144 was inactivated by autoclave, heat and high pressure saturated steam for 20 min at 121 °C (250 °F) with a pressure of 15 pounds per square inch (psi) (103.4 kPa). P144 was previously resuspended until totally dissolution in 100 mM Na₂CO₃ or 50 mM TRIS, both solutions were previously adjusted to pH 9.5 with HCl 1 M (Fluka). Biological activity inactivation was confirmed through proliferation, wound healing and spheroid formation assays, previously described. A chemical analysis of inactivated peptide was carried out by UV/Visible spectrophotometry and High-performance liquid chromatography (HPLC) as described below. Autoclaved P144 was compared to a control with only medium and the corresponding vehicle solution (100 mM Na₂CO₃ or 50 mM TRIS) under the same autoclave process that the one applied to P144.

2.11.2 Time-dependent stability analysis of peptide P144 biological activity

Time stability testing was assessed dissolving peptide P144 at 3 g/mL in 100 mM Na₂CO₃ or 50 mM TRIS. Solutions were incubated at 37 °C for 28 days. Assays were carried out at day 0, 7, 14, 21 and 28 of incubation. The experimental design is schematized in Fig. 12.

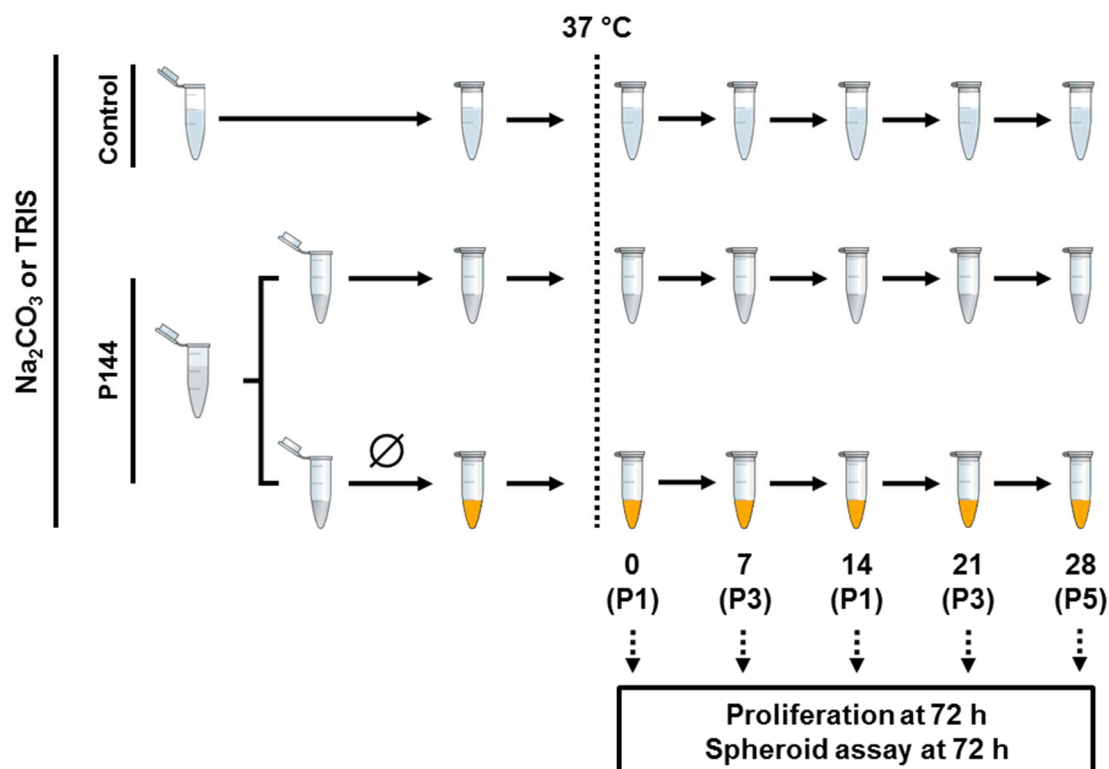


Figure 12. Experimental design schematic representation of P144 biological activity time kinetics analysis. Peptide solutions were prepared at 3 mg/mL. Each time point indicated in days. An aliquot of each tube was used to determine proliferation and migration by spheroid assay. The autoclaved treatment is denoted by \emptyset . Indicated in brackets the cell passage number used in biological assay.

2.11.3 Biological inactivation analysis

The time-dependent stability of P144 biological activity was assessed through proliferation and spheroid formation assays following methods described above.

2.11.4 Analysis of time-dependent chemical stability of peptide P144

The chemical stability was determined by UV/Visible spectrophotometry using NanoPhotometer™ (Implen GmbH, Munich, Germany) and HPLC. Data from nanophotometer were expressed as absorbance (A), calculated as $A = -\log(I/I_0)$, where I_0 is the intensity of light before it enters the sample and I is the intensity of light that has passed through a sample

(transmitted light). For HPLC analysis, an Agilent 1100 Series HPLC System (Agilent Technologies, Santa Clara, CA, USA) equipped with a binary pump system, coupled to a 500 μ L sample loop UV/visible detector, was utilised. The chemical separation was achieved with an Agilent Eclipse XDB-C18 column (150 \times 4.6 mm, 5 μ m, 80 angstrom (\AA)) (Cat No 993967-906, Agilent Technologies, Santa Clara, CA, USA). The mobile phase consisted of a binary gradient of 0.1% (v/v) trifluoroacetic acid in water (eluent A) and in acetonitrile (eluent B). The injection volume was 200 μ L of P144 (1 mg/mL) diluted in 100 mM Na_2CO_3 solution and 50 μ L of P144 (1 mg/mL) in 50 mM TRIS. The flow rate was constant throughout the chromatographic run at 1 mL/min in the following conditions: 20% B (0-2 min), 50% B (2-25 min) and 100% B (35-40 min). An equilibration step was included at the end of the protocol with 25% B. The column temperature was kept at 25 $^\circ\text{C}$. Chromatograms were recorded at 210 nm, 220 nm, 260 nm and 280 nm absorbance wavelength. Data were analysed with HPLC ChemStation Software (Agilent Technologies, Santa Clara, CA, USA).

2.11.5 Surgical intracranial tumour injection

All surgical and animal procedures were carried out in accordance with the ethical guidelines of the University of Regensburg Medical Center. The experiment was approved by the ethical committee of the University of Regensburg (application No 54-2532.1-10/13). For orthotopic model, 24 male mice (30-32 gr) from Charles River were used. Mice were fed with standard pellet diet and provided water *ad libitum* during all the process. Mice were randomized in three different groups with 8 animals per group.

To perform the intracranial injection, mice were IP anaesthetised with a mixture of Ketamine (20 mg/mL), Xylazine (4 mg/mL) and Acepromazine (2 mg/mL) in saline solution in a proportion 11:2:1. Anaesthetised mice were kept at 37 $^\circ\text{C}$ to avoid hypothermia. After confirmation of reflex loss in the animal, mice were identified with metal ear markers and eyes surface were protected with BEPANTHEN (Dexpanthenol 5 gr, Bayer Vital GmbH, Leverkusen, Germany). Mice were placed into a stereotaxic instrument with a source of heat for corporal temperature maintenance and oxygen inhale source. The surgical site was disinfected with 70% isopropanol and an 8-mm incision was made through the scalp skin. A posterior to the incision "pocket" was made undermining the skin for osmotic pump placement (further described). The skull surface was washed with saline solution and a hole was drilled through the skull over the right lateral ventricle at defined stereotaxic coordinates (medial/lateral: -1.5 mm, anterior/posterior: +0.5 mm). Using a syringe (Hamilton, Reno, NV, USA) fixed to the stereotaxic instrument, 5 μ L of 0.9% sterile sodium chloride solution containing 2.5×10^5 U-87 MG cells were injected through stereotactic-guided surgery at a depth of 2.5 mm (dorsal/ventral: -2.5 mm) with an injection flow of 0.25 μ L/min. To define the

injection cell number, a pre-assay with two different amount of injected cells (1×10^4 or 1×10^5) was performed.

2.11.6 Osmotic pump implantation

After intracranial cells injection, a stainless steel intracerebroventricular (ICV) catheter custom length (2.5 mm precut below pedestal) (Cat No 3280PM/PK/SPC, Plastics One, Roanoke, VA) was implanted at the injection site to the same depth (dorsal/ventral: -2.5 mm) and secured with cyanoacrylate gel adhesive (Loctite® 545). The ICV catheter was connected to an Alzet® micro-osmotic pump (Model 1002, Durect Corporation, Cupertino, CA, USA) via flexible polyethylene tubing. The micro-osmotic pump utilised allowed the release of P144 into the intracranial injection point at a flow rate of 0.25 $\mu\text{L/h}$ for 14 days. Following all the surgery proceeding, mice were released from stereotaxic instrument and the incision was closed with surgical skin sutures (Cat No CS-211, Sofsilks™, COVIDIEN, Neustadt an der Donau, Germany). Mice were monitored until total anaesthesia recovery and every 24 h mice were assessed using the scoring system listed in Table 15 until 21 days.

Table 15. Early endpoint parameters and criteria.

Parameter	0 points	1 point	2 points	3 points
Body weight reduction	5%	10%	15%	20%
Behaviour	attention awake, active in the group	quiet, yet in the group	isolate of the group, still interacting with animals in the area	apathetic, indifferent
Defence / Pain response	inconspicuous, normal reaction	significant defensive behaviour	strong defence, aggressiveness, even at slight handling	no defence reaction, even when challenged
Breathing	normal	mildly increased frequency, no restriction in movement	increased frequency, significant decrease in the movement of the animal	frequent high or low breathing to respiratory distress
Motor activity	without deficits	when walking partially uncoordinated	walking uncertain, wavering, significant coordination deficits	paralysis, severe deficits, hemiplegia
Posture/Hide	physiologically	slightly curved back (posture) or slightly ruffled fur	curved back, shaggy fur acts	strongly curved back, ruffled fur (cowering)

Individual early endpoint criteria was determined as soon as animals reached a total of 3 points in a concrete parameter criteria or 8 points derived from the sum of different analysed parameters. Parameters and scoring system were taken and modified from Morton and Griffiths [182].

2.11.7 Assembly and priming of Alzet® osmotic pumps

The different available osmotic pump models are shown in Fig. 13. In order to obtain a correct brain infusion in different treatments, and prior to implantation, Alzet® Osmotic Pumps were assembled and equilibrated following manufacturer’s instructions (Fig. 14). Briefly, stainless steel ICV catheter or cannula was connected to Alzet® micro-osmotic pump (Model 1002) with approximately 1 cm flexible polyethylene tubing to allow free movement of mice’s head and neck. Before the assembly, each osmotic pump were filled with the corresponding solution according treatment protocol: a) 100 mM Na₂CO₃ solution for vehicle control group, b) 3 mg/mL of P144 dissolved in 100 mM Na₂CO₃ solution for treated mice, and c) autoclave 3 mg/mL of P144 in 100 mM Na₂CO₃ solution (as previously described) for P144 inactive treatment group. After filling, a flow moderator was introduced in the pump and free end was connected to the cannula via the polyethylene catheter.

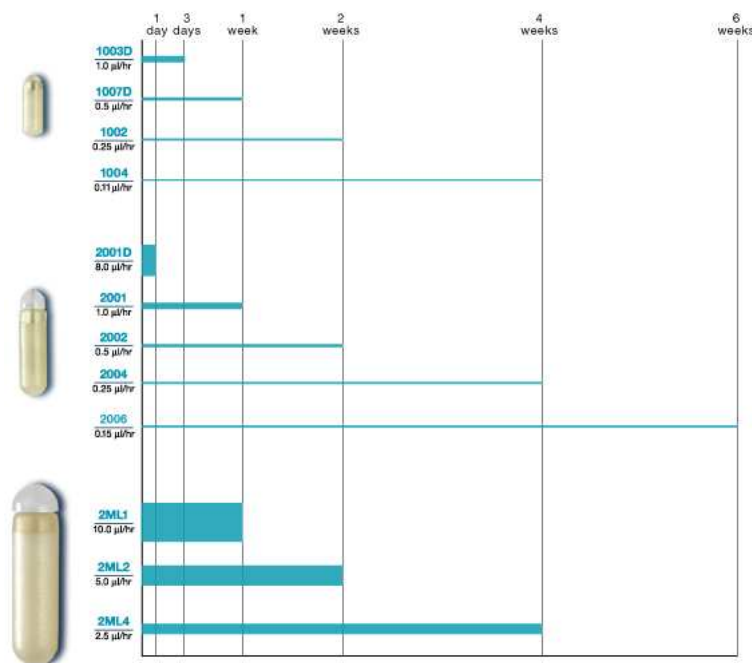


Figure 13. Alzet® osmotic pumps models. The release time allowed by each model for different treatment protocols is indicated [183].

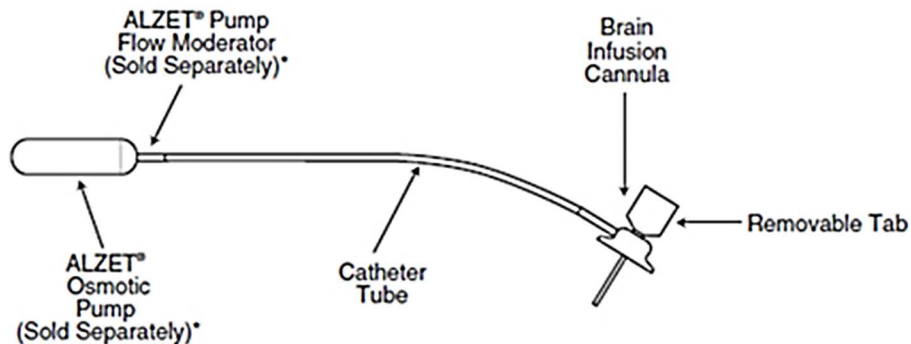


Figure 14. Schematic representation of brain system using Alzet® Osmotic Pumps [183].

After assembly, all joints were fixed with cyanoacrylate gel adhesive and all the system was soaked in 70% ethanol aqueous solution for several minutes to avoid microbial contamination.

To assure the correct pump release rate after implantation, osmotic pumps were equilibrated by O/N incubation of the filled brain infusion assembly with attached osmotic pump in DPBS at 37 °C. This step is essential when osmotic pumps are utilised with a catheter, and also minimizes the risk of clotting within the cannula or tissue occlusion during delivery of the test agent. The technical specifications of the models considered for the orthotopic *in vivo* model are summarized in Table 16.

Table 16. Specifications of osmotic pump models considered for intracranial model.

Model Numbers	1002	1004	2002	2004
Reservoir Volume	100 μ L		200 μ L	
Time of treatment (days)	14	28	14	28
Complete Osmotic Pump				
Length (cm)	1.5		3.0	
Diameter (cm)	0.6		0.7	
Weight (g)	0.4		1.1	
Total Displaced Volume (mL)	0.5		1.0	
Filling Tube				
Length (cm)	1.1		2.2	
Gauge	27		27	
Outside diameter (cm)	0.04		0.04	
Inside diameter (cm)	0.02		0.02	
Flow Moderator				
Length (cm)	1.3		2.4	
Gauge	21		21	
Outside diameter (cm)	0.08		0.08	
Inside diameter (cm)	0.05		0.05	
Weight (g)	0.05		0.2	
Chemical compatibility				
Acids	pH > 1.8			
Bases	pH < 14			
Other compounds	DMSO (up to 50%), ethanol (up to 15%) in water, phosphate buffer, saline (0.9%), serum, distilled water, culture media (1% benzyl alcohol as bacteriostatic)			

2.11.8 Magnetic resonance imaging

Once the treatment period concluded, all mice were scanned in order to obtain *in vivo* images of tumour formation using a 3 Tesla magnetic resonance tomography (MRT) (Siemens Healthcare, Erlangen, Germany). The hardware of the MRI contained a 4-phase channel array coil system for rodents. For best representation of images, mice were measured in two sequences plus two sequences with contrast solution. As contrast solution, Gadovist® (gadobutrol, gadolinium-diethylenetriamine penta-acetic acid:Gd-DTPA) (Bayer Vital GmbH, Leverkusen, Germany) at 1 M in saline solution was used. Mice were immobilized and 0.2 mmol/kg body weight were injected intravenously (IV) in the lateral tail vein using a standard 28G IV cannula. Subsequently, animals were sedated with inhaled 3-4% Isoflurane (B.Braun) plus an oxygen flow rate of 2 Lt/min. Once significant sedation occurred, ear metal tag and osmotic pump were removed and the mouse placed in the MRI. Sedation with 0.7% Isoflurane plus 3-4% O₂ 0.8 Lt/min was maintained during all MRI procedure using a 3 ml syringe nose ventilation in prone position. To maintain corporal

temperature, an integrated heat system of the coil at 38 °C was set. Modified MRI sequences for intracranial mouse model were taken from Pillai *et al* [184]. An axial T1 sequence (TR 1000 ms, TE 18 ms, slice thickness 1 mm, 10 slices) was acquired before and after administration of contrast agent (Gadovist®). An axial T2 sequence was also acquired (TR 4000 ms, TE 68 ms, slice thickness 1 mm, 10 slices).

2.11.9 Animal euthanasia and sample processing

After MRI procedure, mice were deeply anesthetized, chest cavity opened and euthanized by cardiac perfusion with 4% paraformaldehyde (PFA) in PB. Cardiac perfusion procedure was carried out by technician assistant from Department of Neurosurgery from the University Clinic at the University of Regensburg (MTLA Eva Maria Stoll). After decapitation, brain was removed and immersed in PFA 4% in PB during 24 h and then in 30% sucrose in DPBS. After 24-48 h of incubation at 4 °C, brains were snap frozen by soaked in 2-methylbutane at -80 °C. Brains were stored at -80 °C until processing for histology.

2.11.10 Histology

Brains were cut in 10 µm slices using a Leica CM1950 cryostat (Leica Microsystem, Wetzlar, Germany). H&E staining was carried out by the Department of Neuropathology from the University Clinic at the University of Regensburg.

The tumour slides, derived from H&E staining, were used to calculate the tumour size as described by Schmidt *et al* [185] and Ileva *et al* [186]. This method is based in a slab approximation, assuming that cross sections drawn from the tumour at determined intervals represent contiguous layers of tumour and uniform cross sectional areas. Total tumour volume was calculated by summing the volume of these uniform layers (slabs) whose volumes are equal to the layer thickness (10 µm) multiplied by the cross-sectional areas of the tumour. One section was selected at different intervals around 400 µm of tumour length and photographed. ImageJ software [179] was used to calculate the cross sectional area of the tumours, determining the total area of the tumour by outlining the tumour region. Calibration to convert pixels to mm² was made measuring a known distance in a picture taken with the same microscope and setups to adjust the microscope's calibration.

2.12 Statistical analysis

Experiments were performed independently at least three times except those indicated in material and methods and results section. All data are represented as the mean ± standard deviation. Once normality and homogeneity of variance analysis were assessed, a parametric or nonparametric analysis was selected. Statistically significant differences among three or more

groups were analysed by one-way analysis of variance (ANOVA) or two-way ANOVA, followed by post-hoc analysis. Comparisons between two groups were carried out by t-test (as parametric test) or by Mann-Witney U test (as nonparametric test). Descriptions of special statistical analysis in particular assays are detailed in the corresponding sections. The significance level was set to $p < 0.05$ and classified by asterisks as follows: $p < 0.05$ (*); $p < 0.01$ (**); $p < 0.001$ (***) and $p < 0.0001$ (****). The statistical analysis was calculated through GraphPad Prism software for Windows (version 5.04).

RESULTS

RESULTS

I) *IN VITRO* FINDINGS

1. ANALYSIS OF CELLULAR RESPONSE TO P144 IN TWO GLIOBLASTOMA COMMERCIAL CELL LINES

1.1 P144 decreases proliferation

The effect of P144 over the growth of commercial human glioblastoma cell lines was tested in A172 and U-87 MG cell lines by the MTT assay. After 24 h and 48 h of treatment, proliferation measurement was assessed. P144 inhibited the growth of glioblastoma cell lines *in vitro* in a dose-dependent manner (Fig. 15). Proliferation at 24 h was slightly lower than control in A172 cells, but the inhibition was remarkably lower in both cell lines after 48 h. The decrease on proliferation was statistically significant between 10 and 200 $\mu\text{g}/\text{mL}$ of P144 at 48 h in both cell lines. In addition, U-87 MG cells were more sensitive to P144 than A172 cells. In fact, the IC_{50} (half maximal inhibitory concentration) of P144 at 48 h for U-87 MG cell line was close to 16 $\mu\text{g}/\text{mL}$, but at the same dose, the A172 cells nearly showed a 20% inhibition. To analyse if the P144 antiproliferative effect was selective to tumour cell lines, we carried out a MTT assay with normal human astrocytes (NHA) at a concentration rate where p144 induces its highest antiproliferative effect in tumour cell lines (from 25 $\mu\text{g}/\text{mL}$ to 200 $\mu\text{g}/\text{mL}$). NHA cell line did not show statistical reduction on proliferation in the presence of P144. P144, therefore, has a selective antiproliferative effect on glioblastoma cells lines that is not reproducible in nontumour cells (normal astrocytes) under *in vitro* conditions.

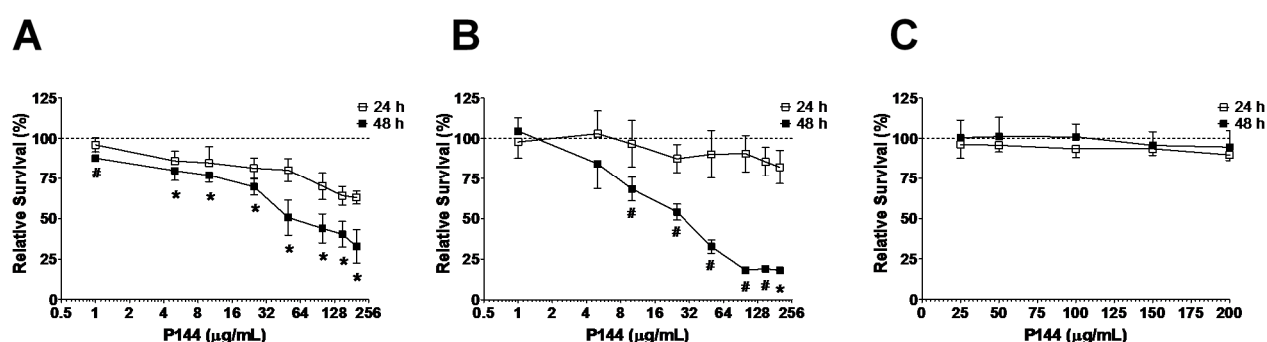


Figure 15. Antiproliferative effect of P144 measured by MTT assay. Proliferation was measured in A172 (A), U-87 MG (B) and NHA (C) cell lines. Concentrations in (A) and (B) are graphed in X-axis in log₂ scale. Data are presented as the mean \pm SD and the dotted line represents the control value (100%). Signs indicate the statistical significance compared to control: (#) statistical significance at 24 h and 48 h, (*) significance only at 48 h (one-way ANOVA for each time with Dunnett as post-test, $p < 0.05$).

1.2 P144 induces apoptosis

To further analyse the role of P144 in cell growth inhibition, apoptosis was evaluated. Cell death by apoptosis was quantified by ELISA (Cell Death Detection ELISA^{Plus}), detecting the presence of mono- and oligonucleosomes in the cytoplasmic fraction after 24 h and 48 h after different treatments. The treatments were: (i) non-treated cells as control; (ii) P144 at 100 µg/mL; (iii) TGF-β1 (200 pg/mL); and (iv) anti-TGF-β1 antibodies (Tβ1Ab) (40 ng/mL). A group of cells treated with Camptothecin at 5 µM was included in order to have a positive control of apoptosis of glioblastoma cell lines in the experimental design. In addition, apoptosis was analysed in cells were TGF-β1 was administered together with P144 or Tβ1Ab. P144 was able to increase apoptosis determined by ELISA in the same magnitude as Tβ1Ab in both glioblastoma cell lines (Fig. 16). The results showed that the apoptosis induced by P144 was close (even higher in the A172 cell line) to that produced by Camptothecin, indicating a clear pro-apoptotic effect in glioblastoma cell lines. Moreover, when TGF-β1 was applied in addition to P144 or anti-TGF-β1, the induction of apoptosis was partially reverted in a significant manner.

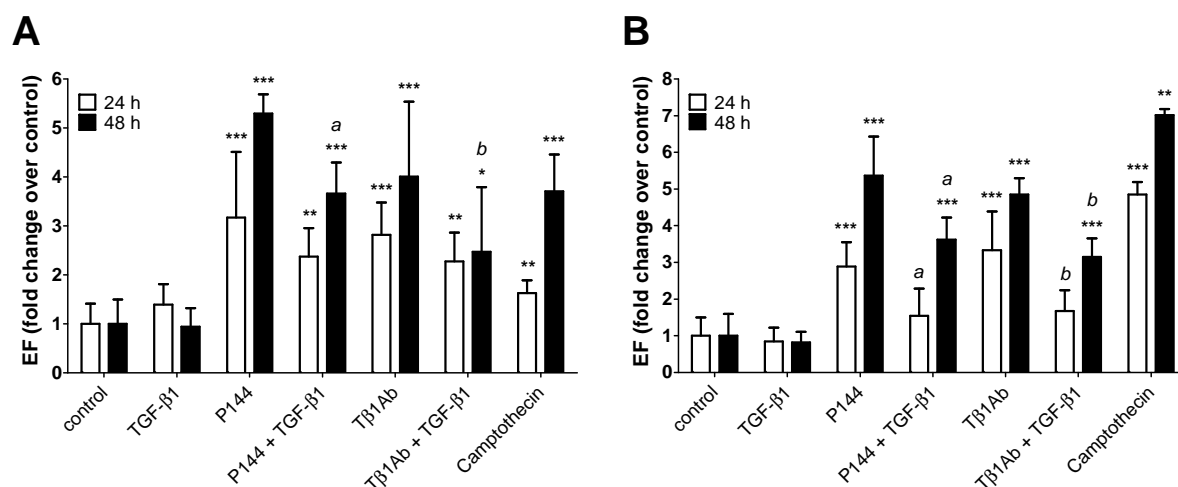


Figure 16. Apoptosis determination by ELISA. Apoptosis was measured in A172 (A) and U-87 MG (B) cell lines. The concentrations used for apoptosis determination were: P144, 100 µg/mL; TGF-β1, 200 pg/mL and anti-TGF-β1 (Tβ1Ab), 40 ng/mL. A treatment with camptothecin at 5 µM was included as a positive control. Enrichment factor was calculated according to manufacturer's specifications. Data were analysed at each time point by one-way ANOVA with Dunnett as post hoc test. A Tukey test was utilized for multiple comparisons. Significance is indicated by (*) for each treatment vs control ($p < 0.05$ (*); $p < 0.01$ (**), and $p < 0.001$ (***)); by (a) for P144 vs P144 + TGF-β1 ($p < 0.05$) and by (b) for Tβ1Ab vs Tβ1Ab + TGF-β1 ($p < 0.05$) comparison. Mean \pm SD are represented. EF: Enrichment factor.

1.3 P144 modifies apoptosis evolution and increases late apoptosis

To evaluate how P144 affects apoptotic kinetics, acridine orange/ethidium bromide (AO/EB) fluorescence staining was performed. Live cells were stained with the vital dye AO (green), whereas EB (red) only penetrated those cells in which the membrane permeability and/or membrane integrity was compromised. The microscopic analysis recognized morphological changes as chromatin condensation, nuclear fragmentation and alterations in the size and shape of cells. The analysis of these characteristics allowed us to classify the green cells into viable or early apoptotic. The red cells were classified as late apoptotic or necrotic cells (Fig. 17 and 18).

A172 and U-87 MG cells were plated in the absence or presence of P144 with a final concentration of 100 µg/mL. The AO/EB staining was performed at different time points and cells were classified in viable (V), early apoptotic (EA), late apoptotic (LA) and necrotic cells (N). In the non-treated cells, uniform green cells were observed and only at long-term incubation some red cells could be observed, probably due to the normal culture evolution. The treatment with P144 increased the amount of red cells through time in both cell lines (Fig. 19).

A172 and U-87 MG cell lines presented an increase of apoptosis in both EA and LA. A172 cells showed a slight increase in the number of cells in EA that was related with an increment in LA (Fig. 20). However, the amount of cells that displayed LA was significantly increased 8 h after P144 treatment and in all subsequent time points. An induction from EA to LA was produced in the A172 cell line. A similar behaviour was observed in the U-87 MG cell line, the rate of generation of apoptotic cells was maintained throughout time and the increase of apoptosis was only evident after 48 h. Apparently, the U-87 MG cell line presents a lower sensitivity to spontaneous apoptosis in comparison to the A172 cell line, probably due to the growth ratio difference between these cell lines. In both cases, the number of necrotic cells was lower and was only observed in the presence of P144 after 12-24 h.

To analyse if the change in distribution through time was statistically significant, a chi-square test for trend was carried out. After 4 h of treatment, significant statistical differences were observed in both cell lines, indicating that the inhibition of TGF- β signalling pathway by P144 significantly changed the ratio of cells in different apoptotic stages present in the culture. In addition, the results confirmed the increase of apoptosis by P144 observed in the ELISA assay (Fig. 16), confirming the capacity of P144 to induce apoptosis and, in a lesser extent, to induce necrosis in GBM cell lines.

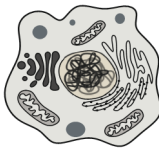
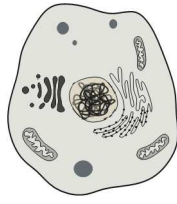
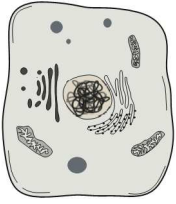

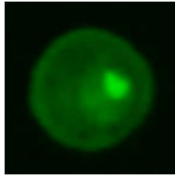
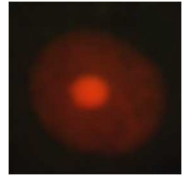
	Viable cell	Reversible swelling	Irreversible swelling	Cell lysis
				
Characteristics		No chromatin condensation	Chromatin pattern conserved Damaged cytoplasmic organelles	Loss of membrane integrity by membrane breakdown
AO/EB dye		Non-detectable	Non-detectable	
				Necrotic cell

Figure 17. Schematic representation of the necrotic process and states detected by AO/EB staining. Schemas were taken from Žanić-Grubišić [187]. Representative pictures of each stage detected are shown.





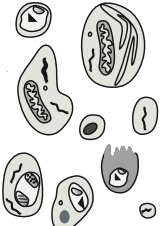
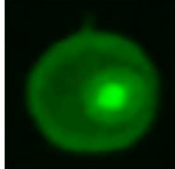

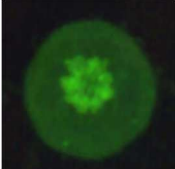
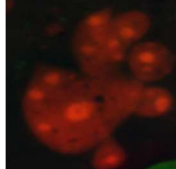
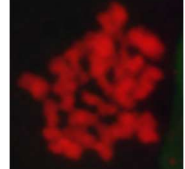
	Viable cell	Cell blebbing	Nuclear collapse	Cell and nuclear fragmentation	Apoptotic bodies
					
Characteristics		Cell shrinkage Chromatin condensation Presence of DNA fragments in cytoplasm	Organelles morphology and cytoplasmic membrane remain intact	Intact cytoplasmic organelles Change in membrane permeability	Cell fragmentation Membrane integrity intact Formation of apoptotic bodies
AO/EB dye					
		Early Apoptosis		Late Apoptosis	

Figure 18. Schematic representation of the apoptotic process and states detected by AO/EB staining. Schemas were modified from Žanić-Grubišić [187]. Representative pictures of each stage detected are shown.

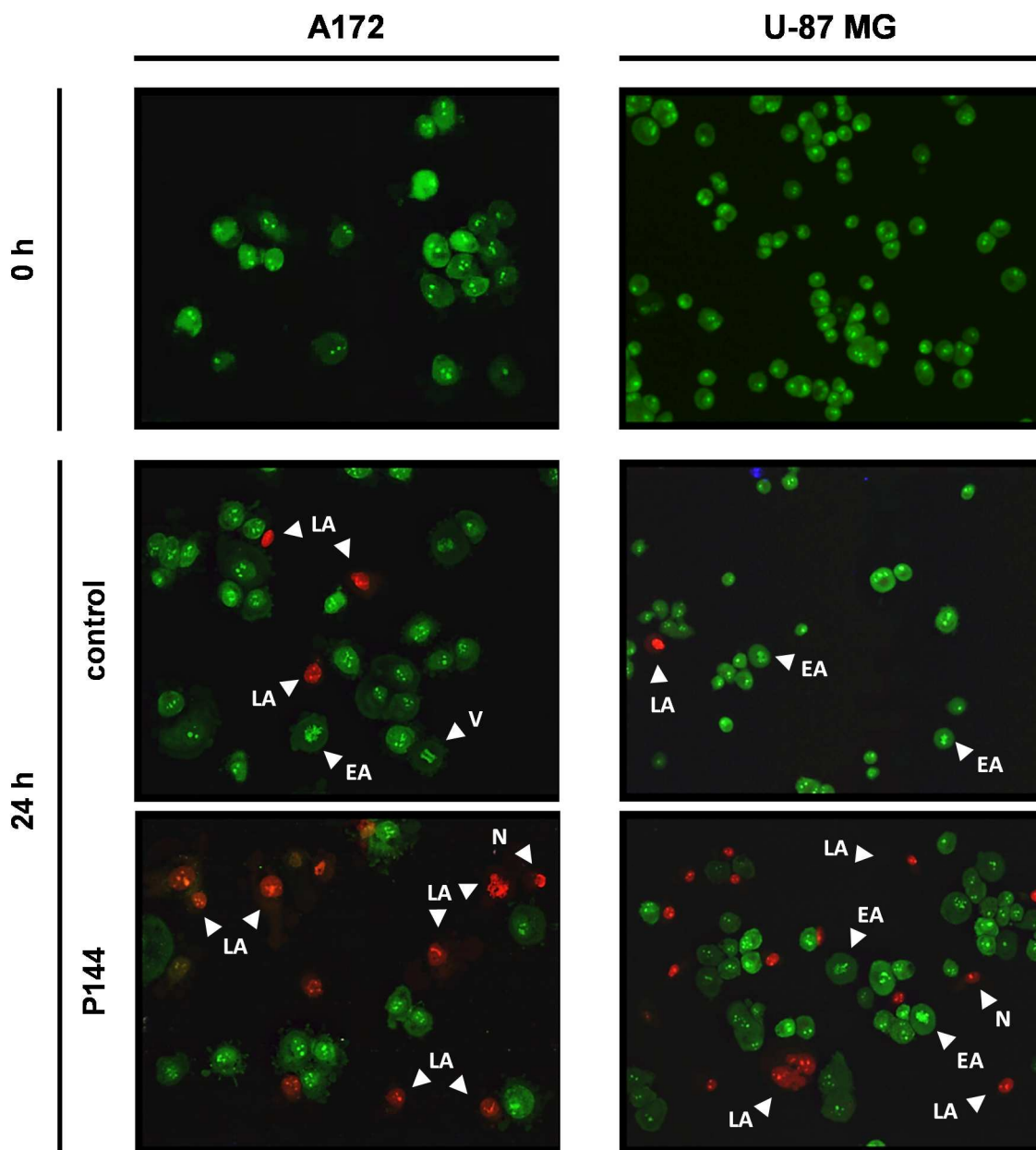


Figure 19. Apoptosis determination by AO/EB staining in A172 and U-87 MG cell lines. Representative pictures (200 \times) showing the increase in red cells rate through time (0 h and 24 h). C: control (non-treated cells). P: P144. Different apoptotic cell stages are indicated by white arrowheads. V: viable. EA: early apoptosis. LA: late apoptosis. N: necrosis.

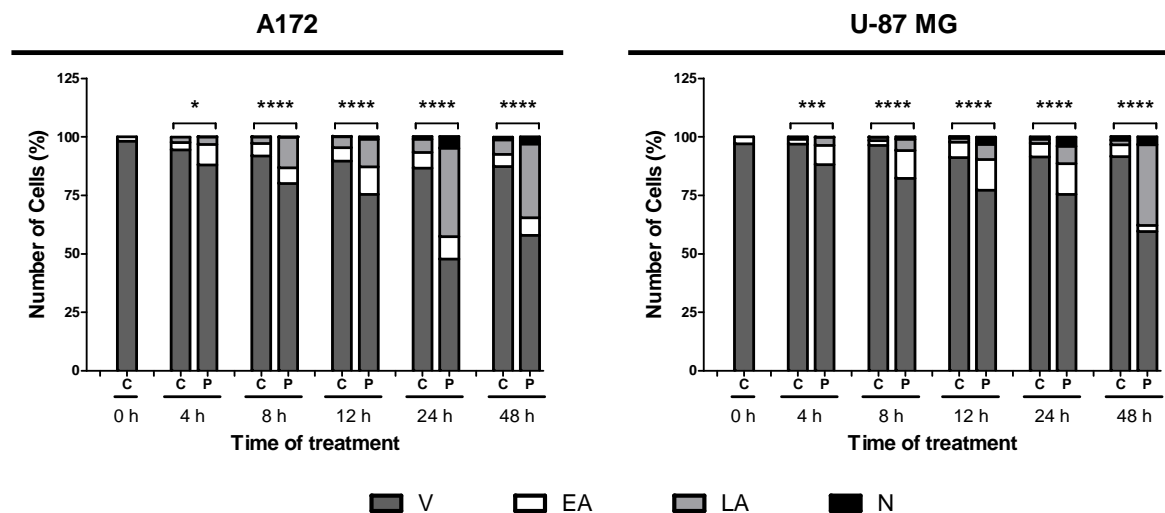


Figure 20. AO/EB staining apoptosis quantification for A172 and U-87 MG cell lines. Quantification of AO/EB staining was performed distinguishing the apoptotic stage of 300 cells per well. Mean percentage value of each stage from three independent assays are graphed. P-values of Chi-square test for trend (control vs P144 at each time point) and obtained significance ($p < 0.05$ (*); $p < 0.001$ (**); and $p < 0.0001$ (***)) are shown. C: control (non-treated cells). P: P144. V: viable. EA: early apoptosis. LA: late apoptosis. N: necrosis.

1.4 P144 impairs anoikis escape in detached cell culture conditions

The loss of cell-to-cell contact with surrounding cells and ECM induces an apoptotic process called anoikis. Usually, tumour cells develop resistance to anoikis and avoid this process [188]. We studied whether the addition of P144 affected the anoikis process under cell culture anchorage-independent conditions. Cells from A172 and U-87 MG cell lines were seeded in 6-well plates with Ultra-Low Attachment surface that prevents the adherent growth of cells to simulate conditions where the anoikis process can be induced. P144 at 100 $\mu\text{g}/\text{mL}$ was added and cells were harvested at different time points. Total protein concentration constitutes an indirect measurement of anoikis. This type of apoptosis is related with a decrease in total protein quantification [189-191].

As shown in Fig. 21, cell growth differences were observed depending on the cell line. A172 cells were not able to grow under detached conditions, the number of cells and spheres formed decreased over time. In contrast, U-87 MG cells were able to grow unattached and developed spheres that increased in size through time. The addition of P144 did not produce cell growth differences in A172 cells, but the size and number of spheres in U-87 MG cell line was affected specially after three days of culture. This observation was confirmed by quantification of total protein (Fig. 22). Total protein content was not affected by the addition of P144 and, in the case of the A172 cell line, remained stable throughout time. Only a decrease in protein levels was

detected at 4 h of treatment. U-87 MG cell line displayed a constant growth pattern under these conditions. The quantity of protein was increased throughout time and P144 produced a decrease in this parameter 3 days after treatment with a significant reduction after 7 days of treatment, coinciding with direct visual observation results.

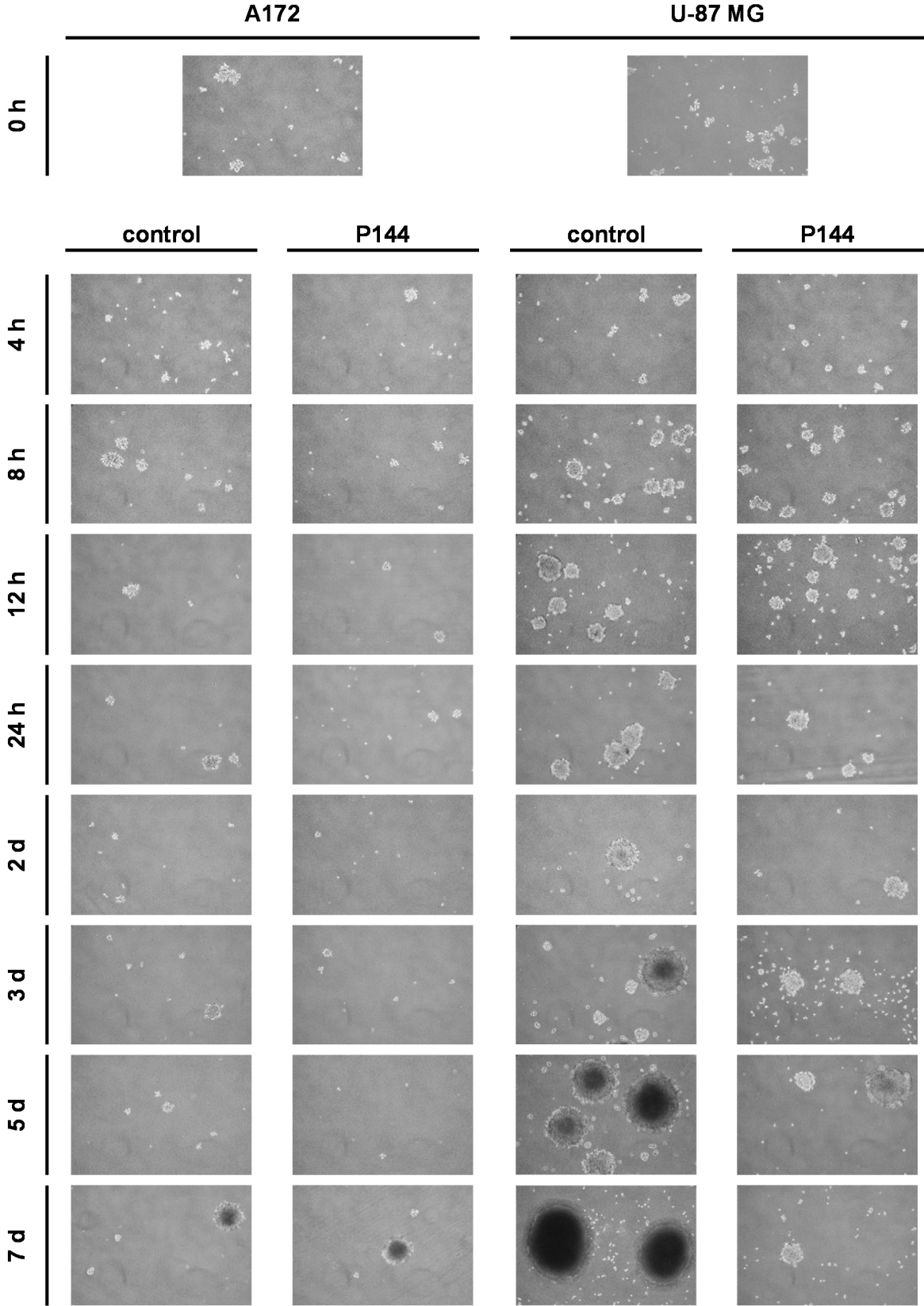


Figure 21. A172 and U-87 MG culture development under induced anoikis by anchorage-independent cell growth conditions. Cell lines were grown in Ultra-Low Attachment 6-well plates and cell culture images monitored through time in the absence or presence of P144. Time points are denoted as hours (h) and days (d).

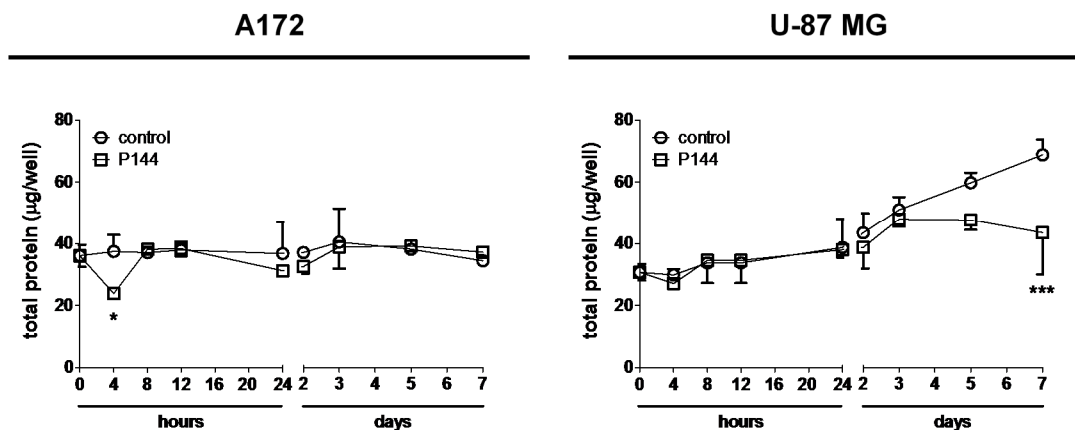


Figure 22. Total protein quantification of A172 and U-87 MG cells under anoikis induced culture conditions. A two-way ANOVA followed by Bonferroni as post hoc test was performed in order to detect significant differences ($p < 0.05$ (*)) and $p < 0.001$ (***) between control and cells treated with P144 throughout time.

Anoikis is an apoptotic process, and based on previous results of visual observation and protein quantification we decided to study apoptotic mechanisms by analysing protein obtained samples by western blot. The expression of BAX, a principal regulator of the apoptotic process, as well as the cleavage by caspases of Lamin A and Lamin C, were determined. In both cell lines, treated cells with P144 displayed an increase in the levels of Lamin A and Lamin C in contrast to the decrease observed in control cells between 4 h and 12 h (Fig. 23). The increase of Lamin A and Lamin C levels was more relevant in the A172 cell line. In addition, BAX levels were increased in both cell lines in a significant manner after 8, 12 and 24 h of treatment. Only U-87 MG cell line displayed a significant increase at day 7 of culture.

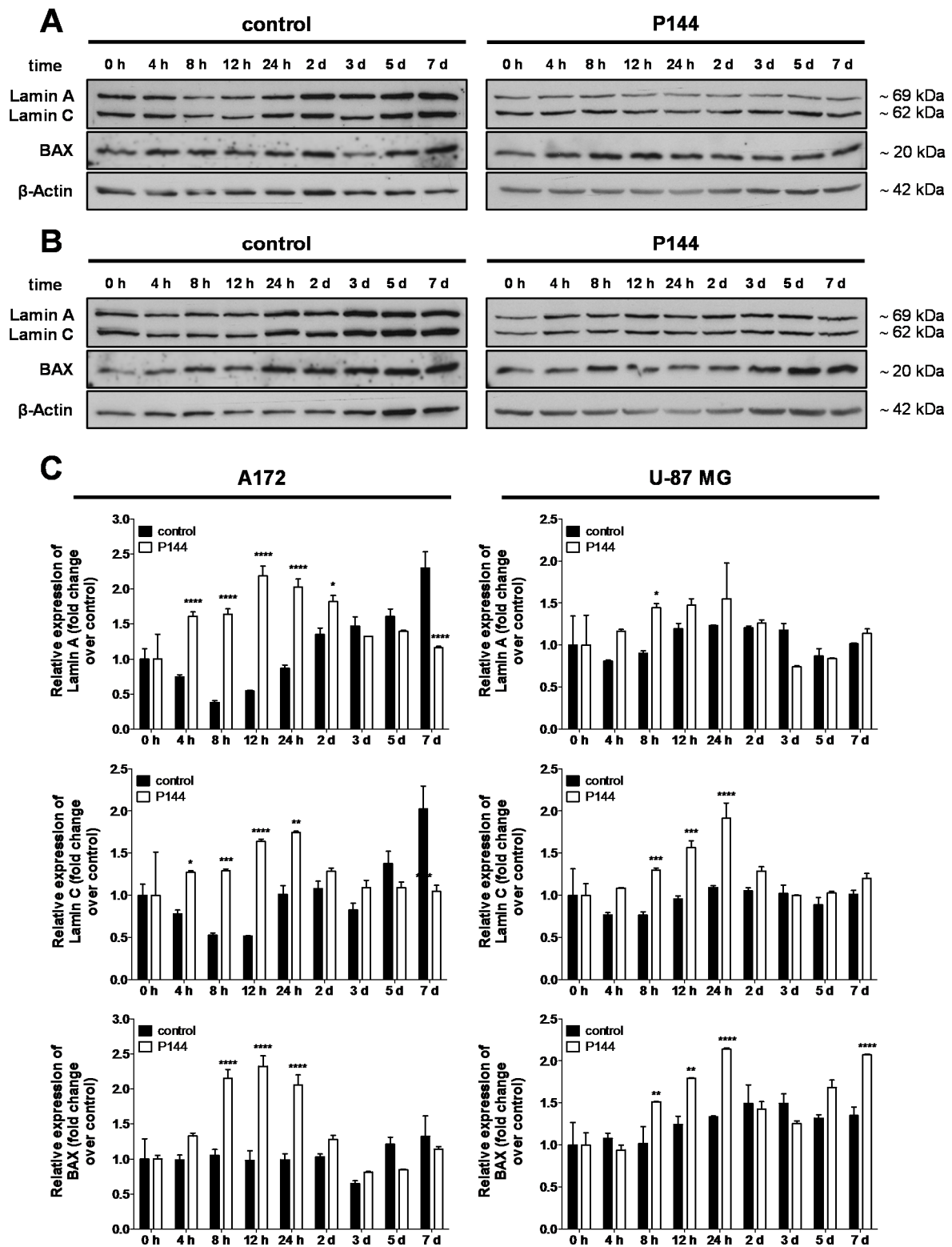


Figure 23. Apoptosis markers analysis in A172 and U-87 MG cell lines under anoikis induction. Protein levels of Lamin A, Lamin C, and BAX were determined by western blot analysis. Representative western blot images from two independent experiments are displayed for A172 (A) and U-87 MG (B) cell lines. In (C), the quantification of relative expression normalized to β -Actin. Asterisks represent significant differences between control and P144 treated cells at each time point, detected by two-way ANOVA plus Bonferroni post-test. Significance level was classified as follows: $p < 0.05$ (*); $p < 0.01$ (**); $p < 0.001$ (***) and $p < 0.0001$ (****).

1.5 P144 inhibits invasiveness and migration

In order to study whether P144 might impair the invasion and migration capacity of glioblastoma cell lines, two assays were performed. Invasiveness of A172 and U-87 MG cell lines were determined by matrigel invasion assay towards FBS [178] in the absence (control) or presence (treated) of P144. Results showed that P144 significantly suppressed cell invasion. In both cell lines, a significant decrease of invasiveness of almost 70% was observed when compared to control cells (Fig. 24).

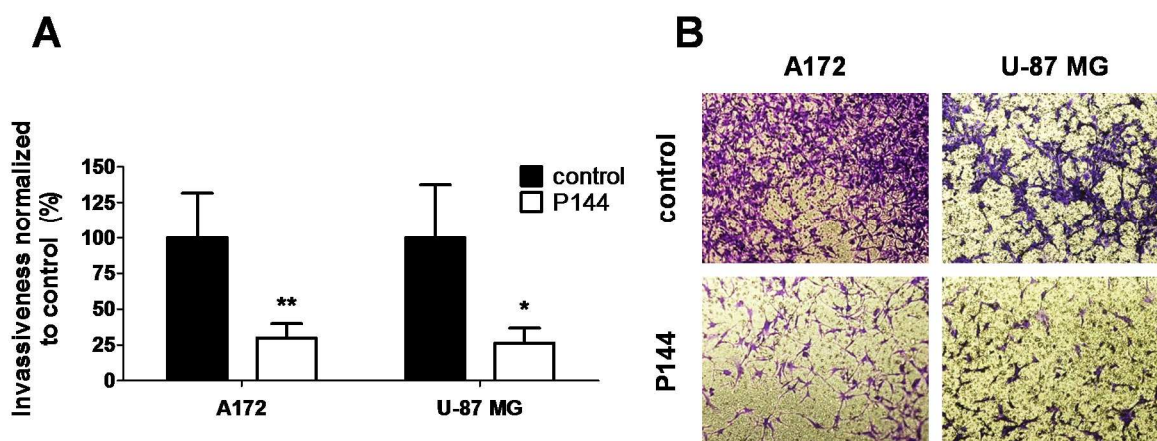


Figure 24. Matrigel invasiveness determination in commercial glioblastoma cell lines. (A) The percentage of invasiveness was calculated by the reduction in the area covered by stained cells normalized to control. Mean \pm SD of three replicates from three independent experiments are represented. Asterisks represent statistical difference (Mann-Whitney U test) for treated cells vs control ($p < 0.05$ (*)) and $p < 0.01$ (**)). In (B) representative images (100 \times of magnification) of each cell line and condition are displayed.

A scratch assay to analyse the inhibition of migration of cell lines treated with P144 was also performed. Cells were grown until total confluence was observed. Then, a scratch was made on the cell monolayer and wound healing was monitored until total coverage of control wounds was achieved (72 h for A172 cells and 48 h for U-87 MG cells). After 48 h in A172, and 24 h in the U-87 MG cell lines, the migratory potential was affected in cells treated with P144 in comparison to control cells (Fig. 25). These results confirmed that the addition of P144 at 100 $\mu\text{g}/\text{mL}$ was able to inhibit migration and invasion of glioblastoma cells *in vitro*.

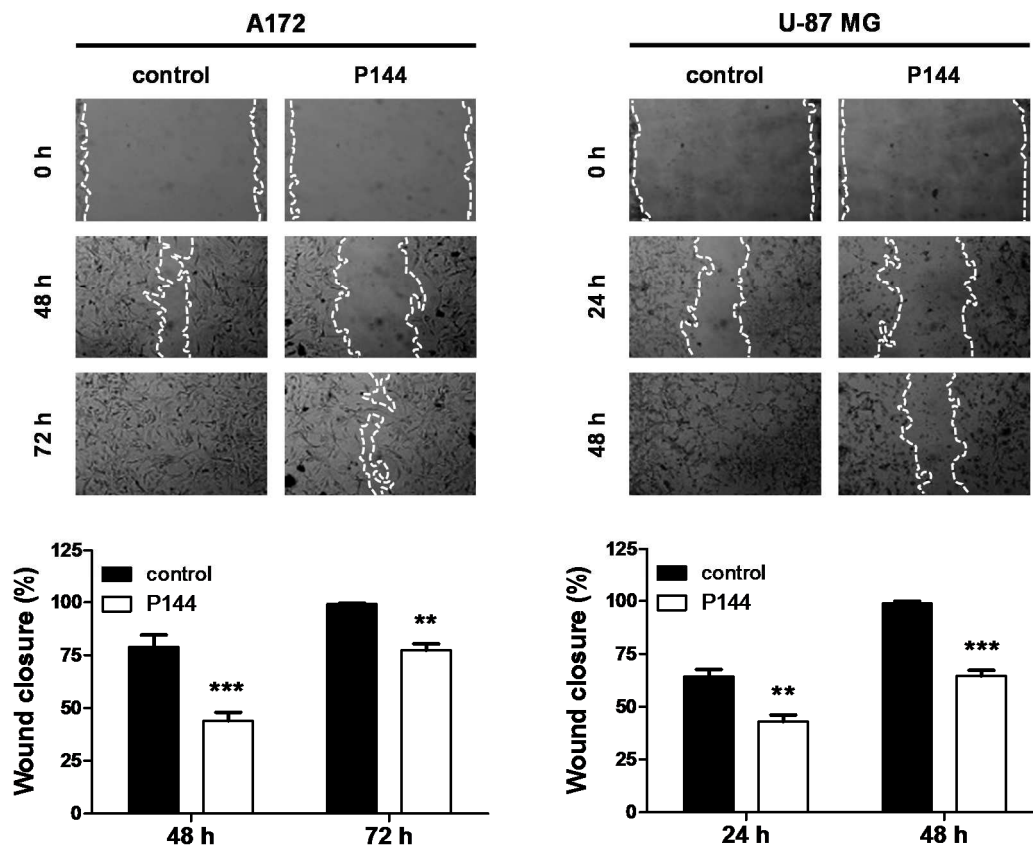


Figure 25. Wound healing assay for A172 and U-87 MG cell lines. Representative images at 100 \times of magnification from three independent assays are shown. The addition of P144 produce a delay in the total cover of the wound compared to control. White dotted lines delimit the cell-free area. The quantification of the assay is graphed. Two-way ANOVA and Bonferroni as post hoc test were performed. Asterisks represent statistical differences at each time point of control vs P144 treatment: $p < 0.01$ (**) and $p < 0.001$ (***).

1.6 P144 impairs tumorigenesis phenotype

The ability of a single tumour cell to survive and proliferate in anchorage-independent conditions is easily measured by a soft agar colony formation assay [192]. In addition, neurosphere formation provides information related to cellular transformation [193, 194]. To analyse whether inhibition of TGF- β signalling pathway produces changes in anchorage-independent growth and cellular transformation, A172 and U-87 MG cell lines were treated with P144 and quantified by colony formation grown in soft agar and by neurosphere formation assays, respectively.

A172 and U-87 MG cell lines were grown in soft agar in the absence or in the presence of P144 at 100 $\mu\text{g}/\text{mL}$, and incubated until colonies were visible at naked eye (4-6 weeks) (Fig. 26). The number of colonies produced by A172 cells was remarkably higher than U-87 MG cell line. P144 was able to significantly reduce colony numbers in a 66.5% for A172 cells and a 76.9% in the U-87 MG cell line. In addition, as shown in Fig. 26, colonies derived from the A172 cell line were

smaller than those produced by the U-87 MG cells. This result indicates that the tumorigenic potential in tested glioblastoma cell lines was significantly reduced by P144 treatment.

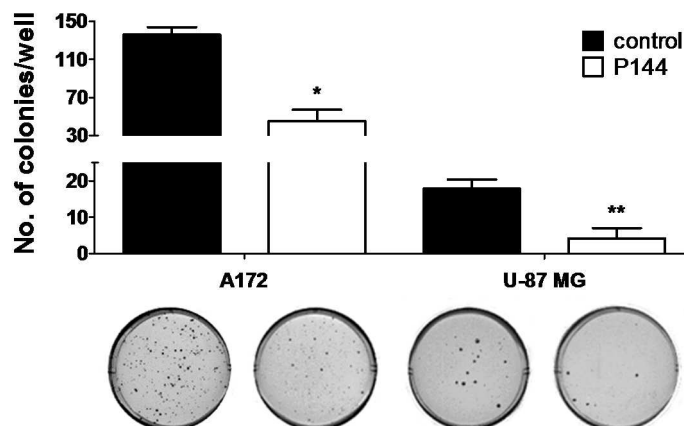


Figure 26. Colony-forming assay in soft agar for A172 and U-87 MG cell lines. The mean \pm SD of number of colonies counted at the end of the assay is represented. Below graph, photographs of most representative well for each condition are shown. Data were analysed by Mann Whitney U test ($p < 0.05$ (*) and $p < 0.01$ (**)).

Moreover, a significant decrease in number and size of neurospheres derived from cells treated with P144 was observed (Fig. 27A). A deeper analysis on the ability of glioblastoma cell lines to generate neurospheres was carried out. Primary neurospheres (obtained in passage 1) were dissociated, and equal number of viable cells were grown in fresh neurospheres medium to generate secondary neurospheres in the presence or absence of P144. The procedure was repeated until passage 3. The inhibitory effect of P144 on the generation of neurospheres increased in a passage-dependent manner in both cell lines (Fig. 27B).

In order to determine whether the decrease produced by P144 in neurosphere formation was due to the inability of cell lines to generate neurospheres in selective medium, the total number of viable cells and neurospheres only in the non-treated cells at each passage was analysed (Fig. 27D). Cell growth and neurospheres formation capacity of A172 in selective medium was maintained only until the 3rd passage, correlating with a significant decrease on viable cells and neurospheres throughout passages. In contrast, the U-87 MG cell line was able to grow and produce neurospheres during 15 passages with no significant reduction in number of viable cells or neurospheres (Fig. 27C and 27E).

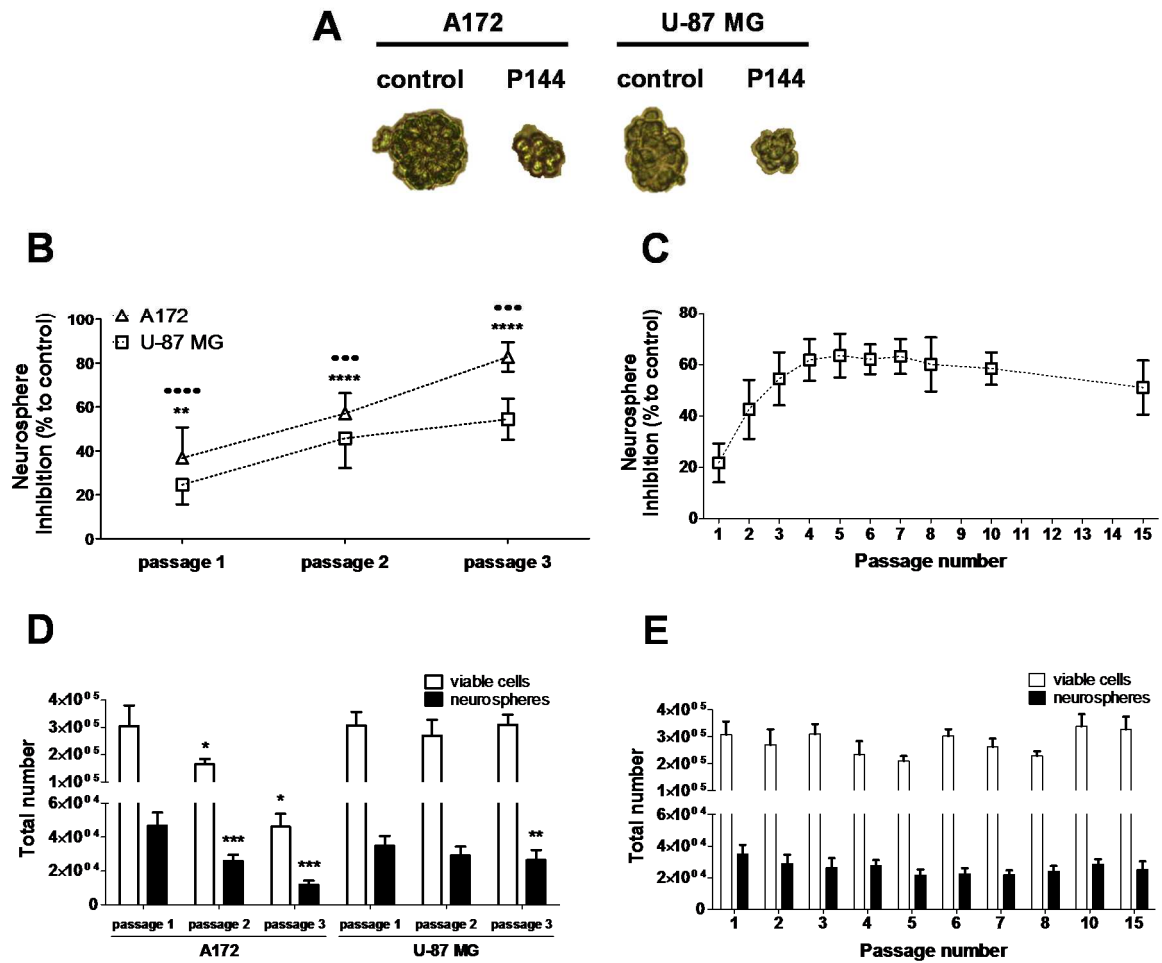


Figure 27. Neurosphere formation inhibition by P144 in A172 and U-87 MG cell lines. (A) Representative images of neurospheres showing the decrease in size and number of cells per neurosphere in P144 treated cultures. Neurosphere formation inhibition through three consecutive passages in both cell lines (B) and until passage 15 in U-87 MG cell line (C) are graphed. Mean \pm SD of percentage of inhibition of neurosphere formation from three independent assays are graphed. Statistical significance compared to control (100%) in each passage are represented in (A) by (•) for A172 and (*) for U-87 MG cell lines. The number of neurospheres and viable cells in non-treated cells until passage 3 in A172 and U-87 MG cells is shown in (D); and until passage 15 only for U-87 MG cells in (E). The statistical analysis in (B) was performed with Mann-Whitney U test and in (D) with Kruskal-Wallis test followed by Dunn multiple comparison test ($p < 0.05$ (*); $p < 0.01$ (**); $p < 0.001$ (***) and $p < 0.0001$ (****)).

2. BRAIN TUMOUR INITIATING CELLS (BTIC) LINES RESPONSE TO P144

2.1 Morphological culture characterization of BTIC under normoxia and hypoxia

Different BTIC lines were selected to determine the effect of P144 on these type of cells (Table 11). Cell culture and assays were carried out in normoxia (5%CO₂/21%O₂) and hypoxia (5%CO₂/3%O₂) conditions. In each assay and determination, the U-87 MG cell line was included for comparison reasons regarding the effect of P144 on BTIC lines. BTIC lines were grown in RHB-A[®] medium supplemented with growth factors (EGF and bFGF, both at 20 ng/ml). This medium allows the propagation, maintenance and expansion of human glioblastoma stem cell lines retaining their neurogenic capacity for over 100 mitotic cycles generations [195, 196].

No changes in cell morphology or size were observed under hypoxic culture conditions (Fig. 28). U-87 MG cells and pro-neural BTIC (RAV19 and RAV57 cell lines) grown in hypoxia displayed a lower growth rate compared to the cells grown in normoxia. In contrast, hypoxia increased the growth of RAV28 cells. In addition, cell adhesion was affected by hypoxic conditions, RAV28 cells grew with increased substrate attachment and cell to cell adhesion. On the other hand, RAV20 cells increased the amount of spheres observed, but maintained its mixed growth type. Finally, the RAV57 cell line displayed a mixed growth pattern under hypoxia, instead of the attached growth type observed in normoxia conditions.

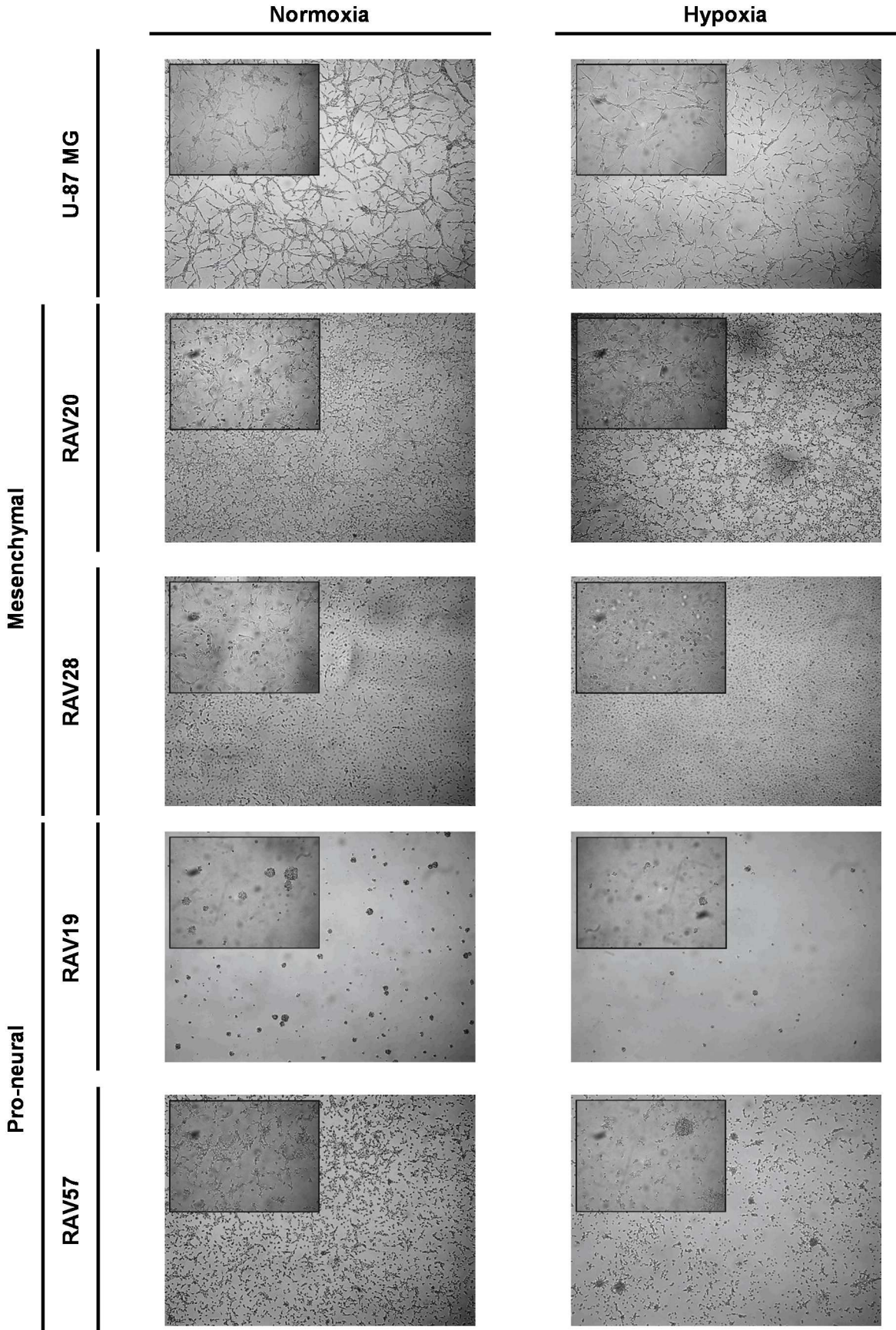


Figure 28. Culture morphology of U-87 MG and BTIC cell lines. Representative pictures (31.25× magnification and 125X inner square) of cell lines used in the present work showing growth characteristics under normoxia and hypoxia conditions.

In comparison with procedures related with the analysis of A172 and U-87 MG commercial cell lines (Results, section 1), two methodological modifications were included. First, P144 was completely dissolved in 100 mM Na₂CO₃ pH 9.5 in order to facilitate culture image analysis in 2D-migration assays, and provide a suitable carrier solution for the intracranial *in vivo* study (Results, section 5). Second, the concentration of P144 was increased from 100 µg/mL to 150 µg/mL, based on previous results where proliferation inhibition (by XTT assay determination) in BTIC was only achieved at high concentrations of peptide (150-200 µg/mL). In addition, proliferation was finally determined by direct count of viable cells due to high variation rate and low reproducibility of the XTT assay (Fig. 29).

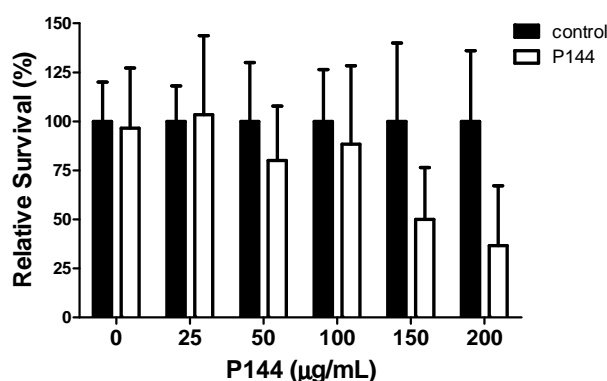


Figure 29. XTT-based proliferation assay determination. Representative data obtained by XTT assay in RAV20 cell line in the presence of different P144 concentrations.

2.2 BTIC cell lines express cancer stem cell markers

Expression levels in BTIC lines of some CSC markers were previously determined in the Neuro-Oncology Department at the University of Regensburg (Dr. rer. nat. Arabel Vollmann-Zwerenz) in passage 4 during isolation and enrichment of BTIC. The CD133 marker was not as highly expressed in normoxia as expected, but the hypoxic growth condition induced a significant increase in expression of this marker in pro-neural BTIC. Additionally, the growth of BTIC in selective media increased the detection of CD15 in all cell lines. The RAV28 cell line was an exception with no significant changes in detected levels of CD133 and CD15 markers, both in normoxia or hypoxia. The U-87 MG cell line exhibited lower values of expression of these stem cell markers, CD133 and CD15, both in normoxia and hypoxia (Table 17).

CD133 and CD15 detection differences are usually used to characterize stem cell subpopulations. Our data highlighted the heterogeneity of BTIC lines. These data confirmed the enrichment in cancer stem cell markers compared to U-87 MG. In the case of RAV28 cells, this

increase was not detected, at least at the initial cell line passages. U-87 MG constitutes a good reference cell line to compare if the effect of P144 on BTIC lines differs significantly due to enrichment and isolation of certain cell subpopulations in selective medium.

Table 17. Expression levels of stem cell markers in U-87 MG and BTIC lines under normoxia and hypoxia conditions.

		CD133		CD15	
		Normoxia	Hypoxia	Normoxia	Hypoxia
	U-87 MG	0.9	1.3	0.01	0.13
Mesenchymal	RAV20	10	7	13	24
	RAV28	0	1	0	0
Pro-neural	RAV19	3	28	39	21
	RAV57	0	58	10	25

Data are expressed as percentage of positive cells. Results from BTIC lines correspond to unpublished data.

2.3 P144 treatment decreases BTIC proliferation ratio

BTIC and U-87 MG proliferation ratio was assessed by direct counting, determining the number of cells that exclude trypan blue dye. All cell lines analysed did not show any difference in the growth pattern between control cells and cells treated with vehicle solution (100 mM Na₂CO₃). The U-87 MG cell line was the most sensitive to P144 antiproliferative effects. In all time points of treatment this cell line showed a significant statistical reduction in proliferation. In contrast, BTIC lines were less sensitive to P144. BTIC lines required 3 days of treatment to present significant changes in RAV19 cells, or even 7 days of treatment in the case of the RAV20 cell line under hypoxia conditions. In general, no remarkable differences in response to P144 between conditions (normoxia and hypoxia) were detected. Results are summarized in Fig. 30.

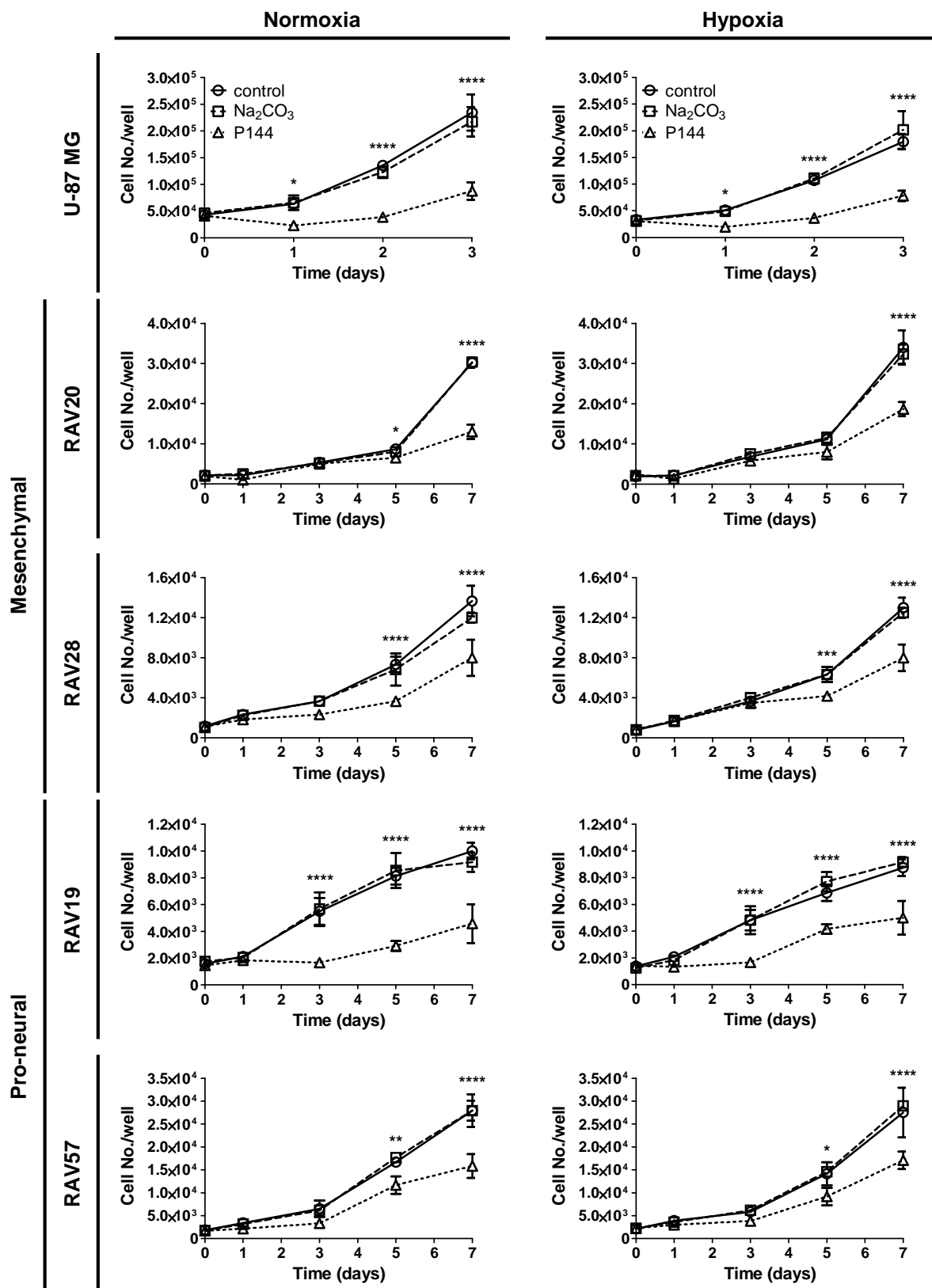


Figure 30. Proliferation analysis in U-87 MG cell line and selected BTIC lines. Data represent the number of viable cells at each time point. Two-way ANOVA and Bonferroni as post hoc test were performed. Asterisks represent statistical differences at each time point of control vs P144 treatment: $p < 0.05$ (*); $p < 0.01$ (**); $p < 0.001$ (***) and $p < 0.0001$ (****). No significant differences were found when control was compared to cells treated with 100 mM Na₂CO₃.

The expression of CSC markers differed between cell lines and conditions (Table 17) indicating that enrichment on BTIC or CSC subpopulation was not uniform across the BTIC lines. We analysed whether an initial change in cell density (and probable CSC subpopulation proportional change) affected the sensitivity to P144 and had an impact on proliferation. For this objective, we studied proliferation only when the maximal reduction was produced in each cell line (3 days for U-87 MG cells and 7 days for BTIC lines). Different numbers of initial cells were tested and a control of non-treated cells for each cell density was included.

There was no variation in results depending on the initial density in the U-87 MG cell line, only a slight increase in the quantity of cells recovered after treatment with P144 at higher density (Fig. 31). BTIC lines showed changes on proliferation in response to P144 according to the initial cell number. RAV20 and RAV19 cells were particularly affected by density both under normoxia and hypoxia conditions, displaying a loss of the effect at high initial cell density. Despite the higher growth ratio of the RAV28 cell line, P144 was able to inhibit proliferation in the same level, in spite of the initial number tested.

RAV57 cells displayed a different behaviour. The cell density did not influence the P144 effect under normoxia. P144 was able to abolish the proliferation in the initial cell densities analysed. Under hypoxia, at the higher cell density examined (30,000 cells), P144 did not produce an effect in proliferation. However, in the other initial cell density analysed, the proliferation under hypoxia conditions with P144 reached similar levels to those observed under normoxia.

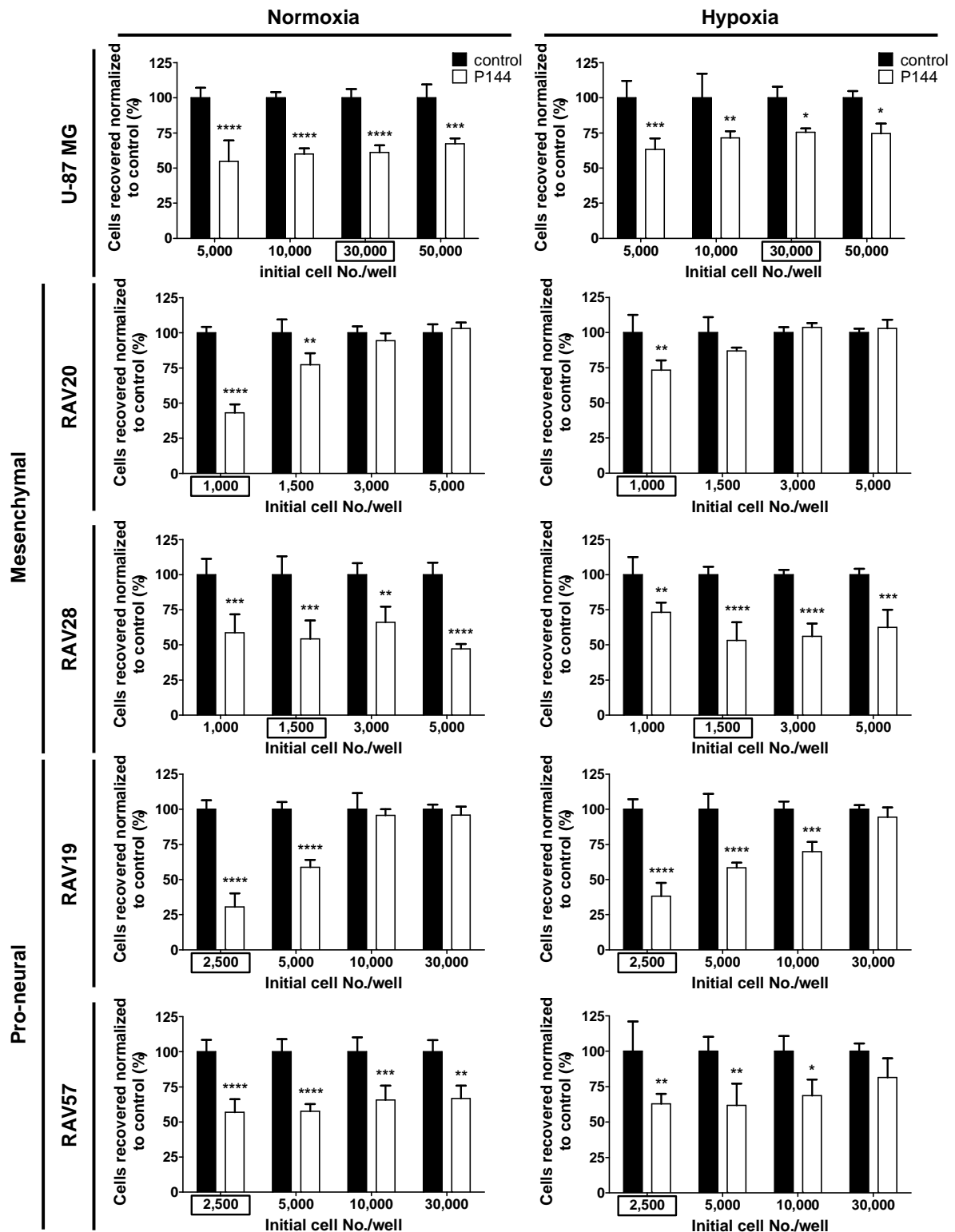


Figure 31. Proliferation analysis at different initial cell density. The Y-axis represents the percentage of viable cells recovery after treatment normalized to control. Numbers in X-axis are the initial number of cells tested. Two-way ANOVA with Bonferroni test to multiple comparisons was carried out. Statistical differences are indicated as follows: $p < 0.05$ (*); $p < 0.01$ (**); $p < 0.001$ (***) and $p < 0.0001$ (****). Values highlighted in a box indicates the initial cells that were tested in the time-course proliferation analysis (Fig. 30).

2.4 P144 treatment impairs clonogenic survival

Clonogenic assays are used to analyse the capacity of a single cell to produce a progeny, a characteristic associated with CSC activity, and how this parameter is affected by a specific treatment [180]. Using limiting dilutions, 1 and 5 cells/well were plated in flat-bottom 96-well plates and treated with P144 to study its effect on clonogenicity. After 1-3 weeks, clones were counted. The analysis of the data was carried out by quantification of plate efficiency (PE = number of clones counted/number of cells plated) and surviving fraction (SF = number of clones counted/[number of cells plated × PE]) [180]. Since PE is depending on the cell line and the cell number plated, the SF was independently calculated for each cell line and for each initial number of cells tested in the presence of P144.

Despite that control cell clone morphology was not affected in normoxia compared to hypoxia growth conditions (Fig. 32), a morphological modification was detected in U-87 MG, RAV20 and RAV57 clones treated with P144.

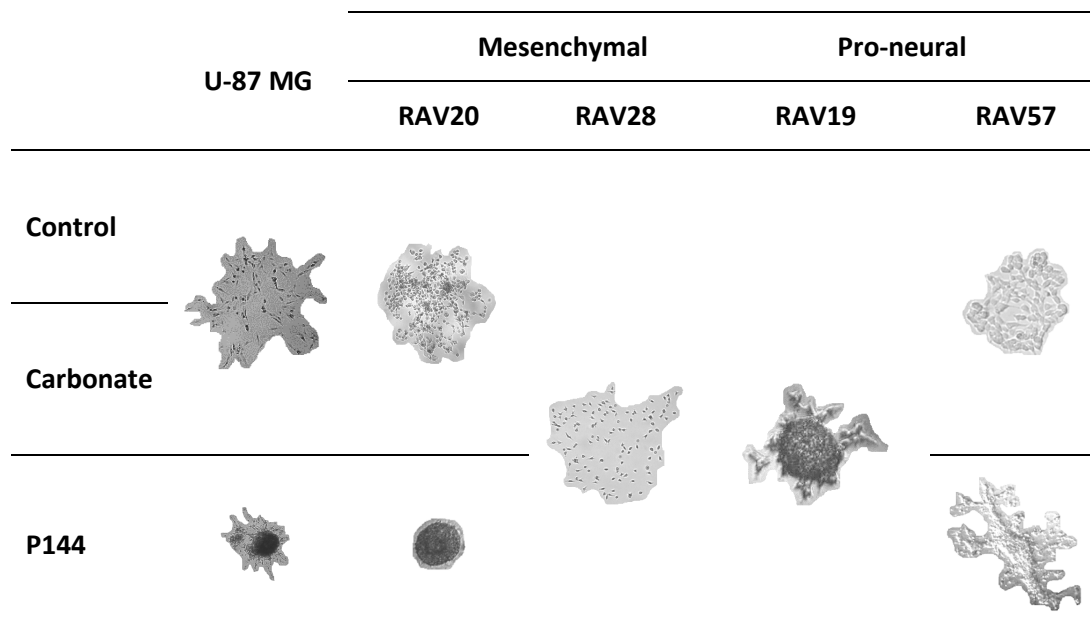


Figure 32. Clonogenic assay derived clones morphology. Representative pictures of clones observed in analysed cell lines in control and treatment groups are shown.

As expected, variation in values of PE were found in the cell lines analysed, since this parameter is characteristic of each cell line (Table 18). The treatment with Na₂CO₃ did not affect the SF in the studied cell lines. The values of clones obtained (SF_{Carbonate}) were near to 100%, indicating an absence of Na₂CO₃ effect in clonogenicity. On the contrary, P144 reduced the percentage of cells able to form colonies in all cell lines and growth conditions: from 44.4% to

63.2% in U-87 MG cells and from 14.9% to 71.1% in BTIC lines. Hypoxia only produced lower percentages when compared to normoxia on SF_{P144} in the U-87 MG cell line and in mesenchymal BTIC in both initial cell numbers tested. In the pro-neural BTIC a clear behaviour was not observed. RAV19 and RAV57 displayed variations in the SF_{P144}, and no correlation with the initial number of cells or growth condition was observed.

Table 18. Clonogenic assay analysis.

	Mesenchymal						Pro-neural				
	U-87 MG			RAV20		RAV28		RAV19		RAV57	
	c/w	N	H	N	H	N	H	N	H	N	H
PE	1	11.7	15.0	21.7	70.0	73.3	43.3	28.3	20.0	30.0	18.3
	5	12.7	12.0	11.7	15.7	30.0	10.7	15.3	31.0	30.3	15.7
SF_{Carbonate}	1	114.3	88.9	92.3	104.8	95.5	88.5	94.1	108.3	105.6	90.9
	5	84.2	111.1	94.3	97.9	105.6	90.6	104.3	89.2	98.9	93.6
SF_{P144}	1	57.1	44.4	46.2	59.5	61.4	53.8	47.1	58.3	55.6	36.4
	5	63.2	50.0	22.9	14.9	71.1	53.1	67.4	61.3	31.9	36.2

Numerical data except cells per well represents percentages. **c/w**: plated cells per well. **N**: normoxia. **H**: hypoxia. **PE**: plate efficiency. **SF_{Carbonate}**: Survival Fraction of cells treated with 100 mM Na₂CO₃ solution. **SF_{P144}**: survival fraction of cells in presence of P144.

2.5 P144 inhibits migration in 2D assays

BTIC lines migration was assessed with two different methodologies, wound healing assay and spheroid assay. In the first one, cells were monitored at different time points until wound closure. Due to the fast growth rate of RAV28 cells, was non-possible to set up the optimal conditions to analyse its migration capacity through wound healing assay. In the other cell lines, no significant differences were detected between vehicle control solution (Na₂CO₃) and non-treated cells (Fig. 33 and 34). In contrast, the migration inhibition displayed by P144 was significant in comparison to the non-treated control in all cell lines. P144 totally abolished the wound healing process in U-87 MG cell line under normoxia and hypoxia conditions. In BTIC lines, migration was also inhibited but at a lower extent than the U-87 MG reference cell line. In all cell lines hypoxia induced a delay in wound closure.

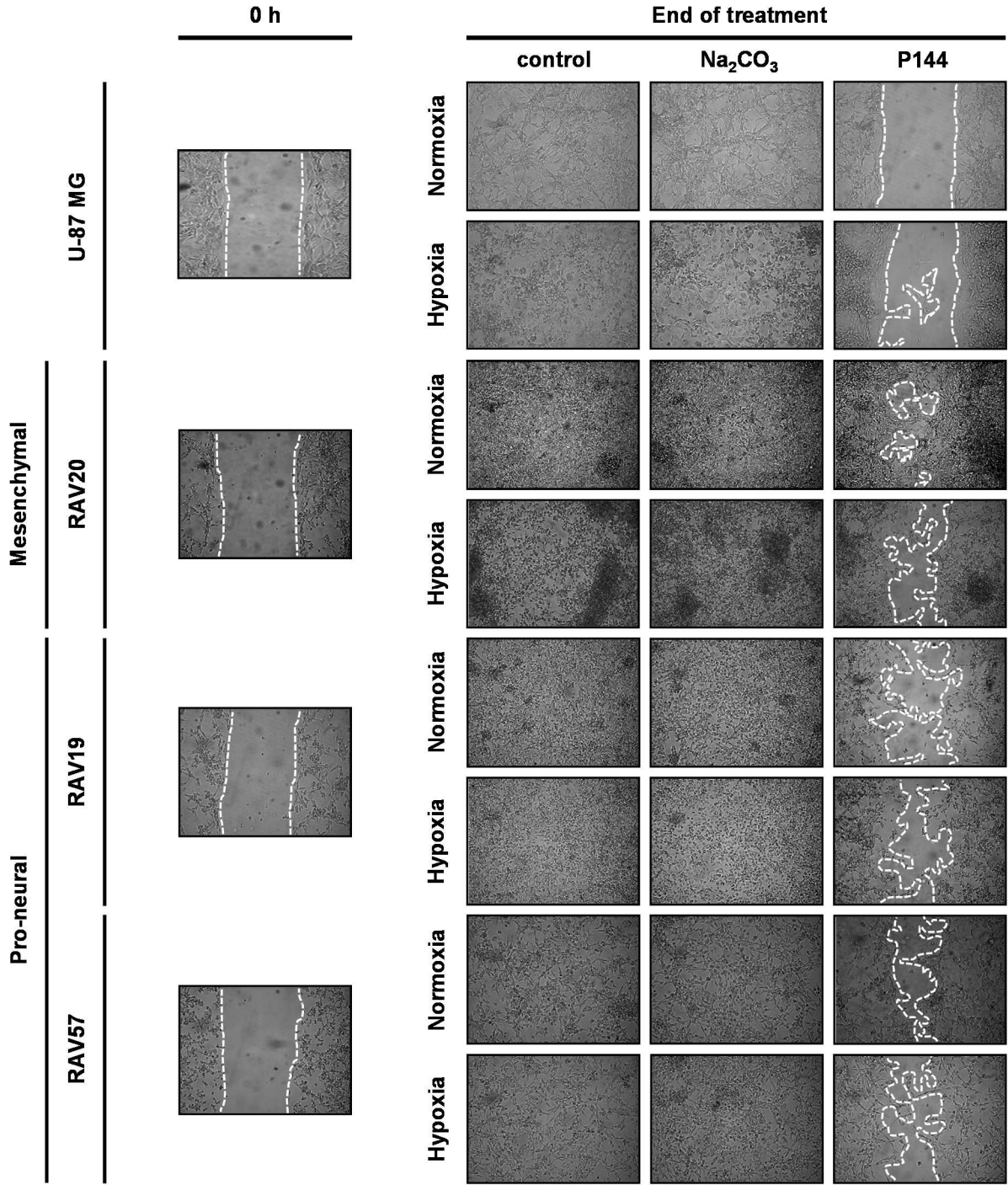


Figure 33. Wound healing assay in U-87 MG and BTIC lines. Representative images (125× of magnification) at time 0 h (left panel) and at the end of treatment in normoxia and hypoxia conditions (right panel) of wound healing assay. Dotted lines circumscribe the cell-free area.

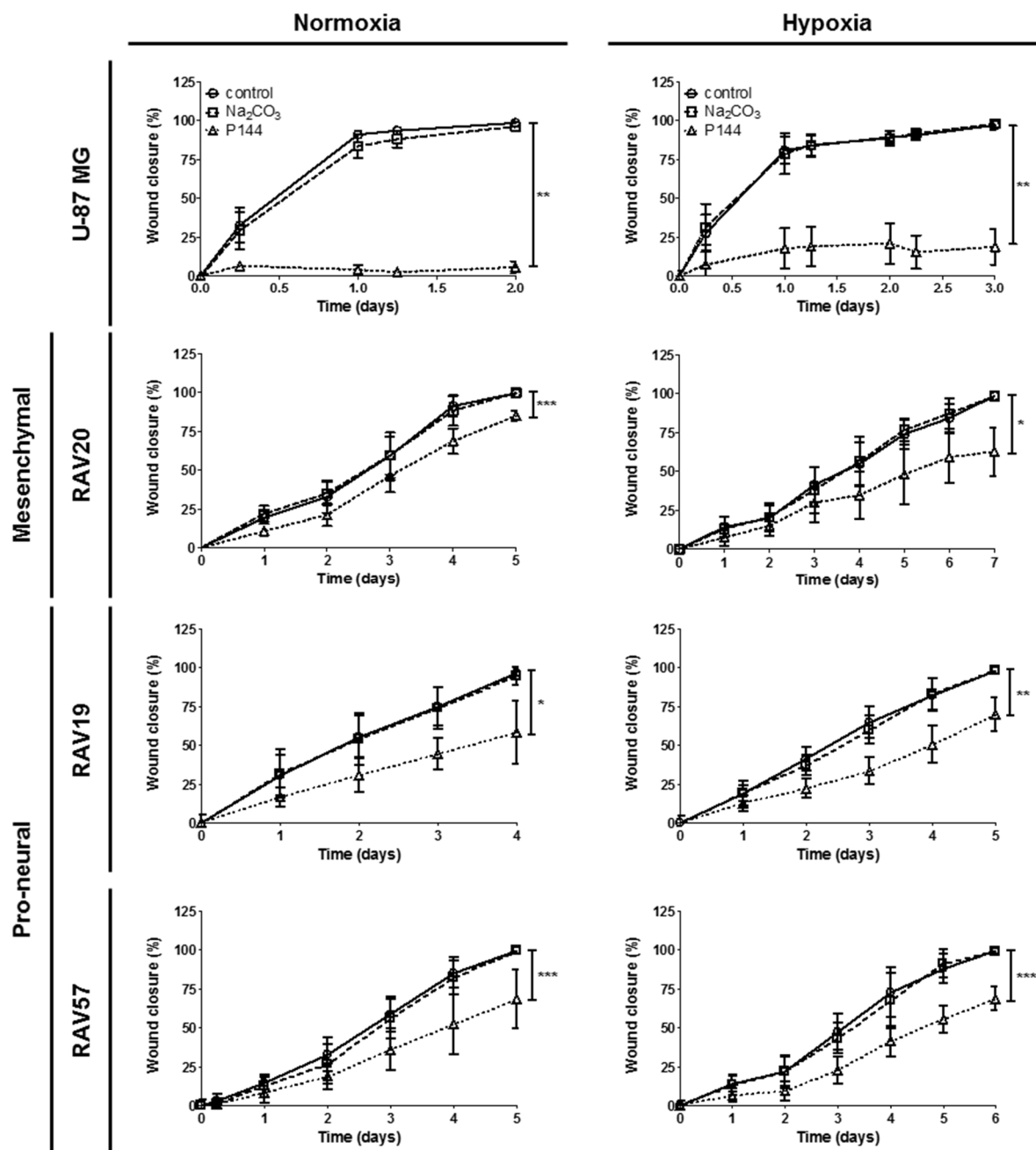


Figure 34. Quantification of wound healing assay in U-87 MG and BTIC lines. The percentage of initial cell-free area covered by cells over time is graphed. Statistical analysis was carried out by one-way ANOVA with Friedman test for repeated measurements and Dunnett as test for multiple comparisons. Asterisks represent the significance of P144 treatment compared to control: $p < 0.05$ (*); $p < 0.01$ (**); and $p < 0.001$ (***). No significant differences between control and Na_2CO_3 solution were found in all cell lines tested.

In order to analyse the influence of cell passage number, three independent assays were performed in U-87 MG and BTIC lines using consecutive passages. Migration measured by wound healing assay was not affected by passage number except in the RAV57 cell line under normoxia (Fig. 35). The RAV57 cell line showed smaller cell-free areas in consecutive passages. The influence of passage number over the wound closure process was not observed in the control or vehicle

group. Correlation between RAV57 passage number and increasing resistance to P144 was analysed for each passage treated with P144 compared to control. The P144 migration inhibition at passage 3 was not significant compared to control group.

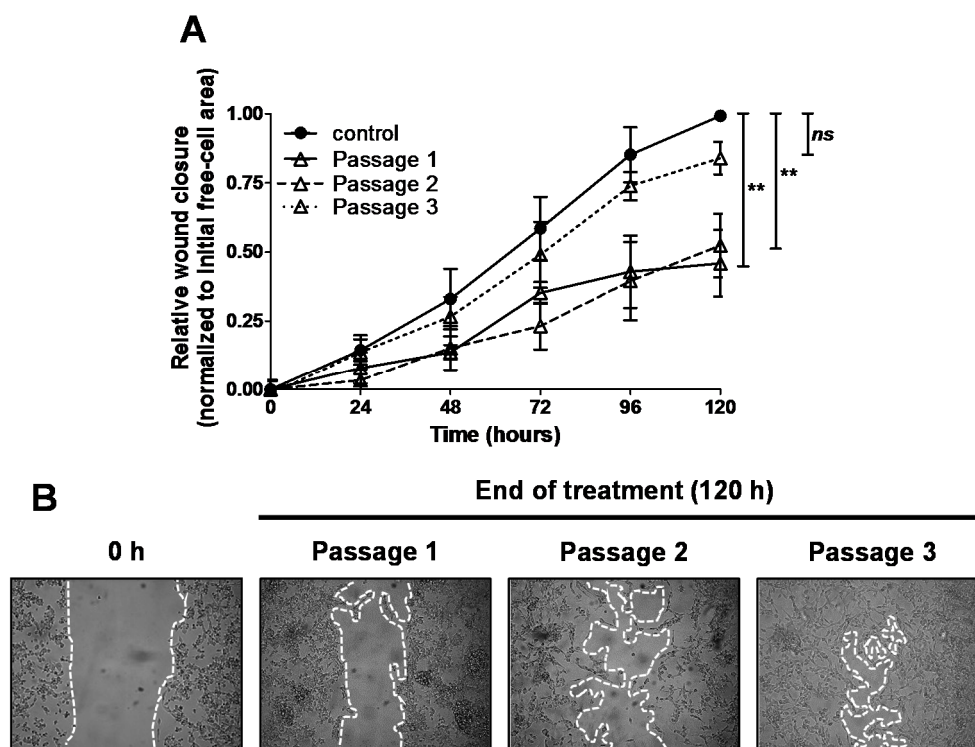


Figure 35. RAV57 cell passage number effect over P144 migration inhibition in wound healing assay. (A) Relative wound closure in treated group normalized to control at different passages. (B) Representative images (125 \times) at 0 h (control) and each passage at the end of treatment (120 h) in the presence of P144. Significance level is denoted by asterisks ($p < 0.01$ (**)).

Spheroid assay was analysed by observation and migration area measurement over time. Similar results in comparison to wound healing assay were obtained. No significant differences were found between non-treated cells and cells treated with the vehicle solution. The migration area developed by the U-87 MG cell line was inhibited with P144 (around 90%) under normoxia and hypoxia. All BTIC lines developed lower rates of inhibition in comparison to P144 treated U-87 MG cell line. RAV20 and RAV19 cell lines displayed low migration capacity under hypoxia. In contrast, the RAV28 cell line displayed a high migration ratio under hypoxia, and developed a higher migration area compared to normoxia control. Significant differences were found in all cell lines and conditions tested, except for the RAV57 cells under normoxia, which showed no P144 effect. Results corresponding to spheroid assay are summarized in Fig. 36 and 37.

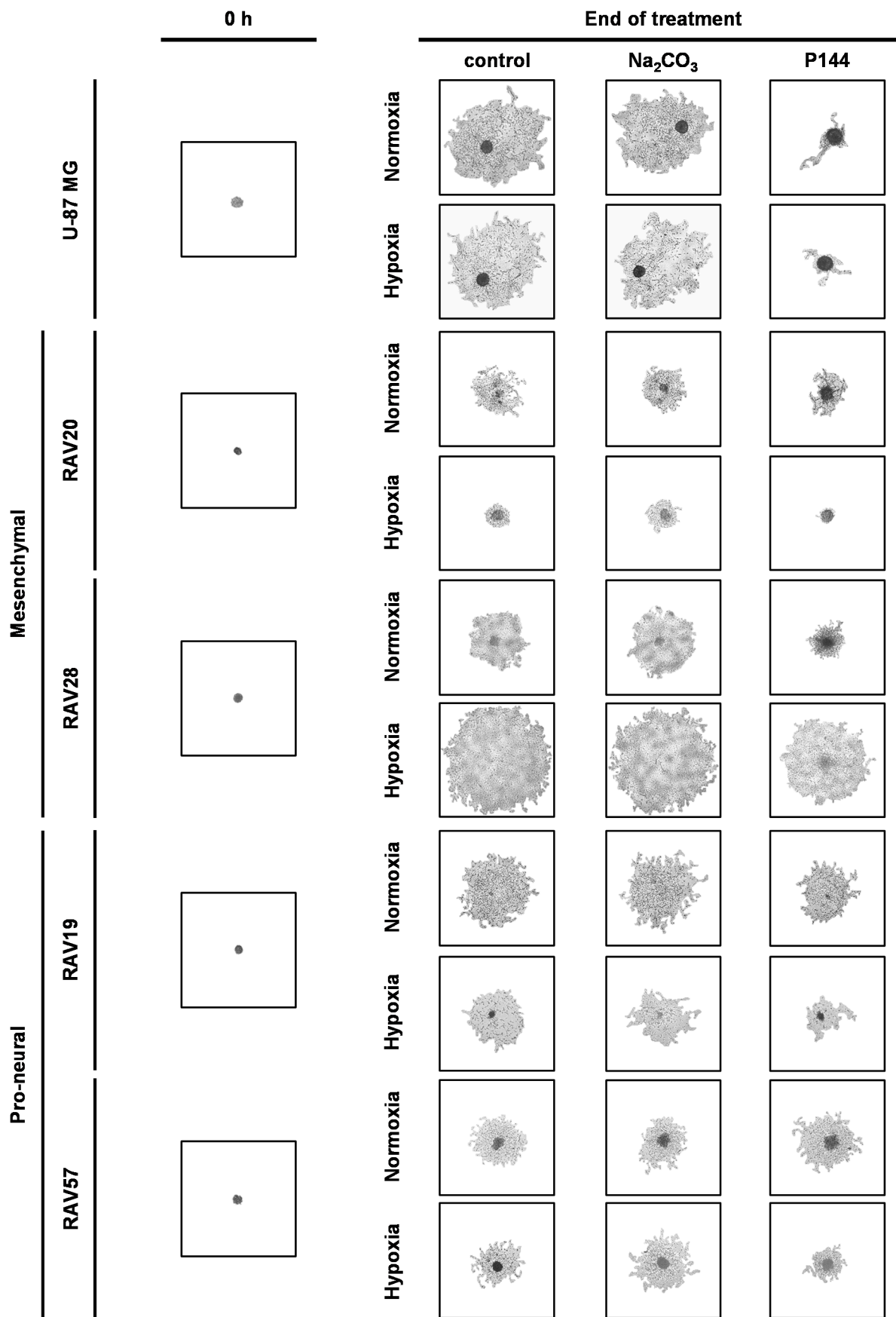


Figure 36. Spheroid assay in U-87 MG and BTIC cell lines. Representative images (31.25×) of initial sphere (left panel) and at the end of treatment under normoxia and hypoxia conditions (right panel). The end of treatment was adjusted to each cell line according the migration pattern in the spheroid assay.

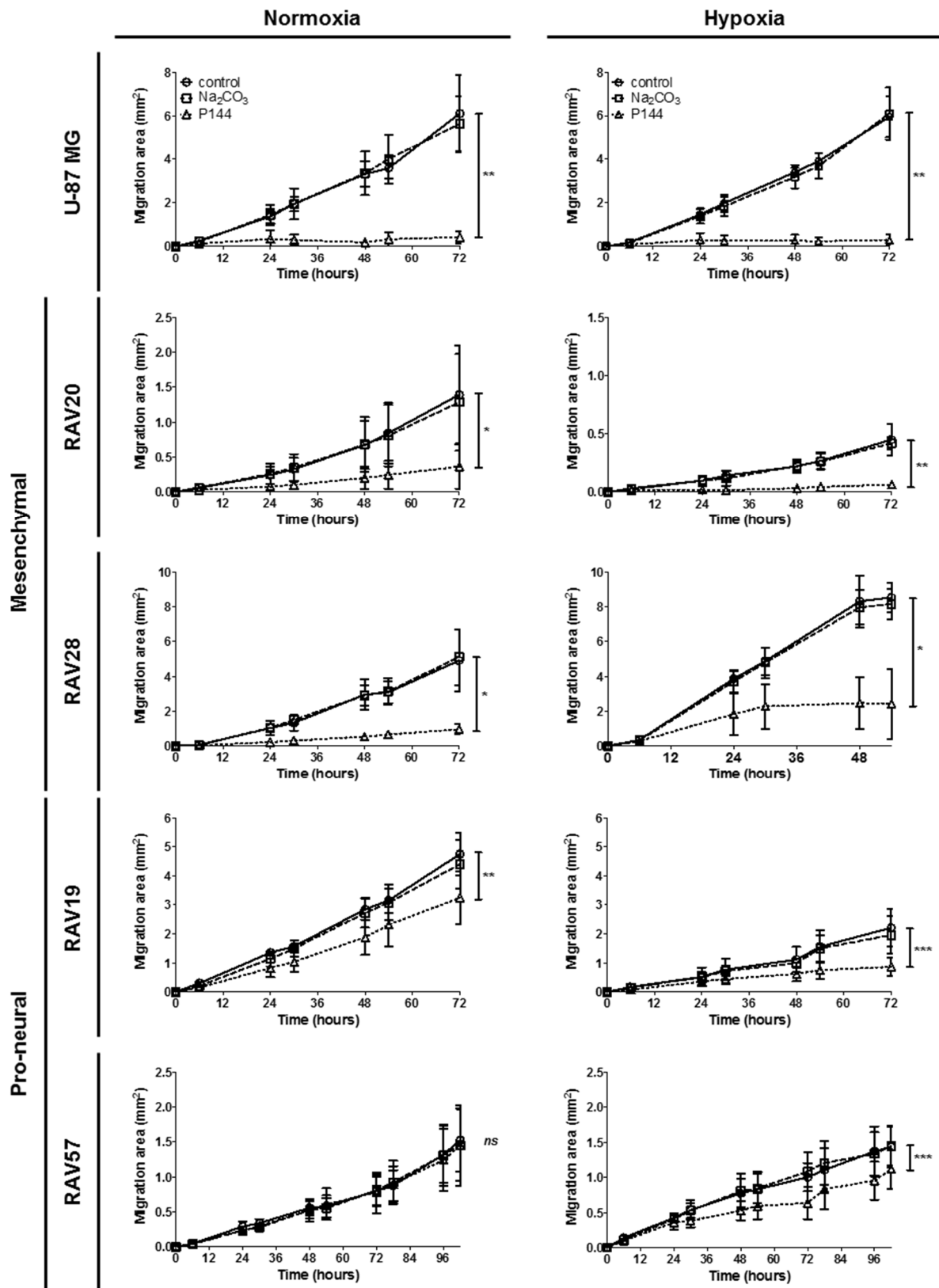


Figure 37. Migration capacity quantification by spheroid assay. Cell migration generated area (mm²) was calculated as the total final area minus the initial core area. Non parametric one-way ANOVA with Friedman test and Dunnett as post hoc test were applied for statistical differences identification. Significance of P144 treatment compared to control is indicated by asterisks ($p < 0.05$ (*); $p < 0.01$ (**); $p < 0.001$ (***)) and no significant by *ns*. In all cell lines, no significant differences between control and Na₂CO₃ solution group were found.

As the RAV57 cell line behaviour in the wound healing assay, RAV20 and RAV19 cell lines were influenced by the passage number. RAV20 cells under normoxia conditions increased their migration capacity as passage number augmented. The non-treated cells increased the migration area in consecutive passages (Fig. 38A). P144 treated spheres apparently showed a loss of response to the peptide. The area of migration in the P144 treated cells was enhanced directly by the passage number. At the same time, RAV19 cells exhibited a change in the behaviour through passages under hypoxia, but instead of increasing its migration capacity, area decreased according to passage number in non-treated spheres (Fig 39A). Spheres treated with P144 displayed a slight decrease in the migration area as passaged number increased.

Despite these observations, further analysis demonstrated an equivalent level of cell migration inhibition by P144 between the three passages analysed in the cell lines RAV20 and RAV19 (Fig. 38B and 39B): cell passage did not influence the response to P144, but increased the migration capacity in the RAV20 cell line and inhibited it in RAV19 cells.

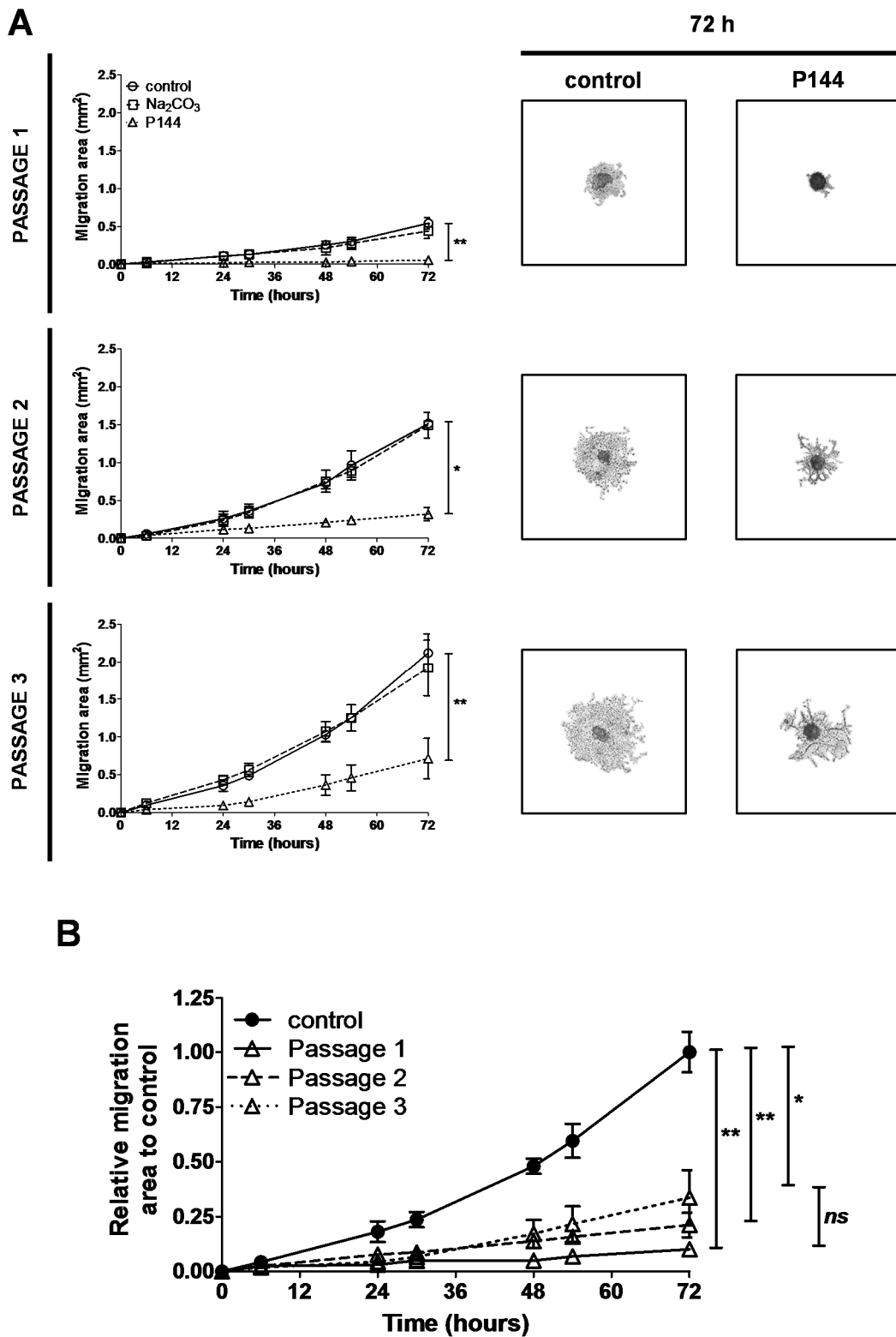


Figure 38. RAV20 cell line migration analysis through passages under normoxia conditions in spheroid assay. (A) Migration area (mm^2) replicates average. Representative images ($31.25\times$) of control and treated spheres are shown in the right panel. (B) Values of relative migration areas of control and treated groups at each passage. One-Way ANOVA with Tukey post hoc test for multiple comparisons confirmed that migration decrease in the treated groups was not affected by passage number. Significance is indicated as follows: $p < 0.05$ (*) and $p < 0.01$ (**).

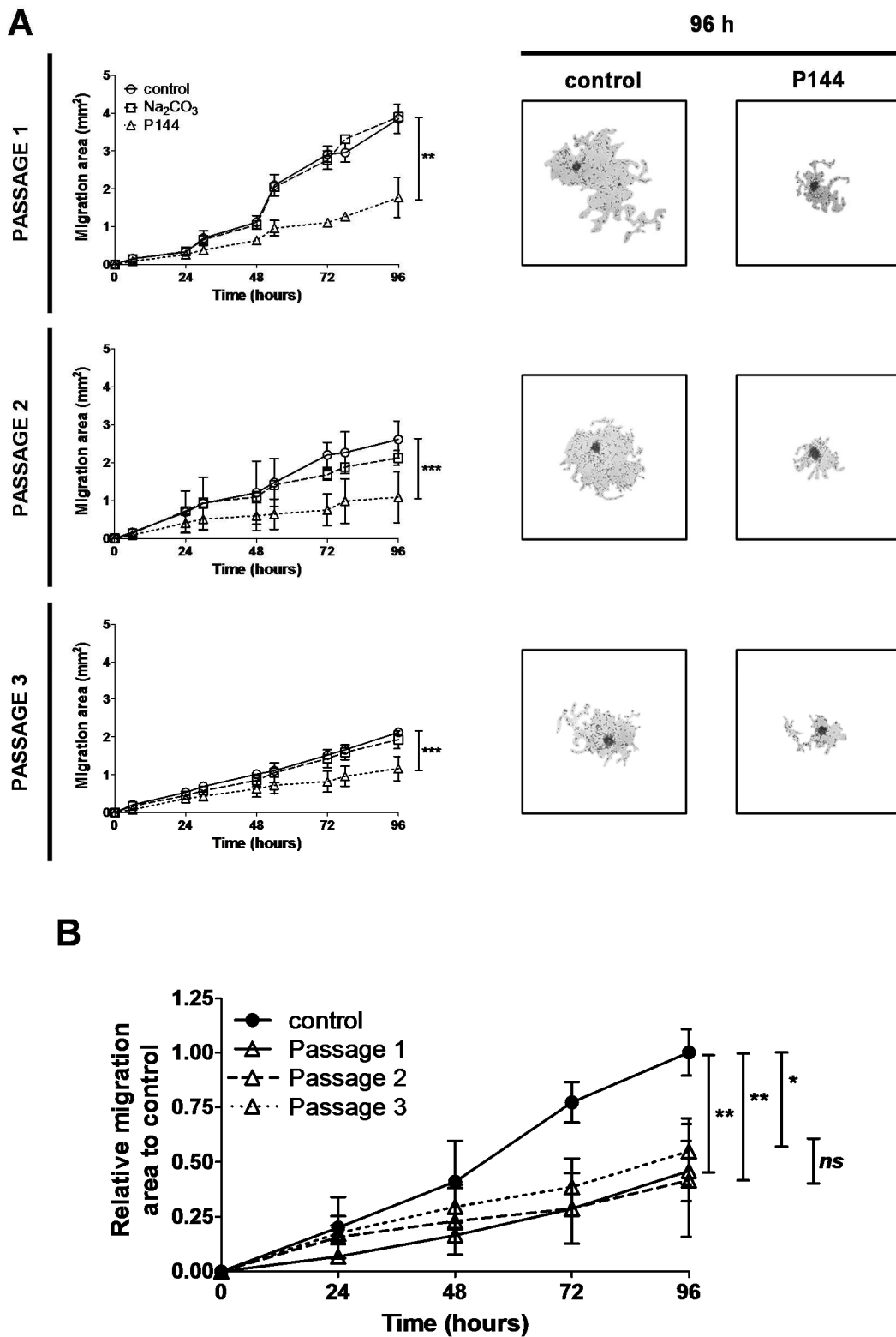


Figure 39. RAV19 cell line migration analysis through passages under hypoxia conditions in spheroid assay. (A) Migration area (mm²) from replicates average over time (left panel) and representative Images (31.25×) of spheres migration at 96 h are included (right panel). (B) Relative migration areas. One-Way ANOVA with Tukey as post-test for multiple comparisons were carried out. Significance is denoted by asterisks ($p < 0.05$ (*); $p < 0.01$ (**); $p < 0.001$ (***)).

2.6 P144 cellular type-dependent inhibition activity

In order to perform a global comparison between the cell line of reference U-87 MG and BTIC lines under normoxia and hypoxia, the inhibition exerted by P144 treatment was calculated. For this purpose, data from proliferation, wound healing and spheroid assays were collected. P144 inhibiting values were normalized to values from non-treated cells and expressed as “percentage of inhibition” for each assay (Table 19). This percentage represents the maximum decrease observed after the P144 treatment (normalize to non-treated cells) for each cell line and assay performed. Data from the clonogenic assay did not represent a statistical representative sample and were not included in the analysis.

The inhibitory percentage values were analysed following different statistical methods. The two-way ANOVA allows variance discrimination from two sources of variation. In this case, cell line and oxygen culture conditions. The two-way ANOVA was performed in order to determine significant differences between: the two culture conditions, normoxia and hypoxia, and between U-87 MG cell line and BTIC lines. The effect of culture condition at each cell line was carried out by t-test method. The corresponding mentioned analyses showed that:

(i) P144 produced a lower inhibition of proliferation under hypoxia condition when compared to normoxia ($p=0,024$). This result suggests that under hypoxia, cells are more resistant to P144 activity. In addition, when BTIC lines were compared to U-87 MG, no significant differences were detected, indicating that P144 produced the equal effect on proliferation in all studied cell lines. Only RAV20 cell line showed a significant difference between normoxia and hypoxia, suggesting a resistance of this cell line to the effect of P144 under hypoxia.

(ii) Hypoxia did not affect the P144 effect on migration (analysed by wound healing assay). However, significant differences were found when BTIC lines were compared to the U-87 MG cell line. BTIC cell lines analysed displayed lower inhibition rates than the U-87 MG cell line. These differences were statistically significant both under normoxia or hypoxia conditions. In addition, the pair comparison in each cell line between normoxia and hypoxia showed a significant difference in U-87 MG, RAV20 and RAV19 cell lines, but not in RAV57 cells, suggesting that the effect of P144 could be related to the cell line type rather than growth conditions.

(iii) Percentages of inhibition from spheroid assay revealed that hypoxia produces a significant impact in the activity of P144 ($p < 0.0001$). In addition, mesenchymal BTIC did not show significant variations compared to the U-87 MG cell line, indicating that P144 produces similar levels of inhibition in RAV20 and RAV28 cell lines. Only pro-neural BTIC (RAV19 and RAV57 cell lines) presented significant differences compared to the U-87 MG cell line, and hypoxia had a significant influence in the P144 effect over this cell lines. This fact indicates that both pro-neural

cell lines were more resistant to P144 migration inhibitory activity and hypoxia clearly affects this response.

Table 19. Percentage of inhibition observed in proliferation, wound healing and spheroid assay in the presence of P144.

		U-87 MG		Mesenchymal				Pro-neural			
				RAV20		RAV28		RAV19		RAV57	
		N	H	N	H	N	H	N	H	N	H
Proliferation	\bar{X}	62.67	56.52	56.91	45.1	41.46	38.46	54.17	42.86	43.28	37.88
	\pm SD	7.02	5.43	5.97	5.16	13.19	10.18	14.43	14.29	9.32	6.94
	Sign.	c		c, d		c		C		c	
Wound Healing assay	\bar{X}	94.44	78.81	17.79	36.41	-	-	43.06	28.88	39.00	34.39
	\pm SD	3.924	10.76	5.325	15.58	-	-	17.91	11.12	20.08	10.18
	Sign.	d		a, b, d		-		a, b, d		a, b	
Spheroid assay	\bar{X}	89.35	94.50	78.39	85.49	81.38	79,28	32.43	57.59	8,694	25.32
	\pm SD	6.48	5.13	12.39	7.56	3.06	12,60	15.97	17.03	10,67	13.99
	Sign.	c		c		c		a, b, c, d		a, b, c, d	

N: normoxia. **H:** hypoxia. \bar{X} : Percentage of inhibition mean. **SD:** standard deviation. **Sign.:** statistical significance observed in different comparisons carried out. Letters indicate statistical significance ($p < 0.05$) in groups comparisons performed: (a) U-87 MG vs each BTIC in normoxia, (b) U-87 MG vs each BTIC in hypoxia, (c) global comparison normoxia vs hypoxia, (d) comparison normoxia vs hypoxia in each cell line. Two-way ANOVA with Bonferroni post-test for multiple comparisons were carried out. For (d), the parametric t-test was performed.

2.7 P144 inhibition correlates with CSC markers expression

When P144 inhibition values obtained for each cell line and assay (Table 19) were correlated with CSC expression markers (Table 17), data displayed a plausible negative correlation (Fig. 40). The expression of CD133 or detection of CD15 was negatively correlated with P144 effect, indicating a probable resistance to P144 related with the CSC expression markers. Although no significant correlation was detected for CD133 (Fig. 40A), a significant negative correlation for CD15 detection ($p = 0.0158$) was found (Fig. 40B). Then, correlation analysis was performed comparing culture conditions (normoxia and hypoxia).

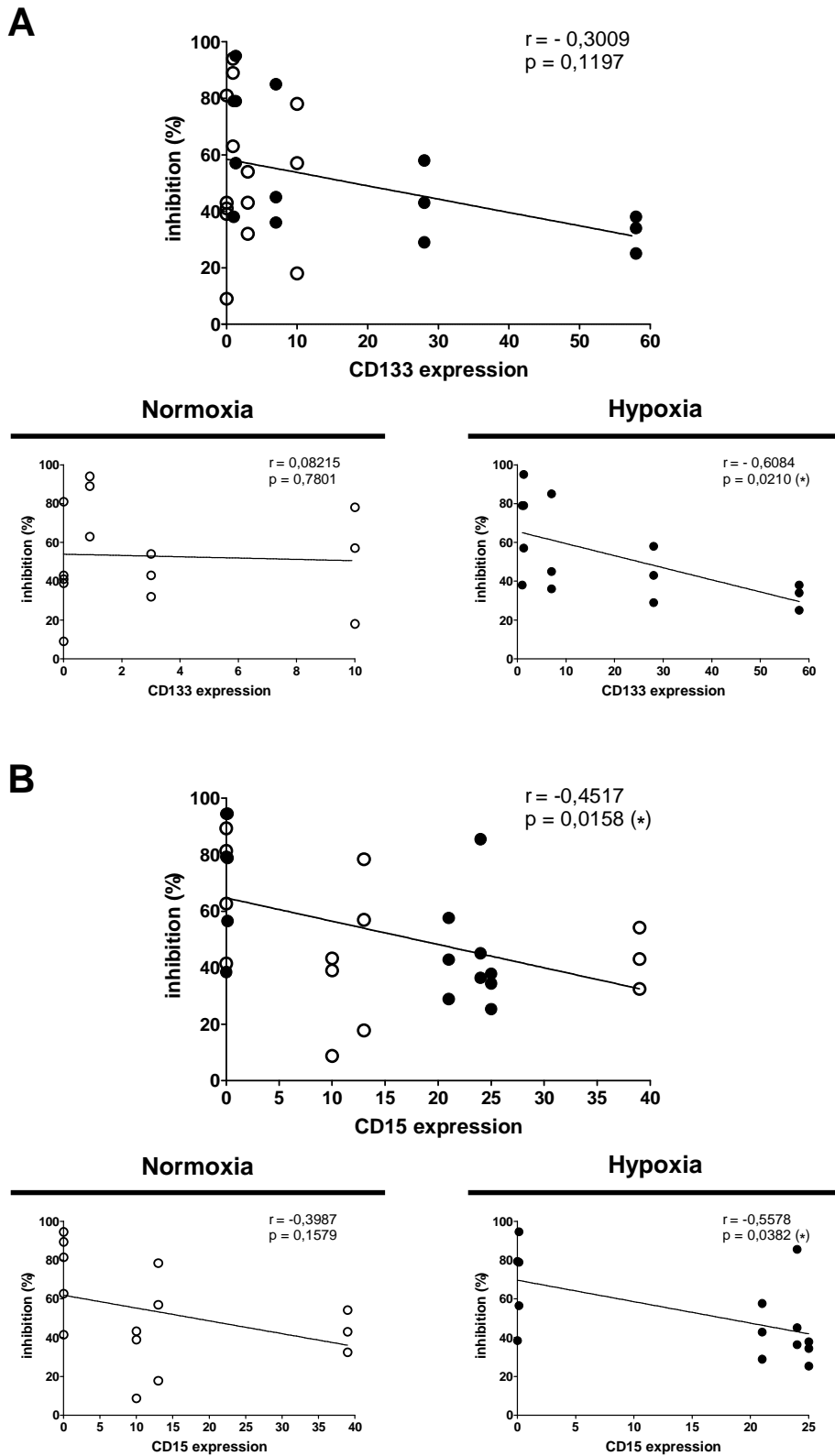


Figure 40. Correlation between CSC markers expression and P144 inhibitory percentages observed in proliferation, wound healing, and spheroid assay. The correlation with CD133 (A) and CD15 (B) expression was carried out by the nonparametric Spearman rank correlation test. Black filled circles correspond to values obtained under hypoxia and the empty circles under normoxia.

As is shown in Fig. 40, no correlation between percentages of inhibition and both CSC expression markers under normoxia was detected. A value of Spearman r coefficient near to zero suggested that under normoxia, the expression of CD133 did not influence the inhibition produced by P144. Moreover, under hypoxia conditions, the detection levels of CD133 or CD15 were correlated negatively with a statistical significance. Results suggest that the effect induced by P144 could be affected by the detected levels of the analysed CSC markers and the hypoxia condition.

3. MOLECULAR ANALYSIS OF TGF- β SIGNALLING PATHWAY INHIBITION BY P144 IN GLIOBLASTOMA A172 AND U-87 MG CELLS

3.1 P144 blocks activation of the TGF- β signalling pathway and nuclear translocation of P-SMAD2

The effect of P144 over SMAD2 phosphorylation was analysed to confirm that *in vitro* effects over cellular responses correlate with the inhibition of the TGF- β signalling pathway. The phosphorylation status of SMAD2 was detected by western blot using total protein extracts of A172 and U-87 MG cells. Cells were treated with P144 (100 μ g/mL) and at different time points, cells were harvested and processed. The time-course assay confirmed that P144 decreased P-SMAD2 levels until 48 h of treatment in both cell lines (Fig. 41A). Besides, an experiment using different control treatments were performed in both cell lines. The treatments (all performed by 4 h) include: (i) non-treated cells, in order to determine the basal level of phosphorylation of SMAD2; (ii) P144 at 100 μ g/mL; (iii) TGF- β 1 (200 pg/mL for A172 cells and 100 pg/mL for U 87 MG cells) as positive control of the TGF- β signalling pathway activation; and (iv) anti-TGF- β 1 antibodies (T β 1Ab) (40 ng/mL) as a control of the TGF- β pathway inhibition by extracellular binding to free TGF- β 1 (as P144) (Fig. 41B). The assay confirmed that the addition of P144 decreases the phosphorylation level of SMAD2. In the same way, cells that were treated with T β 1Ab showed the same profile of SMAD2 phosphorylation inhibition. As expected, the addition of TGF- β 1 strongly increased the phosphorylation levels of SMAD2.

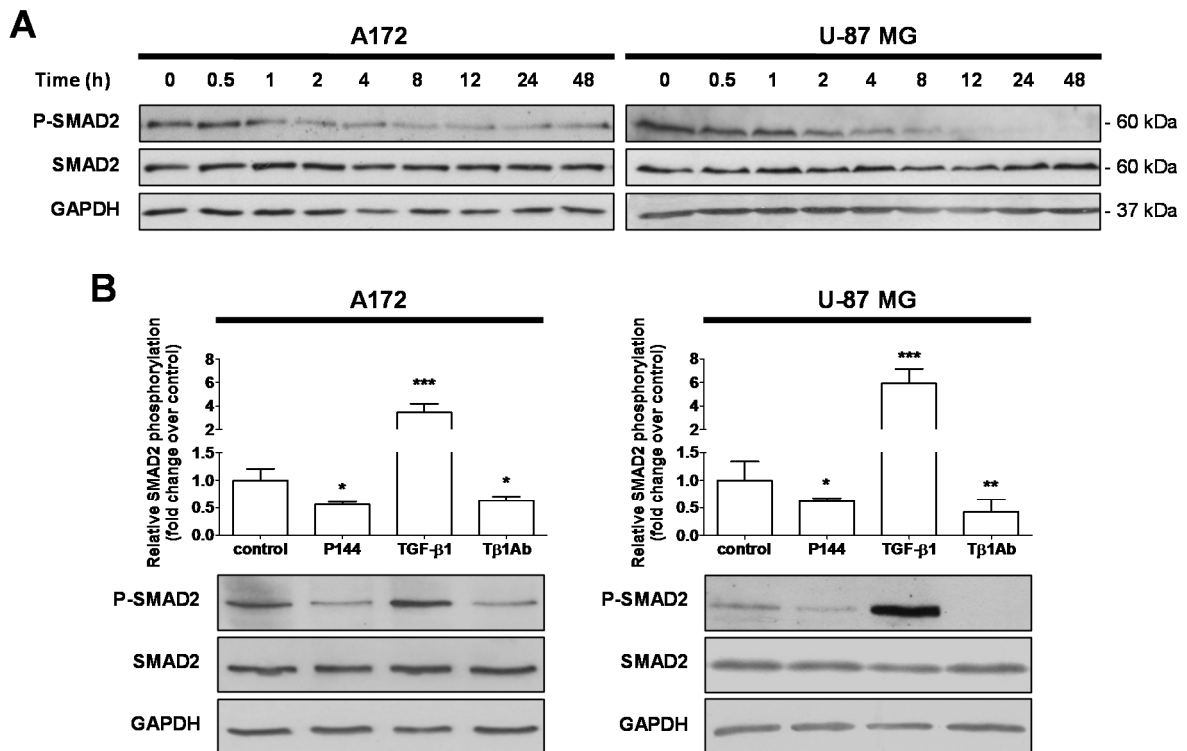


Figure 41. Inhibition of SMAD2 phosphorylation by P144. (A) Kinetics of unphosphorylated (SMAD2) and constitutively active form of SMAD2 (P-SMAD2) in A172 and U-87 MG cell lines in the presence of P144 (100 μ g/mL). (B) Analysis of the TGF- β signalling pathway inhibition in both cell lines. The graphs represent the ratio between P-SMAD2 and SMAD2. Cells were treated for 4 h with P144 (100 μ g/mL), TGF- β 1 (200 pg/mL for A172 cells and 100 pg/mL for U-87 MG cells), or T β 1Ab (40 ng/mL). The significant level is denoted by asterisks as follows: $p < 0.05$ (*); $p < 0.01$ (**); and $p < 0.001$ (***). Most representative western blot pictures from three independent experiments are displayed in (A) and (B).

To examine whether P144 is also able to reduce the activation of the TGF- β signalling pathway induced by the isoform TGF- β 2, cells were treated with recombinant human TGF- β 1 or TGF- β 2. In this experiment, P144 was added together with each TGF- β isoform at increasing concentrations for 4 h. After treatment, the phosphorylation status of SMAD2 was detected by western blot. As is shown in Fig. 42, P144 inhibited the activation of intracellular signalling pathway induced by exogenous TGF- β 1 in a dose-dependent manner. In the same way, addition of the TGF- β 2 isoform was able to activate the signalling pathway and P144 blocked this activation in a dose-dependent manner in both analysed cell lines (A172 and U-87 MG).

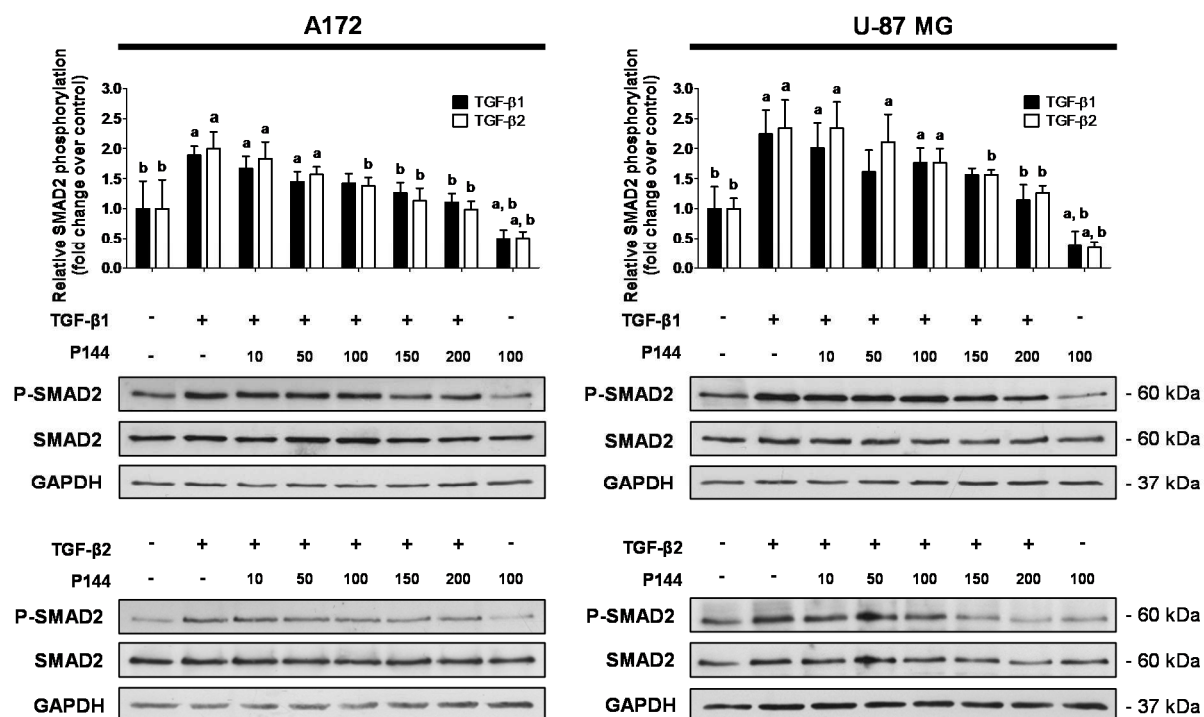


Figure 42. Blockade of TGF- β 1 or TGF- β 2 induced SMAD2 phosphorylation by P144.

Treatments were performed for 4 h. TGF- β 1 and TGF- β 2 concentrations were 200 μ g/mL for A172 and 100 μ g/mL for U-87 MG. Numbers above figures indicate P144 concentration in μ g/mL. Kruskal-Wallis test followed by Dunnet or Tukey as post hoc test for multiple comparisons were performed for each isoform. Significance level ($p < 0.05$) is indicated by (a) for comparisons to control and by (b) when treatments were compared to TGF- β treatment.

In order to demonstrate that inhibition of SMAD2 phosphorylation correlates with a blockade of P-SMAD2 translocation to the nucleus, kinetic analysis with TGF- β 1 was carried out in both cell lines. The nuclear and cytoplasmic P-SMAD2 was detected by western blot. The results are summarized in Fig. 43 and 44. The TGF- β 1 treatment increased cytoplasmic P-SMAD2 levels due to signalling pathway activation that consequently induces enrichment of nuclear P-SMAD2 levels through translocation from the cytoplasm reservoir to the nucleus. Increment of P-SMAD2 in both fractions, cytoplasmic and nuclear, was more remarkable in the U-87 MG cell line. Additionally, the levels of SMAD2 in the A172 cell line were enhanced after 5 min of treatment and then reduced over time. In the U-87 MG cell line, the amount in cytoplasmic fraction of SMAD2 decreased after 5 min of treatment. In nuclear fractions, the total quantity of SMAD2 increased in a time-dependent manner in both cell lines analysed. The decline of total SMAD2 at the cytosolic fraction in response to TGF- β 1 was followed by an increase inside the nucleus, due to SMAD2 phosphorylation and further translocation to the nucleus. As expected, the addition of TGF- β 1 triggered the activation of the TGF- β signalling pathway and produced the translocation of P-SMAD2 to the nucleus in both cell lines.

The analysis of the relative quantity of P-SMAD2 and total SMAD2 (Fig. 43C and 44C) pointed out that when TGF- β 1 is present, the increase observed in the total SMAD2 correlates with the increment of P-SMAD2. In each fraction (cytoplasm and nucleus) similar kinetics were displayed. In A172 cells, P-SMAD2 increased through time in the cytoplasmic fraction due to pathway activation. The nuclear P-SMAD2 fraction behaved the same way but with a delayed kinetics, due to cytoplasm/nuclear translocation. Equal behaviour was observed in the U-87 MG cell line. In the cytoplasmic fraction of both cell lines, the amount of total SMAD2 decreased over time, verifying the P-SMAD2 nuclear translocation.

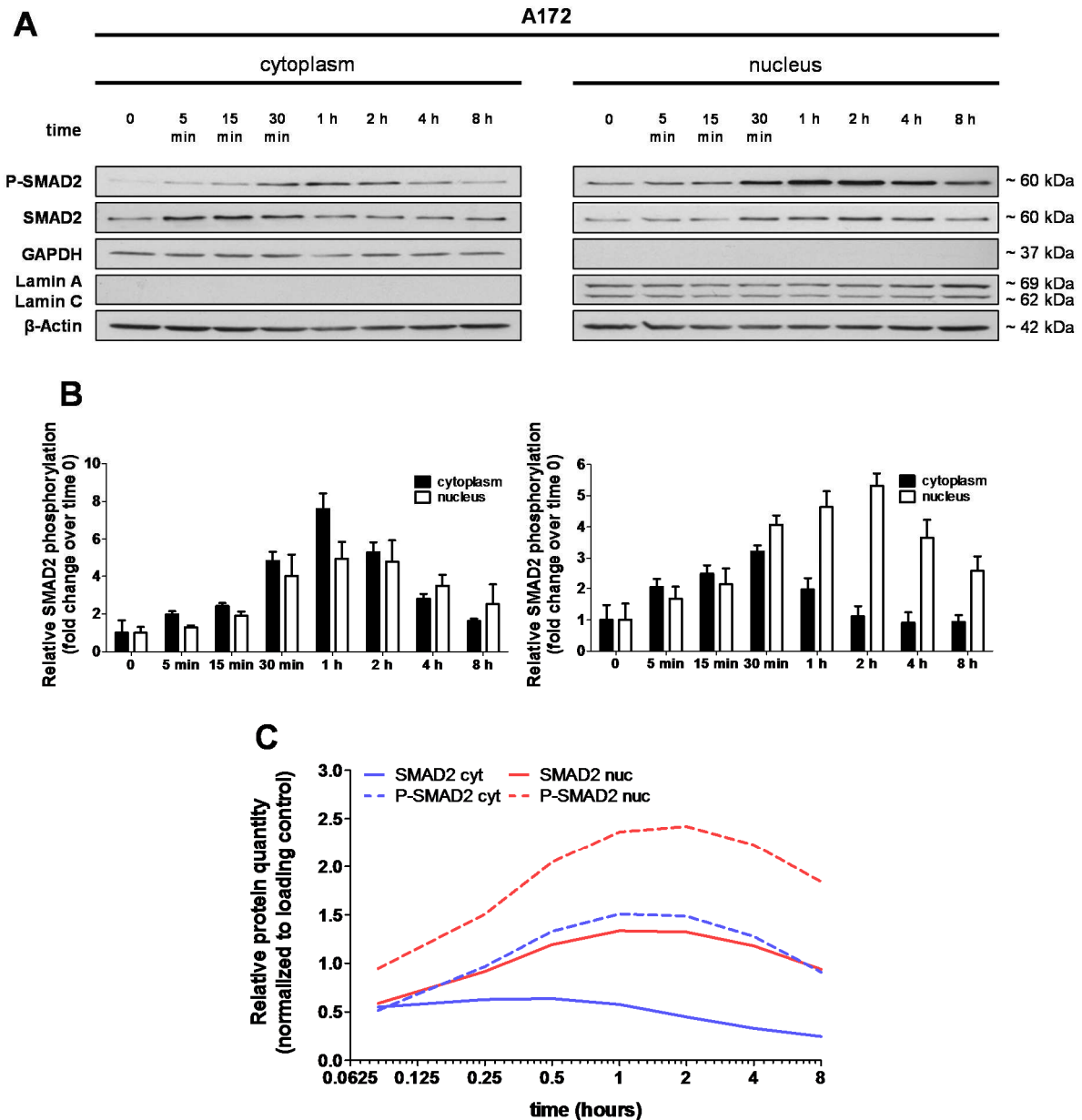


Figure 43. Cytoplasmic and nuclear P-SMAD2/SMAD2 kinetic analysis in A172 cell line treated with TGF- β 1. Representative images from western blot analysis are displayed in (A). Mean \pm SD of data of protein expression normalized to β -Actin and referred to initial time of treatment (0 = zero) from three independent assays are graphed in (B). Time-course analysis of relative quantity of SMAD2 and P-SMAD2 in cytoplasmic fraction (cyt) and nuclear fraction (nuc) are graphed in (C). β -Actin levels was used as loading control. GAPDH and Lamin A/Lamin C were used to indicate the cytoplasmic and nuclear fractions purity, respectively.

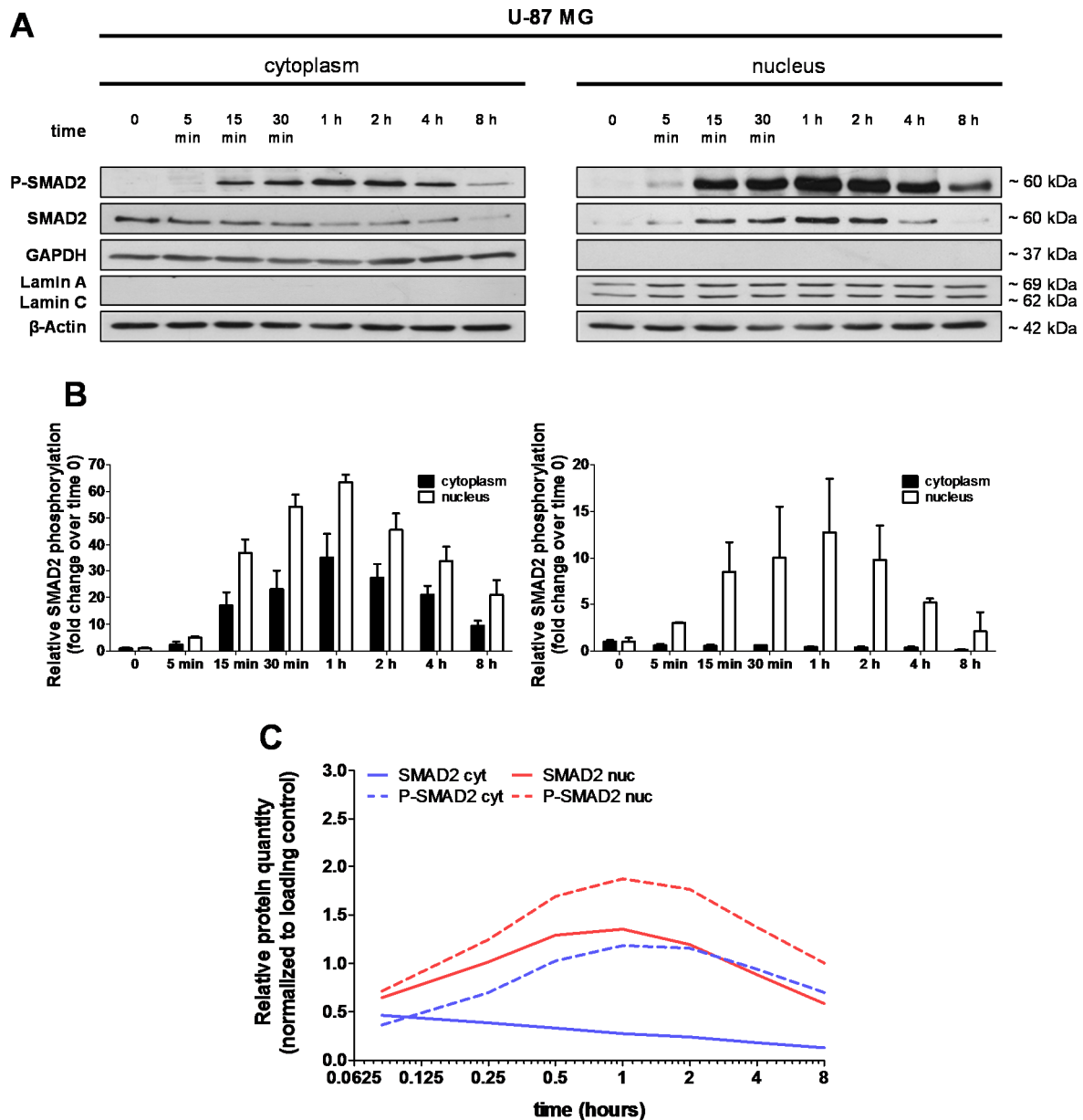


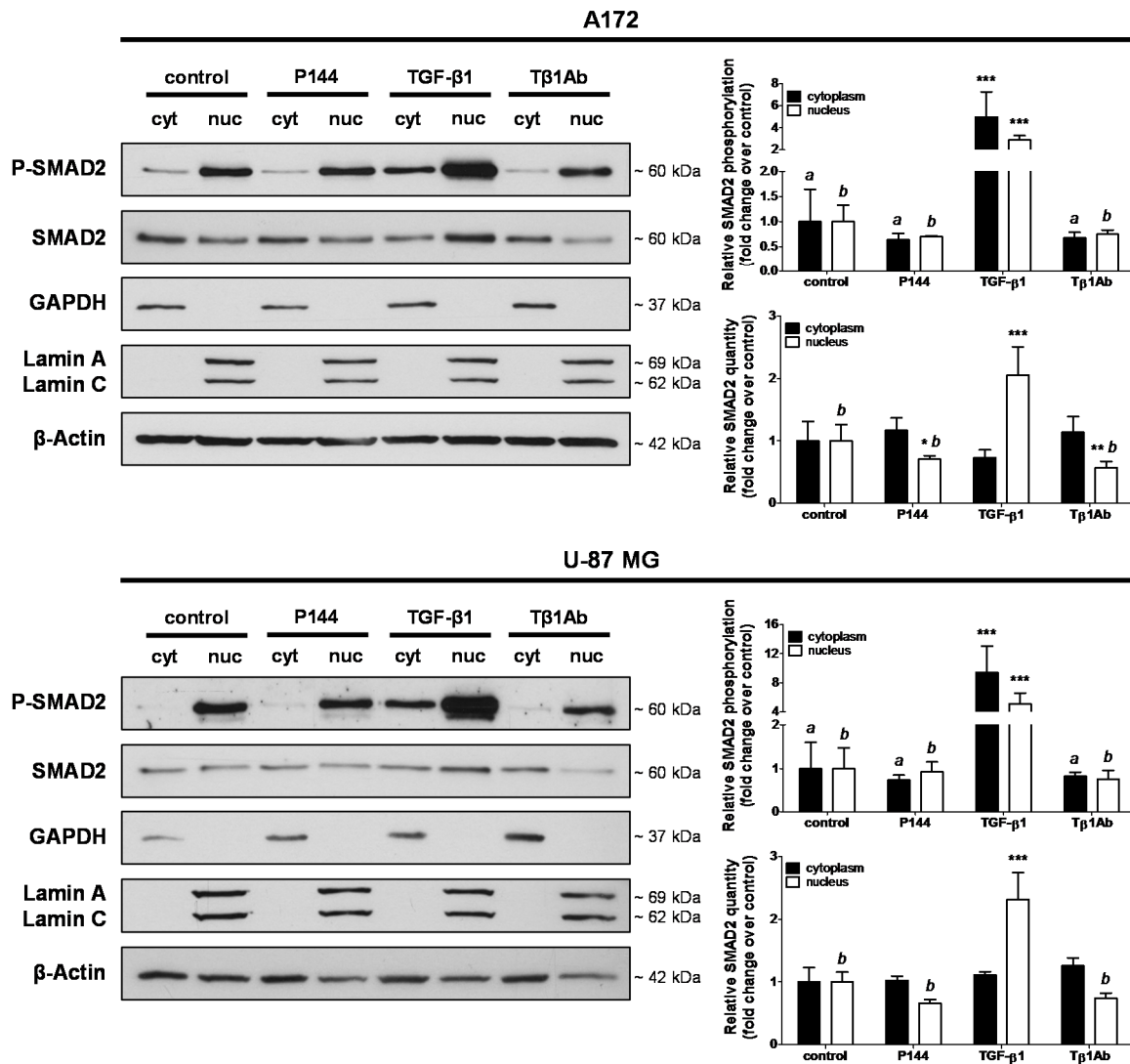
Figure 44. Cytoplasmic and nuclear P-SMAD2/SMAD2 kinetic analysis in U-87 MG cell line treated with TGF- β 1. As in A172, representative images from western blot are included in (A). In (B), protein expression levels of SMAD2 and P-SMAD2 are graphed. The evolution over time of relative quantity of each status of SMAD2 in each cellular fraction analysed are represented in (C).

Two experiments were carried out to analyse the ability of P144 to reduce P-SMAD2 translocation to the nucleus. The amount of P-SMAD2 and SMAD2 were analysed in the cytoplasmic and nuclear fractions 4 h after treatment with P144 (100 μ g/mL), TGF- β 1 (200 pg/mL for A172 cells and 100 pg/mL for U-87 MG) or T β 1Ab (40 ng/mL) (Fig. 45). In both cell lines, TGF- β 1 produced an expected increase in the amount of P-SMAD2 in the cytoplasmic and nuclear fractions. P144 and T β 1Ab decreased basal levels of P-SMAD2 in the two cellular fractions analysed but with no statistical significance. The analysis of total SMAD2, showed a significant increase after

treatment with TGF- β 1 in the nucleus. On the contrary, the treatment with P144 or T β 1Ab produced a statistically significant reduction of levels of SMAD2 in the nuclear fraction in both cell lines. In the cytoplasmic fraction, SMAD2 levels were not significantly altered, compared to control. These findings show P144 ability to bind TGF- β 1 and block its biological activity, reducing the phosphorylation of SMAD2 and the subsequent nuclear translocation of P-SMAD2 to the nucleus.

The second assay was performed to determine whether P144 was able to inhibit the translocation produced by the treatment with exogenous recombinant TGF- β 1. Cell lines were treated with TGF- β 1 together with P144 or T β 1Ab (at concentrations described above) and compared to the non-treated cells (Fig. 46). Quantifications were performed at 1 h that was previously set as the time point of higher TGF- β pathway activation (Fig. 43 and 44).

In the A172 cell line, TGF- β 1 treatment produced a significant increase in the total amount of SMAD2. However, the addition of P144 or T β 1Ab blocked this response and reduced the SMAD2 amount to non-significant levels compared to non-treated cells. The decrease in SMAD2 activation observed in the presence of TGF- β 1 when combined with P144 or T β 1Ab was significant compared with TGF- β 1 treatment. Likewise, P-SMAD2 levels were clearly increased in response to TGF- β 1. Only the addition of P144 was able to significantly decrease the levels of P-SMAD2 in the nucleus. The U-87 MG cell line displayed a similar behaviour. However, not only the addition of P144 but also T β 1Ab significantly reduced the P-SMAD2 levels induced by TGF- β 1.



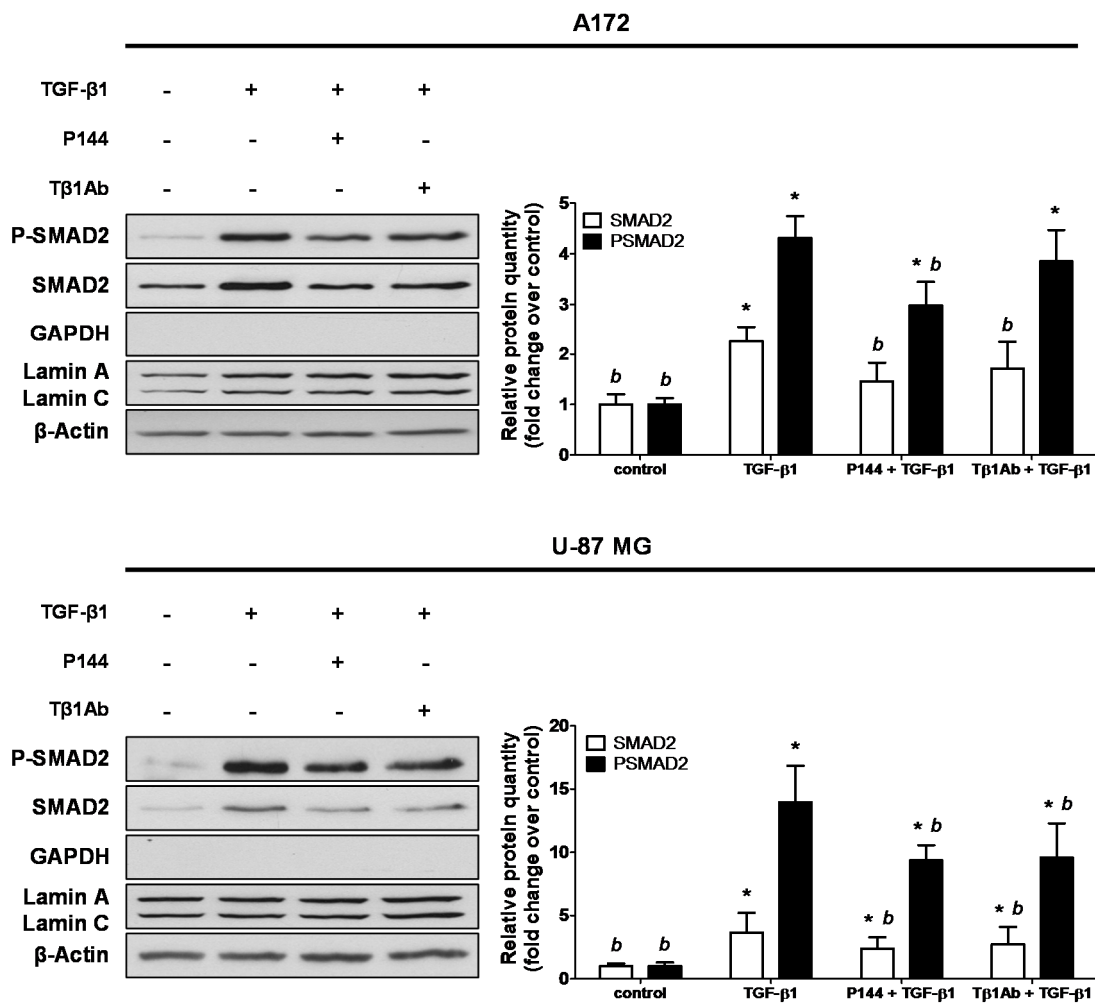


Figure 46. Blockade of TGF- β 1 induced P-SMAD2 nuclear translocation by P144 in A172 and U-87 MG cell lines. Left panel presents representative western blot images showing expression of total SMAD2 and P-SMAD2 in nuclear protein extracts. Right panel presents a graphical representation of relative expression (normalized to β -Actin) from three independent experiments. The Kruskal-Wallis test and Tukey as post hoc test were carried out in order to determine statistical significance between treatments. Asterisks indicate statistical significances between control and the other treatments in each fraction ($p < 0.05$ (*)). Significant level of performed treatments compared to TGF- β 1 group is designated by (b) ($p < 0.05$).

3.2 P144 regulates in vitro SMAD7 and SKI expression

To elucidate a possible molecular mechanism behind the action of P144, a set of genes related with the TGF- β signalling pathway were quantified by RT-qPCR. A kinetic analysis in A172 and U-87 MG cell lines treated with P144 (100 μ g/mL) throughout 12 h was carried out (Fig. 47). P144 induced an increase in *SMAD7* expression in both cell lines. On the contrary, a clear decrease in the expression of *SKI* gene was observed in both cell lines. The downregulation on *SKI* was maintained after 12 h of treatment in the A172 cells, whereas the U-87 MG cell line recovered basal expression levels after 4 h of treatment. *SNON* only showed a significant increase in expression at 2 h in A172 cell line. The expression of *SNON* was not affected by P144 in the U-87 MG cells. No change in the expression of *p21CIP1* or *FOXG1* until 12 h of treatment with P144 was observed. Basal expression of *p15INK4B* was not detected in both cell lines.

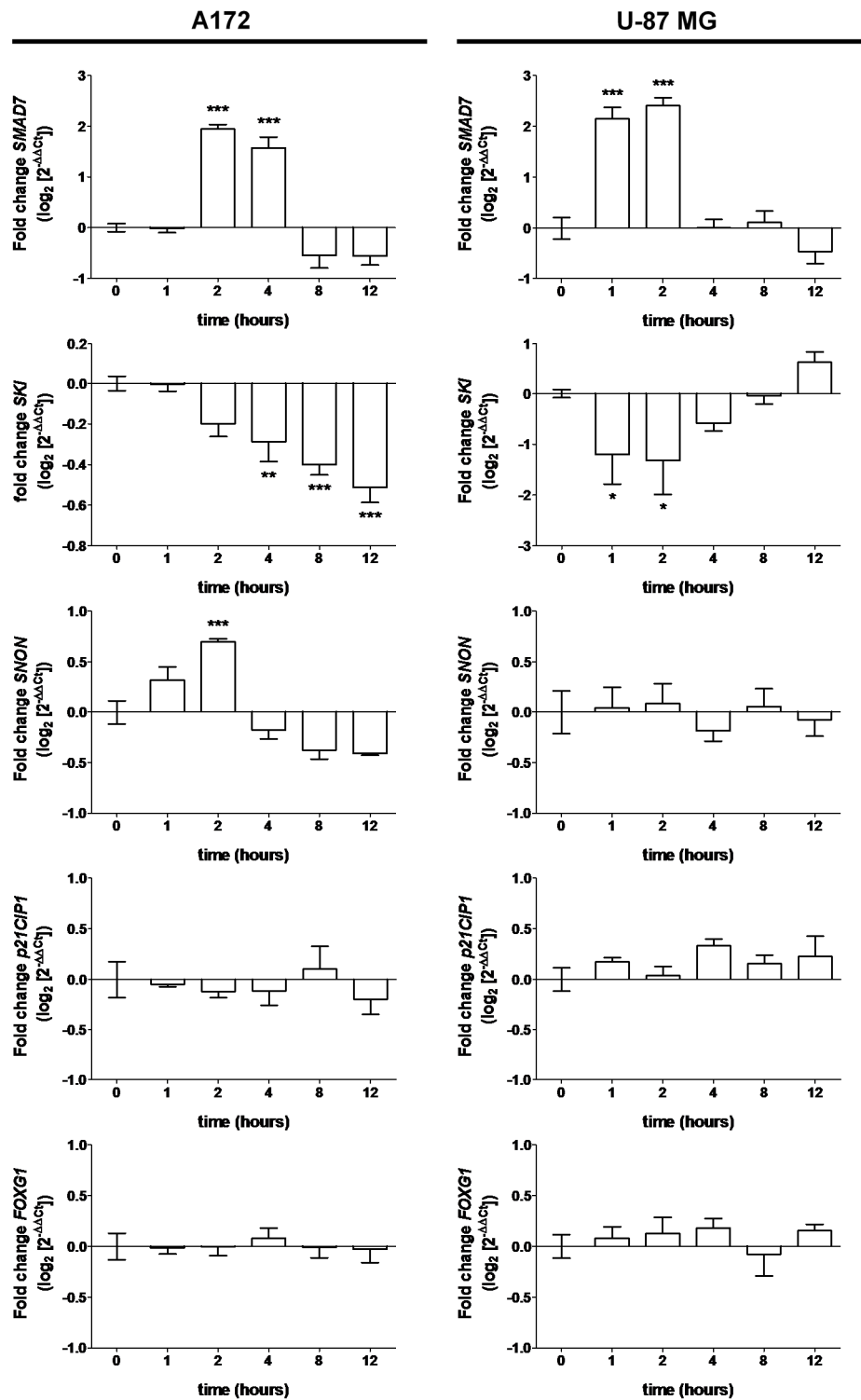


Figure 47. Gene expression kinetics of P144 treated A172 and U-87 MG cell lines. Mean \pm SD from three independent experiments are summarized. Data were processed by the $2^{-\Delta\Delta C_t}$ method and base 2 logarithm values are graphed. To determine the significant differences compared to initial time, a Kruskal-Wallis test followed by Dunnett's multiple comparison test were performed. The significance level was classified as follows: $p < 0.05$ (*); $p < 0.01$ (**); and $p < 0.001$ (***)

Further analysis of gene expression was carried out in the A172 and U-87 MG cell lines in order to determine the expression profile under activation or inhibition conditions of the TGF- β

pathway. Different treatments were performed at those times where a significant change in expression was observed in each cell line. The effect of P144 over the expression of *SMAD7* and *SKI* was confirmed and TGF- β 1 treatment produced the opposite effect compared to P144. Furthermore, T β 1Ab treated cells reproduced the gene expression changes displayed by P144 (Fig. 48). These results confirm the involvement of *SMAD7* and *SKI* genes in the TGF- β 1 signalling pathway in A172 and U-87 MG cell lines. Moreover, the addition of P144 or T β 1Ab together with TGF- β 1 counteract significantly the effect on gene expression induced by TGF- β 1. In the A172 cell line, *SNON* expression was clearly affected by the different treatments performed. However, the expression of *SNON* in the U-87 MG cell line did not show consistent pattern. Results reveal a correlation between gene expression of *SMAD7* and *SKI* and the TGF- β signalling pathway in human GBM cell lines.

The basal expression levels of *SMAD7* and *SKI* genes in A172 and U-87 MG cell lines together with the levels observed after treatment with P144 were compared to the expression profile in the NHA cell line. The A172 cell line displayed significant differences in the basal expression of both genes compared to the NHA cell line, in contrast with the U-87 MG cell line that did not exhibit differences in basal expression of these genes compared to NHA cells. When treatment with P144 in both cell lines was considered, a clear trend in the expression of *SMAD7* and *SKI* genes was noticed (Fig. 49). Expression of *SMAD7* and *SKI* genes was significantly upregulated and downregulated, respectively, by P144.

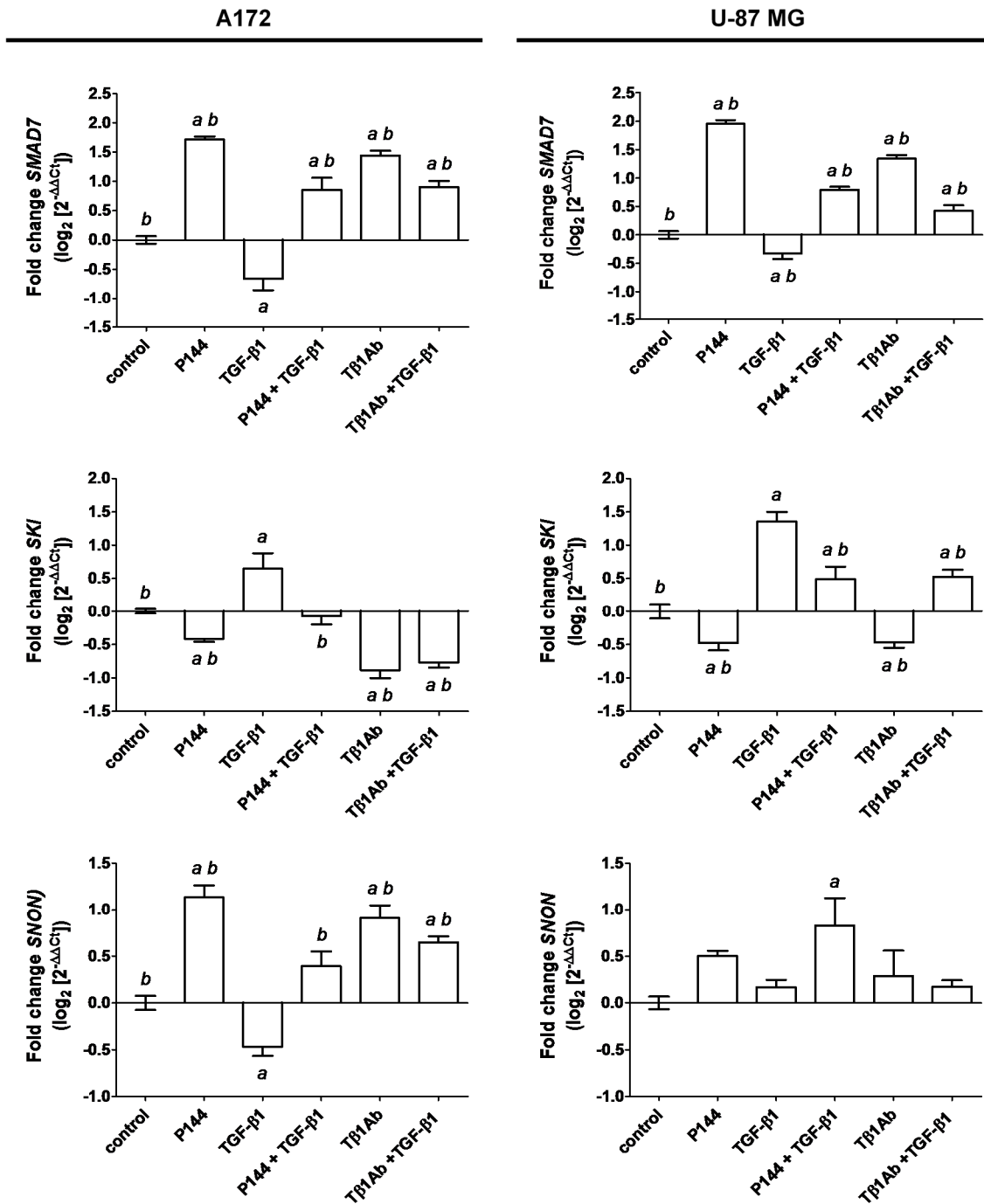


Figure 48. SMAD7, SKI and SNON gene expression analysis in glioblastoma cell lines. Treatments included: control, P144 (100 μg/mL), TGF-β1 (200 pg/mL), P144 + TGF-β1, Tβ1Ab (40 ng/mL) and Tβ1Ab + TGF-β1. Statistical analysis included a Kruskal-Wallis test to detect significant differences and post-test through Dunnett's and Tukey's multiple comparison tests. (a) indicates significant statistical differences between control and treatments and (b) indicates differences within the expression level of TGF-β1 group compared to other treatments.

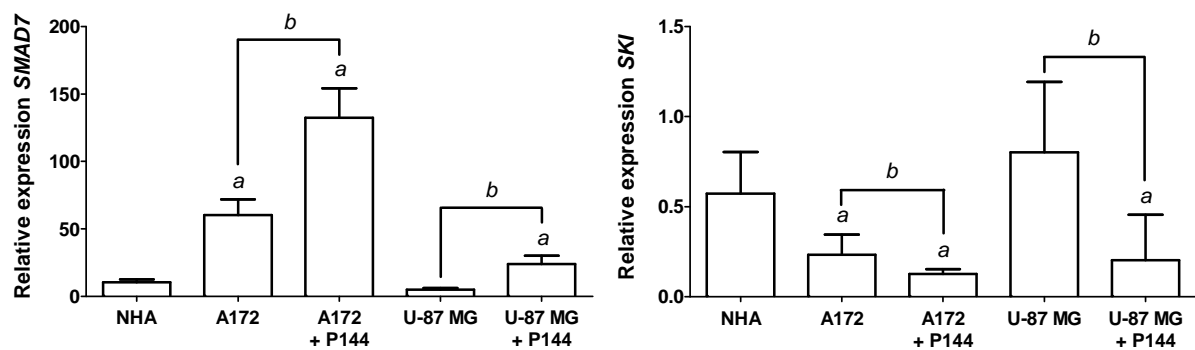


Figure 49. SMAD7 and SKI relative expression in NHA, A172 and U-87 MG cell lines. Values were obtained by the efficiency corrected quantification model. Mean \pm SD are graphed. The statistical analysis included Kruskal-Wallis test for identified differences and Tukey as post hoc test. Significance is indicated by letters: (a) when compared to NHA cell line and (b) difference between non-treated cells and P144 (100 μ g/ml) treated group in each cell line.

To confirm whether the detected changes in gene expression were translated to protein expression, the protein levels of SMAD7 and SKI were assessed by western blot in a time-course assay in the presence of P144 (Fig. 50A). Protein levels correlate well with the gene expression kinetics described above. P144 increased SMAD7 protein levels until 48 h of treatment. Levels of SKI protein were reduced throughout time until 48 h of treatment. These data correlated with P144 kinetic inhibition of SMAD2 phosphorylation (Fig. 41A), where P-SMAD2 reduction corresponds with the increase and decrease of the protein amount of SMAD7 and SKI, respectively.

To validate kinetic results, three different treatments were carried out in the A172 and U-87 MG cell lines. Protein expression was quantified after treatment with P144, TGF- β 1 or T β 1Ab, and in non-treated cells. The treatments were performed for 12 h to ensure detection of significant differences in protein levels. As shown in Fig. 50B, the addition of exogenous TGF- β 1 in glioma cell lines induced the opposite effect over SMAD7 and SKI protein expression in comparison to P144 treated group. Moreover, T β 1Ab that mimics the extracellular P144 blocking of free TGF- β 1, reproduced the effect over SMAD7 and SKI protein levels obtained after the treatment with P144.

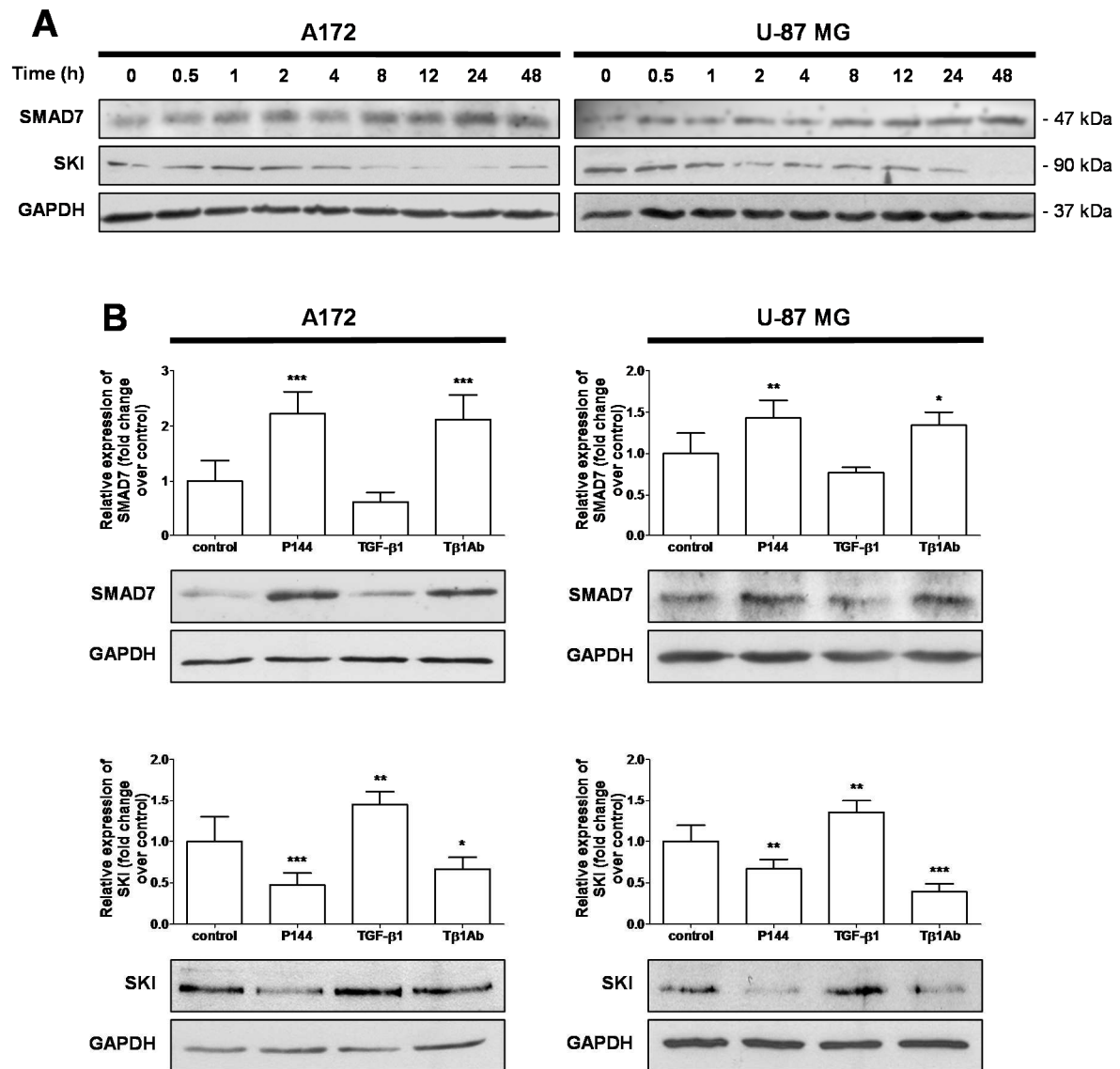


Figure 50. Protein expression of SMAD7 and SKI in A172 and U-87 MG cell lines. (A) Kinetic analysis with P144 (100 μ g/mL). Representative western blot images from two independent assays are shown. (B) Analysis of SMAD7 and SKI protein levels after treatment with P144 (100 μ g/mL), TGF- β 1 (200 pg/mL), or T β 1Ab (40 ng/mL). Most representative western blot pictures and graphics of relative protein quantity of each group are represented. Values were normalized to the loading control protein GAPDH. Statistical analysis was performed with Kruskal-Wallis test plus Dunnet post hoc test and significance differences between treatments marked with asterisks ($p < 0.05$ (*); $p < 0.01$ (**); and $p < 0.001$ (***)).

II) *IN VIVO* FINDINGS

4. EVALUATION OF ANTITUMOUR ACTIVITY OF P144 IN A NUDE MOUSE SUBCUTANEOUS MODEL

4.1 P144 reduces growth rate and increases survival in nude mice implanted human glioblastoma xenografts

A xenograft subcutaneous mouse model was carried out in order to evaluate the *in vivo* potential activity of P144 on tumour growth and development. Since the A172 cell line presents a poor *in vivo* tumorigenic and invasiveness capacity [197], the U-87 MG cell line was selected for this assay. In this model, 20 nude female mice were implanted with tumour cells by subcutaneous injection in the right flank of the lumbar area. Tumour growth measurement and P144 treatment were performed each day. The IP administration of P144 (200 µg/animal) started when tumour mass reached a volume of 500 mm³.

Mice treated with P144 showed a delayed onset and progression of tumour growth compared with control group. Delay in tumour growth was evidenced after 1 day of treatment (10.1% of reduction), reaching a maximal value of 45.5% at day 21 (Fig. 51A). Additionally, these data were correlated with a decrease in the growth ratio, which was statistically significant at day 21, and with a significant increase on survival in mice IP injected with P144 (Fig. 51D and 51B, respectively). Tumours were extracted after 40 days of treatment, or when tumour diameter reached an average measurement of 1.7 cm, and subsequently processed for immunohistochemical staining, gene expression and protein analysis. One mice from the P144 treated group did not develop tumour and was removed from further analysis. All tumour samples exhibited many of the histopathological and biological features of gliomas including a central necrosis area and cells densely arranged in a perpendicular or pseudo-palisading manner around necrotic areas. Cellular pleomorphism, mitoses and areas with microvascular proliferation adjacent to necrosis were identified by microscopic analysis (Fig. 52). These characteristics are typical of human high-grade gliomas.

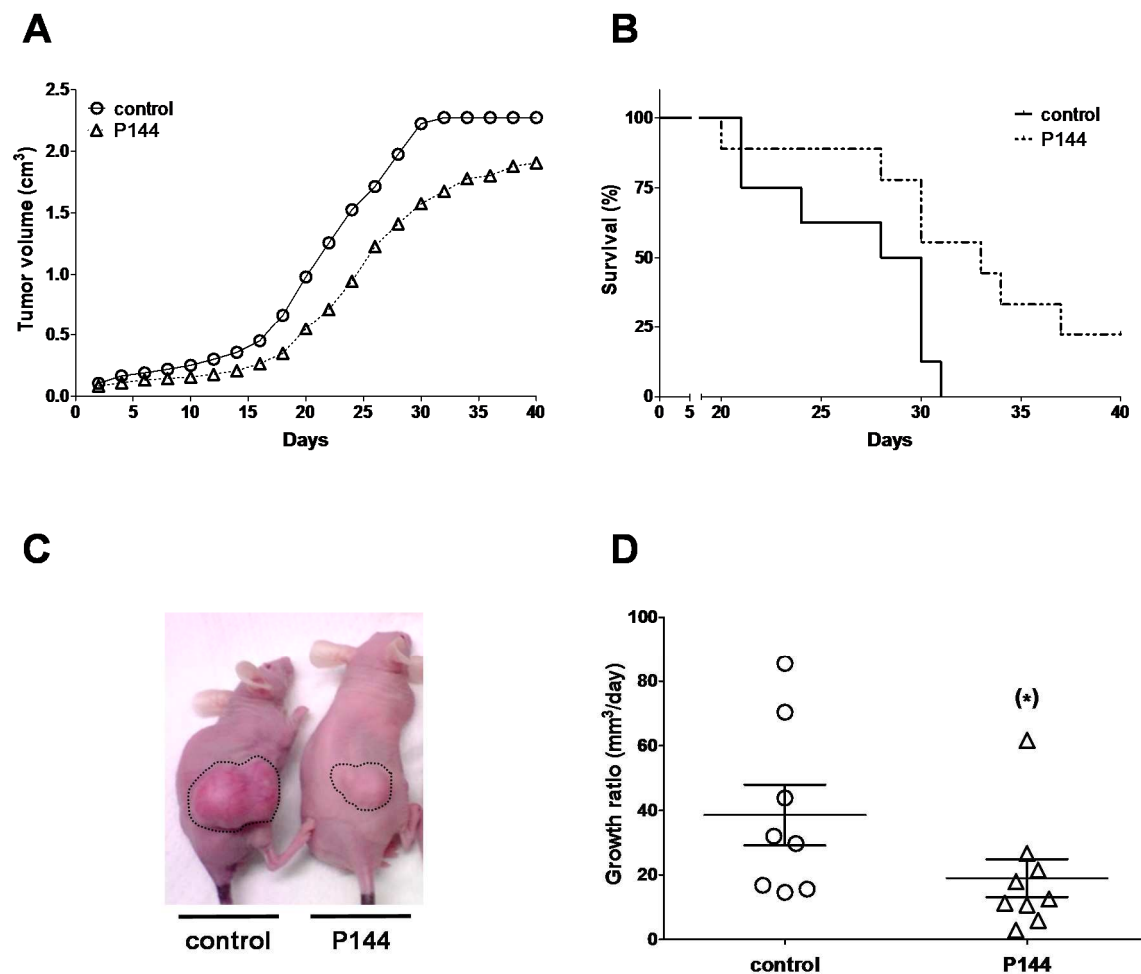


Figure 51. Effect of P144 over U-87 MG xenograft nude mice subcutaneous model. (A) The tumour volume was calculated every day as indicated in Material and Methods section. P144 group shows a significant decrease in the tumour volume (Wilcoxon matched-pairs signed rank test, $p < 0.0001$). (B) Kaplan-Meier curve displayed statistical significance when was analysed by Log-rank (Mantel-Cox) test ($p = 0.024$). (C) Representative pictures of mice from control and P144 treated group after 30 days of treatment. (D) The growth ratio was calculated as the average of the daily increase in the tumour volume until day 21 (Mann Whitney test, $p = 0.046$).

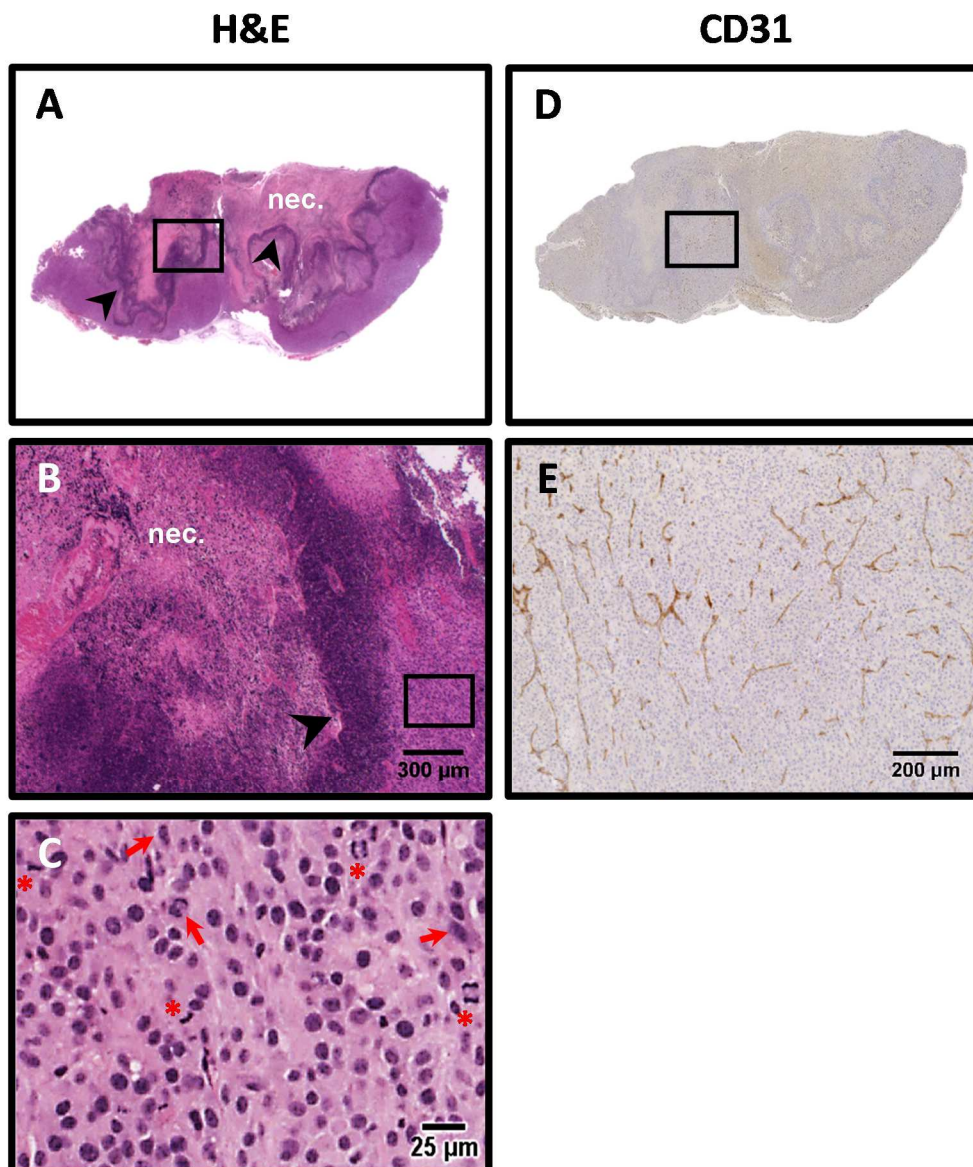


Figure 52. Histological analysis of tumour samples from subcutaneous xenograft model. Representative slide images showing H&E and CD31 immunostaining are shown. In (A) and (D) a slide image including a representative complete tumour. Amplified sections are delimited by a square and represented in the next lower panel. The typical cell types of glioblastoma tumours are shown in (C). In (E) the tumour vasculature development is observed. Tumour samples exhibited multinuclear malignant and pleomorphic cells (red arrows). Mitotic figures are indicated by red asterisks. The H&E in (A) and (B) show the typical cellular arrays arranged in perpendicular manner or pseudopalisading (black arrowheads) surrounding necrotic areas (nec.).

To explain the effect of P144 over tumour volume and growth ratio, apoptosis and angiogenesis was quantified in the tumour tissue samples by IHC. As shown in Fig. 53, P144 produced a decrease on Ki-67 expression levels but without statistical significance, suggesting that the reduction in growth ratio could be explained by a decrease in cell proliferation. The treated tumour samples presented significant lower apoptotic values (Caspase-3 expression) when

compared with controls. Tumour angiogenesis was quantified through CD31 immunohistochemistry and did not show significant differences.

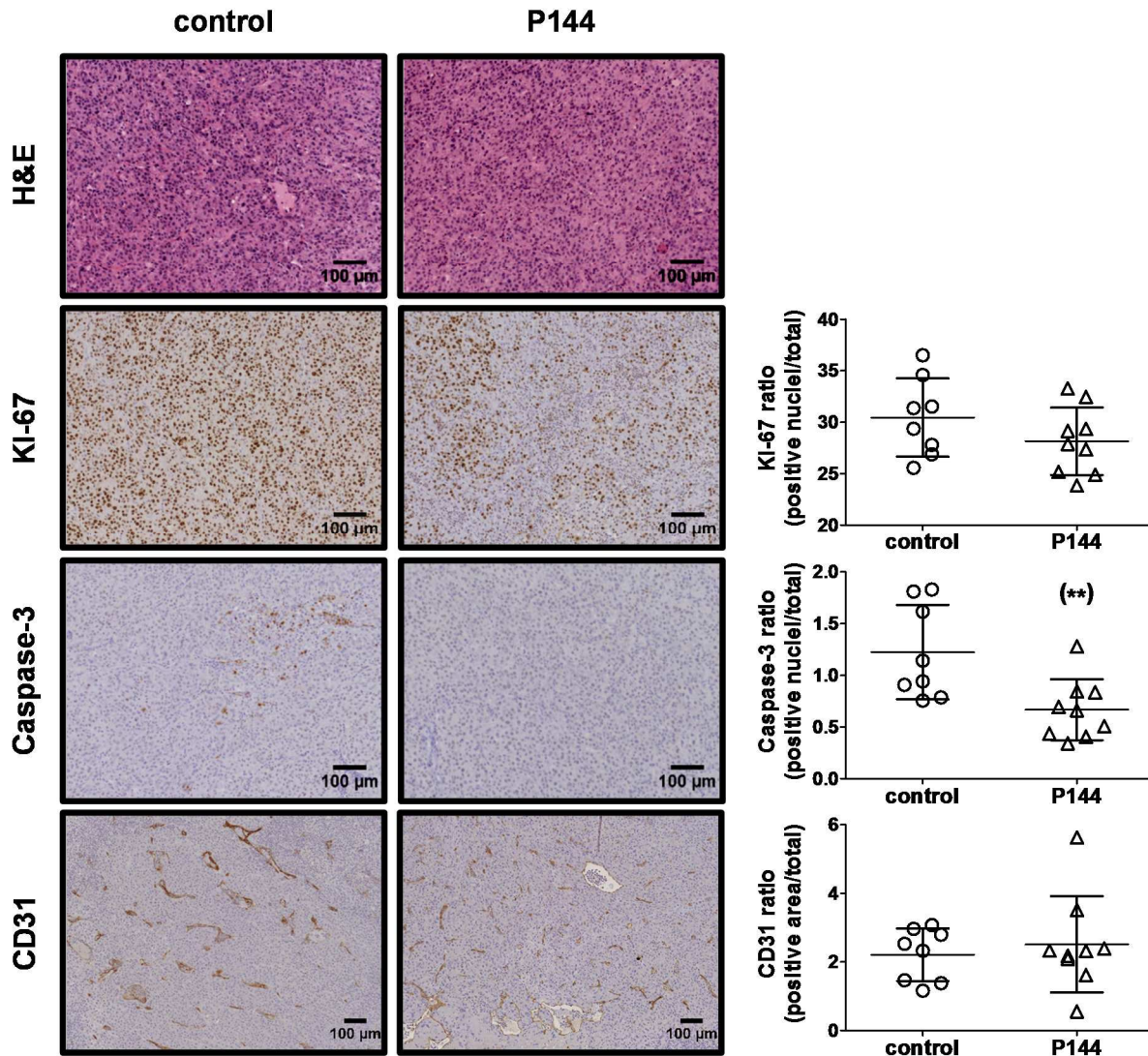


Figure 53. Tumours tissue immunohistochemical quantification of proliferation, apoptosis and angiogenesis. Left panel shows representative tumour tissue images from control and P144 treated group, including H&E and KI-67, Caspase-3, and CD31 IHC staining. ImageJ software based quantification is graphed on the right panel. Data were analysed by Mann Whitney test. Only the decrease observed on Caspase-3 levels in P144 treated group was statistically significant ($p = 0.008$).

4.2 P144 regulates in vivo levels of SMAD7 and SKI

Tumour tissue samples were processed to obtain total mRNA and total protein fractions to further analysis by RT-qPCR and western blot, respectively. The determination of gene expression by RT-qPCR showed that tumours from mice treated with P144 presented an increase of *SMAD7* and a decrease in *SKI* at a transcriptional level (Fig. 54). Both changes were statistically significant

compared to the control group. *SNON* did not vary its expression when compared to control, in accordance with the *in vitro* expression pattern observed in the U-87 MG cell line.

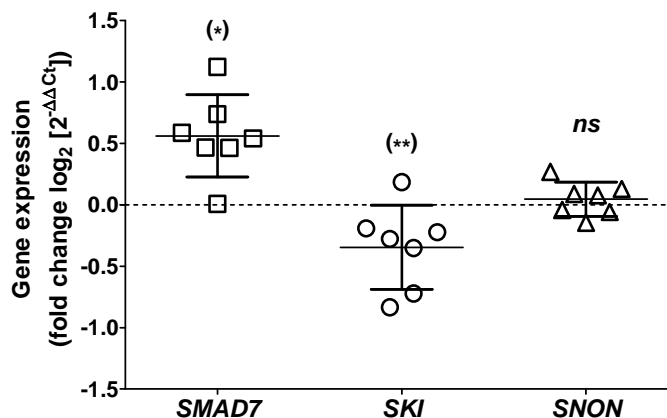


Figure 54. Expression levels of *SMAD7*, *SKI* and *SNON* genes in tumour samples from P144 treated mice. The dotted line represents the expression level referred to the control group for each gene. A Mann-Whitney U test between the expression levels of each gene compared to corresponding control was performed. Significance is indicated with asterisks ($p < 0.05$ (*) and $p < 0.01$ (**)). No significance is denoted by *ns*.

Protein samples derived from tumours were processed and the protein levels of *SMAD7* and *SKI* were determined by western blot. Changes in protein levels of *SMAD7* and *SKI* were detected (Fig. 55). Despite the increase observed in mRNA level, *SMAD7* did not show significant differences when compared to the control group at the protein level. However the decrease in *SKI* gene transcription was translated to a significant decrease at protein level. Moreover, samples were analysed for the detection of phosphorylation status of *SMAD2* protein. The treatment with P144 was able to inhibit the phosphorylation of *SMAD2* after 40 days of daily treatment. This inhibition was statistically significant when compared to the phosphorylation levels of the control group. *In vitro* P144 induced changes in *SMAD7* and *SKI* at the transcriptional and translational levels and the phosphorylation status of *SMAD2* observed were confirmed in tumour samples derived from the subcutaneous *in vivo* assay.

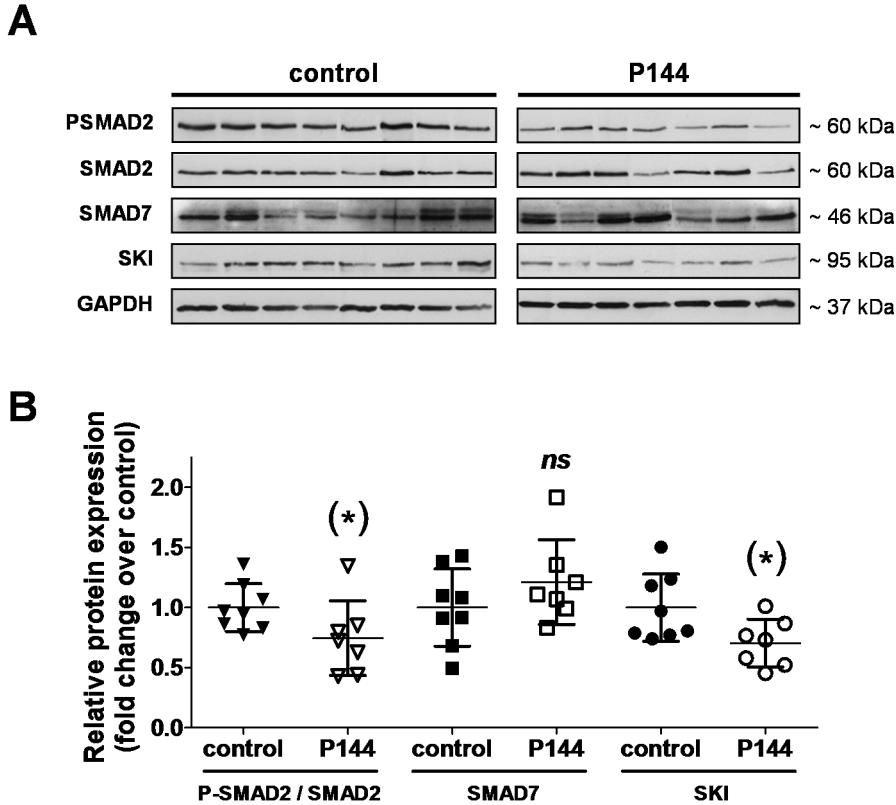


Figure 55. *In vivo* phosphorylation status of SMAD2 and protein level of SMAD7 and SKI. In (A) representative western blots images from three independent determinations are shown. Protein levels were quantified and normalized to GAPDH housekeeping gene. The P-SMAD2 levels were normalized to the total SMAD2 protein content. Values were compared to control samples through Mann-Whitney U test. Asterisks denoted statistical significance ($p < 0.05$ (*)), *ns* indicated no significance.

5. P144 EFFECT ON GLIOBLASTOMA DEVELOPMENT IN THE BRAIN ENVIRONMENT OF A NUDE MICE INTRACRANIAL MODEL

To determine the potential of P144 as a clinical candidate for GBM treatment, an *in vivo* assay was performed based on an intracranial mouse model to generate tumours in the brain environment. For this purpose, several previous tuning assays were carried out in order to define the final conditions and treatments to be performed in the assay.

5.1 P144 presents no *in vitro* residual effect over U-87 MG cell line proliferation

In the subcutaneous tumour xenograft model (Results, section 4), the administration of P144 was performed daily and the peptide stability did not constitute a source of uncertainty over results. However, in the intracranial mouse model coupled to osmotic pumps, a unique P144 solution dosage is continuously delivered to the brain. For this reason, potential P144 residual effect on the target tumour cells as well as chemical and *in vitro* biological stability were studied.

First, we analysed whether U-87 MG tumour cells showed an *in vitro* residual or long-term effect in the proliferation rate after P144 treatment. As further described below, osmotic pumps allow a fixed treatment period. The treatment time cannot be externally manipulated and directly depends on the pump model. To increase or modify the treatment time range in the different pumps, it is necessary to exchange the device with a new filled osmotic pump. In addition, the dosage continuity in the osmotic pump is theoretically calculated, taking into account that several external factors can affect the administered flow and the exact treatment period.

To elucidate the possible P144 residual effect, an *in vitro* assay with the U-87 MG cell line under normoxia conditions was carried out. Cell proliferation was analysed through time in presence of P144. Three days after treatment, the culture medium was replaced with P144-free fresh medium and proliferation was determined during seven days in the absence of P144. A vehicle control solution was included in the assay. As shown in Fig. 56, after three days in presence of P144, no residual effect was noticed over U-87 MG cell proliferation once P144 was eliminated from the medium in comparison with cells not previously exposed to P144. Additionally, data were analysed through linear regression to detect significant differences between the slopes of each treatment. As expected, the results obtained indicated a significant slower growth ratio in cells treated with P144 when compared to control. From day 4 to 11, once P144 was removed, no differences were detected between the growth curves of P144 previously treated cells and non-treated cells, suggesting that U-87 MG previously treated cells showed no residual effect on cell growth.

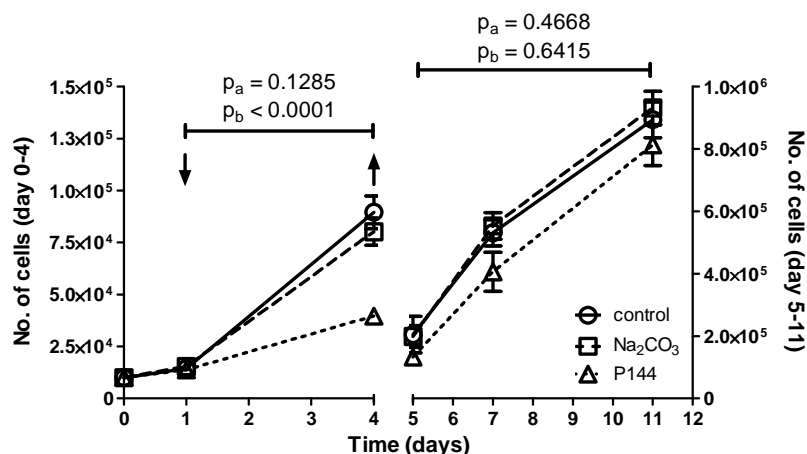


Figure 56. Analysis of potential antiproliferative residual effect of P144 on U-87 MG cell line. Slopes were compared with lineal regression analysis. The significance levels (p values) are designated as p_a for control vs Na_2CO_3 treatment, and p_b control vs P144 treatment. Arrows indicate the initiation (down arrow) and end (up arrow) of P144 treatment.

5.2 P144 biological activity is lost with autoclave treatment

The autoclave effect on P144 as an inactivation method was analysed in order to include an equivalent control group in the *in vivo* assay. A solution of P144 at 1 mg/mL dissolved in 100 mM Na_2CO_3 or 50 mM TRIS was subjected to heat and high pressure saturated steam by autoclave during 20 min. After this procedure, a chemical profile as optical absorbance spectrum and HPLC analysis, as well as the biological activity through cell proliferation, wound healing and spheroid assays were carried out.

Spectral absorbance analysis was determined by spectrophotometry using a NanoPhotometerTM (Implen GmbH). After heat inactivation, modifications in the absorbance spectrum were observed (Fig. 57A). Despite that maximal points of absorbance around 220 and 280 nm were not significantly affected, the general spectrum differed in comparison to the P144 control solution. A slight shift in the highest absorbance peak near to 220 nm and a small increase in the peak at 280 nm in the autoclaved P144 were observed. A deeper analysis was carried out by measuring the maximal absorbance values obtained at 220 nm and 280 nm wavelength (Fig. 57B). Compared to the non-autoclaved P144 solution, the autoclave treatment of P144 in Na_2CO_3 did not produce significant differences when absorbance values were compared. In contrast, when P144 was autoclaved in TRIS solution, a significant increase in absorbance at 220 nm was detected. The ratio between the values at 220 and 280 nm of absorbance were calculated and no statistical differences were found compared to control P144 in both solutions, Na_2CO_3 and TRIS (Fig. 57C).

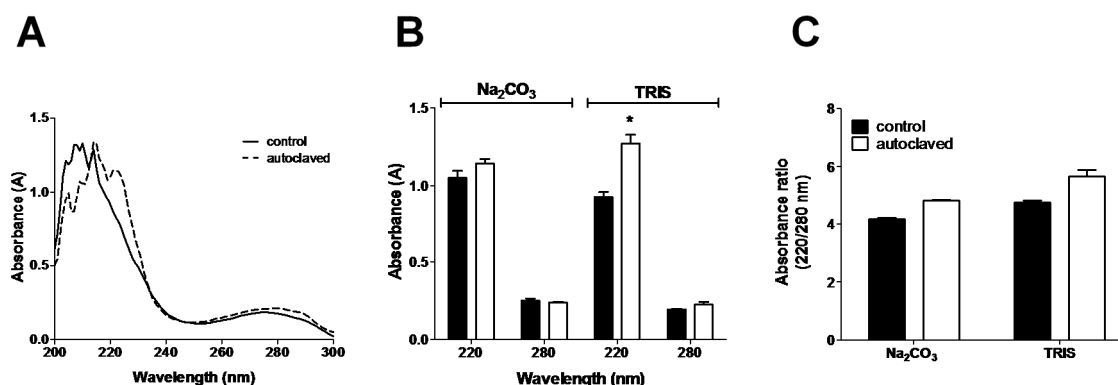


Figure 57. Autoclaved P144 absorbance quantification by spectrophotometry. In (A) the absorbance spectrum from control P144 is superimpose with P144 autoclaved (dotted line). The absorbance values at 220 nm and 228 nm are analysed in (B). The ratio 220 nm/228 nm from absorbance values are graphed in (C). The statistical analysis included a two-way ANOVA with Bonferroni as post hoc test in (B) and Mann-Whitney U test in (C) ($p < 0.05$ (*)). Solutions of peptide were prepared at 1 mg/mL.

A sample of autoclaved P144 at 0.1 mg/mL in Na₂CO₃ was injected in an Agilent 1100 Series HPLC System (Agilent Technologies) to determine possible chemical changes due to inactivation processing. The UV absorbance detection was carried out in four different wave lengths: 210, 220, 260, and 280 nm. Chromatograms, retention times and areas from peaks were examined and compared to the non-autoclaved P144 control in the same solution and concentration.

Control P144 dissolved in Na₂CO₃ generates a well-defined chromatogram profile (Fig. 58). Autoclaved P144 showed the same peaks profile but with several additional peaks with less retention times. Principal peaks retention times (Rt) were not affected; as consequence, the ratio of the retention time (RRt) did not change in both analysed solutions (control and autoclaved samples of P144).

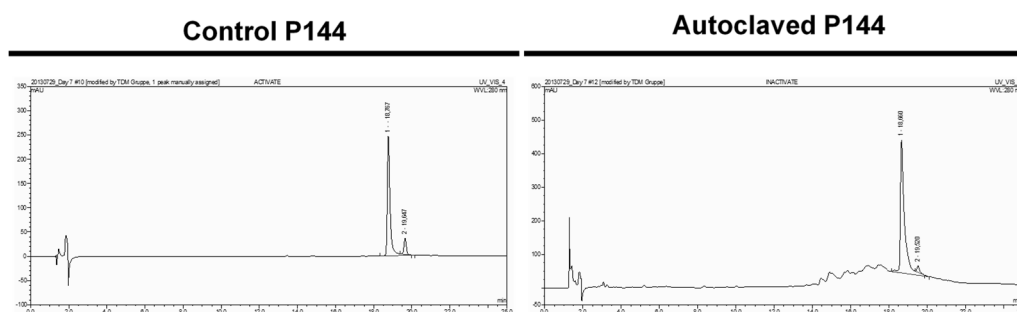


Figure 58. HPLC analysis of autoclaved P144. Representative chromatograms obtained from control and autoclaved P144 at 0.1 mg/mL dissolved in 100 mM Na₂CO₃.

The biological activity of control and autoclaved P144 was analysed through different assays in the U-87 MG cell line grown under normoxia conditions (5% CO₂, 21% O₂). Effect on proliferation was measured after 72 h of treatment with the autoclaved P144 and control P144, dissolved in Na₂CO₃. The significant effect on proliferation previously observed by P144 was totally abolished when P144 was inactivated by heat (Fig. 59A). Moreover, autoclaved P144 solution was neither able to reproduce the P144 inhibitory activity detected in the 2D migration assays. No statistical significant differences were detected on migration determined by wound healing (Fig. 59B) or spheroid assays (Fig. 59C) when autoclaved P144 vs non-treated cells were compared.

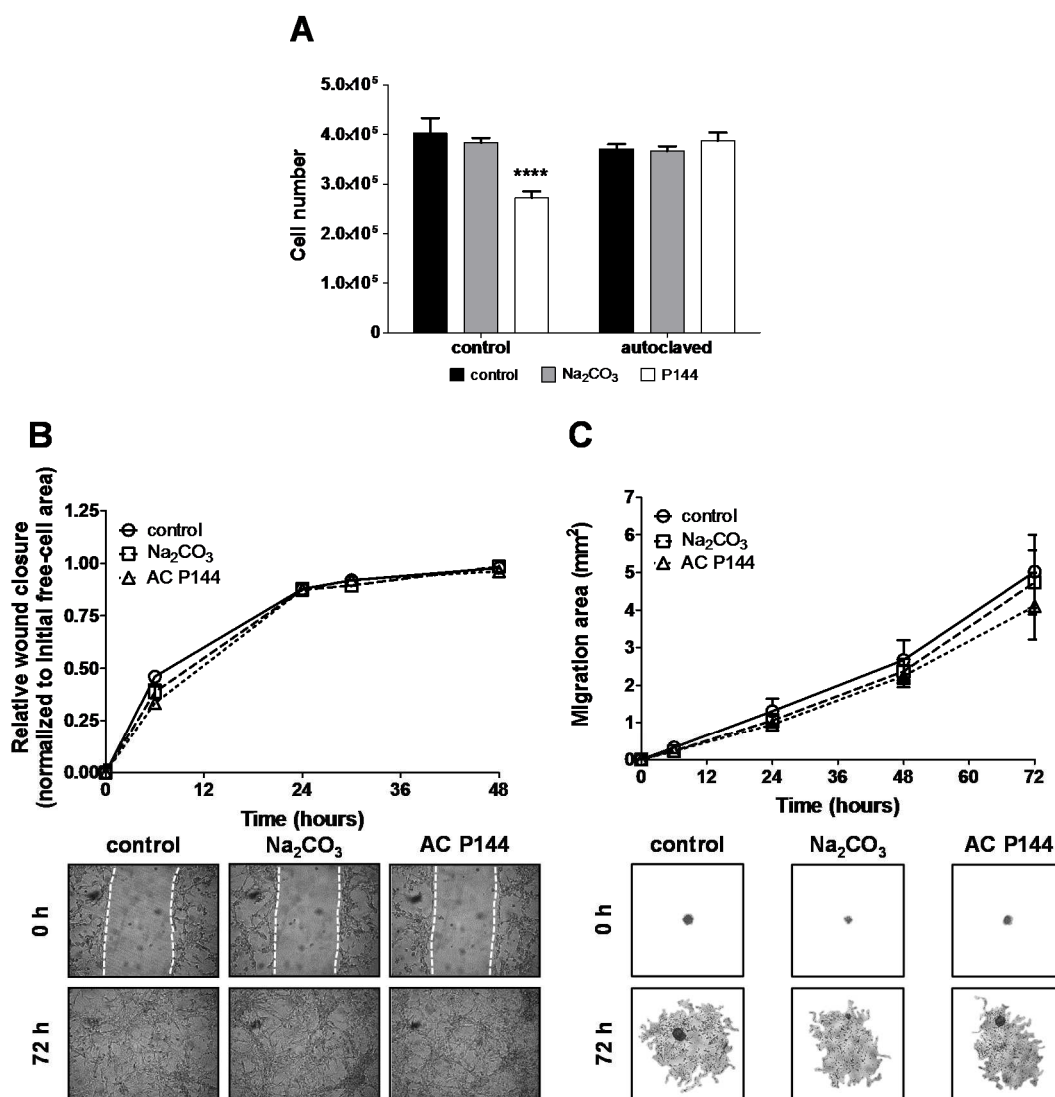


Figure 59. Analysis of autoclaved P144 biological activity. Proliferation (A) was not affected by peptide exposed to heat treatment by autoclave. Asterisks represent the significance found by two-way ANOVA followed by Bonferroni post hoc test ($p < 0.0001$ (****)). Autoclaved P144 activity in wound healing and spheroid assay are displayed in (B) and (C), respectively. Friedman test and post hoc Dunnett test present no statistical differences between groups. Representative figures from wound healing (125 \times) and spheroid assay (31.25 \times) are displayed below graphs. **AC**: autoclaved.

Since autoclave treatment produce a partial and variable buffer solution evaporation, differences in final concentrations between solution with control P144 and solution exposed to autoclave treatment were evaluated. For this purpose, P144 dissolved in Na_2CO_3 at different concentrations before and after heat processing were analysed by absorbance measurement at 220 and 280 nm. Results suggest that P144 concentration after autoclave treatment was approximately double with respect to the P144 control solution with a proportional relation with buffer volume loss (data non-shown).

In all performed assays, a stock solution of P144 at 3 mg/mL was prepared in Na_2CO_3 , and then added to the corresponding cell culture medium to obtain the desired final concentration. To confirm that the biological activity loss after autoclave treatment was not due to changes in final concentration, proliferation after 72 h of treatment (Fig. 60A) and a spheroid assay (Fig. 60B) were performed. Experiments were run with both corrected and non-corrected final volume solutions, upon absorbance obtained concentration. Cell proliferation and migration determined by the spheroid assay were not affected in both cases. This result confirms that the *in vitro* biological activity loss was not related with concentration changes induced by autoclave evaporation, but with chemical modifications produced by the heating autoclave process.

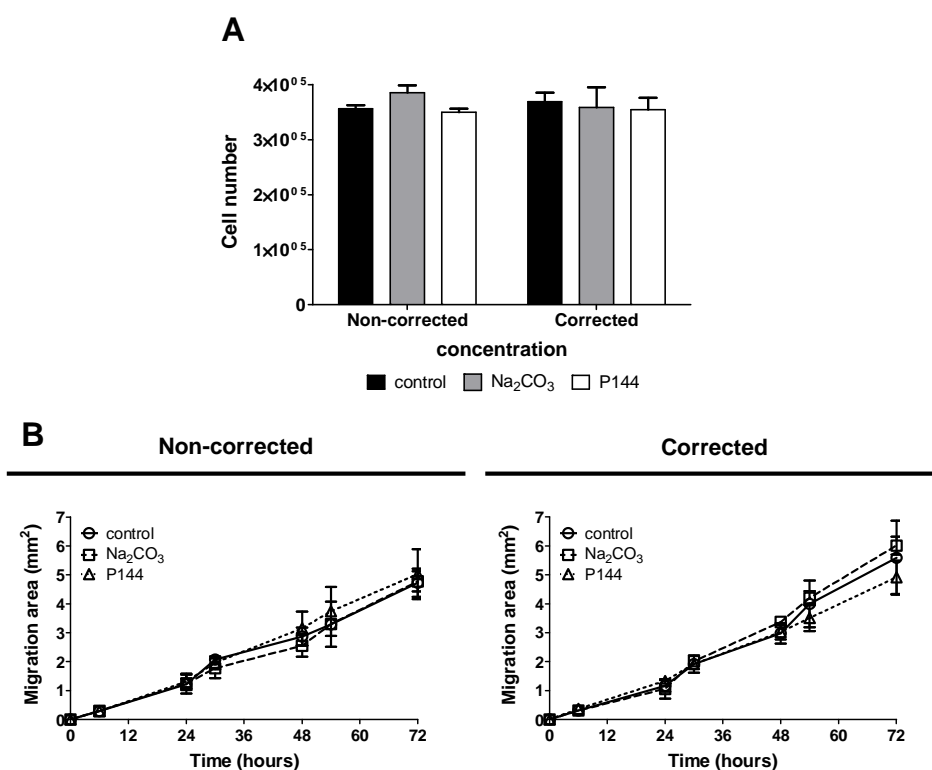


Figure 60. Biological activity analysis of non-corrected and corrected concentrations of autoclaved P144. Proliferation at 72 h (A) and spheroid assay (B) were performed. Two-way ANOVA for (A) and Friedman test for (B) did not find significant differences between groups.

5.3 P144 chemical and in vitro activity time stability

The intracranial *in vivo* assay requires a unique P144 solution load of the osmotic pump that is released over time in a controlled manner. Thus, carrier solution selection must be considered to assure the activity and stability of P144 during the whole treatment period. Few solutions are compatible as *in vivo* carriers for P144 due to its hydrophobicity. Previous analysis determined the solubility efficacy for P144 in these solutions. Then, the stability of P144 was determined in two different carrier solutions: 100 mM Na₂CO₃ and 50 mM TRIS, both at pH 9.5. The incubation was performed at 37 °C for 28 days. At days 0, 7, 14 and 28 of incubation an aliquot of each solution was collected to carry out the different analyses (Fig. 12). The concentration of P144 varied depending on the analysis performed: 1 mg/mL for optical spectrophotometry, 0.1 mg/mL for HPLC analysis and 3 mg/mL stock for biological activity assays.

Kinetics of P144 chemical stability was studied by two different approaches. First, we analysed the spectral absorbance by spectrophotometry to detect variations in P144 absorbance at 220 and 280 nm wavelengths at different time points. Any visible or significant changes in absorbance at these two wavelengths were detected in solutions incubated at 37 °C. Furthermore, the ratio of absorbance 220 nm/280 nm did not show any significant variation during the whole assay period (28 days) of incubation.

Second, P144 dissolved in Na₂CO₃ and TRIS solutions were analysed by HPLC. Two replicates of each time point and each solution were injected and analysed at 210, 220, 260 and 280 nm wavelengths. The chromatograms analysis derived from HPLC showed that P144 solutions generated two peaks as previously reported, with identical chromatogram profile and peaks retention times for all time points and samples analysed. Chromatogram peaks area was quantified with HPLC ChemStation Software (Agilent Technologies) and further analysis was carried out. Fig. 61 shows the analysis of area performed at different wave lengths and time points. P144 peaks area starts to diminish after 14 days of incubation in Na₂CO₃ solution and after 7 days in the case of TRIS solution. Finally, the area ratio between peak 1 and 2 was calculated. Unexpectedly, the ratios varied significantly depending on the solution used to dissolve P144, showing an opposite trend. This ratio increased with time when P144 was dissolved in Na₂CO₃ after 7 days of incubation and maintained constant until day 28. No significant differences were found comparing the ratios obtained at days 7, 14 and 28. The opposite effect was found when incubation was performed in TRIS. The area ratio between peak 1 and 2 decreased directly proportional to time. This decline was statistically significant after 7 days of incubation likewise in the Na₂CO₃ solution group, when compared to the initial time. Significant statistical differences were not found among days 7, 14 and 28.

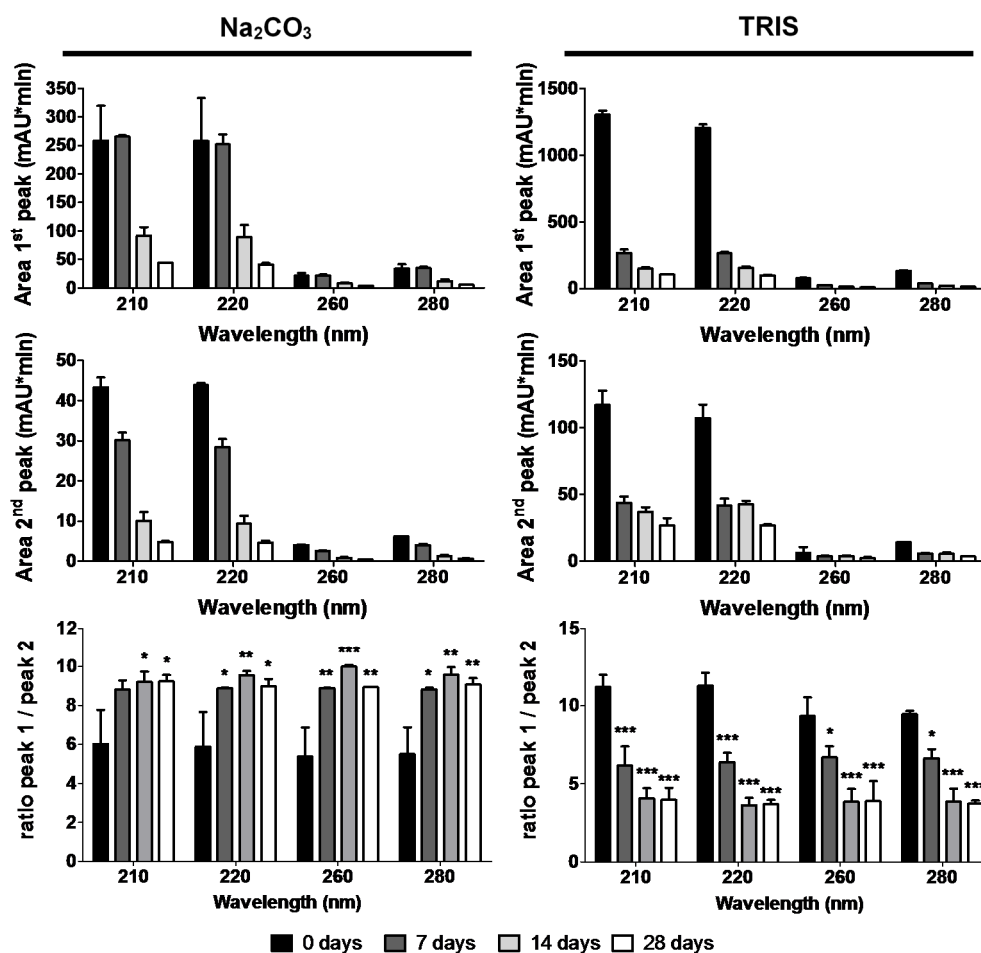


Figure 61. Analysis of P144 chemical stability by HPLC. Peaks area values are expressed as milliabsorbance units per minute (mAU*min) and the mean \pm SD is represented. Area values for peak 1 and 2 plus the ratio between them for P144 dissolved in Na₂CO₃ are displayed in the left panel, and when dissolved in TRIS, in the right panel. Statistical significance was analysed using two-way ANOVA test plus Bonferroni as post hoc test ($p < 0.05$ (*); $p < 0.01$ (**); and $p < 0.001$ (***)).

To confirm whether the P144 biological activity was stable enough over time, a proliferation assay and a spheroid assay were performed. Control and autoclaved P144 in different carrier solutions were analysed. 3 mg/mL P144 solutions in Na₂CO₃ (100 mM) or TRIS (50 mM) at pH 9.5 were prepared and splitted into two samples, one of which was subjected to autoclave treatment. A vehicle control solution was included. All solutions were incubated at 37 °C and at days 0, 7, 14, 21 and 28 of incubation an aliquot of each tube was used to perform the proliferation and the spheroid assays at a P144 final concentration of 150 μ g/mL. For those samples subjected to autoclave, the volume was corrected in order to equalize the final concentration. Cell passage number was considered: stock frozen vials with the same passage number were used for the assays performed at time point 0 and 14 (Fig. 12). Proliferation and migration quantification were performed after 72 h of treatment.

Until 28 days of incubation, control P144 was able to induce a decrease on cell proliferation, but the strength effect decreased with time. This effect was more evident with the peptide dissolved in 50 mM TRIS, reaching a non-significant reduction on proliferation at day 21. Additionally, the autoclaved P144 did not evidence any biological activity at any tested time point during incubation at 37 °C in Na₂CO₃ (Fig. 62A) as well as TRIS as a dissolving solution (Fig. 62B).

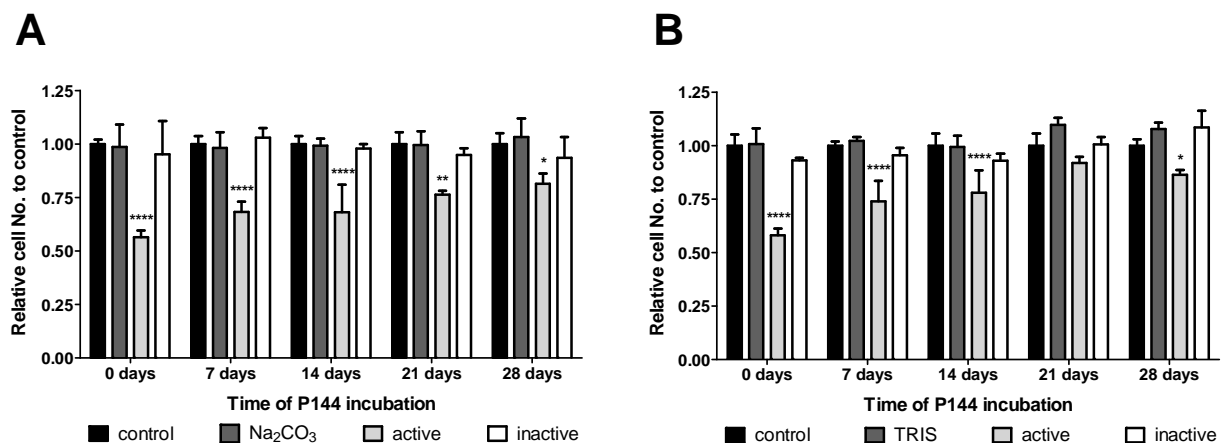


Figure 62. P144 time-dependent biological stability determined by proliferation assay. Na₂CO₃ (A) and TRIS (B) solutions were analysed. Treatments included the carrier solutions without P144, the control P144 at 150 µg/mL and the autoclaved group. Data are presented as the number of cells after treatment, normalized to the control of each time point. Two-way ANOVA and Bonferroni post hoc test detected significant differences between groups, marked by asterisks as follows: $p < 0.05$ (*); $p < 0.01$ (**); and $p < 0.0001$ (****).

Similar results were found when P144 stability in different solutions was assessed in a cell migration assay. The migration area of cells treated with P144 dissolved in Na₂CO₃ increased over time (Fig. 63), but significantly less when compared to the control. The inactive P144 in Na₂CO₃ did not show any biological activity along 28 days of incubation at 37 °C. Similarly, the active P144 dissolved in TRIS lost the migration ability over time (Fig. 64). Inactive P144 in TRIS solution displayed an apparent recovery of its biological activity but this effect did not show a regular trend or correlation with the incubation time.

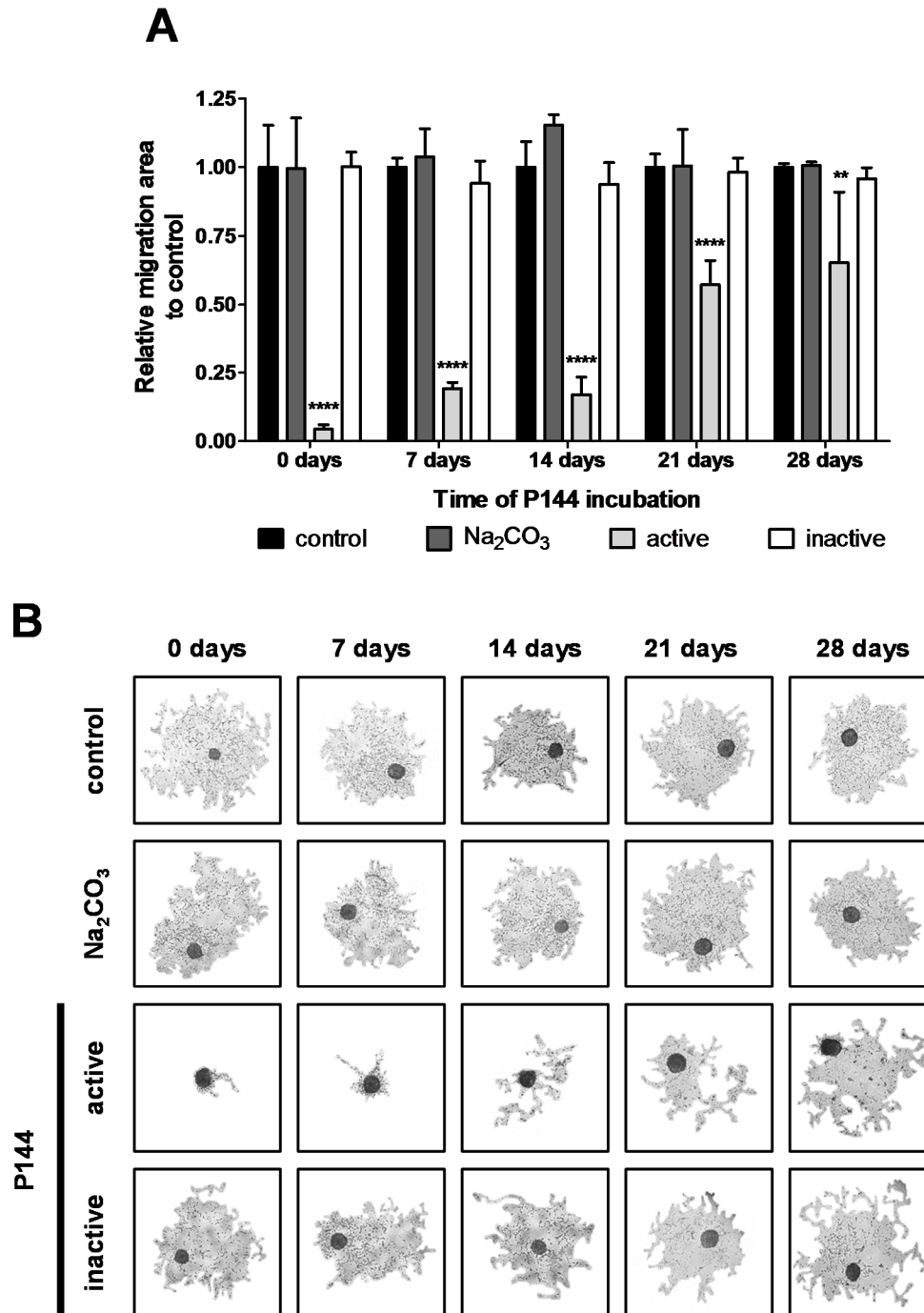


Figure 63. Time-dependent P144 biological activity in Na₂CO₃ as vehicle assessed by migration analysis. The migrated area at 72 h was measured after treatment with the control and autoclaved P144 dissolved in 100 mM Na₂CO₃. A vehicle control solution was included. All solutions were incubated at 37 °C and activity was measured at different time points until day 28. The area was normalized to control and graphed as mean ± SD (A). Two-way ANOVA plus Bonferroni post hoc tests were performed to find significant differences ($p < 0.01$ (**)) and $p < 0.0001$ (****). Representative pictures at 31.25× (B) show the time-course increased migration ability in spheroids treated with the P144 active form.

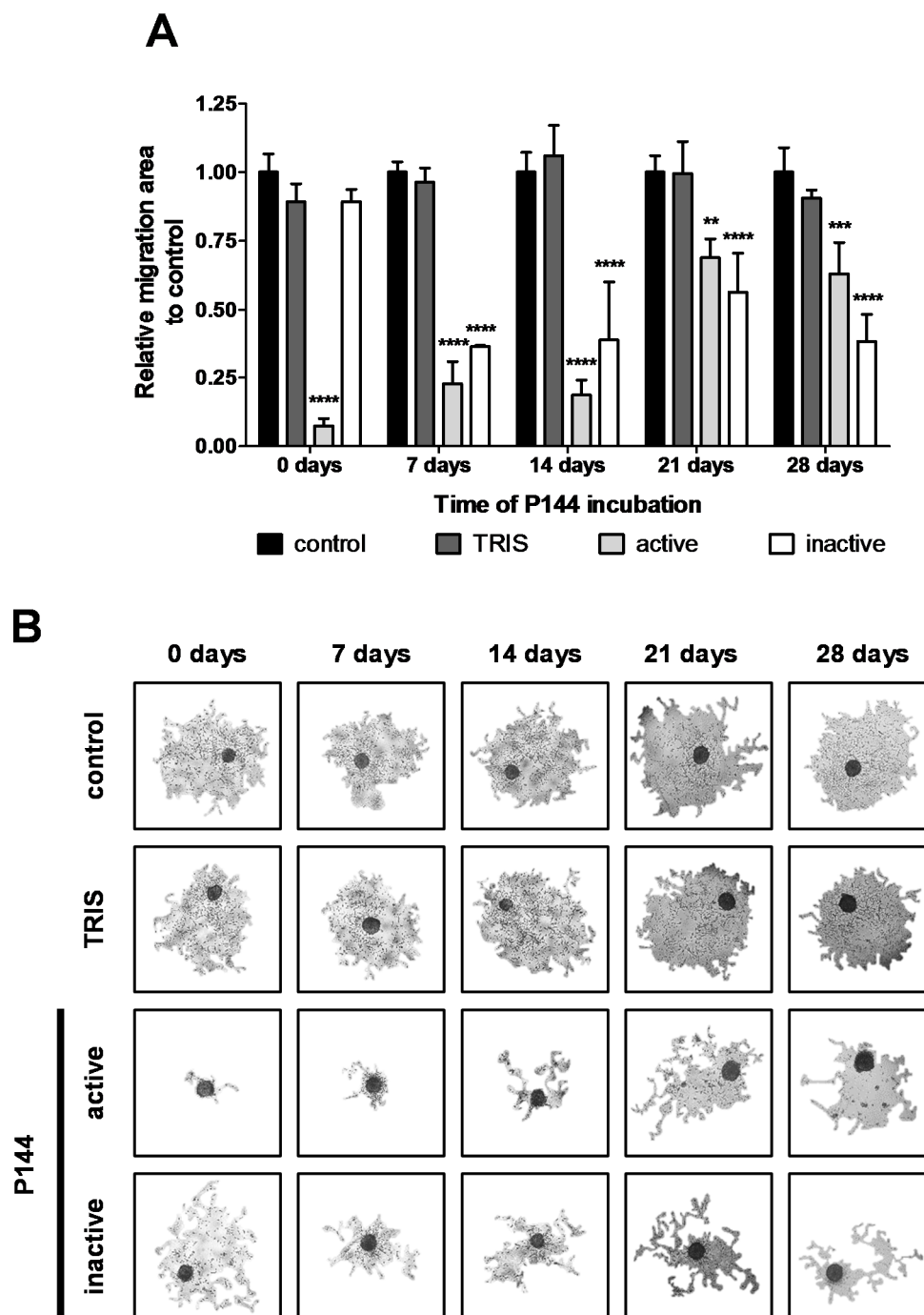


Figure 64. Time-dependent P144 biological activity in TRIS as vehicle assessed by migration analysis. As in Fig. 63, the migration area at 72 h was normalized to control (A). Asterisks represent statistical differences from two-way ANOVA test followed by Bonferroni as post-test ($p < 0.01$ (**); $p < 0.001$ (**); and $p < 0.0001$ (****)). In (B) representative pictures (31.25 \times) of each treatment and time points are displayed.

5.4 P144 in vitro release from Alzet[®] osmotic pump system

Treatment time to test antitumor activity of P144 was considered around 2-3 weeks (Dr. Peter Hau, Dr. Maïke Rüttgers, personal communication) based on previous experience in

intracranial mouse models at University Clinic Neuro-Oncology Department (University of Regensburg). For this purpose, the time of treatment allowed by the different models of Alzet[®] osmotic pumps was examined. Different models of osmotic pumps are available and its choice depends on the animal model, time of treatment (Fig. 13) and reservoir volume allowed. For mice models, pumps with a reservoir volume of 100 or 200 μL are recommended.

Thus, the selected osmotic pump model required specifications compatible with two or more weeks of P144 release period and chemical compatibility with P144 appropriate carrier solution (Table 16). P144 shows solubility in different solutions that can be used as carriers. However, certain solutions present biological toxicity (as DMSO) and others affect the availability of released P144. Both vehicle solutions selected for P144 (Na_2CO_3 and TRIS) were in the compatible pH range and were compatible with osmotic pumps.

Osmotic pumps Model 1002 were filled with high concentrated solutions of P144 in 100 mM Na_2CO_3 (5 mg/mL) or 50 mM TRIS (10 mg/mL). A constant flow of P144 solution was achieved by a flow moderator introduced in the pumps. Each osmotic pump was placed inside a 1.5 mL tube, completely submerged in PBS and incubated at 37 $^\circ\text{C}$. At different time points, an aliquot of PBS was analysed by nanophotometer in order to determine the absorbance at 220 and 280 nm wavelength. Over time P144 release from osmotic pumps to the external solution was quantified by absorbance at both wavelengths (Fig. 65). This assay was carried out to confirm the P144 release from the osmotic pump. However, the assay did not reproduce the precise *in vivo* P144 release kinetics.

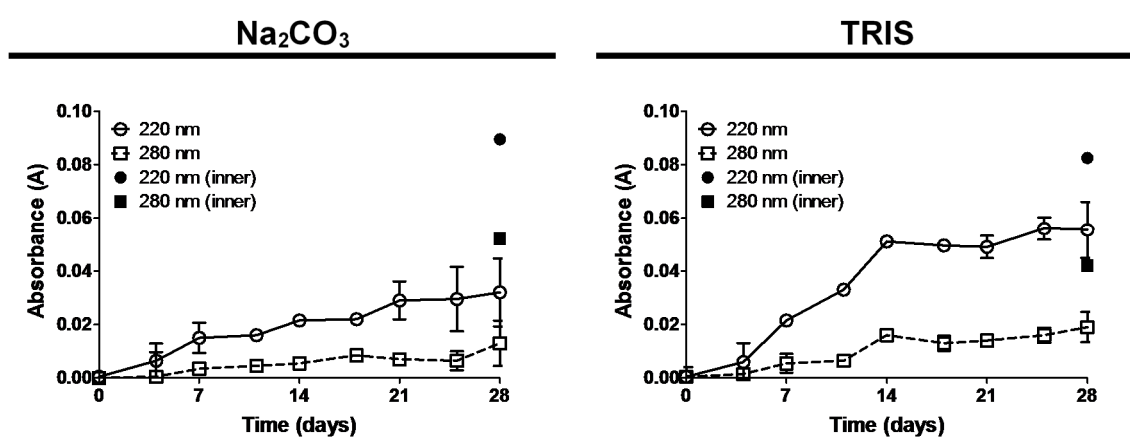


Figure 65. P144 *in vitro* delivery determination from Alzet[®] osmotic pump system. Values are the mean \pm SD of two independent repetitions.

In both solutions the sample absorbance increased over time and reached a constant value after 14 days of incubation. Indeed, the absorbance values obtained with TRIS solution doubled

those for Na_2CO_3 , being consistent with the double concentration of P144 in TRIS compared with the Na_2CO_3 solution. In addition, the remaining solution inside the pump reservoir was recovered at the end of the assay and the absorbance at 220 and 280 nm was determined. Unexpectedly, the values obtained in the inner solution were higher than those found in the external solution, even twofold in the case of Na_2CO_3 .

5.5 U-87 MG cell line intracranial tumours generation

The potential of the U-87 MG cell line to produce tumours *in vivo* was previously tested in the subcutaneous nude mouse model. Since in our hands the cell line was not previously tested in an intracranial model, a pre-assay was performed in order to determine the tumorigenic capacity of the cell line in the brain as well as the optimal number of cells to be injected and the potential effect of the osmotic pump system over tumour development as well as general health status and behaviour of mice. For this purpose, two groups of two nude mice each were injected and monitored during 14 days. Two different quantities of cells were injected, 10,000 or 100,000 cells in 2 μL of PBS. In each group of two mice, one mouse was implanted with a complete osmotic pump system filled with PBS. The general status of animals was not compromised by the osmotic pump system during all the experiment, and weight increase was normal over time in all animals. Furthermore, the cell line tested was able to produce tumours in an intracranial environment that were visualized by MRI. The imaging analysis detected the tumour mass formed in three mice (one animal presented problems with the contrast solution) and the brain implanted osmotic pump system (Fig. 66).

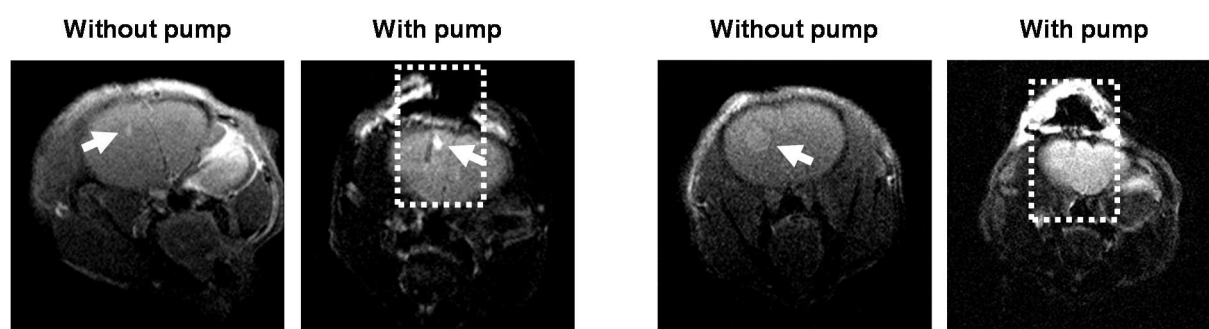


Figure 66. Tumour intracranial model pre-assay. Representative images obtained by MRI are displayed. White arrows indicated the tumour mass and the dotted squared, the cannula of osmotic pump system. In the last animal, due to problems with the contrast solution, the tumour mass could not be detected.

5.6 P144 affects tumour size in the intracranial *in vivo* model

All previous experiments and assays allowed the determination of the final conditions for the *in vivo* intracranial tumour model in nude mice. The number of U-87 MG cells as well as osmotic pump type used, concentration of P144, flow ratio and quantity of peptide delivered, carrier solution and animal groups performed are summarized in Table 20.

Table 20. Final conditions for the intracranial mouse model.

Treatment groups	Vehicle	P144	Inactive P144
Concentration	-	5 mg/mL	≈ 5 mg/mL
Carrier solution	100 mM Na ₂ CO ₃ pH 9.5		
Animals per group	8	8	8
Number of cells injected	250,000 cells in 5 µL of PBS		
Treatment schema	2 weeks of treatment + 1 week without treatment		
Osmotic pump	Alzet® model 1002		
Flow ratio	-	1.25 µg/hr	≈ 1.25 µg/hr
Theoretical delivery concentration	-	30 µg/day	≈ 30 µg/day

After surgery, cell injection, and osmotic pump implantation, animals were monitored as previously described in Materials and Methods section. The weight of each animal was measured each day as well as different characteristics in order to determine the general status of animals according to the scoring system described (Table 15).

Only one mouse from the P144 active group required euthanasia one day before performing the MRI at day 22, due to the high scoring value obtained. All mice showed body weight gaining during the *in vivo* assay period. However, a decrease after day 14 was observed in the P144 treated group (Fig. 67). This time point coincided with the end of P144 theoretical release from the osmotic pump.

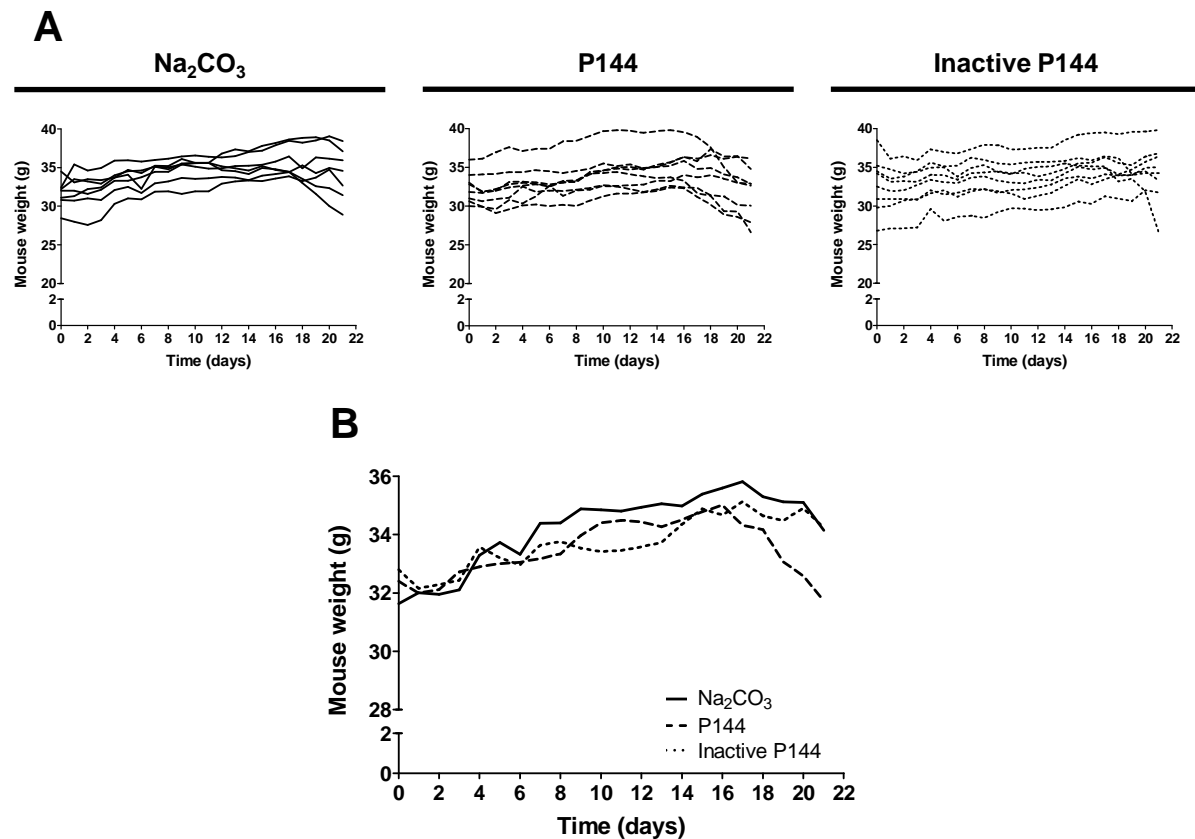


Figure 67. Body weight evolution. Individual mouse daily weight of each treatment group was registered (A). The average per treatment group is represented in (B).

After treatment schema, animals were prepared for MRI. Once the images were taken, animals were sacrificed by perfusion and brains extracted and processed for its storage. Then, brains were cut with cryostat and slides processed for histological staining.

A tumour mass was detected by MRI in all mice, except in two mice that died during the imaging acquirement process. Additionally, MRI allowed detection of cannula implantation place, confirming a correct position in all cases. Furthermore, the H&E staining confirmed the presence and position of tumours observed by MRI (Fig. 68).

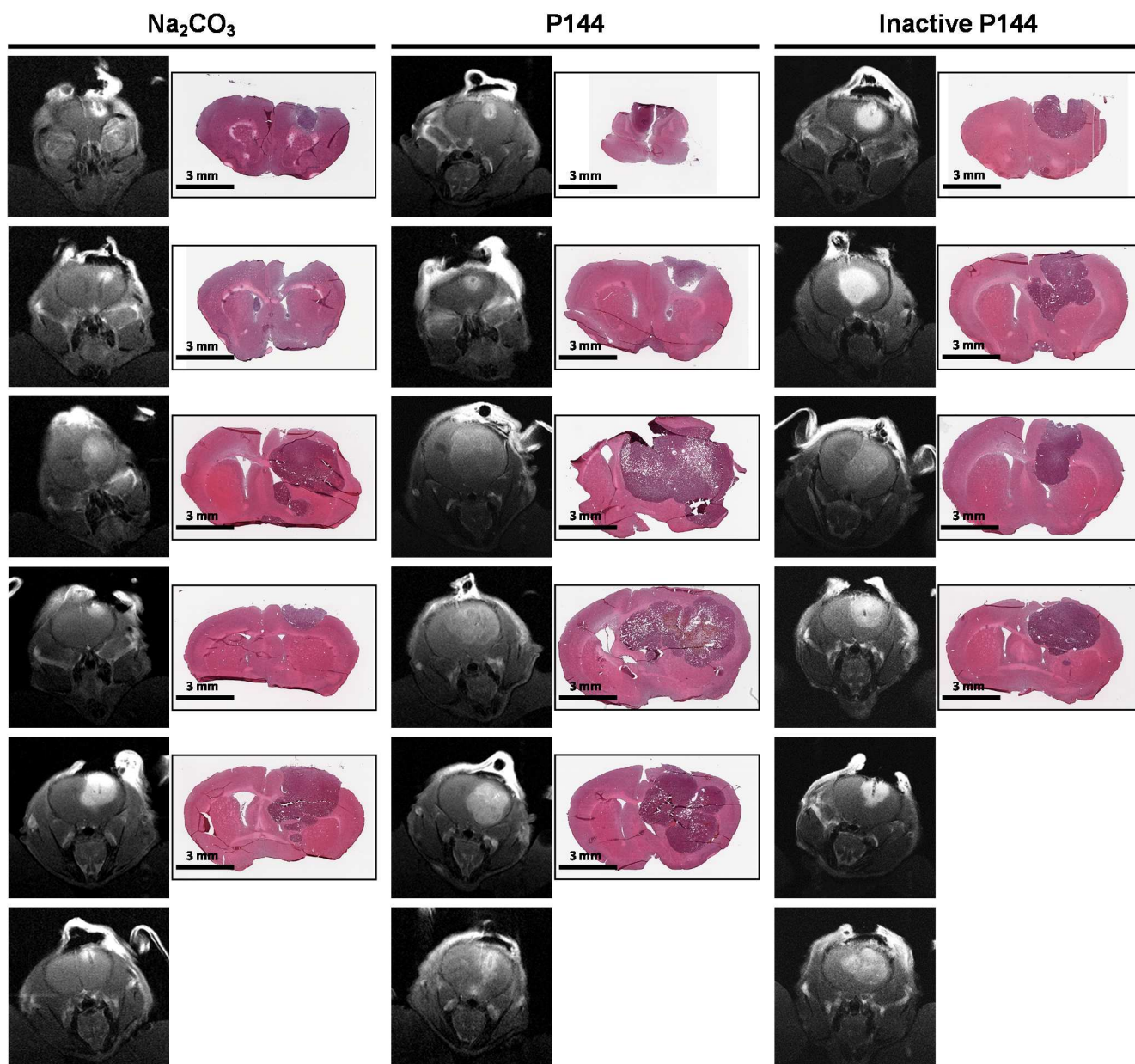


Figure 68. Magnetic Resonance Imaging and H&E. Both MRI as H&E was performed for each animal and treatment group. H&E staining missing correspond to brains that were reserved for further analysis.

The H&E staining allowed the tumour volume quantification. Since intracranial tumour cells related surgery and osmotic pump implantation requires around 1 h per animal, each treatment group of mice was processed the same day and divided in two subgroups of 4 animals, using for each subgroup a different cell suspension derived from the same cell passage. This protocol aspect was taken into account for the statistical analysis. A two way ANOVA followed by Bonferroni post hoc test allowed to consider the potential source variation upon different cell suspension used (Fig. 69). P144 treated mice displayed an increase in tumour volume when compared to control.

Moreover, no differences were detected when the inactive P144 group was compared with control.

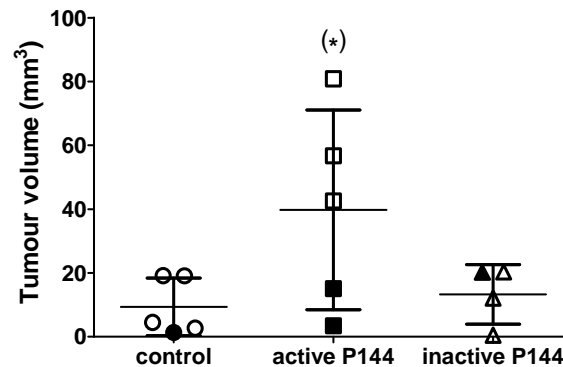


Figure 69. Intracranial tumour volume analysis. The statistical analysis of the tumour volume included a two way ANOVA plus Bonferroni as post hoc test. Significance level is indicated by asterisks ($p < 0.05$ (*)). The signs black filled represent mice implanted with the first cell suspension, and the non-filled signs, with the second cell suspension.

Tumours derived from treatment with P144 showed areas with a cell morphology consistent to apoptotic cells. This morphology was detected in the other groups but in low proportion (Fig. 68). This observation, led us to hypothesize that the increase in the tumour volume was influenced with an increase in apoptosis. To analyse this aspect, a quantification of apoptosis in the H&E samples was carried out.

H&E stained sections were examined for apoptotic cells. Apoptotic cells were characterized by cell shrinkage, with condensed hyperchromatic nodular, ring-like or beaded nuclear chromatin, and often had deeply eosinophilic cytoplasm surrounded by a clear "halo". Counts of apoptotic cells were performed using 40 \times objective. All identified apoptotic cells in the tumour were counted and an apoptotic index was defined as the total number of apoptotic cells in at least 100 tumour cells [198]. This quantification was performed five times in different representative areas of the tumour from the slides where the maximum area of tumour section was detected.

The analysis revealed that tumour samples derived from the inactive P144 treated mice showed similar values in apoptotic cells compared to control. The samples from P144 treated mice displayed an increase in apoptotic cells. However, a Kruskal-Wallis test did not detect significant difference in these values between groups (Fig. 70).

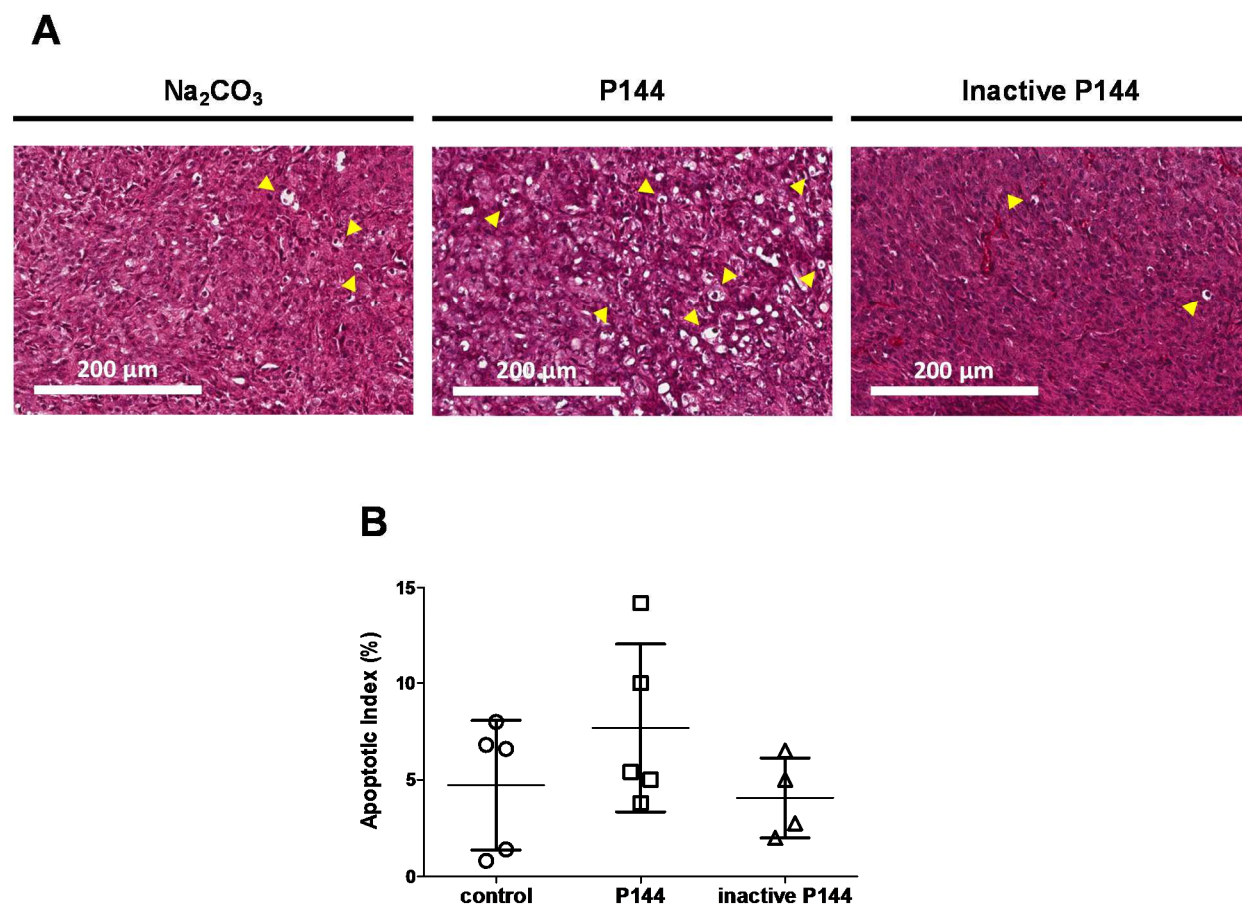


Figure 70. Apoptosis quantification in H&E slides. The measurement was carried out through the determination of an apoptotic index. In (A) representative pictures (20 \times) of each treatment group are shown. Arrow heads indicates cells with an apoptotic morphology. In (B), the average value from 5 determination for each sample is graphed. The Kruskal-Wallis test performed did not detect significant differences between treatment groups.

DISCUSSION

DISCUSSION

1) Evaluation of response to P144 in A172 and U-87 MG glioblastoma cell lines

GBM corresponds to the most malignant and lethal form of gliomas and accounts for around 60-70% of all astrocytic tumours [4, 5]. Despite its low incidence, GBM has the poorest overall survival (0.05-4.7% of five years survival after diagnosis) in comparison to other tumours of the CNS [9, 13]. The median survival for GBM is 12-15 months after diagnosis, even with maximal surgical resection, adjuvant radiotherapy, and chemotherapy [4]. In the last years the improvement in GBM survival can be measured in weeks [17].

Molecular studies have identified important genetic events in GBM [25] confirming the molecular base of the heterogeneity of this type of tumour [1]. Several regulatory pathways are implied in the origin, development and growth of different tumours as GBM. Among them, the TGF- β signalling pathway plays a pivotal role in tumours regulating progression, infiltration and radio- and chemoresistance [101-103]. Targeting of TGF- β or its downstream signalling constitutes a promising therapeutic approach [123, 151].

An increasing number of inhibitors of the TGF- β pathway are under clinical development [105] and include different strategies [101] for the treatment of diverse diseases and malignancies [149]. The inhibition of the TGF- β signalling pathway showed reduction of tumour progression and improvement in overall survival in clinical trials [105]. Antagonizing the biological effect of TGF- β is a promising experimental strategy to combat GBM [108]. Preclinical models demonstrated potent antitumour activity of TGF- β inhibition alone or in combination with radiochemotherapy. These findings have promoted the development and testing of TGF- β targeting agents in patients with GBM (Table 8). Initial studies showed good tolerability and safety of TGF- β targets, but efficacy remains to be demonstrated [108]. Here, we analysed the therapeutic potential of P144, designed to directly bind to active extracellular TGF- β 1, blocking the signalling pathway and further biological functions [156, 157].

First clinical trials attempts with TGF- β pathway inhibitors were focused on fibrosis related clinical indications. In the last years, most clinical trials are testing safety and efficacy of these compounds over different tumours and metastatic processes, including GBM [149]. Many aspects should be considered when P144 data, obtained in the present work, are compared against other TGF- β pathway inhibitors in the context of tumour development and particularly in GBM. These factors included: inhibitor molecular type (small molecules, antisense oligonucleotides, peptides, antibodies and soluble receptors), pathway inhibited step (extracellular, membrane receptor kinase activity, cytoplasmic mRNA and nuclear gene expression) (Fig. 10) and pharmacological

profile (molecular weight, solubility, toxicity, antigenicity, pharmacokinetic, half-life, bioavailability, and tissue penetration). All these aspects generate relevant chemical, pharmacological and strategic variations among different inhibitors, making clear that every inhibitor could generate different therapeutic and/or adverse effects. Therefore, comparisons between results obtained with different inhibitors of TGF- β pathway should be taken with caution in each experimental model or clinical context. Even similar compounds acting at the same pathway level could differ importantly in their activity. For example, P144 and P17 are peptides of similar length (14-15 amino acids) and molecular weight (1,5-2 kDa) described as extracellular binding inhibitors of active TGF- β [158, 159] but their activity profiles substantially differ depending on tumour models and *in vitro* vs *in vivo* analysis. For instance, P17 has no activity in glioblastoma *in vitro* assays such as proliferation and apoptosis, but presents *in vivo* antitumoural activity (data not shown), in contrast to the P144 strong effect in all described glioblastoma assays and in non-small-cell lung cancer lymph nodes metastasis [172]. In other models P17 was able to develop a strong *in vitro* and *in vivo* antitumoural effect, in the context of colorectal cancer liver metastasis [199].

For evaluation of tumour treatment response, several reliable *in vitro* and *in vivo* methods have been developed [200]. The rationale of classical anticancer therapy has been focused on cell proliferation which constitutes the cell culture initial step in therapeutic evaluation of new anticancer compounds. Cell counting or dye-based assays such as MTT, are quick and robust methods to estimate the total number of surviving cells [200, 201]. In this work, the P144 effect on proliferation was firstly assessed by the MTT assay. The treatment with P144 significantly reduced the proliferation of GBM commercial cell lines. It is important to note that P144 presents no effect over proliferation in the NHA non-tumour cell line, in accordance with good tolerability and safety of previous TGF- β targeting agents initial studies [108]. For many years, the main scientific effort was focused on the identification of cancer cells specific surviving targets, since the standard therapy of cancer is limited by its toxicity to normal cells. The goal of therapy is to exploit the differences between normal and cancer cells. Currently, there are no truly cancer-specific targets [202]. TGF- β signalling, in addition to its importance in GBM, has several pivotal functions in normal tissues and cells. TGF- β has a suppressive role in embryogenesis of CNS and adult brain [101, 203]. It has been proved that particularly TGF- β 1 produces a growth-inhibiting effect not only in astroglia and microglia but also in other CNS cells as NSC [203]. Our results evidence that P144 probably has a selective antiproliferative effect on glioblastoma cells lines, but not over nontumour CNS cells (specifically on the NHA cell line) under *in vitro* conditions. The absence of P144 effect over NHA proliferation (Fig. 15C) supports P144 as a promising therapeutic candidate for the treatment of GBM without side effects on normal tissue.

However, the possible effects of P144 TGF- β inhibition on normal brain tissue need further research.

The MTT results lead us to consider that the effect of P144 over cell proliferation could be a partial consequence of additional cellular processes. The determination of apoptosis by ELISA indicates that P144 clearly increases the apoptotic levels in GBM cell lines (Fig. 16). Moreover, when TGF- β 1 was added in the presence of P144 or T β 1Ab, the induction of apoptosis was partially reverted in a significant manner. This result evidences an antiapoptotic effect of TGF- β 1 in the cell lines analysed. It has been described that TGF- β 1 inhibits caspases activity in fibroblasts inducing its proliferation [204]. This antiapoptotic effect by TGF- β mediated by other factors was also suggested in the U-87 MG cell line [205]. The protective action on apoptosis exerted by TGF- β was also described in myelo-monocytic leukemic cells by Xu *et al* [206] confirming that the treatment with TGF- β 1 in leukemic cells induces a protective effect on apoptosis. The T β RI kinase activity inhibitor, LY2109761, induced apoptosis in these cells and when added simultaneously, the inhibitor abolished the protective effect of TGF- β 1 in a similar manner to our results. The autocrine loop produced by the overexpression of TGF- β 1 and/or TGF- β 2 promotes GBM progression [110, 111] including an antiapoptotic effect that is neutralised *in vitro* by P144 in GBM cell lines.

Further analysis using AO/EB staining in A172 and U-87 MG cell lines confirmed an increase in later apoptosis and, slightly, in necrosis (Fig. 19 and 20). Cells under growth arrest can undergo apoptosis. Indeed, a correlation between apoptosis and therapeutic response in several tumours indicates that apoptosis is a goal of cancer therapy [202]. However, most common cancers and specially GBM do not easily undergo apoptosis since resistance to apoptosis is an established hallmark in GBM and other tumours [42, 202]. Efforts to detect alterations in the molecular pathway of apoptosis have been made in the past years. Numerous mechanisms are implicated in the resistance to apoptosis. The apoptotic process constitutes an attractive target for GBM treatment, since it presents the possibility to enhance current treatments in combination with other therapeutics [44, 202]. Our data suggest that the decrease on proliferation is related with the increase of apoptosis.

The induction of apoptosis by P144 on A172 and U-87 MG cell lines was initially investigated by cytometry analysis of phosphatidylserine (PS) exposure, which is an early and widespread event in apoptosis activation [207]. For this reason, apoptosis induction by antitumour compounds is usually confirmed by PS exposure at initial times of treatment. The treatment with P144 did not produce detectable exposure of PS in both cell lines (data not shown), suggesting a lack of an early activation of apoptosis by P144. However, the results were only obtained at one short time point and were not conclusive. This finding, together with ELISA and AO/EB determinations, led us to

hypothesise that P144 did not directly produce the activation of apoptosis. The increase in apoptosis could be explained through the activation of other cellular processes or regulatory pathways. In conclusion, P144 produced a growth arrest on glioblastoma cell lines *in vitro*, probably by an inhibition of cell proliferation and an indirect induction of apoptosis. These results support the possible therapeutic potential of P144 against GBM treatment.

As previously described, anoikis is an apoptotic process involved in development and tissue homeostasis. A failure in the anoikis programme results in cell proliferation at ectopic sites [45]. Resistance to anoikis is a characteristic of cancer cells that sustains invasiveness and metastatic potential [41]. Despite GBM is not characterized by metastasis (only 0.4% of cases) [133], anoikis resistance is an attractive target against GBM progression and recurrence [45]. In this work, P144 was able to impair anoikis escape, measured as a decrease in protein content in cells under anchorage-independent conditions [189-191]. The total amount of protein was affected by P144 in both GBM commercial cell lines analysed (Fig. 22), besides the fact that A172 was not able to grow under these nonadherent cell culture conditions. Since anoikis is a cell death programme executed by the same molecular machinery as apoptosis, levels of apoptosis-related proteins were measured to confirm the induction of this process [41]. The induction of BAX protein and degradation of Lamins have been reported in several human cancer cell lines as part of the apoptosis process [208]. Additionally, the activation of BAX is the major initiator of the intrinsic pathway of apoptosis and plays a crucial role in anoikis conditions [46]. We confirmed the induction of anoikis by P144, measuring the level of the BAX and the degradation of Lamin A and Lamin C (Fig. 23). Compared to control, P144 significantly increased the levels of BAX in both cell lines after 8 h of treatment, confirming the induction of anoikis. However, in the first time points analysed, levels of Lamin A and Lamin C showed a decrease in the control cells, in contrast to the increased levels observed in the P144 treated group. The decrease in Lamin A and Lamin C levels indicates a degradation of these proteins in control cells. This result could be explained by an activation of apoptosis in the culture due to nonadherent growth conditions since Lamin A and Lamin C is cleaved by caspase activation, event that was described as crucial for apoptotic induction in cancer cells [43]. In the control cells, we can assume that culture conditions induced anoikis in GBM cell lines. After 24 h, the cells apparently displayed an escaping process to avoid anoikis that induces proliferation under anchorage-independent conditions in the U-87 MG cell line. Contrarily to the control cells, levels of Lamin A and Lamin C were increased by P144. Several studies have indicated that an intact Lamin A can prevent or at least delay the execution of apoptosis, preventing chromatin condensation and fragmentation. In this way the Lamin composition could prevent or delay apoptosis [209]. The increasing levels of Lamin A and Lamin C could constitute an escaping mechanism from the anoikis process induced by P144 in GBM cell

lines *in vitro*. It should be stated that an active role of Lamins in the induction, but also in the prevention of apoptosis is beginning to emerge indicating the vital role of these proteins in cell survival. Clearly, the research on the role of Lamins in cancer has just begun [209].

Anoikis is regulated by many different signalling pathways depending on the cell type and expressed oncogenes. A better understanding of the molecular mechanisms involved in anoikis resistance would assist in the development of anticancer drugs to eradicate circulating or infiltrative tumour cells [210]. In GBM, anoikis is a process more related with cell invasiveness and migration. Escaping anoikis could explain, in part, the high infiltrative behaviour of GBM [211, 212]. Furthermore, the role of TGF- β in the regulation of anoikis has been described [212, 213]. For these reasons, anoikis resistance is an attractive target that can impair tumour progression, metastasis, and the brain infiltration of tumour cells in tissues not compromised by GBM [45]. Our results allow us to conclude that, on the one hand, the U-87 MG cell line was able to escape from anoikis in suspension cell cultures to further proliferate under this condition. On the other hand, P144 was able to induce anoikis in detached cells by the induction of BAX. Apparently, the increase on Lamin A and Lamin C levels could indicate an attempt to escape from apoptosis induced by P144 in commercial GBM cell lines. As in other assays, anoikis is a cell line-dependent process; for instance the detached A172 cells were not able to proliferate. The implication of anoikis in GBM is under study and emerging as a therapeutic target [214, 215]. The implication of TGF- β in the induction of anoikis has been described for several tumours [101]. However, in GBM the regulation of anoikis by the TGF- β pathway still remains to be elucidated. An indirect regulation of this process through TGF- β has only been described in mouse glioma cell lines [212]. Further assays must be carried out in order to identify the precise mechanism by which P144 induces anoikis in GBM cells and whether escaping mechanisms are involved.

Proliferation is not the unique parameter to be considered in the evaluation of new cancer treatment therapeutics. In the last years, the observation of tumour invasion led to the development of different *in vitro* techniques that allow for cell invasion/migration analyses. These techniques are being widely used in the discovery and evaluation of new therapeutic compounds [201]. Since invasive and migration properties of GBM are pivotal characteristics that mediate the infiltrative and aggressive growth behaviour of this tumour [216], we tested the P144 inhibitory potential over migration and invasion in GBM cell lines. The treatment with P144 not only significantly affected the invasion capacity (Fig. 24) of both cell lines analysed but also its migration capacity *in vitro* (Fig. 25). In the wound healing assay, the scratch in the treated cells was not covered even when in the control group the wound was totally healed. Recent studies point out the importance of focussing on established or novel therapeutic agents identification that are capable of impairing migration and invasion in gliomas. The finding of new agents that represent

novel anti-invasive candidates may improve the clinical management of CNS tumours, especially GBM [217]. Currently, several anti-invasive therapies for GBM treatment are under development. However, a low percentage of clinical trials are based on signalling pathways directly targeting the invasion/migration tumour capacity. This type of therapy would enhance the treatment by interrupting migration of escaping cells, making them more susceptible to the standard therapy, and limiting tumour spread [218]. Our experiments evidence that P144 inhibits migration and invasion of GBM cells lines *in vitro*, increasing its value as a potential candidate for GBM treatment.

The anchorage-independent growth correlates with tumorigenesis and malignant transformation, and is easily measured by colony forming assay in soft agar. In addition, the neurosphere formation phenotype provides information related with the cellular transformation grade and is associated with clinical outcome, becoming a predictor of progression in gliomas [193, 194]. P144 inhibited the formation of colonies in soft agar in both cell lines analysed (Fig. 26). The treatment with P144 decreased the number of colonies in U-87 MG and A172 cell lines. Interestingly, in A172 cell line, not only the number was affected but also the size of the colonies generated. It must be considered that the experimental endpoint of this assay is the surviving fraction of clonogenic cells after a treatment period defined until colonies could be observed with the naked eye [200]. The cells descending from a single surviving clonogenic cell defines a colony. The reduction in the number of colonies in both cell lines analysed after P144 treatment could further support the therapeutic potential of P144. Additionally, the observation of smaller colonies in the P144 treated group in the A172 cell line confirmed the P144 antiproliferative effect besides the clonogenic inhibition. Evaluation of more than one endpoint as well as other culture conditions must be considered in the performance of this assay to further confirm the specific influence of clonogenic inhibition and antiproliferative effect of P144 on final results. However, in the effectiveness evaluation of a drug monotherapy or in combination with other therapeutic strategies, the use of this kind of *in vitro* assays before proceeding to *in vivo*, is an imperative prerequisite [200].

The capacity of P144 to exert an antiproliferative effect on GBM derived neurospheres was also tested in A172 and U-87 MG cell lines (Fig. 27). The neurosphere formation assay does not only predict cellular transformation. It can also be used as an indicator of CSC phenotype and self-renewal capacity [80]. P144 reduced in a significant manner the neurosphere formation, both in A172 as in U-87 MG cell lines. However, this effect was cell line-dependent. The self-renewal ability was higher in U-87 MG since its neurospheres were able to be subcultured at least during 15 passages. It is widely accepted that not all tumour cell lines display the same response to anticancer agents. This could constitute the explanation for the results observed in the neurosphere assay. The underlying reasons for intertumour heterogeneity are poorly understood.

In our case, the specific mutation pattern of downstream pathways present in each cell line can affect the response to P144 in neurosphere growth. Making conclusions about whether P144 is able to target the CSC subpopulation is difficult with this only assay. The limitations of this technique have already been described. The adherent culture of GBM CSC has been reported and is replacing the neurospheres cultures. This technique presents 90-100% efficiency, compared with less than 30% for neurosphere cultures in CSC isolation. It is argued that adherent cultures provide uniform access to the EGF and bFGF growth factors, which suppress differentiation and enable expansion of highly pure CSC populations. Thus, although neurosphere assays represent a robust and widely used *in vitro* method for propagating CSC cultures, the limitations mentioned above require a critical evaluation of their use in specific experimental settings [83]. For the reasons exposed, we must limit the conclusions about the P144 effect on CSC subpopulations. However, our results demonstrate that P144 reduces tumorigenesis and cellular transformation *in vitro*, suggesting an effect against malignancy of gliomas.

It is interesting to note some differences in the response to P144 displayed by A172 and U-87 MG cell lines. The reduced capacity of A172 to develop neurospheres (Fig. 27D), its low resistance to anoikis (Fig. 21 and 22) and even the different sensitivity responding to TGF- β 1 treatment (compare Fig. 43 and 44), reflect the heterogeneity displayed by GBM cell lines. These differences in the response to a specific treatment were early identified in the resistance to radiotherapy [219] and evidence the genetic heterogeneity background of GBM cell lines. The genetic heterogeneity presented by different GBM-derived cell lines seems to influence their responses to antitumour agents. The analysis of the different responses observed and the study of a molecular mechanism underlying in a set of cell lines, could reveal new information related to resistance mechanism as well as the identification of new therapeutic targets and the possibility to increase the response to a specific treatment [219-223]. The differential response to TGF- β was also described in GBM cell lines [224]. The analysis of the treatment with P144 in a set of commercial GBM cell lines could constitute another approach in order to evaluate the potential of P144 for the treatment against GBM and could highlight the molecular mechanism behind.

2) *In vitro* analysis of P144 effect over CSC subpopulation

The relevant role displayed by CSC in the development of different types of tumours promoted the investigation of this subpopulation in GBM [60]. Cells with stem-like properties have been isolated from freshly resected human GBM. This subset of neoplastic cells, which appear to be resistant to standard therapies, can explain why tumours recur and that only by their eradication a tumour can be successfully treated [93]. Therefore, therapies targeting CSC to differentiate or die represent a novel strategy with a great potential in the treatment of GBM [42,

93, 131]. Due to the involvement of TGF- β signalling pathway in GBM progression [28] and in the maintenance of GBM CSC subpopulation [106], therapies based on the inhibition of TGF- β pathway constitute a promising therapeutic strategy [101]. Thus, we analysed the effect of P144 on BTIC lines. Different characteristics were analysed through several *in vitro* assays under two incubation conditions, normoxia and hypoxia. Hypoxia condition was included since it plays a role in malignant transformation in GBM promoting clonal selection of resistant cells to hypoxic stress [34] and the development of GBM CSC [92]. Four BTIC lines previously established in the Neuro-Oncology Department at the University of Regensburg were used. After isolation, cell lines were classified according to their expression signature in pro-neural and mesenchymal subtypes, and the expression of CSC markers was assessed [176, 225]. The analysis of the CSC markers expression (Table 17) confirmed the initial identification. The pro-neural BTIC cell lines analysed showed a significant CD133 and CD15 expression that was increased under hypoxia. On the contrary, a clear expression pattern for these markers was not observed in cell lines classified as mesenchymal. This observation is in agreement with the characteristics proposed for each CSC group (Table 4) [92].

Proliferation, migration and clonogenic assays were performed in BTIC and in the U-87 MG cell line in the presence or absence of P144 (Results, section 2). A previous work showed that TGF- β regulates proliferation, migration and tumorigenicity in BTIC lines [225]. Here, we showed that inhibition of TGF- β signalling by P144 significantly affects these characteristics. However, the inhibition magnitude did not reach the levels observed in the U-87 MG cell line. This finding agrees with the observation that CSC could be responsible for the increased resistance to chemotherapy in GBM [42]. Likewise, when clonogenicity was analysed, all cell lines treated with P144 displayed a reduction in the capacity to produce progeny, in accordance with previous work in which inhibition of TGF- β signalling impaired clonogenicity and self-renewal capacity in GBM CSC [226].

According to the molecular pattern, two distinct types of GBM CSC have been identified, mesenchymal and pro-neural. Phenotypically, these two CSC subtypes are different, being the mesenchymal subtype more aggressive [90-92]. Here, we analysed two cell lines from each subtype. A clear difference in the response to P144 was not identified, suggesting that the molecular background in the cell lines analysed do not affect the responsiveness to P144. Beier *et al* [225] described that the pro-neural subtype showed a deficiency in the T β RII receptor and is resistant to the regulatory effects of TGF- β . However, P144 treatment affected both CSC subtypes in the same magnitude, at least in the cell lines analysed. The different response to TGF- β inhibition observed in GBM CSC can be explained by the genetic background of GBM in different patients [111]. Despite the deficiency of T β RII in the pro-neural subtype, P144 was able to affect proliferation and the migration potential as well as the clonogenicity ability in cell lines analysed

from these subtype. It is clear that P144 is able to bind TGF- β and thereby to inactivate the pathway [160]. Nevertheless, it must be considered the different regulation points that are involved in TGF- β signalling to explain the effect observed even when a deficiency in T β RII is present. The interaction of other signalling mediators with T β RI or T β RII or the action of other adaptor proteins could explain the effect of P144 despite the deficiency in some of the canonical receptors [106]. Further experiments must be carried out to determine the underlying molecular mechanism of P144 and, in this way, increase its therapeutic potential targeting the CSC subpopulation.

Tumour hypoxia observed in GBM negatively affects therapy outcome and is largely thought to be responsible for insufficient *in vivo* efficacy of *in vitro* identified compounds [128]. The P144 activity was clearly affected under hypoxia in the BTIC lines analysed. The expression of CSC markers, signalling pathways and resistance to therapy are modulated under hypoxia conditions [93]. Moreover, the association of hypoxia with tumour invasion, resistance to radiation and chemotherapy and poor survival of GBM patients could be explained by CSC [38]. In GBM CSC, hypoxia increases the expression of several CSC markers as CD133 and SOX2 [227]. In the BTIC lines studied, this effect of hypoxia on the CD133 and CD15 markers was observed. Trying to eradicate CSC through targeting the hypoxia effects is a very valuable area that may open new perspectives for GBM therapeutics and increase the therapeutic efficiency of new compounds [38, 93].

We cannot discard that CSC subpopulation enrichment did not reach 100% efficiency, probably affected by consecutive passages and our growth conditions including culture medium. Further, we can consider that the initial representative amount of CSC present in culture differs in each cell line. The differences observed in the antiproliferative effect of P144 with different initial cell densities support this hypothesis (Fig. 31). The phenotypical changes throughout passages observed in the RAV20 and RAV19 cell lines in spheroid assay (Fig. 38 and 39) could indicate changes in the BTIC lines due to enrichment of CSC. Only RAV57 displayed an increased resistance to P144 in the wound healing assay (Fig. 35). Trying to obtain more information whether the resistance to P144 treatment derives from the CSC subpopulation, a correlation analysis was carried out. We found a negative correlation between the expression of CSC markers and the percentage of inhibition produced by P144. This finding could support the hypothesis that CSC are responsible for the resistance to standard therapies in GBM [93]. CSC could be more resistant to the P144 effect; however, we must be careful with this conclusion. The evaluation of P144 on CSC must be carried out through specific assays. It has been reported that P17, another TGF- β inhibitory peptide, decreased the expression of CSC markers as CD44 and SOX2 in adenocarcinoma cell lines [174]. Whether P144 has similar effects on GBM CSC is not yet elucidated. Current

limitations and issues in the clear identification of this cells subset in GBM [83] lead to develop other required assays to confirm our hypothesis. For instance, the effect of P144 on the expression of specific GBM CSC markers, as well as its evaluation in isolated CSC (as CD133 positive and/or negative fraction) must be considered.

3) In vitro characterization of TGF- β signalling pathway inhibition by P144

The subsequent step after TGF- β binding to its membrane receptors includes the recognition and phosphorylation of SMAD2 protein. This phosphorylation is a pivotal event in the initiation of TGF- β signalling pathway, followed by other steps of signal transduction [101]. Therefore, the determination of the phosphorylation status of SMAD2 is a direct evidence of the activation or inhibition of the canonical TGF- β signalling pathway. In addition, A172 and U-87 MG cell lines have been widely used for the study of different aspects of the TGF- β signalling pathway in GBM. The study of inhibitory compounds [228-230], regulatory elements and processes [122, 231-235], and therapeutic strategies [230, 236, 237] have been tested in these cell lines since different studies confirmed a functional and intact TGF- β signalling that allow these cell lines to respond to TGF- β [238, 239].

P144 was able to block SMAD2 phosphorylation over time (Fig. 41A). In A172 and U-87 MG cell lines, P144 inhibited the activation of TGF- β pathway in the same magnitude that the T β 1Ab treatment did. On the contrary, exogenous TGF- β 1 treatment induced the pathway in both cell lines (Fig. 41B). Additionally, P144 was able to inhibit the phosphorylation of SMAD2 not only *in vitro* but also *in vivo* (Fig. 55). These findings confirm the ability of P144 to inhibit the phosphorylation of SMAD2 under *in vivo* conditions in a subcutaneous mouse model.

Since the isoform TGF- β 2 is considered to be a key factor in GBM progression [28, 110], we determined the ability of P144 to bind and block the biological activity of both isoforms, TGF- β 1 and TGF- β 2. The phosphorylation status of SMAD2 was assessed in cells treated with TGF- β 1 or TGF- β 2 (Fig. 42), together with the addition of P144. The P-SMAD2 levels decreased in a dose-dependent manner with the treatment with P144. It was recently described that the three isoforms of TGF- β are broadly expressed in patients-derived GBM and, apparently, the expression of all three isoforms are controlled by a common pathway not yet identified [240]. This finding suggests that targeted approaches focusing on a particular isoform are unlikely to be successful in glioblastoma [240]. The failure in the evaluation of TGF- β 2 antisense oligonucleotides (e.g. AP-12009) could be partially explained by the interaction in the GBM biology of the three TGF- β isoforms. Acting only over one could lead the other isoforms to counteract the produced inhibition. The ability of P144 to bind not only the TGF- β 1 isoform but also TGF- β 2 supports the therapeutic potential for the treatment against GBM.

After receptor-mediated SMAD2/3 phosphorylation, the phosphorylated SMAD2/3 forms a complex with SMAD4 and moves to the nucleus [101, 102]. The different assays carried out confirmed that the inhibition produced by P144 in the SMAD2 phosphorylation is also translated to a blockade of the nuclear translocation (Fig. 43 and 44). It is well established that SMAD proteins have a ligand-independent constant shuttle process between cytoplasm and nucleus mediated by different transport mechanisms [102]. Our results were in agreement with some observations made by Schmierer and Hill [241] that proposed a mechanism to explain the nuclear translocation of SMAD proteins. For instance, this work pointed out that the phosphorylation kinetics match with nuclear accumulation kinetics, both reaching a maximum after 45 min of TGF- β treatment. Furthermore, they proposed that probably there is no cytoplasmic pool of P-SMAD2 since after activation, P-SMAD2 is translocated to the nucleus. Both observations were highlighted in our analyses.

4) Analysis of therapeutic potential of P144 in mouse models

For technical reasons, scientists mainly used ectopically-implanted, subcutaneous-growing tumour models. Most preclinical data on new anticancer drugs were obtained using transplanted tumour cells frequently as xenografts of human origin. Considerable scepticism about the value of ectopic tumours arose when some new drugs in clinical trials were not as effective as in the preclinical setting. However, a detailed comparison of preclinical results and clinical data reveals that ectopically-implanted tumour models can be remarkably predictive when experiments are performed under clinically relevant conditions [200].

Investigation of human tumours requires an immunodeficient host as nude mice to avoid tissue rejection [200, 242]. In the *in vivo* evaluation of P144, a subcutaneous xenograft nude mouse model was assessed as a first approximation. Several considerations in the development of the subcutaneous model were taking into account. For instance, to confirm the cytological neoplastic origin of generated tumours [243], a histological analysis was performed, and the generated tumours showed the typical morphology of GBM (Fig. 52). Moreover, the evaluation of an objective response in clinical trials enrolled patients requires a measurable disease at baseline [243]. When treatment begins at the moment when a tumour nodule is established (a tumour growth delay study), the results are more convincing than results in a tumour growth inhibition study (whether treatment begins the day after or on the day of tumour cell implantation). Tumour growth delay is a better model of clinical disease, and may be the most important estimate of preclinical antitumour effectiveness, because it mimics most closely clinical endpoints and requires observation of mice during disease progression period [244]. For this reason, the

treatment with P144 in mice was started at the time when a measurable tumour mass was detected.

The treatment with P144 impaired not only the tumour growth but also increased the survival of the treated group (Fig. 51A and 51B). The tumour growth assay is robust, standardized, widely accepted and used in most experiments to study anticancer agents *in vivo* [200]. P144 produced a delay in the growth that generates an increase in the survival, probably because the endpoint established was related with the tumour mass. The delay in growth provides not only evidence for further drug evaluation in clinical trials, but also helps to design further clinical trials [200]. The delay in the tumour growth, as well as the increase in the survival, supports the therapeutic potential of P144.

In order to analyse whether the effect on tumour mass was due to the ability of P144 to impair different cellular process, IHC staining was performed. Proliferation, apoptosis, and angiogenesis was quantified by IHC in tumour samples extracted after reached the tumour size endpoint (Fig. 53). Despite a clear effect on proliferation and apoptosis was observed *in vitro*, contradictory results were obtained *in vivo*. Proliferation showed only a non-significant decrease and, in contrast to observed *in vitro*, apoptosis was significantly decreased. It is obvious that cell cultures represent an artificial and simplified system. Unlike the situation *in vitro*, a tumour is a 3-dimensional complex consisting of interaction of several cell types. Vascularization, perfusion, and thereby, drug access to the tumour cells are not evenly distributed. This last issue is an important source of heterogeneity in tumour response to drugs that does not exist *in vitro*. However, in our case, a clear effect on tumour growth was detected; including a significant decrease in the tumour growth ratio after 21 days of treatment (Fig. 51D).

The disagreement between the IHC analysis and the P144 effect on tumour growth and survival could be explained by the endpoint utilised. The development of endpoints requires a careful examination of: (i) the experimental objectives and scientific endpoints; (ii) the characteristics of the tumour system and the possible adverse effect on the host; (iii) the effect of additional experimental challenge; (iv) the onset of critical phases (e.g. tumour associated disease, lethality or drug toxicity); (v) the animal model; and (vi) the quality of animal care [245]. In this first *in vivo* approach, our experimental objective was to obtain data regarding tumour growth and response. This kind of experimental design elucidates the growth pattern of the tumour in control mice as well as the effect of the drug on the tumour growth pattern [244]. It is important to note that the endpoint of the tumour growth delay is a time to reach a volume but not a volume at a given time point. The difficulty is that no consensus was reached about the optimal endpoint size to report data from growth delay assays [200]. In this case, the importance of the tumours

response observation period must be taken into consideration. At early days of treatment, the resolution among the groups analysed could be very limited; however, when the tumour observation period is extended, differences could become clear [244]. Due to resources availability we could not perform a time-course *in vivo* assay, where information related with how P144 affects different processes and molecular markers at different time points could be obtained. It is clear that further assays must be carried out to confirm the therapeutic potential of P144 in *in vivo* models considering, for instance, evaluation of tumour characteristics at different time points to evaluate the effect of P144 on tumour progression over time.

Despite that the subcutaneous xenograft model is easy to monitor and quantify, several limitations have been described in this model regarding evaluation of new drugs for GBM treatment [242, 246]. At first, the absence of normal brain parenchyma environment, followed by the lack of BBB, are known to affect drug delivery and clearance kinetics. Also, the absence of brain immune-privileged conditions does not permit ascertainment of potential neurotoxic effects of therapeutic agents. Finally, the large number of cells implanted to induce tumour growth greatly differs from single cell transformation and further induction of spontaneous tumour development [246].

Our next step was the evaluation of P144 treatment in an orthotopic model using the U-87 MG cell line and Alzet® osmotic pumps for P144 delivery. Although technically more demanding, orthotopic xenograft models of human glioma cell lines or tumour explants are preferred [246]. The *in vivo* assay performed corresponds to a growth inhibition study, where the treatment starts on the day of tumour cell implantation [244]. Additionally, osmotic pumps allowed a constant P144 delivery directly to the injection site [242] bypassing BBB related issues [246]. Analysis of obtained results (Fig. 68 and 69) generated two conclusions. On the one hand, autoclaved P144 did not produce any significant variation in tumour size compared to control. On the other hand, the P144 treated mice displayed a significant increase in tumour size. Initially, it could be considered that P144 is not effective when it is administered in the brain environment. However, a number of considerations must be done:

(i) The possible P144 residual effect was assessed *in vitro* in the U-87 MG cell line (Fig. 56), and no residual effect was detected, suggesting a reconsideration of the treatment schema for P144 in the *in vivo* assay. An evaluation of P144 residual effect must be considered to confirm *in vitro* results.

(ii) When the treatment protocol as well as the treatment formulation may be stressful or toxic or may have physiologic effects that could alter the viability of the tumour cells, *in vivo* assays should also include a vehicle-treated control (the compounds and solutions that were used to

prepare the drug formulation) [200, 247]. Due to the hydrophobic profile of P144 [159], the solubilisation of P144 depends on pH and on the chemical properties of the vehicle control. In this work, we analysed two different vehicle solutions *in vitro*, Na₂CO₃ and TRIS. Chemical and biological stability of P144 was determined in these solutions.

(iii) Despite no detectable chemical properties modification of P144 were detected over time in performed assays, biological stability of P144 was compromised (Fig. 62, 63 and 64). In general, P144 biological stability was affected in the same magnitude in both solutions. Only slight differences in P144 biological activity reduction were noticed depending on vehicle solution. For instance, the results observed in the spheroid assay were significantly affected due to solidification or gelation of the P144 solution in TRIS buffer. This characteristic that was transferred to the culture medium where the spheroid assay was carried out (direct observation), could explain the inhibitory effect observed on cell migration ability. Despite the fact that the treatment period coincides with the higher P144 biological stability period *in vitro*, we are not able to assure whether under *in vivo* conditions the stability of P144 varies from that observed *in vitro*. Furthermore, the vehicle solution could affect the activity of P144. *In vivo* analysis of P144 stability in different vehicle solutions must be carried out to confirm if the *in vivo* results are related to unconsidered external factors or due to the brain environment influencing P144 antitumour activities.

(iv) Similar considerations must be taken with autoclaved P144. The analysis performed on P144 subjected to the autoclave process indicates its complete biological inactivation, not only *in vitro* but also *in vivo*. After autoclave treatment, P144 was not able to reproduce the previously observed *in vitro* effects on cell proliferation and migration (Fig. 59). Mice treated with inactive P144 showed the same tumour size than vehicle control group (Fig. 69). Autoclave procedure generates an easy, low-cost and fast equivalent negative control avoiding the use of scramble peptides that must be generated *de novo* by chemical synthesis at high cost. However, the detailed molecular characterization of P144 after autoclave treatment (heat and high pressure saturated steam) will determine what changes in the structure of P144 lead to loss of the biological activity. This knowledge could facilitate the understanding of the underlying molecular mechanism as well as the identification of specific modifications that might increase the biological effect and the therapeutic potential of P144.

All the previous experiments performed before the intracranial *in vivo* assay lead us to consider the osmotic pump as a compatible system for P144 administration. Indeed, the release of P144 from this system was assessed *in vitro* (Fig. 65). However, the correct P144 delivery into the injection place must be assured. The analysis of H&E slides identified increase tendency in

apoptosis within the tumour mass of P144 treated group (Fig. 70). However, the presence of perinuclear halos could be also the result of technical issues such as delayed in fixation in frozen sections [248]. The real biological mechanism related with this observation must be elucidated by further analysis. Similarly to the subcutaneous *in vivo* assay, the IHC analysis of cellular processes as proliferation and apoptosis, as well as specific markers quantification like SMAD2 phosphorylation status, can provide useful information related with P144 activity over intracranial generated tumours. In addition, IHC analysis can highlight the potential influence of P144 in the surrounding normal brain tissue.

Despite the consistent results obtained in the subcutaneous model regarding to the arrest of the tumour growth and the increase in the survival produced by P144, the orthotopic intracranial *in vivo* model did not reveal antitumour activity by P144. Numerous GBM studies still involve subcutaneous mouse models in a poorly vascularized environment in contrast with the natural habitat of GBM, the highly vascularized brain parenchyma [249]. Additionally, in the work of Blouw *et al* [249] the involvement of hypoxia could explain the differences in the results obtained when a subcutaneous model is compared with an intracranial model. Similarly to our results, they observed a radical change in tumour behaviour when the site of implantation was changed from the subcutaneous environment to the intracranial space [249]. The importance of hypoxia in GBM progression and behaviour has been previously described. Indeed, the oxygen concentration in healthy brain tissue (2.5-12.5%) is high in comparison to GBM, which display oxygen concentrations that varies from mild hypoxia (0.5-2.5%) to moderate-severe hypoxia (0.1-0.5%) [93]. It is important to emphasize that the microenvironment has to be taken into consideration in the evaluation of new therapeutics for GBM treatment. When inoculated at a site different from their natural environment, tumours could display different behaviours, most commonly in subcutaneous sites. Subcutaneous tumours, in general, become encapsulated, lose their metastatic behaviour, and, indeed, could respond differently to a specific treatment [249]. Both hypoxia and environment factors could explain the different results obtained in both *in vivo* assays as well as the absence of typical histologic characteristics of GBM (as pseudopalisading cells and necrotic foci) in the intracranial tumours (compare Fig. 52 and Fig. 68).

In addition, we must take into consideration that due to time/resources limitations, and solubility restriction of P144, only one concentration was tested in the intracranial model. Valuable information will be obtained if different concentrations and carrier solutions for P144 are evaluated *in vivo*. Moreover, an analysis of the evolution of tumour growth could be of vital importance in the intracranial model. In contrast to the subcutaneous model where the evolution was easily measured, the intracranial model has limitations to evaluate this parameter over time. The tumour mass was measured at the end of the assay as a final result. P144 could produce an

effect at early stages of tumour evolution and the increase in size could be an adaptation to the treatment that we are not able to detect under this model conditions. The determination of another end point in an intracranial *in vivo* model could allow us to analyse tumour progression with the P144 treatment. This technique will allow survival ratio analysis as performed in the subcutaneous model. Preclinical information is considered decisive before clinical trial evaluation. However, due to limitations and external factors, an *in vivo* positive result could lead to a failure in clinical trials [200, 246]. The treatment with P144 alone increased survival in the treated group from subcutaneous xenografts *in vivo*, coinciding with other reports for several TGF- β inhibitors [226, 230, 250]. These findings support the P144 therapeutic potential.

The heterogeneity of GBM was already described. Moreover, the heterogeneous genetic background of GBM in different patients could explain wide differences in the treatment response [251]. For instance, the unmethylation of *MGMT* gene produces resistance to TMZ treatment [127]. This is only one reason whereby combined therapy in GBM must be considered [252]. Efforts are focused in personalized therapy and the combined treatment that could enhance the therapeutic efficacy of other cytotoxic agents and counteract side effects [251, 253]. The combination of TGF- β inhibitors with current and new chemotherapies is widely considered and under study [131, 153, 251, 253-255]. This approach must be analysed for P144. The obtained information could be applied to determine the appropriate patient population for the TGF- β signalling therapy [255] or increase the therapeutic benefit of other targets. For example, the LY2109761 inhibitor not only prolongs survival in GBM *in vivo* but also enhanced the radiation response in an orthotopic mouse model [226]. First step could be the evaluation of P144 with the current therapies for GBM: TMZ and radiation. As with LY2109761, a study compared its combination with TMZ and radiation. Interestingly, the TGF- β inhibitor was able to induce an increase in survival combined with TMZ in an unmethylated *MGMT* gene cell line [230]. These data support the idea that inhibition of TGF- β pathway can enhance current therapies and, apparently, counteract tumour drug resistance. Next step could be based on combination of P144 with inhibitors of other GBM hallmarks as hypoxia (targeting HIFs), angiogenesis (targeting VEGF pathway), and/or immunotherapies [153]. This kind of assays could reveal the real therapeutic potential of P144.

A final consideration regarding cell line selection for the *in vivo* assays must be discussed. The most commonly used models include cell lines established from glioma biopsies taken from patients. Among these, the U-87 MG cell line is one of the most utilised [246]. The U-87 MG cell line was established in 1975 from a female GBM patient [256]. The tumours generated by this cell line are highly cellular; however they only show a well-delineated tumour mass with a nondiffusive infiltrative growth pattern. The U-87 MG cells harbour fewer than 512 homozygous mutated genes

due to the phenotypic and gene expression alterations gathered during the original tumour explant adaptation to monolayer culture conditions. Despite its extended use, as a result of these genetic background, several groups have reported that preclinical glioma models with this cell line could have limited use as cancer drug clinical efficacy predictor [246]. Several techniques that improve surgical orthotopic implantation and further therapeutic evaluation have been proposed. The improvements include transplantation of intact fragments of human cancers directly taken from patients, to single cell suspensions from tumours or primary cultures [242]. Other cell lines and intracranial models must be considered for the *in vivo* evaluation of P144 as a GBM therapeutic option. For instance, genetically engineered models that generate equivalent tumours to human disease. These “molecular” models address deficiencies of implantable models, as the tumour initiation method or the BBB gap and reactive brain wound produced by the intracranial implantation [246]. Furthermore, the *in vivo* evaluation of P144 using the BTIC lines must be considered as a further step. Isolated cells with a CSC-like phenotype can reproduce the overall glioma behaviour generating diffuse invasion of the tumour cells into the surrounding normal brain [246]. This assay will not only provide information about the efficacy of P144 in the brain environment, but will also identify the specific effect of P144 on this particular subset of GBM cells.

5) P144 modulation of SMAD7 and SKI expression (in vitro and in vivo findings)

Many different molecular mechanisms that allow tumour cells to escape from TGF- β tumour suppressive effects have been described. In these regulatory processes, the expression levels of endogenous factors play an important role in the switching of tumour response to TGF- β [113, 114]. To study whether P144 affects some of these factors, several genes were selected for expression quantification after treatment with P144 (Fig. 47), since we considered that P144 could modulate or affect these tumour cells escaping programmes. In normal cells, TGF- β induces two cyclin-dependent kinase inhibitors, p21CIP1 and p15INK4B, that promote cell cycle arrest [113, 115, 257]. In both cell lines analysed, A172 and U-87 MG, no expression of *p15INK4B* gene was detected. Despite that the regulation of the TGF- β pathway over this gene was previously described [115, 257, 258], the majority of GBM commercial cell lines present homozygous deletions of the *p15INK4B* gene [112, 115]. It is clear that the loss or decrease in *p15INK4B* expression plays an important role in the development of resistance to the TGF- β growth inhibitory effect in gliomas [115].

In the absence of *p15INK4B* expression, other compensatory mechanisms by which TGF- β can block cell cycle progression are present [115]. In gliomas, the expression of *FOXG1*, selectively prevents the induction of *p21CIP1* by TGF- β and the further proliferation inhibition. Since FOXG1

allows tumour cells to escape from p21CIP1-mediated cell cycle arrest induced by TGF- β [113], gene expression of both genes was assessed. Changes in the kinetic expression pattern with P144 were not observed in these genes. However, diverse gene responses are implicated in the cytostatic mechanisms of TGF- β . Tumour cells that have selectively lost the antiproliferative response while still retaining other TGF- β gene responses, could have suffered a selective loss of growth-inhibitory SMAD cofactors [258]. According to the raw Ct values, high basal mRNA level of *p21CIP1* was detected in A172 and U-87 MG cell lines. This observation supports the idea that GBM cell lines displayed the escaping of the antiproliferative effect of TGF- β through activation of this cyclin-dependent kinase inhibitor that was observed in other tumour types [259]. Despite P144 was not able to modulate the expression of *p21CIP1* or its repressor *FOXG1*, the molecular mechanism behind the P144 effect needs further analysis. Determination of protein level of p21CIP1 and p15INK4B as other cyclin-dependent kinase inhibitors could help to elucidate the probable mechanism. Additionally, the intracellular location of modulators of this mechanism as FOXG1 [259] could exert a regulation process that is not affected at transcriptional level. A deeper analysis of these different involved factors could help to elucidate the underlying mechanism of P144.

Other regulators that mediated not only the escaping from antiproliferative control but also the switch to proto-oncogene functions of TGF- β signalling are SKI and SNON proteins. These proteins are two well-known negative regulators of the TGF- β signalling that are overexpressed in different tumours [113]. These factors modulate the TGF- β pathway response by interacting with SMAD2, 3, and 4, repressing the transcription induced by TGF- β [260, 261]. P144 treatment represses the expression of *SKI* in both cell lines. *SNON* was only affected in the A172 cell line. Initially, these results seem contradictory because P144 represses two repressors of TGF- β signalling that could lead to activation of the same pathway. However, like TGF- β pathway, these two regulators have both oncogenic and tumour suppressor properties depending on target cells and context [260]. It has been reported that overexpression of *SKI* antagonizes the normal growth inhibitory response to TGF- β and enables transformed cells to grow in the presence of TGF- β [262]. In this context, the negative regulation induced by P144 in the expression of *SKI* could lead to a growth arrest in GBM cells. Additionally, the regulation of both genes by TGF- β showed contradictory effects. For instance, Liu *et al* [262] reported that the treatment with TGF- β produced a decrease at short exposure, but prolonged treatment (2 h) induced an increase in the mRNA levels of *SNON*.

It is obvious that *SKI* and *SNON* present different regulation steps. However, data from different studies suggest that the levels of *SKI* and *SNON* are elevated in tumour cells, and this excess can modulate the tumour response to TGF- β [261, 262]. Even more, the downregulation of

SKI and *SNON* reduces *in vitro* and *in vivo* lung, breast and pancreatic tumour cell growth [261]. P144 was able to modulate the expression of *SKI* in both cell lines, although *SNON* expression was affected only in the A172 cell line, as mentioned above. The different expression pattern could respond to inherent differences of cell lines. Furthermore, the induced changes in *SKI* transcription were translated to a protein level decrease in both cell lines. The result shows the modulation of *SKI* by P144 and TGF- β (Fig. 48 and 50). The modulation on expression of this gene at transcriptional and translational level could explain the impairment observed in the different parameters studied *in vitro*. Additionally, the fact that *SNON* was affected in one of the cell lines analysed does not exclude the participation of this gene in the molecular mechanism of P144. A detailed analysis of the expression and protein levels of both genes, *SKI* and *SNON*, in other GBM cell lines treated with P144 could highlight the implication of each gene in the response produced by P144.

Another regulatory element that has been related with TGF- β function repression is SMAD7. SMAD7 is an inhibitory SMAD that regulates TGF- β signalling by a negative feedback loop [109, 113]. Similarly to the TGF- β pathway as well as to *SKI*, SMAD7 presents a dual role in the control of tumour growth [116]. The treatment with P144 produced a clear modulation of *SMAD7* expression both at transcriptional and translational levels (Fig. 48 and 50). This modulation was the opposite of that produced by P144 on *SKI*, since P144 increased the expression of *SMAD7* at mRNA and protein levels. Emerging evidence has revealed that SMAD7 may not be just an inhibitor of TGF- β signalling but functions as a promoter of invasion and metastasis in multiple cancers. This dual role must be considered in the development of therapeutic strategies. For instance, the overexpression of SMAD7 is positively related to numerous cancers. It is reasonable for these cancers to take advantage of the inhibitory activity of SMAD7 to overcome the TGF- β -mediated proliferation suppression. However, SMAD7 expression continuously increases along with cancer progression [263]. The induction of SMAD7 for therapeutic implications is being tested. For instance, a hepatocyte growth factor synthetic analogue (BB3) showed antifibrotic properties in animal models inducing the expression of SMAD7 [149]. There is no doubt that SMAD7 is a critical node for tumour development and a promising therapeutic target in cancer [263]. Our results support this idea and confirm that the inhibitory ability of P144 implies the modulation of SMAD7. However, drug design and/or clinical implications targeting SMAD7 should consider its switching role in cancer progression [263].

The interaction of *SKI* and SMAD7 with the TGF- β signalling pathway and its relation with tumour escaping mechanisms has been widely described. A clear expression pattern at mRNA and protein levels of these regulators in A172 and U-87 MG cell lines after treatment with P144 was consistently confirmed. This result allows us to conclude that the treatment with P144 regulates

the expression of both proteins in GBM. To confirm the significance of both proteins in GBM, we compared the expression levels of *SKI* and *SMAD7* with those obtained in the NHA cell line (Fig. 49). If *SKI* and *SMAD7* are involved in the modulation of the TGF- β pathway in GBM, and furthermore, in the P144 molecular mechanism, we will observe variations in the expression. In the adult brain, *SKI* expression is increased in areas that retain a certain proliferative potential [264]. It has been reported that *SKI* expression in GBM cell lines could be higher or similar compared to normal astrocytes [257]. On the other hand, expression of *SMAD7* in astrocytes showed downregulation and/or similar levels to those obtained in GBM cell lines [112, 115, 257, 265]. The basal expression level of both genes varies in the GBM cell lines analysed. The treatment with P144 modulates the expression of *SKI* and *SMAD7* in GBM cell lines showing a clear trend compared to NHA cell line. Additionally, the decrease in *SKI* and the increase in *SMAD7* produced by the P144 treatment were reproduced in the *in vivo* samples derived from the subcutaneous xenograft model at mRNA and protein levels (Fig. 54 and 55).

The previous results confirmed that P144 exerts its action through *SKI* and *SMAD7* modulation *in vitro* and *in vivo*. However, the exact molecular mechanism remains to be elucidated. It has been described that *SKI* negatively regulates the expression of *SMAD7* [266]. Furthermore, the regulation of *SKI* involves different mechanisms as transcription regulation, ubiquitination and other post-translational modifications [261]. The *in vitro* kinetic analysis of *SKI* and *SMAD7* showed a tight correlation between these two proteins, but we are not able to detect which event goes first, the decrease of *SKI* or the expression increase of *SMAD7*. Our results only allow us to make hypotheses related with the molecular elements underlying the P144 activity. To elucidate the precise mechanism we must analyse other regulatory elements. It is possible that P144 produces a decrease in the expression of *SKI* leading to an increase in *SMAD7* expression, since the negative regulation on *SMAD7* is lost. On the contrary, an increase in the protein level of *SMAD7* could induce the ubiquitination process by which its expression is regulated [101, 102]. The increase in the expression of *SMAD7* could induce an activation of ubiquitination that indirectly affects *SKI* expression, since it is regulated by the same process [261]. The measure of the expression of SMURFs could highlight and give information to explain our results. Owing to the absence of data from other regulatory elements in our model, it is hard to propose a possible molecular mechanism for P144. It is clear that *SKI* and *SMAD7* proteins are regulated not only by P144, as its expression is under the regulation of the TGF- β pathway, since the treatment with TGF- β produces the opposite effect than P144. To our knowledge, the presented work is the first one to describe an upregulation of *SMAD7* and downregulation of *SKI* by inhibiting the TGF- β pathway in GBM. Only one work describes that the induced overexpression of *SMAD7* by an expression vector in U251 GBM cell line, inhibited proliferation and invasion, but induced

apoptosis [265]. Moreover, the first, and probably the only evidence that SKI plays a role in GBM was recently described by Jiang *et al* [267]. The fact that P144 modulates the expression of protein elements with therapeutic potential as SKI [261] and SMAD7 [149, 263], support our hypothesis of the high potential of P144 as a therapy strategy for the treatment of GBM.

CONCLUSIONS

CONCLUSIONS

1) P144 treatment clearly reduced different cell processes implicated in GBM progression in A172 and U-87 MG human glioblastoma cell lines. Cell proliferation, migration, invasiveness and tumorigenicity were significantly impaired by P144 in these cell lines. Altogether, these results confirm the P144 value as a potential candidate for GBM treatment.

2) Apoptosis was significantly induced in P144 treated A172 and U-87 MG cell lines. Moreover, P144 blocked the protective antiapoptotic effect of TGF- β in these cell lines, and increased later apoptosis and, slightly, necrosis. The analysis showed that P144 probably induces apoptosis in an indirect manner as a consequence of cell cycle arrest. The induction of anoikis by P144 was confirmed in A172 and U-87 MG cell lines under anchorage-independent conditions. The significant upregulation of BAX and Lamins A and C produced by P144 confirmed the induction of this apoptotic subtype process.

3) Neurosphere assay results pointed out that TGF- β signalling inhibition by P144 in A172 and U-87 MG cell lines impaired the self-renewal capacity of a putative CSC subpopulation. Brain Tumour Initiating Cells (BTIC), isolated from human GBM biopsies, treated with P144 confirmed these results. P144 reduced proliferation, migration and self-renewal capacity measured by clonogenic assay. No differences between pro-neural and mesenchymal BTIC subtypes were observed in this experimental context.

4) The antitumoural activity of P144 was significantly impaired under hypoxia. This effect was detected in concrete assays (proliferation and spheroid assay) and BTIC cell lines. Even though the mechanism that link hypoxia and resistance to P144 activity remains unrevealed, the induction of CD133 and CD15 under hypoxia might participate in this cellular response.

5) Quantification of SMAD2 phosphorylation status confirmed the P144 inhibitory effect over TGF- β signalling pathway in A172 and U-87 MG cell lines, by blocking SMAD2 phosphorylation, its consequent nuclear translocation, and TGF- β target genes transcriptional regulation.

6) P144 consistently upregulated SMAD7 and downregulated SKI at transcriptional and translational levels in A172 and U-87 MG cell lines. These findings strongly suggest the implication of SMAD7 and SKI in the molecular mechanism triggered by P144 and its participation in the regulation of the TGF- β signalling pathway. TGF- β treatment produced the opposite effects to P144 on *SMAD7* and *SKI* transcription and when combined, P144 neutralized the exogenous TGF- β effects over these genes.

7) Despite that P144 chemical structure apparently was not affected over time, its biological activity was significantly impaired. P144 biological activity was maintained until day 14 of

incubation at 37 °C in vehicle solutions, Na₂CO₃ and TRIS buffers. These data could help in the design of further *in vitro* and *in vivo* analysis of P144 activity.

8) Complete inactivation of P144 biological activity by autoclave was confirmed and validated *in vitro* and *in vivo*. Cell proliferation, migration, as well as tumour growth in an intracranial U-87 MG orthotopic nude mouse model, were not affected by inactive P144. Altogether, these results confirm that autoclave treatment is an easy, fast, nonreversible and reproducible method for P144 biological inactivation.

9) P144 significantly impaired tumour growth in a subcutaneous U-87 MG xenograft nude mouse model that leads to an increase on survival. However, the IHC analysis was not able to confirm a significant proliferation decrease or apoptosis increase, probably due to the selected assay endpoint. Additionally, SMAD7, SKI and P-SMAD2 in tumour derived samples were modulated by P144 treatment in the same manner as previously described *in vitro*.

10) Intratumoural administration of P144 via Alzet® osmotic pumps in an intracranial orthotopic nude mouse model, led to an increase in tumour size. Although this result could suggest the inability of P144 to exert its effect in a brain environment, further analysis must be considered to confirm this observation. The identification of over time cellular processes as proliferation, apoptosis or necrosis are essential to highlight the underlying mechanism that could explain tumour size increase.

REFERENCES

REFERENCES

1. Jovcevska I, Kocevar N, Komel R. Glioma and glioblastoma - how much do we (not) know? *Mol Clin Oncol*. 2013;**1**(6):935-41.
2. Bailey P, Cushing H. A classification of the tumors of the glioma group on a histogenetic basis with a correlated study of prognosis, by Percival Bailey and Harvey Cushing (with 108 illustrations): Philadelphia, London. J. B. Lippincott Company; 1926.
3. Louis DN, Ohgaki H, Wiestler OD, Cavenee WK, Burger PC, Jouvet A, Scheithauer BW, Kleihues P. The 2007 WHO classification of tumours of the central nervous system. *Acta Neuropathol*. 2007;**114**(2):97-109.
4. Wen PY, Kesari S. Malignant gliomas in adults. *N Engl J Med*. 2008;**359**(5):492-507.
5. Agnihotri S, Burrell KE, Wolf A, Jalali S, Hawkins C, Rutka JT, Zadeh G. Glioblastoma, a brief review of history, molecular genetics, animal models and novel therapeutic strategies. *Arch Immunol Ther Exp (Warsz)*. 2013;**61**(1):25-41.
6. Kleihues P, Louis DN, Scheithauer BW, Rorke LB, Reifenberger G, Burger PC, Cavenee WK. The WHO classification of tumors of the nervous system. *J Neuropathol Exp Neurol*. 2002;**61**(3):215-25; discussion 26-9.
7. Cancer Research UK. 2015 [Last access May 2015]. Available from: www.cancerresearchuk.org.
8. GLOBOCAN. 2012 [Last access May 2015]. Available from: www.globocan.iarc.fr.
9. Ostrom QT, Gittleman H, Stetson L, Virk SM, Barnholtz-Sloan JS. Epidemiology of gliomas. *Cancer Treat Res*. 2015;**163**:1-14.
10. Urbanska K, Sokolowska J, Szmidi M, Sysa P. Glioblastoma multiforme - an overview. *Contemp Oncol (Pozn)*. 2014;**18**(5):307-12.
11. Stummer W. Surgical Management of Glial Cancers. In: Watts C, editor. *Emerging Concepts in Neuro-Oncology*: Springer London; 2013. p. 143-59.
12. Di Stefano AL, Enciso-Mora V, Marie Y, Desestret V, Labussiere M, Boisselier B, Mokhtari K, Idbaih A, Hoang-Xuan K, Delattre JY, Houlston RS, Sanson M. Association between glioma susceptibility loci and tumour pathology defines specific molecular etiologies. *Neuro Oncol*. 2013;**15**(5):542-7.
13. Ostrom QT, Bauchet L, Davis FG, Deltour I, Fisher JL, Langer CE, Pekmezci M, Schwartzbaum JA, Turner MC, Walsh KM, Wrensch MR, Barnholtz-Sloan JS. The epidemiology of glioma in adults: a "state of the science" review. *Neuro Oncol*. 2014;**16**(7):896-913.
14. Dziurzynski K, Chang SM, Heimberger AB, Kalejta RF, McGregor Dallas SR, Smit M, Soroceanu L, Cobbs CS, Hcmv, Gliomas S. Consensus on the role of human cytomegalovirus in glioblastoma. *Neuro Oncol*. 2012;**14**(3):246-55.
15. Solomon IH, Ramkissoon SH, Milner DA, Jr., Folkert RD. Cytomegalovirus and glioblastoma: a review of evidence for their association and indications for testing and treatment. *J Neuropathol Exp Neurol*. 2014;**73**(11):994-8.
16. Karnofsky DA, Burchenal JH. The clinical evaluation of chemotherapeutic agents in cancer. New York, NY: Columbia University Press; 1949. p. 196.
17. Chesler DA, Berger MS, Quinones-Hinojosa A. The potential origin of glioblastoma initiating cells. *Front Biosci (Schol Ed)*. 2012;**4**:190-205.
18. Aguilar-Morante D, Morales-Garcia JA, Sanz-SanCristobal M, Garcia-Cabezas MA, Santos A, Perez-Castillo A. Inhibition of glioblastoma growth by the thiadiazolidinone compound TDZD-8. *PLoS One*. 2010;**5**(11):e13879.
19. Karsy M, Huang T, Kleinman G, Karpel-Massler G. Molecular, histopathological, and genomic variants of glioblastoma. *Front Biosci (Landmark Ed)*. 2014;**19**:1065-87.
20. Kernohan JW, Mabon RF, et al. A simplified classification of the gliomas. *Proc Staff Meet Mayo Clin*. 1949;**24**(3):71-5.

21. Daumas-Duport C, Scheithauer B, O'Fallon J, Kelly P. Grading of astrocytomas. A simple and reproducible method. *Cancer*. 1988;**62**(10):2152-65.
22. Zulch KJ. Principles of the new World Health Organization (WHO) classification of brain tumors. *Neuroradiology*. 1980;**19**(2):59-66.
23. Huse JT, Holland EC. Targeting brain cancer: advances in the molecular pathology of malignant glioma and medulloblastoma. *Nat Rev Cancer*. 2010;**10**(5):319-31.
24. Ohgaki H, Kleihues P. The definition of primary and secondary glioblastoma. *Clin Cancer Res*. 2013;**19**(4):764-72.
25. Cancer Genome Atlas Research N. Comprehensive genomic characterization defines human glioblastoma genes and core pathways. *Nature*. 2008;**455**(7216):1061-8.
26. Safa AR, Saadatzadeh MR, Cohen-Gadol AA, Pollok KE, Bijangi-Vishehsaraei K. Glioblastoma stem cells (GSCs) epigenetic plasticity and interconversion between differentiated non-GSCs and GSCs. *Genes Dis*. 2015;**2**(2):152-63.
27. Parker NR, Khong P, Parkinson JF, Howell VM, Wheeler HR. Molecular heterogeneity in glioblastoma: potential clinical implications. *Front Oncol*. 2015;**5**:55.
28. Alifieris C, Trafalis DT. Glioblastoma multiforme: Pathogenesis and treatment. *Pharmacol Ther*. 2015.
29. Cohen AL, Colman H. Glioma biology and molecular markers. *Cancer Treat Res*. 2015;**163**:15-30.
30. Tso CL, Shintaku P, Chen J, Liu Q, Liu J, Chen Z, Yoshimoto K, Mischel PS, Cloughesy TF, Liao LM, Nelson SF. Primary glioblastomas express mesenchymal stem-like properties. *Mol Cancer Res*. 2006;**4**(9):607-19.
31. Karsy M, Gelbman M, Shah P, Balumbu O, Moy F, Arslan E. Established and emerging variants of glioblastoma multiforme: review of morphological and molecular features. *Folia Neuropathol*. 2012;**50**(4):301-21.
32. Colman H, Aldape K. Molecular predictors in glioblastoma: toward personalized therapy. *Arch Neurol*. 2008;**65**(7):877-83.
33. Tysnes BB, Mahesparan R. Biological mechanisms of glioma invasion and potential therapeutic targets. *J Neurooncol*. 2001;**53**(2):129-47.
34. Jensen RL. Hypoxia in the tumorigenesis of gliomas and as a potential target for therapeutic measures. *Neurosurg Focus*. 2006;**20**(4):E24.
35. Rong Y, Durden DL, Van Meir EG, Brat DJ. 'Pseudopalisading' necrosis in glioblastoma: a familiar morphologic feature that links vascular pathology, hypoxia, and angiogenesis. *J Neuropathol Exp Neurol*. 2006;**65**(6):529-39.
36. Jensen RL. Brain tumor hypoxia: tumorigenesis, angiogenesis, imaging, pseudoprogression, and as a therapeutic target. *J Neurooncol*. 2009;**92**(3):317-35.
37. Amberger-Murphy V. Hypoxia helps glioma to fight therapy. *Curr Cancer Drug Targets*. 2009;**9**(3):381-90.
38. Yang L, Lin C, Wang L, Guo H, Wang X. Hypoxia and hypoxia-inducible factors in glioblastoma multiforme progression and therapeutic implications. *Exp Cell Res*. 2012;**318**(19):2417-26.
39. Elmore S. Apoptosis: a review of programmed cell death. *Toxicol Pathol*. 2007;**35**(4):495-516.
40. Palumbo S, Miracco C, Pirtoli L, Comincini S. Emerging roles of microRNA in modulating cell-death processes in malignant glioma. *J Cell Physiol*. 2014;**229**(3):277-86.
41. Galluzzi L, Vitale I, Abrams JM, Alnemri ES, Baehrecke EH, Blagosklonny MV, Dawson TM, Dawson VL, El-Deiry WS, Fulda S, Gottlieb E, Green DR, Hengartner MO, Kepp O, Knight RA, Kumar S, Lipton SA, Lu X, Madeo F, Malorni W, Mehlen P, Nunez G, Peter ME, Piacentini M, Rubinsztein DC, Shi Y, Simon HU, Vandenabeele P, White E, Yuan J, Zhivotovsky B, Melino G, Kroemer G. Molecular definitions of cell death subroutines: recommendations of the Nomenclature Committee on Cell Death 2012. *Cell Death Differ*. 2012;**19**(1):107-20.
42. Kogel D, Fulda S, Mittelbronn M. Therapeutic exploitation of apoptosis and autophagy for glioblastoma. *Anticancer Agents Med Chem*. 2010;**10**(6):438-49.

43. Shahzidi S, Brech A, Sioud M, Li X, Suo Z, Nesland JM, Peng Q. Lamin A/C cleavage by caspase-6 activation is crucial for apoptotic induction by photodynamic therapy with hexaminolevulinate in human B-cell lymphoma cells. *Cancer Lett.* 2013;**339**(1):25-32.
44. Eisele G, Weller M. Targeting apoptosis pathways in glioblastoma. *Cancer Lett.* 2013;**332**(2):335-45.
45. Paoli P, Giannoni E, Chiarugi P. Anoikis molecular pathways and its role in cancer progression. *Biochim Biophys Acta.* 2013;**1833**(12):3481-98.
46. Simpson CD, Anyiwe K, Schimmer AD. Anoikis resistance and tumor metastasis. *Cancer Lett.* 2008;**272**(2):177-85.
47. Modrek AS, Bayin NS, Placantonakis DG. Brain stem cells as the cell of origin in glioma. *World J Stem Cells.* 2014;**6**(1):43-52.
48. Hadjipanayis CG, Van Meir EG. Brain cancer propagating cells: biology, genetics and targeted therapies. *Trends Mol Med.* 2009;**15**(11):519-30.
49. Sampetean O, Saya H. Characteristics of glioma stem cells. *Brain Tumor Pathol.* 2013;**30**(4):209-14.
50. Galli R, Gritti A, Bonfanti L, Vescovi AL. Neural stem cells: an overview. *Circ Res.* 2003;**92**(6):598-608.
51. Vescovi AL, Galli R, Reynolds BA. Brain tumour stem cells. *Nat Rev Cancer.* 2006;**6**(6):425-36.
52. Martino G, Pluchino S, Bonfanti L, Schwartz M. Brain regeneration in physiology and pathology: the immune signature driving therapeutic plasticity of neural stem cells. *Physiol Rev.* 2011;**91**(4):1281-304.
53. Ziegler AN, Levison SW, Wood TL. Insulin and IGF receptor signalling in neural-stem-cell homeostasis. *Nat Rev Endocrinol.* 2015;**11**(3):161-70.
54. Jhanwar-Uniyal M, Labagnara M, Friedman M, Kwasnicki A, Murali R. Glioblastoma: molecular pathways, stem cells and therapeutic targets. *Cancers (Basel).* 2015;**7**(2):538-55.
55. Reya T, Morrison SJ, Clarke MF, Weissman IL. Stem cells, cancer, and cancer stem cells. *Nature.* 2001;**414**(6859):105-11.
56. Wurth R, Barbieri F, Florio T. New molecules and old drugs as emerging approaches to selectively target human glioblastoma cancer stem cells. *Biomed Res Int.* 2014;**2014**:126586.
57. Galli R, Binda E, Orfanelli U, Cipelletti B, Gritti A, De Vitis S, Fiocco R, Foroni C, Dimeco F, Vescovi A. Isolation and characterization of tumorigenic, stem-like neural precursors from human glioblastoma. *Cancer Res.* 2004;**64**(19):7011-21.
58. Ignatova TN, Kukekov VG, Laywell ED, Suslov ON, Vrionis FD, Steindler DA. Human cortical glial tumors contain neural stem-like cells expressing astroglial and neuronal markers *in vitro*. *Glia.* 2002;**39**(3):193-206.
59. Cruceru ML, Neagu M, Demoulin JB, Constantinescu SN. Therapy targets in glioblastoma and cancer stem cells: lessons from haematopoietic neoplasms. *J Cell Mol Med.* 2013;**17**(10):1218-35.
60. Binda E, Reynolds BA, Vescovi AL. Glioma stem cells: turpis omen in nomen? (The evil in the name?). *J Intern Med.* 2014;**276**(1):25-40.
61. Kahlert UD, Bender NO, Maciaczyk D, Bogiel T, Bar EE, Eberhart CG, Nikkhah G, Maciaczyk J. CD133/CD15 defines distinct cell subpopulations with differential *in vitro* clonogenic activity and stem cell-related gene expression profile in *in vitro* propagated glioblastoma multiforme-derived cell line with a PNET-like component. *Folia Neuropathol.* 2012;**50**(4):357-68.
62. Lathia JD, Venere M, Rao MS, Rich JN. Seeing is believing: are cancer stem cells the Loch Ness monster of tumor biology? *Stem Cell Rev.* 2011;**7**(2):227-37.
63. Singh SK, Hawkins C, Clarke ID, Squire JA, Bayani J, Hide T, Henkelman RM, Cusimano MD, Dirks PB. Identification of human brain tumour initiating cells. *Nature.* 2004;**432**(7015):396-401.
64. Yan K, Yang K, Rich JN. The evolving landscape of glioblastoma stem cells. *Curr Opin Neurol.* 2013;**26**(6):701-7.
65. Kenney-Herbert E, Al-Mayhani T, Piccirillo SG, Fowler J, Spiteri I, Jones P, Watts C. CD15 Expression Does Not Identify a Phenotypically or Genetically Distinct Glioblastoma Population. *Stem Cells Transl Med.* 2015;**4**(7):822-31.

66. Yamamuro S, Okamoto Y, Sano E, Ochiai Y, Ogino A, Ohta T, Hara H, Ueda T, Nakayama T, Yoshino A, Katayama Y. Characterization of glioma stem-like cells from human glioblastomas. *Int J Oncol*. 2015;**47**(1):91-6.
67. Son MJ, Woolard K, Nam DH, Lee J, Fine HA. SSEA-1 is an enrichment marker for tumor-initiating cells in human glioblastoma. *Cell Stem Cell*. 2009;**4**(5):440-52.
68. Hennen E, Faissner A. LewisX: a neural stem cell specific glycan? *Int J Biochem Cell Biol*. 2012;**44**(6):830-3.
69. Cheng L, Wu Q, Huang Z, Guryanova OA, Huang Q, Shou W, Rich JN, Bao S. L1CAM regulates DNA damage checkpoint response of glioblastoma stem cells through NBS1. *EMBO J*. 2011;**30**(5):800-13.
70. Held-Feindt J, Schmelz S, Hattermann K, Mentlein R, Mehdorn HM, Sebens S. The neural adhesion molecule L1CAM confers chemoresistance in human glioblastomas. *Neurochem Int*. 2012;**61**(7):1183-91.
71. Jackson M, Hassiotou F, Nowak A. Glioblastoma stem-like cells: at the root of tumor recurrence and a therapeutic target. *Carcinogenesis*. 2015;**36**(2):177-85.
72. Ogden AT, Waziri AE, Lochhead RA, Fusco D, Lopez K, Ellis JA, Kang J, Assanah M, McKhann GM, Sisti MB, McCormick PC, Canoll P, Bruce JN. Identification of A2B5+CD133- tumor-initiating cells in adult human gliomas. *Neurosurgery*. 2008;**62**(2):505-14; discussion 14-5.
73. De Franceschi N, Hamidi H, Alanko J, Sahgal P, Ivaska J. Integrin traffic - the update. *J Cell Sci*. 2015;**128**(5):839-52.
74. Lathia JD, Gallagher J, Heddleston JM, Wang J, Eyler CE, Macswords J, Wu Q, VasANJI A, McLendon RE, Hjelmeland AB, Rich JN. Integrin alpha 6 regulates glioblastoma stem cells. *Cell Stem Cell*. 2010;**6**(5):421-32.
75. Hale JS, Otvos B, Sinyuk M, Alvarado AG, Hitomi M, Stoltz K, Wu Q, Flavahan W, Levison B, Johansen ML, Schmitt D, Neltner JM, Huang P, Ren B, Sloan AE, Silverstein RL, Gladson CL, DiDonato JA, Brown JM, McIntyre T, Hazen SL, Horbinski C, Rich JN, Lathia JD. Cancer stem cell-specific scavenger receptor 36 drives glioblastoma progression. *Stem Cells*. 2014;**32**(7):1746-58.
76. Ying M, Tilghman J, Wei Y, Guerrero-Cazares H, Quinones-Hinojosa A, Ji H, Laterra J. Kruppel-like factor-9 (KLF9) inhibits glioblastoma stemness through global transcription repression and integrin alpha6 inhibition. *J Biol Chem*. 2014;**289**(47):32742-56.
77. Zoller M. CD44, Hyaluronan, the Hematopoietic Stem Cell, and Leukemia-Initiating Cells. *Front Immunol*. 2015;**6**:235.
78. Brown DV, Daniel PM, D'Abaco GM, Gogos A, Ng W, Morokoff AP, Mantamadiotis T. Coexpression analysis of CD133 and CD44 identifies proneural and mesenchymal subtypes of glioblastoma multiforme. *Oncotarget*. 2015;**6**(8):6267-80.
79. Bayin NS, Modrek AS, Placantonakis DG. Glioblastoma stem cells: Molecular characteristics and therapeutic implications. *World J Stem Cells*. 2014;**6**(2):230-8.
80. Ajani JA, Song S, Hochster HS, Steinberg IB. Cancer stem cells: the promise and the potential. *Semin Oncol*. 2015;**42 Suppl 1**:S3-17.
81. Jin X, Jin X, Jung JE, Beck S, Kim H. Cell surface Nestin is a biomarker for glioma stem cells. *Biochem Biophys Res Commun*. 2013;**433**(4):496-501.
82. Reynolds BA, Weiss S. Generation of neurons and astrocytes from isolated cells of the adult mammalian central nervous system. *Science*. 1992;**255**(5052):1707-10.
83. Wan F, Zhang S, Xie R, Gao B, Campos B, Herold-Mende C, Lei T. The utility and limitations of neurosphere assay, CD133 immunophenotyping and side population assay in glioma stem cell research. *Brain Pathol*. 2010;**20**(5):877-89.
84. Suslov ON, Kukekov VG, Ignatova TN, Steindler DA. Neural stem cell heterogeneity demonstrated by molecular phenotyping of clonal neurospheres. *Proc Natl Acad Sci U S A*. 2002;**99**(22):14506-11.

85. Jiang Y, Boije M, Westermarck B, Uhrbom L. PDGF-B Can sustain self-renewal and tumorigenicity of experimental glioma-derived cancer-initiating cells by preventing oligodendrocyte differentiation. *Neoplasia*. 2011;**13**(6):492-503.
86. Brescia P, Richichi C, Pelicci G. Current strategies for identification of glioma stem cells: adequate or unsatisfactory? *J Oncol*. 2012;**2012**:376894.
87. Han L, Shi S, Gong T, Zhang Z, Sun X. Cancer stem cells: therapeutic implications and perspectives in cancer therapy. *Acta Pharmaceutica Sinica B*. 2013;**3**(2):65-75.
88. Kreso A, Dick JE. Evolution of the cancer stem cell model. *Cell Stem Cell*. 2014;**14**(3):275-91.
89. Cheng L, Ramesh AV, Flesken-Nikitin A, Choi J, Nikitin AY. Mouse models for cancer stem cell research. *Toxicol Pathol*. 2010;**38**(1):62-71.
90. Bhat KP, Balasubramanian V, Vaillant B, Ezhilarasan R, Hummelink K, Hollingsworth F, Wani K, Heathcock L, James JD, Goodman LD, Conroy S, Long L, Lelic N, Wang S, Gumin J, Raj D, Kodama Y, Raghunathan A, Olar A, Joshi K, Pelloski CE, Heimberger A, Kim SH, Cahill DP, Rao G, Den Dunnen WF, Boddeke HW, Phillips HS, Nakano I, Lang FF, Colman H, Sulman EP, Aldape K. Mesenchymal differentiation mediated by NF-kappaB promotes radiation resistance in glioblastoma. *Cancer Cell*. 2013;**24**(3):331-46.
91. Mao P, Joshi K, Li J, Kim SH, Li P, Santana-Santos L, Luthra S, Chandran UR, Benos PV, Smith L, Wang M, Hu B, Cheng SY, Sobol RW, Nakano I. Mesenchymal glioma stem cells are maintained by activated glycolytic metabolism involving aldehyde dehydrogenase 1A3. *Proc Natl Acad Sci U S A*. 2013;**110**(21):8644-9.
92. Nakano I. Stem cell signature in glioblastoma: therapeutic development for a moving target. *J Neurosurg*. 2015;**122**(2):324-30.
93. Bar EE. Glioblastoma, cancer stem cells and hypoxia. *Brain Pathol*. 2011;**21**(2):119-29.
94. Cavazos DA, Brenner AJ. Hypoxia in astrocytic tumors and implications for therapy. *Neurobiol Dis*. 2015.
95. Gillespie DL, Aguirre MT, Ravichandran S, Leishman LL, Berrondo C, Gamboa JT, Wang L, King R, Wang X, Tan M, Malamas A, Lu ZR, Jensen RL. RNA interference targeting hypoxia-inducible factor 1alpha via a novel multifunctional surfactant attenuates glioma growth in an intracranial mouse model. *J Neurosurg*. 2015;**122**(2):331-41.
96. Lim KS, Lim KJ, Price AC, Orr BA, Eberhart CG, Bar EE. Inhibition of monocarboxylate transporter-4 depletes stem-like glioblastoma cells and inhibits HIF transcriptional response in a lactate-independent manner. *Oncogene*. 2014;**33**(35):4433-41.
97. Marampon F, Gravina GL, Zani BM, Popov VM, Fratticci A, Cerasani M, Di Genova D, Mancini M, Ciccarelli C, Ficorella C, Di Cesare E, Festuccia C. Hypoxia sustains glioblastoma radioresistance through ERKs/DNA-PKcs/HIF-1alpha functional interplay. *Int J Oncol*. 2014;**44**(6):2121-31.
98. Xu H, Rahimpour S, Nesvick CL, Zhang X, Ma J, Zhang M, Zhang G, Wang L, Yang C, Hong CS, Germanwala AV, Elder JB, Ray-Chaudhury A, Yao Y, Gilbert MR, Lonser RR, Heiss JD, Brady RO, Mao Y, Qin J, Zhuang Z. Activation of hypoxia signaling induces phenotypic transformation of glioma cells: implications for bevacizumab antiangiogenic therapy. *Oncotarget*. 2015;**6**(14):11882-93.
99. Cheng L, Bao S, Rich JN. Potential therapeutic implications of cancer stem cells in glioblastoma. *Biochem Pharmacol*. 2010;**80**(5):654-65.
100. Heldin CH. Targeting the PDGF signaling pathway in tumor treatment. *Cell Commun Signal*. 2013;**11**:97.
101. Kubiczkova L, Sedlarikova L, Hajek R, Sevcikova S. TGF-beta - an excellent servant but a bad master. *J Transl Med*. 2012;**10**:183.
102. Weiss A, Attisano L. The TGFbeta superfamily signaling pathway. *Wiley Interdiscip Rev Dev Biol*. 2013;**2**(1):47-63.
103. Massague J. TGFbeta signalling in context. *Nat Rev Mol Cell Biol*. 2012;**13**(10):616-30.
104. Stover DG, Bierie B, Moses HL. A delicate balance: TGF-beta and the tumor microenvironment. *J Cell Biochem*. 2007;**101**(4):851-61.

105. Kaminska B, Kocyk M, Kijewska M. TGF beta signaling and its role in glioma pathogenesis. *Adv Exp Med Biol.* 2013;**986**:171-87.
106. Sakaki-Yumoto M, Katsuno Y, Derynck R. TGF-beta family signaling in stem cells. *Biochim Biophys Acta.* 2013;**1830**(2):2280-96.
107. Heldin CH, Moustakas A. Role of Smads in TGFbeta signaling. *Cell Tissue Res.* 2012;**347**(1):21-36.
108. Joseph JV, Balasubramanian V, Walenkamp A, Kruyt FA. TGF-beta as a therapeutic target in high grade gliomas - promises and challenges. *Biochem Pharmacol.* 2013;**85**(4):478-85.
109. Principe DR, Doll JA, Bauer J, Jung B, Munshi HG, Bartholin L, Pasche B, Lee C, Grippo PJ. TGF-beta: duality of function between tumor prevention and carcinogenesis. *J Natl Cancer Inst.* 2014;**106**(2):djt369.
110. Hau P, Jachimczak P, Schlaier J, Bogdahn U. TGF-beta2 signaling in high-grade gliomas. *Curr Pharm Biotechnol.* 2011;**12**(12):2150-7.
111. Caja L, Bellomo C, Moustakas A. Transforming growth factor beta and bone morphogenetic protein actions in brain tumors. *FEBS Lett.* 2015;**589**(14):1588-97.
112. Kaminska B, Kocyk M, Kijewska M. TGF Beta Signaling and Its Role in Glioma Pathogenesis. In: Barańska J, editor. *Glioma Signaling.* Advances in Experimental Medicine and Biology. **986**: Springer Netherlands; 2013. p. 171-87.
113. Seoane J. Escaping from the TGFbeta anti-proliferative control. *Carcinogenesis.* 2006;**27**(11):2148-56.
114. Inman GJ. Switching TGFbeta from a tumor suppressor to a tumor promoter. *Curr Opin Genet Dev.* 2011;**21**(1):93-9.
115. Rich JN, Zhang M, Datto MB, Bigner DD, Wang XF. Transforming growth factor-beta-mediated p15(INK4B) induction and growth inhibition in astrocytes is SMAD3-dependent and a pathway prominently altered in human glioma cell lines. *J Biol Chem.* 1999;**274**(49):35053-8.
116. Stolfi C, Marafini I, De Simone V, Pallone F, Monteleone G. The dual role of Smad7 in the control of cancer growth and metastasis. *Int J Mol Sci.* 2013;**14**(12):23774-90.
117. Li Y, Turck CM, Teumer JK, Stavnezer E. Unique sequence, ski, in Sloan-Kettering avian retroviruses with properties of a new cell-derived oncogene. *J Virol.* 1986;**57**(3):1065-72.
118. Luo K, Stroschein SL, Wang W, Chen D, Martens E, Zhou S, Zhou Q. The Ski oncoprotein interacts with the Smad proteins to repress TGFbeta signaling. *Genes Dev.* 1999;**13**(17):2196-206.
119. Nomura N, Sasamoto S, Ishii S, Date T, Matsui M, Ishizaki R. Isolation of human cDNA clones of ski and the ski-related gene, sno. *Nucleic Acids Res.* 1989;**17**(14):5489-500.
120. Bonni S, Bonni A. SnoN signaling in proliferating cells and postmitotic neurons. *FEBS Lett.* 2012;**586**(14):1977-83.
121. Ikushima H, Todo T, Ino Y, Takahashi M, Miyazawa K, Miyazono K. Autocrine TGF-beta signaling maintains tumorigenicity of glioma-initiating cells through Sry-related HMG-box factors. *Cell Stem Cell.* 2009;**5**(5):504-14.
122. Penuelas S, Anido J, Prieto-Sanchez RM, Folch G, Barba I, Cuartas I, Garcia-Dorado D, Poca MA, Sahuquillo J, Baselga J, Seoane J. TGF-beta increases glioma-initiating cell self-renewal through the induction of LIF in human glioblastoma. *Cancer Cell.* 2009;**15**(4):315-27.
123. Rycaj K, Tang DG. Cancer stem cells and radioresistance. *Int J Radiat Biol.* 2014;**90**(8):615-21.
124. Stopschinski BE, Beier CP, Beier D. Glioblastoma cancer stem cells--from concept to clinical application. *Cancer Lett.* 2013;**338**(1):32-40.
125. Stupp R, Mason WP, van den Bent MJ, Weller M, Fisher B, Taphoorn MJ, Belanger K, Brandes AA, Marosi C, Bogdahn U, Curschmann J, Janzer RC, Ludwin SK, Gorlia T, Allgeier A, Lacombe D, Cairncross JG, Eisenhauer E, Mirimanoff RO, European Organisation for R, Treatment of Cancer Brain T, Radiotherapy G, National Cancer Institute of Canada Clinical Trials G. Radiotherapy plus concomitant and adjuvant temozolomide for glioblastoma. *N Engl J Med.* 2005;**352**(10):987-96.
126. Wilson TA, Karajannis MA, Harter DH. Glioblastoma multiforme: State of the art and future therapeutics. *Surg Neurol Int.* 2014;**5**:64.

127. Krakstad C, Chekenya M. Survival signalling and apoptosis resistance in glioblastomas: opportunities for targeted therapeutics. *Mol Cancer*. 2010;**9**:135.
128. Rohwer N, Cramer T. Hypoxia-mediated drug resistance: novel insights on the functional interaction of HIFs and cell death pathways. *Drug Resist Updat*. 2011;**14**(3):191-201.
129. Gray LH, Conger AD, Ebert M, Hornsey S, Scott OC. The concentration of oxygen dissolved in tissues at the time of irradiation as a factor in radiotherapy. *Br J Radiol*. 1953;**26**(312):638-48.
130. van Tellingen O, Yetkin-Arik B, de Gooijer MC, Wesseling P, Wurdinger T, de Vries HE. Overcoming the blood-brain tumor barrier for effective glioblastoma treatment. *Drug Resist Updat*. 2015;**19**:1-12.
131. US National Institutes of Health. 2015 [Last access June 2015]. Available from: www.clinicaltrials.gov.
132. Louveau A, Smirnov I, Keyes TJ, Eccles JD, Rouhani SJ, Peske JD, Derecki NC, Castle D, Mandell JW, Lee KS, Harris TH, Kipnis J. Structural and functional features of central nervous system lymphatic vessels. *Nature*. 2015.
133. Seoane J, De Mattos-Arruda L. Escaping out of the brain. *Cancer Discov*. 2014;**4**(11):1259-61.
134. Bastien JI, McNeill KA, Fine HA. Molecular characterizations of glioblastoma, targeted therapy, and clinical results to date. *Cancer*. 2015;**121**(4):502-16.
135. Céline SG, Tatiana L, Ana X-M, Marta P, Bruno MC. Mechanisms of Aggressiveness in Glioblastoma: Prognostic and Potential Therapeutic Insights. 2013.
136. Prados M, Consortium ftIFEPCT. A "PRECISION MEDICINE" STRATEGY FOR RECURRENT GLIOBLASTOMA. *Neuro Oncol*. 2014;**16**(suppl 3):iii49.
137. Ma D, Sarkaria J, Peng S, Byron S, Craig D, Carpten J, Berens M, O'Neill B, Schroeder M, Tran N. GE-19GENOMICS GUIDED THERAPEUTIC APPROACH FOR THE TREATMENT OF GLIOBLASTOMA MULTIFORME (GBM) USING NEXT GENERATION SEQUENCING (NGS) TECHNOLOGIES. *Neuro Oncol*. 2014;**16**(suppl 5):v100.
138. Weller M, Stupp R, Hegi M, Wick W. Individualized Targeted Therapy for Glioblastoma: Fact or Fiction? *The Cancer Journal*. 2012;**18**(1):40-4.
139. Ampie L, Woolf EC, Dardis C. Immunotherapeutic advancements for glioblastoma. *Front Oncol*. 2015;**5**:12.
140. Muragaki Y, Maruyama T, Iseki H, Tanaka M, Shinohara C, Takakura K, Tsuboi K, Yamamoto T, Matsumura A, Matsutani M, Karasawa K, Shimada K, Yamaguchi N, Nakazato Y, Sato K, Uemae Y, Ohno T, Okada Y, Hori T. Phase I/IIa trial of autologous formalin-fixed tumor vaccine concomitant with fractionated radiotherapy for newly diagnosed glioblastoma. Clinical article. *J Neurosurg*. 2011;**115**(2):248-55.
141. Bloch O. Immunotherapy for malignant gliomas. *Cancer Treat Res*. 2015;**163**:143-58.
142. Wurth R, Pattarozzi A, Gatti M, Bajetto A, Corsaro A, Parodi A, Siritto R, Massollo M, Marini C, Zona G, Fenoglio D, Sambuceti G, Filaci G, Daga A, Barbieri F, Florio T. Metformin selectively affects human glioblastoma tumor-initiating cell viability: A role for metformin-induced inhibition of Akt. *Cell Cycle*. 2013;**12**(1):145-56.
143. Carra E, Barbieri F, Marubbi D, Pattarozzi A, Favoni RE, Florio T, Daga A. Sorafenib selectively depletes human glioblastoma tumor-initiating cells from primary cultures. *Cell Cycle*. 2013;**12**(3):491-500.
144. Sampson JH, Heimberger AB, Archer GE, Aldape KD, Friedman AH, Friedman HS, Gilbert MR, Herndon JE, 2nd, McLendon RE, Mitchell DA, Reardon DA, Sawaya R, Schmittling RJ, Shi W, Vredenburgh JJ, Bigner DD. Immunologic escape after prolonged progression-free survival with epidermal growth factor receptor variant III peptide vaccination in patients with newly diagnosed glioblastoma. *J Clin Oncol*. 2010;**28**(31):4722-9.
145. Emler DR, Gupta P, Holgado-Madruga M, Del Vecchio CA, Mitra SS, Han SY, Li G, Jensen KC, Vogel H, Xu LW, Skirboll SS, Wong AJ. Targeting a glioblastoma cancer stem-cell population defined by EGF receptor variant III. *Cancer Res*. 2014;**74**(4):1238-49.

146. Jiang H, Gomez-Manzano C, Aoki H, Alonso MM, Kondo S, McCormick F, Xu J, Kondo Y, Bekele BN, Colman H, Lang FF, Fueyo J. Examination of the therapeutic potential of Delta-24-RGD in brain tumor stem cells: role of autophagic cell death. *J Natl Cancer Inst.* 2007;**99**(18):1410-4.
147. Kroeger KM, Muhammad AK, Baker GJ, Assi H, Wibowo MK, Xiong W, Yagiz K, Candolfi M, Lowenstein PR, Castro MG. Gene therapy and virotherapy: novel therapeutic approaches for brain tumors. *Discov Med.* 2010;**10**(53):293-304.
148. van Putten EH, Dirven CM, van den Bent MJ, Lamfers ML. Sitimagene ceradenovec: a gene-based drug for the treatment of operable high-grade glioma. *Future Oncol.* 2010;**6**(11):1691-710.
149. Santibanez JF, Quintanilla M, Bernabeu C. TGF-beta/TGF-beta receptor system and its role in physiological and pathological conditions. *Clin Sci (Lond).* 2011;**121**(6):233-51.
150. B3C newswire Antisense Pharma Changes Name to Isarna Therapeutics 2015 [Last access June 2015]. Available from: <http://www.b3cnewswire.com>.
151. Han J, Alvarez-Breckenridge CA, Wang QE, Yu J. TGF-beta signaling and its targeting for glioma treatment. *Am J Cancer Res.* 2015;**5**(3):945-55.
152. Flavell RA, Sanjabi S, Wrzesinski SH, Licona-Limon P. The polarization of immune cells in the tumour environment by TGFbeta. *Nat Rev Immunol.* 2010;**10**(8):554-67.
153. Neuzillet C, Tijeras-Raballand A, Cohen R, Cros J, Faivre S, Raymond E, de Gramont A. Targeting the TGFbeta pathway for cancer therapy. *Pharmacol Ther.* 2015;**147**:22-31.
154. Calone I, Souchelnytskyi S. Inhibition of TGFbeta signaling and its implications in anticancer treatments. *Exp Oncol.* 2012;**34**(1):9-16.
155. Lee SH, Leem HS, Jeong SM, Lee K. Bevacizumab accelerates corneal wound healing by inhibiting TGF-beta2 expression in alkali-burned mouse cornea. *BMB Rep.* 2009;**42**(12):800-5.
156. Llopiz D, Dotor J, Casares N, Bezunartea J, Diaz-Valdes N, Ruiz M, Aranda F, Berraondo P, Prieto J, Lasarte JJ, Borrás-Cuesta F, Sarobe P. Peptide inhibitors of transforming growth factor-beta enhance the efficacy of antitumor immunotherapy. *Int J Cancer.* 2009;**125**(11):2614-23.
157. Loureiro J, Aguilera A, Selgas R, Sandoval P, Albar-Vizcaino P, Perez-Lozano ML, Ruiz-Carpio V, Majano PL, Lamas S, Rodriguez-Pascual F, Borrás-Cuesta F, Dotor J, Lopez-Cabrera M. Blocking TGF-beta1 protects the peritoneal membrane from dialysate-induced damage. *J Am Soc Nephrol.* 2011;**22**(9):1682-95.
158. Dotor J, Lopez-Vazquez AB, Lasarte JJ, Sarobe P, Garcia-Granero M, Riezu-Boj JI, Martinez A, Feijoo E, Lopez-Sagaseta J, Hermida J, Prieto J, Borrás-Cuesta F. Identification of peptide inhibitors of transforming growth factor beta 1 using a phage-displayed peptide library. *Cytokine.* 2007;**39**(2):106-15.
159. Ezquerro IJ, Lasarte JJ, Dotor J, Castilla-Cortazar I, Bustos M, Penuelas I, Blanco G, Rodriguez C, Lechuga Mdel C, Greenwel P, Rojkind M, Prieto J, Borrás-Cuesta F. A synthetic peptide from transforming growth factor beta type III receptor inhibits liver fibrogenesis in rats with carbon tetrachloride liver injury. *Cytokine.* 2003;**22**(1-2):12-20.
160. Zarranz-Ventura J, Fernandez-Robredo P, Recalde S, Salinas-Alaman A, Borrás-Cuesta F, Dotor J, Garcia-Layana A. Transforming growth factor-beta inhibition reduces progression of early choroidal neovascularization lesions in rats: P17 and P144 peptides. *PLoS One.* 2013;**8**(5):e65434.
161. Serrati S, Margheri F, Pucci M, Cantelmo AR, Cammarota R, Dotor J, Borrás-Cuesta F, Fibbi G, Albin A, Del Rosso M. TGFbeta1 antagonistic peptides inhibit TGFbeta1-dependent angiogenesis. *Biochem Pharmacol.* 2009;**77**(5):813-25.
162. Murillo-Cuesta S, Rodriguez-de la Rosa L, Contreras J, Celaya AM, Camarero G, Rivera T, Varela-Nieto I. Transforming growth factor beta1 inhibition protects from noise-induced hearing loss. *Front Aging Neurosci.* 2015;**7**:32.
163. Hermida N, Lopez B, Gonzalez A, Dotor J, Lasarte JJ, Sarobe P, Borrás-Cuesta F, Diez J. A synthetic peptide from transforming growth factor-beta1 type III receptor prevents myocardial fibrosis in spontaneously hypertensive rats. *Cardiovasc Res.* 2009;**81**(3):601-9.

164. Ruiz-de-Erenchun R, Dotor de las Herrerias J, Hontanilla B. Use of the transforming growth factor-beta1 inhibitor peptide in periprosthetic capsular fibrosis: experimental model with tetraglycerol dipalmitate. *Plast Reconstr Surg.* 2005;**116**(5):1370-8.
165. San-Martin A, Dotor J, Martinez F, Hontanilla B. Effect of the inhibitor peptide of the transforming growth factor beta (p144) in a new silicone pericapsular fibrotic model in pigs. *Aesthetic Plast Surg.* 2010;**34**(4):430-7.
166. Santiago B, Gutierrez-Canas I, Dotor J, Palao G, Lasarte JJ, Ruiz J, Prieto J, Borrás-Cuesta F, Pablos JL. Topical application of a peptide inhibitor of transforming growth factor-beta1 ameliorates bleomycin-induced skin fibrosis. *J Invest Dermatol.* 2005;**125**(3):450-5.
167. First Word Pharma. 2015 [Last access August 2015]. Available from: www.firstwordpharma.com.
168. Gil-Guerrero L, Dotor J, Huibregtse IL, Casares N, Lopez-Vazquez AB, Rudilla F, Riezu-Boj JI, Lopez-Sagaseta J, Hermida J, Van Deventer S, Bezunartea J, Llopiz D, Sarobe P, Prieto J, Borrás-Cuesta F, Lasarte JJ. *In vitro* and *in vivo* down-regulation of regulatory T cell activity with a peptide inhibitor of TGF-beta1. *J Immunol.* 2008;**181**(1):126-35.
169. Diaz-Valdes N, Basagoiti M, Dotor J, Aranda F, Monreal I, Riezu-Boj JI, Borrás-Cuesta F, Sarobe P, Feijoo E. Induction of monocyte chemoattractant protein-1 and interleukin-10 by TGFbeta1 in melanoma enhances tumor infiltration and immunosuppression. *Cancer Res.* 2011;**71**(3):812-21.
170. Margheri F, Schiavone N, Papucci L, Magnelli L, Serrati S, Chilla A, Laurenzana A, Bianchini F, Calorini L, Torre E, Dotor J, Feijoo E, Fibbi G, Del Rosso M. GDF5 regulates TGFβ-dependent angiogenesis in breast carcinoma MCF-7 cells: *in vitro* and *in vivo* control by anti-TGFβ peptides. *PLoS One.* 2012;**7**(11):e50342.
171. Medina-Echeverez J, Fioravanti J, Diaz-Valdes N, Frank K, Aranda F, Gomar C, Ardaiz N, Dotor J, Umansky V, Prieto J, Berraondo P. Harnessing high density lipoproteins to block transforming growth factor beta and to inhibit the growth of liver tumor metastases. *PLoS One.* 2014;**9**(5):e96799.
172. Salvo E, Garasa S, Dotor J, Morales X, Pelaez R, Altevogt P, Rouzaut A. Combined targeting of TGF-beta1 and integrin beta3 impairs lymph node metastasis in a mouse model of non-small-cell lung cancer. *Mol Cancer.* 2014;**13**:112.
173. Vicent S, Luis-Ravelo D, Anton I, Garcia-Tunon I, Borrás-Cuesta F, Dotor J, De Las Rivas J, Lecanda F. A novel lung cancer signature mediates metastatic bone colonization by a dual mechanism. *Cancer Res.* 2008;**68**(7):2275-85.
174. Zubeldia IG, Bleau AM, Redrado M, Serrano D, Agliano A, Gil-Puig C, Vidal-Vanaclocha F, Lecanda J, Calvo A. Epithelial to mesenchymal transition and cancer stem cell phenotypes leading to liver metastasis are abrogated by the novel TGFbeta1-targeting peptides P17 and P144. *Exp Cell Res.* 2013;**319**(3):12-22.
175. Atherton E, Logan CJ, Sheppard RC. Peptide synthesis. Part 2. Procedures for solid-phase synthesis using N[small alpha]-fluorenylmethoxycarbonylamino-acids on polyamide supports. Synthesis of substance P and of acyl carrier protein 65-74 decapeptide. *Journal of the Chemical Society, Perkin Transactions 1.* 1981(0):538-46.
176. Moeckel S, Meyer K, Leukel P, Heudorfer F, Seliger C, Stangl C, Bogdahn U, Proescholdt M, Brawanski A, Vollmann-Zwerenz A, Riemenschneider MJ, Bosserhoff AK, Spang R, Hau P. Response-predictive gene expression profiling of glioma progenitor cells *in vitro*. *PLoS One.* 2014;**9**(9):e108632.
177. Ribble D, Goldstein NB, Norris DA, Shellman YG. A simple technique for quantifying apoptosis in 96-well plates. *BMC Biotechnol.* 2005;**5**:12.
178. Gallo-Oller G, Rey JA, Dotor J, Castresana JS. Quantitative method for *in vitro* matrigel invasiveness measurement through image analysis software. *Mol Biol Rep.* 2014;**41**(10):6335-41.
179. Rasband WS, ImageJ. National Institutes of Health, Bethesda, Maryland, USA. 1997-2014. Available from: <http://imagej.nih.gov/ij>.
180. Franken NA, Rodermond HM, Stap J, Haveman J, van Bree C. Clonogenic assay of cells *in vitro*. *Nat Protoc.* 2006;**1**(5):2315-9.

181. IBIDI. 2015 [Last access April 2015]. Available from: www.ibidi.com.
182. Morton DB, Griffiths PH. Guidelines on the recognition of pain, distress and discomfort in experimental animals and an hypothesis for assessment. *Vet Rec.* 1985;**116**(16):431-6.
183. ALZET. 2015 [Last access April 2015]. Available from: www.alzet.com.
184. Pillai DR, Dittmar MS, Baldaranov D, Heidemann RM, Henning EC, Schuierer G, Bogdahn U, Schlachetzki F. Cerebral ischemia-reperfusion injury in rats--a 3 T MRI study on biphasic blood-brain barrier opening and the dynamics of edema formation. *J Cereb Blood Flow Metab.* 2009;**29**(11):1846-55.
185. Schmidt KF, Ziu M, Schmidt NO, Vaghasia P, Cargioli TG, Doshi S, Albert MS, Black PM, Carroll RS, Sun Y. Volume reconstruction techniques improve the correlation between histological and *in vivo* tumor volume measurements in mouse models of human gliomas. *J Neurooncol.* 2004;**68**(3):207-15.
186. Ileva LV, Bernardo M, Young MR, Riffle LA, Tatum JL, Kalen JD, Choyke PL. *In vivo* MRI virtual colonography in a mouse model of colon cancer. *Nat Protoc.* 2014;**9**(11):2682-92.
187. Žanić-Grubišić T. 2015 [Last access August 2015]. Available from: <http://www.ifcc.org/>.
188. Frisch SM, Sreaton RA. Anoikis mechanisms. *Curr Opin Cell Biol.* 2001;**13**(5):555-62.
189. Beaufort N, Corvazier E, Hervieu A, Choqueux C, Dussiot M, Louedec L, Cady A, de Bentzmann S, Michel JB, Pidard D. The thermolysin-like metalloproteinase and virulence factor LasB from pathogenic *Pseudomonas aeruginosa* induces anoikis of human vascular cells. *Cell Microbiol.* 2011;**13**(8):1149-67.
190. Smit MA, Geiger TR, Song JY, Gitelman I, Peeper DS. A Twist-Snail axis critical for TrkB-induced epithelial-mesenchymal transition-like transformation, anoikis resistance, and metastasis. *Mol Cell Biol.* 2009;**29**(13):3722-37.
191. Smit MA, Peeper DS. Zeb1 is required for TrkB-induced epithelial-mesenchymal transition, anoikis resistance and metastasis. *Oncogene.* 2011;**30**(35):3735-44.
192. Borowicz S, Van Scoyk M, Avasarala S, Karuppusamy Rathinam MK, Tauler J, Bikkavilli RK, Winn RA. The soft agar colony formation assay. *J Vis Exp.* 2014(92):e51998.
193. Laks DR, Masterman-Smith M, Visnyei K, Angenieux B, Orozco NM, Foran I, Yong WH, Vinters HV, Liao LM, Lazareff JA, Mischel PS, Cloughesy TF, Horvath S, Kornblum HI. Neurosphere formation is an independent predictor of clinical outcome in malignant glioma. *Stem Cells.* 2009;**27**(4):980-7.
194. Wang L, Zhao H, Cui K, Yao L, Ren M, Hao A, Smollen P, Nie F, Jin G, Liu Q, Wong ST. Identification of novel small-molecule inhibitors of glioblastoma cell growth and invasion by high-throughput screening. *Biosci Trends.* 2012;**6**(4):192-200.
195. Sun Y, Pollard S, Conti L, Toselli M, Biella G, Parkin G, Willatt L, Falk A, Cattaneo E, Smith A. Long-term tripotent differentiation capacity of human neural stem (NS) cells in adherent culture. *Mol Cell Neurosci.* 2008;**38**(2):245-58.
196. Pollard SM, Yoshikawa K, Clarke ID, Danovi D, Stricker S, Russell R, Bayani J, Head R, Lee M, Bernstein M, Squire JA, Smith A, Dirks P. Glioma stem cell lines expanded in adherent culture have tumor-specific phenotypes and are suitable for chemical and genetic screens. *Cell Stem Cell.* 2009;**4**(6):568-80.
197. Mercapide J, Lopez De Cicco R, Castresana JS, Klein-Szanto AJ. Stromelysin-1/matrix metalloproteinase-3 (MMP-3) expression accounts for invasive properties of human astrocytoma cell lines. *Int J Cancer.* 2003;**106**(5):676-82.
198. Forones NM, Carvalho APS, Giannotti-Filho O, Lourenço LG, Oshima CTF. Cell proliferation and apoptosis in gastric cancer and intestinal metaplasia. *Arq Gastroenterol.* 2005;**42**:30-4.
199. Gonzalez-Zubeldia I, Dotor J, Redrado M, Bleau AM, Manrique I, de Aberasturi AL, Villalba M, Calvo A. Co-migration of colon cancer cells and CAFs induced by TGFbeta(1) enhances liver metastasis. *Cell Tissue Res.* 2015;**359**(3):829-39.
200. Zips D, Thames HD, Baumann M. New anticancer agents: *in vitro* and *in vivo* evaluation. *In Vivo.* 2005;**19**(1):1-7.
201. Eccles SA, Box C, Court W. Cell migration/invasion assays and their application in cancer drug discovery. *Biotechnol Annu Rev.* 2005;**11**:391-421.

202. Blagosklonny MV. Prospective strategies to enforce selectively cell death in cancer cells. *Oncogene*. 2004;**23**(16):2967-75.
203. Aigner L, Bogdahn U. TGF-beta in neural stem cells and in tumors of the central nervous system. *Cell Tissue Res*. 2008;**331**(1):225-41.
204. Chen HH, Zhao S, Song JG. TGF-beta1 suppresses apoptosis via differential regulation of MAP kinases and ceramide production. *Cell Death Differ*. 2003;**10**(5):516-27.
205. Sun J, Liu SZ, Lin Y, Cao XP, Liu JM. TGF-beta promotes glioma cell growth via activating Nodal expression through Smad and ERK1/2 pathways. *Biochem Biophys Res Commun*. 2014;**443**(3):1066-72.
206. Xu Y, Tabe Y, Jin L, Watt J, McQueen T, Ohsaka A, Andreeff M, Konopleva M. TGF-beta receptor kinase inhibitor LY2109761 reverses the anti-apoptotic effects of TGF-beta1 in myelo-monocytic leukaemic cells co-cultured with stromal cells. *Br J Haematol*. 2008;**142**(2):192-201.
207. Martin SJ, Reutelingsperger CP, McGahon AJ, Rader JA, van Schie RC, LaFace DM, Green DR. Early redistribution of plasma membrane phosphatidylserine is a general feature of apoptosis regardless of the initiating stimulus: inhibition by overexpression of Bcl-2 and Abl. *J Exp Med*. 1995;**182**(5):1545-56.
208. Ho YS, Lee HM, Chang CR, Lin JK. Induction of Bax protein and degradation of lamin A during p53-dependent apoptosis induced by chemotherapeutic agents in human cancer cell lines. *Biochem Pharmacol*. 1999;**57**(2):143-54.
209. Broers JL, Ramaekers FC. The role of the nuclear lamina in cancer and apoptosis. *Adv Exp Med Biol*. 2014;**773**:27-48.
210. Kim YN, Koo KH, Sung JY, Yun UJ, Kim H. Anoikis resistance: an essential prerequisite for tumor metastasis. *Int J Cell Biol*. 2012;**2012**:306879.
211. Russo MA, Paolillo M, Sanchez-Hernandez Y, Curti D, Ciusani E, Serra M, Colombo L, Schinelli S. A small-molecule RGD-integrin antagonist inhibits cell adhesion, cell migration and induces anoikis in glioblastoma cells. *Int J Oncol*. 2013;**42**(1):83-92.
212. Silginer M, Weller M, Ziegler U, Roth P. Integrin inhibition promotes atypical anoikis in glioma cells. *Cell Death Dis*. 2014;**5**:e1012.
213. Munoz NM, Baek JY, Grady WM. TGF-beta has paradoxical and context dependent effects on proliferation and anoikis in human colorectal cancer cell lines. *Growth Factors*. 2008;**26**(5):254-62.
214. Davies MA, Lu Y, Sano T, Fang X, Tang P, LaPushin R, Koul D, Bookstein R, Stokoe D, Yung WK, Mills GB, Steck PA. Adenoviral transgene expression of MMAC/PTEN in human glioma cells inhibits Akt activation and induces anoikis. *Cancer Res*. 1998;**58**(23):5285-90.
215. Seol HJ, Chang JH, Yamamoto J, Romagnuolo R, Suh Y, Weeks A, Agnihotri S, Smith CA, Rutka JT. Overexpression of CD99 Increases the Migration and Invasiveness of Human Malignant Glioma Cells. *Genes Cancer*. 2012;**3**(9-10):535-49.
216. Giese A, Bjerkvig R, Berens ME, Westphal M. Cost of migration: invasion of malignant gliomas and implications for treatment. *J Clin Oncol*. 2003;**21**(8):1624-36.
217. Cockle JV, Picton S, Levesley J, Ilett E, Carcaboso AM, Short S, Steel LP, Melcher A, Lawler SE, Bruning-Richardson A. Cell migration in paediatric glioma; characterisation and potential therapeutic targeting. *Br J Cancer*. 2015;**112**(4):693-703.
218. Williams S, Patrice. The Role of Glycogen Synthase Kinase in Glioblastoma Multiforme Migration and Invasion: The Ohio State University; 2011.
219. Shu HK, Kim MM, Chen P, Furman F, Julin CM, Israel MA. The intrinsic radioresistance of glioblastoma-derived cell lines is associated with a failure of p53 to induce p21(BAX) expression. *Proc Natl Acad Sci U S A*. 1998;**95**(24):14453-8.
220. Godoy PR, Mello SS, Magalhaes DA, Donaires FS, Nicolucci P, Donadi EA, Passos GA, Sakamoto-Hojo ET. Ionizing radiation-induced gene expression changes in TP53 proficient and deficient glioblastoma cell lines. *Mutat Res*. 2013;**756**(1-2):46-55.
221. Jane EP, Premkumar DR, Pollack IF. Bortezomib sensitizes malignant human glioma cells to TRAIL, mediated by inhibition of the NF- κ B signaling pathway. *Mol Cancer Ther*. 2011;**10**(1):198-208.

222. Leone R, Giussani P, De Palma S, Fania C, Capitanio D, Vasso M, Brioschi L, Riboni L, Viani P, Gelfi C. Proteomic analysis of human glioblastoma cell lines differently resistant to a nitric oxide releasing agent. *Mol Biosyst.* 2015;**11**(6):1612-21.
223. Yao KC, Komata T, Kondo Y, Kanzawa T, Kondo S, Germano IM. Molecular response of human glioblastoma multiforme cells to ionizing radiation: cell cycle arrest, modulation of the expression of cyclin-dependent kinase inhibitors, and autophagy. *J Neurosurg.* 2003;**98**(2):378-84.
224. Piek E, Westermarck U, Kastemar M, Heldin CH, van Zoelen EJ, Nister M, Ten Dijke P. Expression of transforming-growth-factor (TGF)-beta receptors and Smad proteins in glioblastoma cell lines with distinct responses to TGF-beta1. *Int J Cancer.* 1999;**80**(5):756-63.
225. Beier CP, Kumar P, Meyer K, Leukel P, Bruttel V, Aschenbrenner I, Riemenschneider MJ, Fragoulis A, Rummele P, Lamszus K, Schulz JB, Weis J, Bogdahn U, Wischhusen J, Hau P, Spang R, Beier D. The cancer stem cell subtype determines immune infiltration of glioblastoma. *Stem Cells Dev.* 2012;**21**(15):2753-61.
226. Zhang M, Kleber S, Rohrich M, Timke C, Han N, Tuettenberg J, Martin-Villalba A, Debus J, Peschke P, Wirkner U, Lahn M, Huber PE. Blockade of TGF-beta signaling by the TGFbetaR-I kinase inhibitor LY2109761 enhances radiation response and prolongs survival in glioblastoma. *Cancer Res.* 2011;**71**(23):7155-67.
227. Bar EE, Lin A, Mahairaki V, Matsui W, Eberhart CG. Hypoxia increases the expression of stem-cell markers and promotes clonogenicity in glioblastoma neurospheres. *Am J Pathol.* 2010;**177**(3):1491-502.
228. González Juncá A. Study of molecular mechanisms implicated in the TGF-beta oncogenic effect in Glioma: Universitat de Barcelona; 2013.
229. Wang P, Yu J, Yin Q, Li W, Ren X, Hao X. Rosiglitazone suppresses glioma cell growth and cell cycle by blocking the transforming growth factor-beta mediated pathway. *Neurochem Res.* 2012;**37**(10):2076-84.
230. Zhang M, Herion TW, Timke C, Han N, Hauser K, Weber KJ, Peschke P, Wirkner U, Lahn M, Huber PE. Trimodal glioblastoma treatment consisting of concurrent radiotherapy, temozolomide, and the novel TGF-beta receptor I kinase inhibitor LY2109761. *Neoplasia.* 2011;**13**(6):537-49.
231. Joseph JV, Conroy S, Tomar T, Eggens-Meijer E, Bhat K, Copray S, Walenkamp AM, Boddeke E, Balasubramanyian V, Wagemakers M, den Dunnen WF, Kruyt FA. TGF-beta is an inducer of ZEB1-dependent mesenchymal transdifferentiation in glioblastoma that is associated with tumor invasion. *Cell Death Dis.* 2014;**5**:e1443.
232. Lv S, Zhang J, Han M, Wang W, Zhang Y, Zhuang D, Shi R, Bian R, Yao C. Nucleolin promotes TGF-beta signaling initiation via TGF-beta receptor I in glioblastoma. *J Mol Neurosci.* 2015;**55**(1):1-6.
233. Sasaki A, Naganuma H, Satoh E, Kawataki T, Amagasaki K, Nukui H. Participation of thrombospondin-1 in the activation of latent transforming growth factor-beta in malignant glioma cells. *Neurol Med Chir (Tokyo).* 2001;**41**(5):253-8; discussion 8-9.
234. Seliger C, Leukel P, Moeckel S, Jachnik B, Lottaz C, Kreutz M, Brawanski A, Proescholdt M, Bogdahn U, Bosserhoff AK, Vollmann-Zwerenz A, Hau P. Lactate-modulated induction of THBS-1 activates transforming growth factor (TGF)-beta2 and migration of glioma cells *in vitro*. *PLoS One.* 2013;**8**(11):e78935.
235. Yu Y, Ran Q. Nuclear SMAD2 restrains proliferation of glioblastoma. *Cell Physiol Biochem.* 2015;**35**(5):1756-63.
236. Hardee ME, Marciscano AE, Medina-Ramirez CM, Zagzag D, Narayana A, Lonning SM, Barcellos-Hoff MH. Resistance of glioblastoma-initiating cells to radiation mediated by the tumor microenvironment can be abolished by inhibiting transforming growth factor-beta. *Cancer Res.* 2012;**72**(16):4119-29.
237. Satoh E, Naganuma H, Sasaki A, Nagasaka M, Ogata H, Nukui H. Effect of irradiation on transforming growth factor-beta secretion by malignant glioma cells. *J Neurooncol.* 1997;**33**(3):195-200.

238. Isoe S, Naganuma H, Nakano S, Sasaki A, Satoh E, Nagasaka M, Maeda S, Nukui H. Resistance to growth inhibition by transforming growth factor-beta in malignant glioma cells with functional receptors. *J Neurosurg.* 1998;**88**(3):529-34.
239. Shinojima N, Hossain A, Takezaki T, Fueyo J, Gumin J, Gao F, Nwajei F, Marini FC, Andreeff M, Kuratsu J, Lang FF. TGF-beta mediates homing of bone marrow-derived human mesenchymal stem cells to glioma stem cells. *Cancer Res.* 2013;**73**(7):2333-44.
240. Frei K, Gramatzki D, Tritschler I, Schroeder JJ, Espinoza L, Rushing EJ, Weller M. Transforming growth factor-beta pathway activity in glioblastoma. *Oncotarget.* 2015;**6**(8):5963-77.
241. Schmierer B, Hill CS. Kinetic analysis of Smad nucleocytoplasmic shuttling reveals a mechanism for transforming growth factor beta-dependent nuclear accumulation of Smads. *Mol Cell Biol.* 2005;**25**(22):9845-58.
242. Liu M, Hicklin D. Human Tumor Xenograft Efficacy Models. In: Teicher BA, editor. *Tumor Models in Cancer Research.* Cancer Drug Discovery and Development: Humana Press; 2011. p. 99-124.
243. Eisenhauer EA, Therasse P, Bogaerts J, Schwartz LH, Sargent D, Ford R, Dancey J, Arbuck S, Gwyther S, Mooney M, Rubinstein L, Shankar L, Dodd L, Kaplan R, Lacombe D, Verweij J. New response evaluation criteria in solid tumours: revised RECIST guideline (version 1.1). *Eur J Cancer.* 2009;**45**(2):228-47.
244. Teicher B. Preclinical Tumor Response End Points. In: Teicher BA, editor. *Tumor Models in Cancer Research.* Cancer Drug Discovery and Development: Humana Press; 2011. p. 571-605.
245. Wallace J. Humane endpoints and cancer research. *ILAR J.* 2000;**41**(2):87-93.
246. Stylli SS, Luwor RB, Ware TM, Tan F, Kaye AH. Mouse models of glioma. *J Clin Neurosci.* 2015;**22**(4):619-26.
247. Rockwell S. Tumor-Cell Survival. In: Teicher B, editor. *Tumor Models in Cancer Research.* Cancer Drug Discovery and Development: Humana Press; 2002. p. 617-31.
248. Wesseling P, Kros JM, Jeuken JWM. The pathological diagnosis of diffuse gliomas: towards a smart synthesis of microscopic and molecular information in a multidisciplinary context. *Diagn Histopathol.* 2011;**17**(11):486-94.
249. Blouw B, Song H, Tihan T, Bosze J, Ferrara N, Gerber HP, Johnson RS, Bergers G. The hypoxic response of tumors is dependent on their microenvironment. *Cancer Cell.* 2003;**4**(2):133-46.
250. Tran TT, Uhl M, Ma JY, Janssen L, Sriram V, Aulwurm S, Kerr I, Lam A, Webb HK, Kapoun AM, Kizer DE, McEnroe G, Hart B, Axon J, Murphy A, Chakravarty S, Dugar S, Protter AA, Higgins LS, Wick W, Weller M, Wong DH. Inhibiting TGF-beta signaling restores immune surveillance in the SMA-560 glioma model. *Neuro Oncol.* 2007;**9**(3):259-70.
251. Nacif M, Shaker O. Targeting Transforming Growth Factor- β (TGF- β) in Cancer and Non-Neoplastic Diseases. *J Cancer Ther.* 2014;**Vol.05No.07**:13.
252. Reardon DA, Wen PY. Therapeutic advances in the treatment of glioblastoma: rationale and potential role of targeted agents. *Oncologist.* 2006;**11**(2):152-64.
253. Connolly EC, Freimuth J, Akhurst RJ. Complexities of TGF-beta targeted cancer therapy. *Int J Biol Sci.* 2012;**8**(7):964-78.
254. Fabregat I, Fernando J, Mainez J, Sancho P. TGF-beta signaling in cancer treatment. *Curr Pharm Des.* 2014;**20**(17):2934-47.
255. Yingling JM, Blanchard KL, Sawyer JS. Development of TGF-beta signalling inhibitors for cancer therapy. *Nat Rev Drug Discov.* 2004;**3**(12):1011-22.
256. Pontén J. Neoplastic Human Glia Cells in Culture. In: Fogh J, editor. *Human Tumor Cells in Vitro:* Springer US; 1975. p. 175-206.
257. Zhang L, Sato E, Amagasaki K, Nakao A, Naganuma H. Participation of an abnormality in the transforming growth factor-beta signaling pathway in resistance of malignant glioma cells to growth inhibition induced by that factor. *J Neurosurg.* 2006;**105**(1):119-28.
258. Seoane J, Pouponnot C, Staller P, Schader M, Eilers M, Massague J. TGFbeta influences Myc, Miz-1 and Smad to control the CDK inhibitor p15INK4b. *Nat Cell Biol.* 2001;**3**(4):400-8.

259. Chan DW, Liu VW, To RM, Chiu PM, Lee WY, Yao KM, Cheung AN, Ngan HY. Overexpression of FOXG1 contributes to TGF-beta resistance through inhibition of p21WAF1/CIP1 expression in ovarian cancer. *Br J Cancer*. 2009;**101**(8):1433-43.
260. Miyazono K, Suzuki H, Imamura T. Regulation of TGF-beta signaling and its roles in progression of tumors. *Cancer Sci*. 2003;**94**(3):230-4.
261. Deheuninck J, Luo K. Ski and SnoN, potent negative regulators of TGF-beta signaling. *Cell Res*. 2009;**19**(1):47-57.
262. Liu X, Sun Y, Weinberg RA, Lodish HF. Ski/Sno and TGF-beta signaling. *Cytokine Growth Factor Rev*. 2001;**12**(1):1-8.
263. Luo L, Li N, Lv N, Huang D. SMAD7: a timer of tumor progression targeting TGF-beta signaling. *Tumour Biol*. 2014;**35**(9):8379-85.
264. Tesseur I, Wyss-Coray T. A role for TGF-beta signaling in neurodegeneration: evidence from genetically engineered models. *Curr Alzheimer Res*. 2006;**3**(5):505-13.
265. Quan YH. Empirical Study on Effect of Smad7 to U251 Glioblastoma Cell: Jilin University; 2007.
266. Denissova NG, Liu F. Repression of endogenous Smad7 by Ski. *J Biol Chem*. 2004;**279**(27):28143-8.
267. Jiang H, Jin C, Liu J, Hua D, Zhou F, Lou X, Zhao N, Lan Q, Huang Q, Yoon JG, Zheng S, Lin B. Next generation sequencing analysis of miRNAs: MiR-127-3p inhibits glioblastoma proliferation and activates TGF-beta signaling by targeting SKI. *OMICS*. 2014;**18**(3):196-206.

PUBLICATIONS

PUBLICATIONS

1) [Quantitative method for in vitro matrigel invasiveness measurement through image analysis software.](#)

Gabriel Gallo-Oller, Juan A. Rey, Javier Dotor, Javier S. Castresana.

Molecular Biology Reports

October 2014. Volume 41, Issue 10, pp 6335-6341.

2) *Genome-wide microarray expression and genomic alterations by array-CGH analysis in neuroblastoma stem like cells*

Raquel Ordonez, **Gabriel Gallo-Oller**, Soledad Martinez-Soto, Sheila Legarra, Noemie Pata-Merci, Justine Guegan, Giselle Danglot, Alain Bernheim, Barbara Melendez, Juan A. Rey, Javier S. Castresana.

PloS one

November 13, 2014. Volume 9, Issue 11, e113105.

3) *Transforming Growth Factor-Beta inhibitory peptide (P144). Effects over human glioblastoma-molecular and cell biology.*

Gabriel Gallo-Oller, Javier Dotor, Javier S. Castresana.

2015. Under preparation.



Genome-Wide Microarray Expression and Genomic Alterations by Array-CGH Analysis in Neuroblastoma Stem-Like Cells

Raquel Ordóñez¹✉, Gabriel Gallo-Oller¹✉, Soledad Martínez-Soto¹, Sheila Legarra¹, Noémie Pata-Merci², Justine Guegan², Giselle Danglot², Alain Bernheim², Bárbara Meléndez³, Juan A. Rey⁴, Javier S. Castresana¹*

1 Department of Biochemistry and Genetics, University of Navarra School of Sciences, Pamplona, Spain, **2** Institut Gustave Roussy, Villejuif, France, **3** Molecular Pathology Research Unit, Department of Pathology, Virgen de la Salud Hospital, Toledo, Spain, **4** IdiPaz Research Unit, La Paz University Hospital, Madrid, Spain

Abstract

Neuroblastoma has a very diverse clinical behaviour: from spontaneous regression to a very aggressive malignant progression and resistance to chemotherapy. This heterogeneous clinical behaviour might be due to the existence of Cancer Stem Cells (CSC), a subpopulation within the tumor with stem-like cell properties: a significant proliferation capacity, a unique self-renewal capacity, and therefore, a higher ability to form new tumors. We enriched the CSC-like cell population content of two commercial neuroblastoma cell lines by the use of conditioned cell culture media for neurospheres, and compared genomic gains and losses and genome expression by array-CGH and microarray analysis, respectively (in CSC-like versus standard tumor cells culture). Despite the array-CGH did not show significant differences between standard and CSC-like in both analyzed cell lines, the microarray expression analysis highlighted some of the most relevant biological processes and molecular functions that might be responsible for the CSC-like phenotype. Some signalling pathways detected seem to be involved in self-renewal of normal tissues (Wnt, Notch, Hh and TGF- β) and contribute to CSC phenotype. We focused on the aberrant activation of TGF- β and Hh signalling pathways, confirming the inhibition of repressors of TGF- β pathway, as *SMAD6* and *SMAD7* by RT-qPCR. The analysis of the Sonic Hedgehog pathway showed overexpression of *PTCH1*, *GLI1* and *SMO*. We found overexpression of *CD133* and *CD15* in SIMA neurospheres, confirming that this cell line was particularly enriched in stem-like cells. This work shows a cross-talk among different pathways in neuroblastoma and its importance in CSC-like cells.

Citation: Ordóñez R, Gallo-Oller G, Martínez-Soto S, Legarra S, Pata-Merci N, et al. (2014) Genome-Wide Microarray Expression and Genomic Alterations by Array-CGH Analysis in Neuroblastoma Stem-Like Cells. PLoS ONE 9(11): e113105. doi:10.1371/journal.pone.0113105

Editor: Shree Ram Singh, National Cancer Institute, United States of America

Received: June 13, 2014; **Accepted:** October 14, 2014; **Published:** November 13, 2014

Copyright: © 2014 Ordóñez et al. This is an open-access article distributed under the terms of the Creative Commons Attribution License, which permits unrestricted use, distribution, and reproduction in any medium, provided the original author and source are credited.

Data Availability: The authors confirm that all data underlying the findings are fully available without restriction. All relevant data are accessible to from the Array Express database with the following accession numbers: E-MTAB-2866 and E-MTAB-2867.

Funding: G. Gallo-Oller was supported by a fellowship from the Departamento de Educación of Gobierno de Navarra, Pamplona. This research was supported in part by grants from the Departamento de Salud del Gobierno de Navarra, Caja Navarra (project 13912), Fundación Universitaria de Navarra, Pamplona; and Fondo de Investigación Sanitaria (PI-081849 to JSC and PI-101972 to JAR), Madrid. The funders had no role in study design, data collection and analysis, decision to publish, or preparation of the manuscript.

Competing Interests: Coauthor Javier S. Castresana is a PLOS ONE Editorial Board member. Javier S. Castresana confirms that this does not alter the authors' adherence to PLOS ONE editorial policies and criteria.

* Email: jscastresana@unav.es

✉ These authors contributed equally to this work.

Introduction

Neuroblastoma is a neuroendocrine tumor of unknown etiology, derived from primordial neural crest cells which afterwards develop into adrenal medulla and sympathetic ganglia [1]. It is one of the most prevalent cancers in childhood and nearly 50% of the cases take place in children younger than two years. The estimated 5-years survival rate is 90% and 50% for patients with non-high-risk and high-risk neuroblastoma, respectively. Most neuroblastomas occur sporadically and develop with very diverse clinical behavior, from spontaneous regression to aggressive malignant progression and resistance to chemotherapy [2,3].

The actual treatment of neuroblastoma depends on the clinic stage of the tumor, but it is commonly based on radiopharmaceutical therapy in combination with surgery [4]. Current studies

and clinical trials are combining conventional chemotherapy with monoclonal antibodies, stem cell transplants and retinoids, but because of the complexity of this pathology, progress remains extremely slow [5].

Some authors propose that this diverse clinical behavior of neuroblastoma might be due to molecular differences in cell subpopulations [6]. The cancer stem cells (CSC) model might be an explanation for this heterogeneous behavior [7]. This model proposes that only a small subpopulation with characteristics of stem cells within the tumor has the ability to proliferate and maintain its growth. Even if a tumoral mass shows a substantial decrease in size in response to therapy, if the CSC are spared, it will regrow leading to a relapse [8,9]. Some studies propose that CSC operate with the machinery and developmental programs

expressed in normal stem cells [10,11]. There is growing evidence of some signalling pathways involved in self-renewal of both normal and tumor tissues as Wnt [12,13], Sonic Hedgehog (Hh) [14,15], Notch [16,17] and Transforming Growth Factor Beta (TGF- β) [18–20] signalling pathways, that might contribute to tumorigenesis when deregulated [14,21].

In this line, the development of new therapies based in molecular targets may be of great value for the treatment of neuroblastoma. The observation of some pathways acting on multiple levels to promote the development of neuroblastoma and CSC subpopulation, has prompted new therapeutic strategies to treat not only this neoplasm but other brain and nervous system tumors [2,18,22].

Therefore, this project performs a genomic analysis of CSC-like by array-CGH and expression array, with special focus on altered signalling pathways that might explain the stem cell phenotype of the CSC subpopulation. The aim of this study is to provide a powerful tool to open up new targets for therapy or redirect current cancer treatments towards CSC in order to achieve total elimination of tumor cell population and improve treatment effectiveness.

Materials and Methods

Cell lines culture

Two commercial neuroblastoma-derived cell lines were used: SK-N-DZ cell line (ATCC N^oCRL-2149) provided by the American Type Culture Collection (ATCC, Manassas, VA, USA) and SIMA cell line (DSMZ N^o ACC 164) provided by the German Collection of Microorganisms and Cell Cultures (DSMZ, Braunschweig, Germany). Both were grown as monolayer with DMEM/GlutaMAX medium supplemented with 10% fetal bovine serum, 5% non-essential aminoacids, 1% penicillin/streptomycin and 0.1% amphotericin B. To obtain the neurospheres cultures in order to enrich them in CSC-like cells, after chemical dissociation of SK-N-DZ and SIMA cell lines, 5×10^5 cells were transferred to 25 cm² flasks (positioned vertically) and grown in suspension with 5 ml of selective medium: DMEM-F12/GlutaMAX plus 1% penicillin/streptomycin and 0.1% amphotericin B, supplemented with Epidermal Growth Factor (EGF) (20 ng/ml), Fibroblast Growth Factor Basic (FGFb) (20 ng/ml) and B27 Supplement (1X). All cultures were maintained at 37°C in a humidified atmosphere of 5% CO₂/95% air.

DNA/RNA isolation and reverse transcription

DNA from 1×10^6 cells pellet was extracted using Wizard Genomic DNA Purification Kit (Promega, Madison, WI, USA) and total RNA from 2×10^6 cells pellet, employing Illustra RNAspin Mini Kit (GE Healthcare, Buckinghamshire, UK) following manufacturer's instructions in both cases. DNA and RNA samples were stored at -20°C and -80°C until utilization, respectively. DNA and RNA concentrations were measured with a SmartSpec Spectrophotometer (Bio-Rad, Hercules, CA, USA). Reverse transcription was carried out from 2 μg of total RNA (previously denatured at 65°C for 5 min) with a mixture of 0.5 μg of random primers, 0.5 mM dNTPs, 10 mM DTT, First-Strand buffer 1X and 200U SuperScript II Reverse Transcriptase (Invitrogen, Carlsbad, CA, USA) in a total volume of 40 μl . The mixture was incubated for 10 min at 25°C , 50 min at 42°C and 15 min at 70°C , followed by chilling on ice. The cDNA was diluted 1/5 and stored at -80°C until utilization.

Array-CGH

DNA samples were analyzed using a 244K microarray (Agilent Technologies, Santa Clara, CA, USA). Oligonucleotide aCGH processing was performed as detailed in the manufacturer's protocol (version 4.0; <http://www.agilent.com>). Data were extracted from scanned images using feature extraction software (version A.8.5.3, Agilent). Raw data text files from the latter were then imported for analysis into CGH Analytics 3.4.40. Aberrations were detected with the ADM2 algorithm and filtering options of a minimum of 5 probes and $\text{abs}(\log_2\text{Ratio}) > 0.3$. Aberration segments were individually reviewed using build 35, hg17 of UCSC. Anomalies that were localized to regions with high-copy repetitive or GC-rich DNA sequences including telomeric regions were excluded. Gains and losses for the oligonucleotide dataset were defined as a linear ratio ≥ 1.2 or ≤ 0.8 , respectively. High and low-level amplification events were defined as a linear ratio ≥ 4 or $2 < \text{ratio} < 4$, respectively. The data are described in accordance with MIAME guidelines and have been deposited in ArrayExpress under E-MTAB-2866 accession number. All the analysis and statistics related with the array-CGH was performed at Institut Gustave Roussy by the bioinformatics team.

Microarray experiment, data normalization and analysis

SurePrint G3 human Gene Expression Microarray Kit (Agilent, ID:028004) was used to analyze the transcriptional profiles of all samples. This array contains 42,404 60-mer oligonucleotides targeting 27,988 Entrez Gene RNAs and 7,419 lincRNAs (long intergenic non coding RNAs) in an $8 \times 60\text{K}$ format slide (each slide contains 8 arrays of 60,000 features with 1440 spots reserved for internal quality control). The transcripts used can be checked in the EMBL-EBI Database (<http://www.ebi.ac.uk/arrayexpress/arrays/A-GEOD-14550>).

Array performance and analysis were carried out at the Institut Gustave Roussy, using the Agilent Feature Extraction software. Data sets were normalized using quantile normalization, and fold change between cell line and neurospheres was calculated for each gene. The whole dataset was filtered by intensity of the probes. Spots with too high intensities (saturating intensities) and irregular spots (spots inside whose neighbouring pixel showed very different intensities) were not further considered. Likewise, genes with a signal-to-noise ratio lower than 6 fold the average standard deviation observed for all negative control probes were excluded. Finally, >1 fold-change between normalized gene expression measured in neurospheres (or CSC-like cells) versus standard cell lines was used as the criteria to select differentially expressed genes.

The list of differentially expressed genes in both cell lines was imported and classified by DAVID (Database for Annotation, Visualization and Integrated Discovery, <http://david.abcc.ncifcrf.gov/>), version 6.7 [23–25]. Enriched categories in biological processes and molecular function were defined by a p value < 0.05 and more than 2 genes differentially expressed in each category. After the enrichment analysis, a classification by PANTHER (Protein ANalysis THrough Evolutionary Relationships, www.pantherdb.org/) Data Base [26–28] was performed. Finally, a deeper pathway analysis was carried out by comparing the same set of genes with the NCBI BioSystems Database (<http://www.ncbi.nlm.nih.gov/biosystems>). Microarray expression data are available at ArrayExpress with accession number E-MTAB-2867.

Real-Time polymerase chain reaction (RT-qPCR)

A first screening of our primer library was performed according to the microarray data and pathway analysis. 44 pairs of primers were selected and aligned with the mRNA and DNA sequences obtained from RefSeq (<http://www.ncbi.nlm.nih.gov/RefSeq/>)

and UCSC Genome Browser (<http://genome.ucsc.edu/>). A deeper analysis of each pair of primers was performed with Primer3 (<http://primer3.sourceforge.net/>) and Primer Blast (<http://www.ncbi.nlm.nih.gov/tools/primer-blast/>) in order to obtain product length, %GC, melting temperature (T_m), self-complementarity or possible products on unintended templates. After the computational analysis, 17 out of 44 primers (Table 1) were selected for further studies. RT-qPCRs were performed in order to define the optimal T_m for each pair of primers. The melting curves obtained were analyzed to check amplification efficiency in each temperature, and detect additional peaks displaced from the desired amplicon peak (determined by agarose gels checking size and identifying possible intron amplifications). For the quantitative PCR reaction, 2.5 μ l of the generated cDNA was added to a PCR mix containing 12.5 μ l SYBR Green Supermix (Bio-Rad, Hercules, CA, USA) and 12.5 pM forward and reverse primers, in a total volume of 25 μ l. The reaction was performed according to the following protocol: 10 min at 95°C, followed by 40 cycles of 15 s at 95°C, 30 s at the specific T_m for each primer (Table 1) and 20 s at 72°C. A melting curve was added at the end of the protocol as a quality control. All samples were run in triplicate and three independent experiments were carried out. Gene expression levels between samples were normalized using the expression levels of the *HPRT1* gene. Relative gene expression was analyzed according to the $2^{-\Delta\Delta C_t}$ method [29].

Statistical analysis

The statistical analysis of arrays are detailed in the description for each technique. The data of gene expression measured by RT-qPCR was graph as the mean \pm standard deviation. The $2^{-\Delta\Delta C_t}$ values were analysed for normality distribution and homogeneity of variance. Since the data did not show normality distribution, the statistical significance between groups was compared by pairs (the expression level of each gene in standard cultures vs neurospheres cultures) with the non-parametric Mann-Whitney U test. The significance level was set as $p < 0.05$. The statistical program GraphPad Prism for Windows version 5.04 was used.

Results

Genomic profile by array-CGH analysis

To identify the potential common chromosomal alterations indicating possible zones implicated in the CSC-like phenotype, an array-CGH analysis was performed. In the case of SK-N-DZ, we only found six chromosomal regions amplified and no deleted region. SIMA cell line showed more regions of gain and loss, specifically 10 and 30 regions, respectively (data summarized in Table 2). Notwithstanding we did not find any region that was lost or gained in both cell lines and the significance was found only in some points of the genome, we identified numerous chromosomal sequences with copy number variants (CNV) both in SK-N-DZ and SIMA cell lines (Table 2). Whole genome profiles are presented in Figure 1. Among the genes that were included in these regions identified by the array-CGH, the analysis by PANTHER did not show any pattern or group of genes directly related with signalling pathways involved in the CSC-like phenotype. Only a few genes were associated with pathways already described in tumorigenesis and stemness (as p53) but were not principal effectors and its position was downstream, including genes that were related with different regulation points and pathways (data not shown) making the analysis difficult. Despite these results, we noticed that several amplified areas included CpG islands (Table 2). Using the miRBase of the University of

Manchester (www.mirbase.org), we were able to identify the microRNAs included in the gained areas of the chromosomes 1, 2 and 12 (Table 3).

Gene expression profiles by microarray analysis

In order to characterize the differentially expressed genes in CSC-like compared to the standard tumor cell line, mRNA expression was analyzed by microarray analysis. After the first intensity filter, 25,368 genes out of the whole dataset of 42,405 (~60%), reached the minimum quality threshold and were selected for the differential expression analysis. When setting a threshold value of >1 fold-change, 4,831 genes (~11.4%) were identified as differentially expressed in SK-N-DZ neurospheres and 6,613 genes (~15.6%) in SIMA neurospheres. Figure 2A shows the number of genes differentially up and downregulated in each cell line. Among these gene sets, only 757 genes have significantly changed expression in both cell lines (Figure 2B). The sets of genes up and downregulated for each cell line are summarized in Table S1 and the genes shared by both cell lines are represented in Tables S2, S3 and S4.

Differentially expressed genes with >1 fold-change in microarray analysis were categorized according to the biological processes they are involved in, and to the molecular functions they code for, by using the DAVID database. Among all categories, those that appeared significantly altered or enriched ($p < 0.05$ and more than 2 genes differentially expressed in both cell lines by category) were selected for further studies (Table 4).

Further analysis of the significantly enriched categories and signalling pathways involved was performed with PANTHER database and information from the NCBI BioSystems database. As a result, we observed significant alteration in representative signalling pathways known to be also involved in stem cell self-renewal, as Wnt, Notch, Hh and TGF- β (Figure 3).

Biological processes and signalling pathways expression in CSC-like subpopulation

The expression microarray experiment showed up a high percentage of genes altered in neurospheres (Figures 2 and 3). A complete analysis of the data highlighted some of the most relevant biological processes and molecular functions affected (Table 4) that might be responsible for the CSC-like phenotype of this subpopulation. First, we observed an apparent alteration of ion transporters. In our analysis, several genes of Ca^{2+} and K^{+} channels showed up as differentially expressed, as *KCNMA1* and *CACNA1G*. Secondly, we detected alterations in some of the most commonly studied signalling pathways in brain tumors and stem cell development: Wnt, Notch, Hh and TGF- β .

Analyzing Wnt signalling pathway, we observed downregulation of some of the upstream regulators of the pathway: *FZD8* (Frizzled receptor), *PRKCH* (protein kinase C) and *FRAT1*, inhibitor of GSK3-mediated phosphorylation of β -catenin, and therefore a positive regulator of the pathway that could act as a proto oncogene [30,31]. The upregulation of *POU5F1* as a downstream target of the pathway was also noticed.

In Notch signalling pathway, overexpression of the activator ligand of the pathway, *JAG1* was identified. We also detected upregulation of *HES7*, one of the final targets of the pathway [32,33]. This evidence showed an apparent activation of the pathway in CSC-like comparing with the standard cell line.

Expression microarray data showed upregulation of *PTH1L*, the main inhibitor of Hh signalling pathway, but also one of the gene targets of the pathway which transcription would be increased if the pathway is active, as we confirmed with the RT-qPCR data (Figure 4A).

Table 1. Primer sequences.

Gene	Primer sequence (5'–3')	Ref Seq Acc. #	Tm (°C)	Product (bp)
<i>PTCH</i>	F: GGCAGCGGTAGTAGTGGTGTTTC	NM_000264.3	64	191
	R: TGTAGCGGGTATTGTCGTGTGTG			
<i>SHH</i>	F: AGGCTGATGACTCAGAGGTGT	NM_000193.2	64	144
	R: GCCCTCGTAGTCAGAGACT			
<i>GLI1</i>	F: TTCCTACCAGAGTCCCAAGT	NM_005269.2	64	185
	R: CCCTATGTGAAGCCCTATTT			
<i>GLI2</i>	F: GCCATATGTGTGTGAGCACGA	NM_005270.4	64	110
	R: TCTTGACAGATGAGGGTTTCTCG			
<i>GLI3</i>	F: CGAACAGATGTGAGCGAGAA	NM_000168.5	64	185
	R: TTGATCAATGAGGCCCTCTC			
<i>SMO</i>	F: CAGTTCCGGGACTATGTGCTATG	NM_005631.4	64	101
	R: GAAGGCTCGGGCATTCTTG			
<i>SUFU</i>	F: CCTCAGATCGTTGGTGTCT	NM_016169.3	58	132
	R: CCCCTCCGATGTCAGTT			
<i>TGFBR1</i>	F: CGTCAGGTTCTGGCTCAGGTT	NM_004612.2	58	184
	R: TCTGCCTCACGGAACACGAA			
<i>TGFBR2</i>	F: ACGTTCAGAAGTCGGATGTGG	NM_001024847.2	64	142
	R: TGTGAAACTTGACTGCACCGT			
<i>TFGB2</i>	F: GCCTGAACAACGGATTAGGC	NM_001135599.2	64	124
	R: ATCGAAGGAGAGCCATTCCG			
<i>TFGB3</i>	F: ATGATGATCCCCACACCG	NM_003239.2	64	153
	R: CTTCCAGCCAGATCCTGTG			
<i>BAMBI</i>	F: AGCTACATCTCATCTGGCTGC	NM_012342.2	64	187
	R: CATGGGTGAGTGGGAATTTG			
<i>SMAD6</i>	F: AATCCGCCACCTCCCTAC	NM_005585.4	64	131
	R: GAATTCACCCGGAGCAGTGA			
<i>SMAD7</i>	F: CCAACTGCAGACTGTCCAGATGCT	NM_005904.3	58	136
	R: ATGCCACCACGCACCGTGT			
<i>JAG1</i>	F: ATGGGCCCCGAATGTAACAG	NM_000214.2	64	117
	R: ATCACAGTACAGGCCTTGCC			
<i>CD133</i>	F: TCCGGGTTTTGGATACACCTTA	NM_001145847.1	64	155
	R: CTGCAGGTGAAGAGTGCCGTAA			
<i>CD15</i>	F: AGGAGGTGATGTGGACAGCG	NM_002033.3	58	160
	R: AACTACGAGCGTTTGTGCC			
<i>HPRT</i>	F: TGACACTGGCAAAACAATGCA	NM_000194.2	64/58	94
	R: GGTCTTTTACCAGCAAGCT			

F: forward and R: reverse, reference sequences accession number (RefSeq Acc. #), optimal melting temperature (Tm) in Celsius (°C) and size of the PCR product in base pairs (bp).

doi:10.1371/journal.pone.0113105.t001

Likewise, when analyzing TGF- β signalling pathway, the expression microarray data suggested an activation of the pathway (Figure 4B). Ligands like *TGFB3* and *BMP8B* were upregulated, as well as the signal transducer *SHC*. Quite the contrary, we found downregulation of inhibitory SMADs (like *SMAD6* and *SMAD7*) and the pseudoreceptor *BAMBI*, which could sequester ligands and inhibit signal transduction by different mechanisms [34].

Parallel behaviour in SK-N-DZ and SIMA stem-like cells

RT-qPCR was performed in order to corroborate the expression microarray results. In both cell lines, we confirmed the decrease in the expression of *SMAD6*, *SMAD7* and *BAMBI*, as

the increase observed in *JAG1*. The results suggested that the CSC-like subpopulation of both cell lines could have a similar expression profile after enrichment with the neurosphere assay (Figure 5A).

Hh and TGF- β analysis in SIMA stem-like cells

Based on our previous experience in both Hh and TGF- β signalling pathways, further expression analysis by RT-qPCR was performed on some of the most relevant components of both signalling networks in SIMA cell line (Figure 4). Results confirmed Hh aberrant activation by overexpression of its key components as *PTCH1*, *GLI1* and *SMO*. Likewise, TGF- β seemed to be

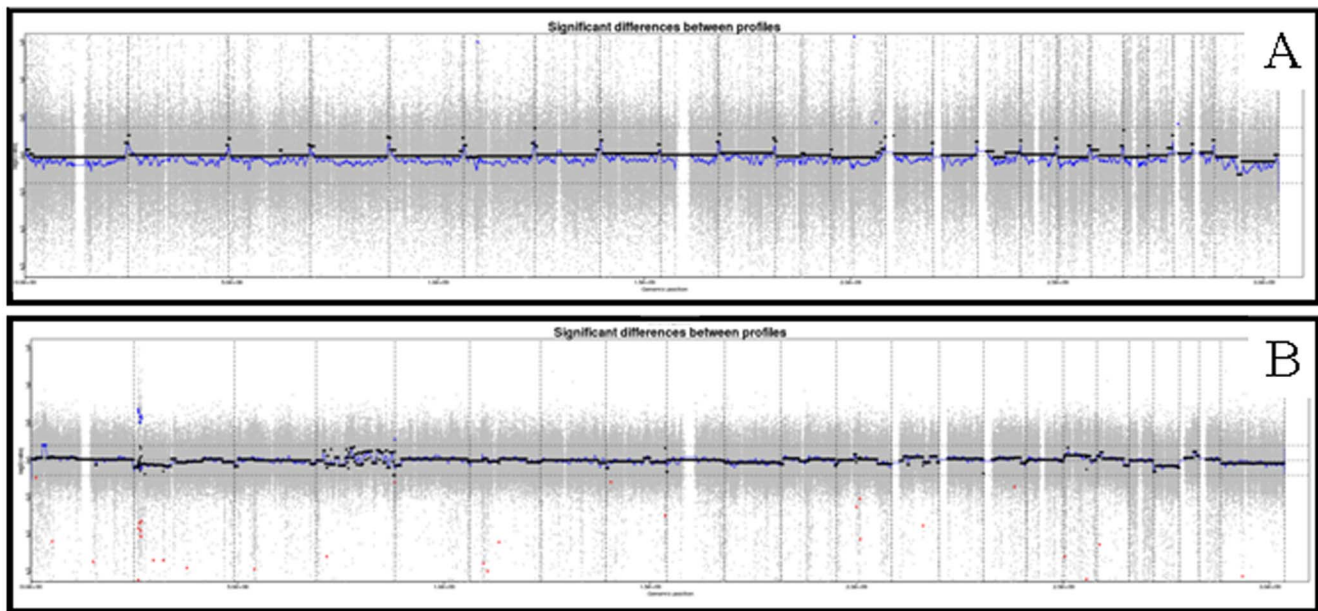


Figure 1. Whole chromosome plots. Array-CGH from SK-N-DZ (A) and SIMA (B) cell lines. The X-axis represents the chromosomes while the Y-axis represent the normalized log₂ ratio fluorescence intensity thresholds -1 (loss) and 1 (gain). The results show gains and losses of small chromosomal regions.

doi:10.1371/journal.pone.0113105.g001

activated by overexpression of its receptors (*TGFBRI* and *TGFB2*) and ligands (*TGFB2*), (despite *TGFB3* is downregulated even though it is also a ligand of the pathway), and downregulation of its repressors (*SMAD6*, *SMAD7* and *BAMBI*). We confirmed by RT-qPCR the increase of the levels of mRNA of *JAG1*, a Notch activating ligand that is related with TGF- β pathway [35]. Its upregulation supports Notch activation as aforementioned.

Expression of stem-cell markers

To confirm the enrichment of the isolated population in CSC-like cells, analysis of CSC-specific cell surface markers was performed. RT-qPCR on *CD133* and *CD15* was carried out in both SK-N-DZ and SIMA neurospheres (Figure 5B). On the basis of these results, SIMA culture was highly enriched in CSC-like cells as shown by the significant increase in CSC surface markers expression. An interesting point is that SK-N-DZ subpopulation did not show any overexpression of the stem-cell markers analyzed.

Discussion

The heterogeneous clinical behavior of neuroblastoma tumors has been widely studied [36–39]. It is already described that genomic rearrangements cannot explain per se this heterogeneity neither the CSC-like subpopulation [40]. In this work, we hypothesized that this heterogeneity might be due to genomic rearrangements together with changes in the expression profile of tumor cell subpopulations, particularly in CSC-like cells. In connection with this model, the genomic profile of CSC-like cells and the regulatory mechanisms or signalling pathways involved in CSC promotion could explain the heterogeneity and biology of this subpopulation and help to its identification in neuroblastoma.

Chromosomal aberrations are common in neuroblastoma, including numerical whole chromosomal gains, segmental chromosomal gains and losses and somatic mutations [2]. However,

array-CGH did not show large modified areas in the genome of CSC-like subpopulations neither individually nor shared by both cell lines (Table 2). Despite this result, we identified other genetic elements involved in the biology of neuroblastoma and in the regulation of several tumors as CNV [41–43] and CpG islands [44–46] (Table 2). Both elements are being investigated as possible therapeutic targets in neuroblastoma [5] and were already identified in other tumors confirming their therapeutic potential [47–51]. These results suggest the fact that these two elements could be involved in tumorigenesis and CSC-like cells generation in neuroblastoma, and, as in other tumors, this might be a starting point to develop or improve current therapies. This is the case of decitabine (5-aza-2'-deoxycytidine). This agent interferes with DNA methylation but the preclinical assays show that it must be administered at doses that are not tolerable in order to produce a biological effect [52]. Our findings propose a genetic basis for the effectivity of this kind of compounds in neuroblastoma highlighting the importance for further research in demethylating agents.

In addition, some microRNAs were identified in lost and gained areas (Table 3). In the last years, these elements have become promising therapeutic targets in neuroblastoma [53]. For example, in amplified loci of SIMA neurospheres, *hsa-mir-4254* and *hsa-mir-4262* were identified (Table 3). These two microRNAs were already related with the stem cell phenotype [54], supporting the hypothesis that the CSC might be using the same regulatory machinery as normal stem cells [10,11]. Other microRNA identified were *hsa-mir-4420*, *hsa-mir-4429* and *hsa-mir-4497*, all described as possible new microRNAs involved in malignant human B cells regulation [55], and *hsa-mir-3605*, a novel microRNA linked to human cervical cancer [56].

In contrast, the expression array results indicated a modified expression pattern in CSC-like cells including changes in different processes and cell functions (Figures 2, 3 and Table 4). Different studies indicated some of the most important pathways involved in the development and maintenance of CSC subpopulation. Among them, the most remarkable are Wnt, Notch, Hh and TGF- β ,

Table 2. Overview on gained (G) and lost (L) chromosomal regions detected by array-CGH.

Cristartend	Size (Kb)	Cytogenetic localization Status	log ₂ ratio	CNV	miRNA	CpGIs	Genes
SK-N-DZ							
1:10532178:10567923	35.75	1p36.22	2.50	2	-	2	<i>DFFA, PEX14</i>
6:33258397:33259821	1.43	6p21.32	1.51	-	-	-	<i>PFDN6, RGL2</i>
8:145921822:145943761	21.94	8q24.3	2.66	2	-	2	
12:57591347:57628354	37.01	12q13.3	1.58	-	-	4	<i>LRP1, NXPH4, SHMT2</i>
12:110214797:110344458	129.66	12q24.11	0.43	2	1	4	<i>TRPV4, GLTP, TCHP</i>
21:10701592:11087870	386.28	21p11.2	0.42	98	-	3	<i>BAGE2, TPTE, BAGES, BAGE</i>
SIMA							
1:277394203:7252011	9.51 × 10 ³	1p36.11	0.20	206	5	163	<i>WASF2, AHDC1, FGR, IFI6, FAM76A, STX12, PPP1R8, SCARNA1, C1orf38, RPA2, SMPDL3B, XKR8, EYA3, SPCS2, PTAFR, DNAJC8, ATP1F1, SESN2, MED18, PHACTR4, RCC1, TRNAUTAP, SNORD99, SNORA61, SNORA44, SNORA16A, RAB42, TAF12, RNU11, GMEB1, YTHDF2, OPRD1, EPB41, TMEM20</i>
2:10490105:10743367	253.26	2p25.1	0.68	15	-	5	<i>HPCAL1, ODC1, NOL10</i>
2:11755630:11905792	150.16	2p25.1	0.65	6	-	5	<i>GREB1, NTSR2, LPIN1</i>
2:11959615:12260468	300.85	2p25.1	0.64	14	1	-	<i>LPIN1</i>
2:14397903:14490030	92.13	2p24.3	0.51	5	-	-	
2:14726070:15319138	593.07	2p24.3	0.51	13	-	1	<i>FAM84A, NBAS</i>
2:15743981:15893191	149.21	2p24.3	0.58	2	-	-	<i>DDX1</i>
2:17683283:17860174	176.89	2p24.2	0.60	4	-	2	<i>RAD51AP2, VSNL1, SMC6</i>
2:18422521:18741209	318.69	2p24.2	0.56	11	-	-	<i>NTSC1B, RDH14</i>
4:190747562:190817136	69.58	4q35.2	0.28	52	-	2	
1:12169416:12228108	58.69	1p36.22	-0.23	2	-	1	<i>TNFRSF8, TNFRSF1B</i>
1:150530677:150531841	1.17	1q21.3	-1.35	-	-	-	<i>ADAMTSL4</i>
1:51760113:51770840	10.73	1p32.3	-1.08	-	-	-	<i>TTC39A</i>
12:48380644:48389191	8.55	12q13.11	-0.62	-	-	-	<i>COL2A1</i>
12:57593050:57606248	13.20	12q13.3	-0.51	-	-	1	<i>LRP1</i>
12:57925800:57926884	1.08	12q13.3	-1.05	1	-	-	<i>DCTN2</i>
13:76141342:76151800	10.46	13q22.2	-0.87	1	-	-	<i>UCHL3</i>
15:74635420:74707504	72.08	15q24.1	-0.35	2	-	3	<i>CYP11A1, SEMA7A</i>
17:3594077:3595092	1.02	17p13.2	-1.28	1	-	-	<i>P2RX5</i>
17:56283529:56284308	0.78	17q22	-1.59	-	-	-	<i>MKS1</i>
18:7013911:7023395	9.48	18p11.31	-1.12	-	-	-	<i>LAMA1</i>
2:10923316:10924881	1.57	2p25.1	-1.60	-	-	-	<i>ATP6V1C2, PDIA6</i>
2:11312145:11718686	406.54	2p25.1	-0.91	18	1	3	<i>PQLC3, ROCK2, E2F6, GREB1</i>
2:128393779:128398576	4.80	2q14.3	-1.44	5	-	-	<i>MYO7B, LIM52</i>
2:13527222:13726873	199.65	2p24.3	-0.84	22	-	-	
2:16396225:16608842	212.62	2p24.3	-0.94	12	-	-	

Table 2. Cont.

Cr:startend	Size (Kb)	Citogenetic localization	Status	log ₂ ratio	CNV	miRNA	CpGIsI	Genes
2:16719258:17667981	948.72	2p24.2	L	-1.02	34	-	-	FAM49A
2:17864935:18277059	412.12	2p24.2	L	-0.81	26	-	3	SMC6, GEN1, MSGN1, KCNS3
2:47273218:47294502	21.29	2p21	L	-1.33	-	-	-	TTC7A, CALM2
2:71191955:71205512	13.56	2p13.3	L	-1.33	-	-	1	ATP6V1B1
2:71246290:71263795	17.51	2p13.3	L	-1.83	3	-	-	OR7E91P
3:49155018:49156532	1.51	3p21.31	L	-1.45	-	-	-	USP19
4:19082476:190874516	49.74	4q35.2	L	-0.29	6	-	1	FRG1
4:25780740:25785945	5.21	4p15.2	L	-1.28	-	-	-	SEL1L3
6:33258397:33260455	2.06	6p21.32	L	-1.38	-	-	-	PFDN6, RGL2
6:43258794:43266869	8.08	6p21.1	L	-1.48	1	-	-	SLC22A7
6:71018884:71038982	20.10	6q13	L	-1.09	-	-	-	-
8:11415447:11565691	150.25	8p23.1	L	-0.29	40	-	9	BLK, GATA4
8:143008634:143243125	234.49	8q24.3	L	-0.74	18	-	2	-
X:53224324:53225545	1.22	Xp11.22	L	-1.55	1	-	-	KDM5C

Chromosome:Chromosomal start position:Chromosomal end position (Cr:start:end). Number of polymorphisms or Copy Number Variants (CNV) in the region. Number of miRNA (miRNA) contained in the region. CpG islands (CpGIsI). doi:10.1371/journal.pone.01113105.t002

which have been already described for different tumors and especially in brain tumors [14]. In neuroblastoma, Wnt and Notch genes have been identified as possible CSC-like markers. The difficulty in the identification of specific genes and accurate markers of CSC-like lies in the heterogeneity of this tumor and the poor knowledge related with this subpopulation, since no specific and definitive gene expression profile has been proposed for neuroblastoma CSC-like cells [57].

Interestingly, the expression pattern in CSC-like cells involves not only Wnt and Notch but also Hh and TGF- β signalling pathways. For example, deregulation of several genes of Wnt pathway was detected. The results indicated a decrease in the expression of upstream regulators as *FZD8*, *PRKCH* and *FRAT1* and an increase in the downstream target *POU5F1*, suggesting the inactivation of Wnt signalling pathway. *POU5F1* was described in several tumors (urothelial, prostatic, cervical, breast and lung) and is implicated in different functions as chemoresistance, prognosis marker, proliferation, apoptosis, migration and invasion [58–61]. In addition to all these functions, this gene plays an important role in stemness and self-renewal of stem cells in normal and tumor tissues [60,62,63] and was found to be overexpressed and correlated with the progression of neuroblastoma [64]. This gene could interact with members from other pathways as TGF- β , Notch and Wnt [65,66] working together in the regulation of stem cell pluripotency. Our results show alterations not only in *POU5F1* but also in members of TGF- β , Notch and Wnt signalling pathways indicating the potential of this gene to be used as a new therapeutic target. Our findings are supported by other works that described its potential in other tumors [62,64,67] and as a possible new CSC marker in neuroblastoma [67–69].

In this context, an apparent activation of Notch pathway was detected in neurospheres. It has been demonstrated that inhibition of Notch in cancer cells has the potential to slow down cell proliferation and induce apoptosis, despite the extensive crosstalk of this pathway with other major cancer pathways as Ras, Akt, NF- κ B, Wnt, Hh and TGF- β [70–72]. This might happen because in neuroblastoma as in other tumors, the CSC subpopulation seems to be especially sensitive to inhibition of stem cell pathways as Notch [73].

Additionally, Hh was activated in CSC-like cells by upregulation of transcription targets and activators (*PTCH1*, *SMO* and *GLI1*) regardless downregulation of *GLI2*. It is known that *GLI2* is a bi-functional transcription factor, with activator and repressor regions. Therefore the pathway could still be activated if *GLI2* is silenced depending on the context [74,75]. In neuroblastoma CSC-like the Gli factors act through cooperative functional interactions in target gene regulation [76] although in our case it seems that *GLI2* does not play an important role. Alike, the TGF- β signalling pathway is activated in neurospheres cultures (Figure 4B) despite the downregulation of *TGFB3*, a ligand of the pathway. A possible explanation could be that the downregulation of *BAMBI* (Figure 4B) would let a greater proportion of ligands free, increasing the concentration of extracellular ligands and consequently facilitating the activation of the pathway or acting as a negative regulator of the TGF- β pathway [34]. Interestingly, *JAG1*, one of the targets of TGF- β [77] and also the main activator of Notch signalling pathway is upregulated, supporting Notch signalling pathway activation. Kurpinski *et al* described *JAG1* as a crosstalk point between these two pathways in the regulation of muscular stem cells [78] which probably suggests an important role of this gene in the generation of CSC-like cells in neuroblastoma. These findings also give us the possibility of studying targets as *JAG1* that participate in several genetic pathways involved in CSC-like cells phenotype.

Table 3. MicroRNA identified in array-CGH analysis.

Citogenetic localization	miRNA
SK-N-DZ	
12q24.11	hsa-mir-4497
SIMA	
1p36.11	hsa-mir-4420; hsa-mir-4254; hsa-mir-5585; hsa-mir-3605; hsa-mir-552
2p25.1	hsa-mir-4262; hsa-mir-4429

doi:10.1371/journal.pone.0113105.t003

It is clear that the expression profile that we observed in the CSC-like cells is similar to other profiles described for this subpopulation in different tumors including neuroblastoma. The identification of CSC is based on the expression of different markers, but in the case of neuroblastoma it remains unclear which markers are accurate to identify this subpopulation, due to its heterogeneity. Our findings show differences between the two cell lines used (Figure 5B) in two CSC markers widely described: *CD133* and *CD15*. This result could highlight the limitations of

neurospheres culture [79] since it was proved that differences in the culture conditions could affect the enrichment and isolation of CSC-like cells [80]. However, since the genes related with CSC followed a similar pattern in both cell lines, the more plausible explanation is that the phenotype of CSC-like cells is not yet fully characterized in neuroblastoma [57]. Coulon *et al* [57] questioned the expression of *CD133* to identify CSC in neuroblastoma, highlighting the need of characterization of other CSC markers or expression profiles that allow the recognition of this subpopulation.

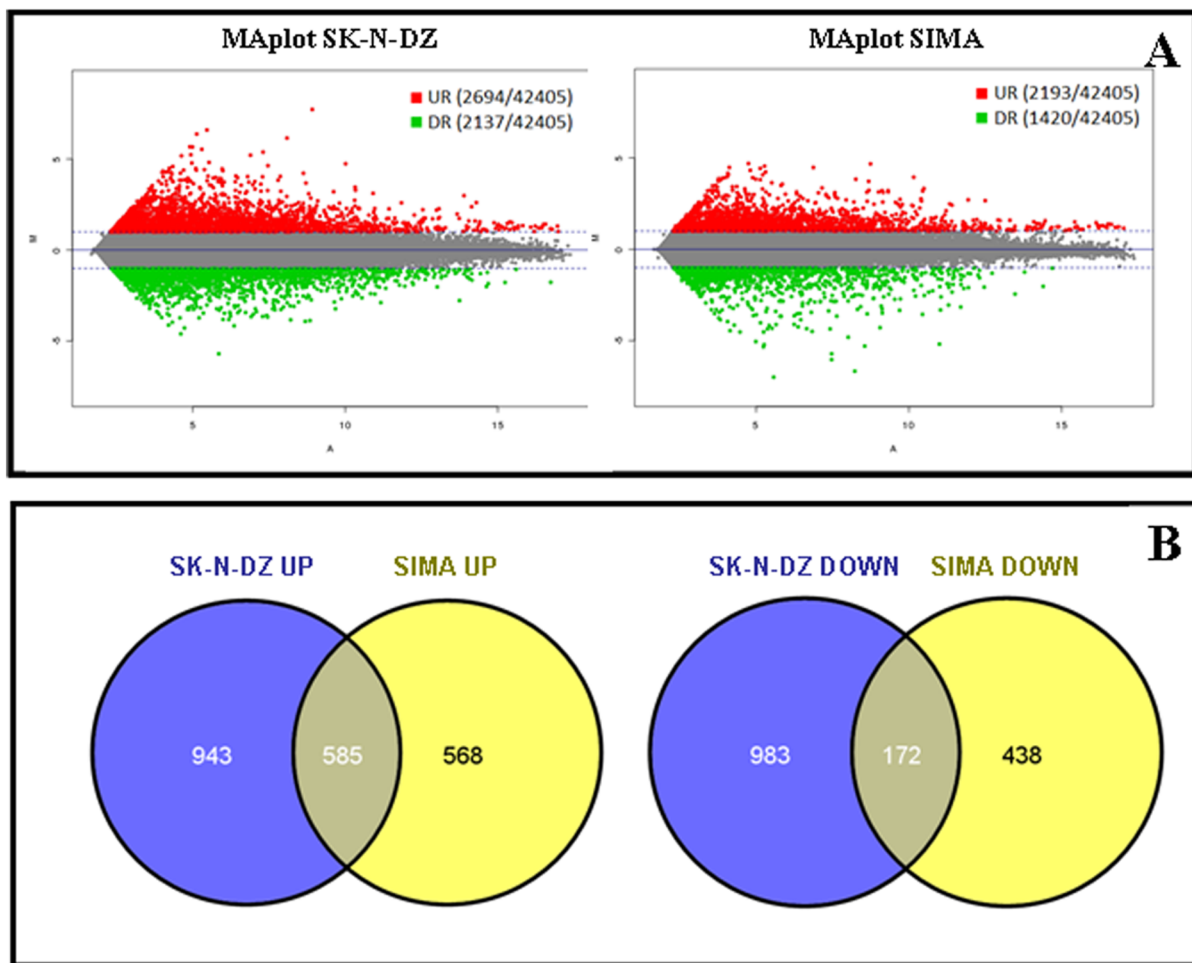


Figure 2. Upregulated (UR, red) and downregulated (DR, green) genes (>1 fold-change) in neurospheres compared to standard cells lines SK-N-DZ and SIMA (A), represented with MAplots, were the Y-axis represents the red/green intensity ratio "M" and the X-axis the average intensity "A". Venn diagrams illustrating the number of differentially expressed genes in SK-N-DZ and SIMA neurospheres compared to standard cell lines (B). The overlapping area represents the set of genes altered in both cell lines.

doi:10.1371/journal.pone.0113105.g002

Table 4. DAVID generated categories.

	# Genes	p value	Genes ID
Biological processes (GO)			
GO:0042127~regulation of cell proliferation	30	3.97×10^{-4} (**)	<i>FGFR2, NAMPT, ACVRL1, FGFR3, ERBB3, PPARG, MITF, TGFB3, TNFSF12, JAG1, FLT3LG, EDNRA, CD9, S1PR3, INS, TGM2, TESC, LYN, PTPRF, SF1, PTPRU, DHRS2, TNFSF13B, ID2, DBP, CHRM1, MYO16, PDGFRB, PTCH1, MCTS1</i>
GO:0007179~transforming growth factor beta receptor signalling pathway	7	8.85×10^{-4} (**)	<i>AMHR2, SMAD9, ACVRL1, ID1, SMAD6, TGFB3, BAMBI</i>
GO:0000165~MAPKKK cascade	11	2.51×10^{-3} (**)	<i>NRTN, DUSP2, FGFR3, ADORA2B, INS, LRRN3, TGFB3, ROR2, TNFRSF19, FGD4, DUSP6</i>
GO:0030509~BMP signalling pathway	5	9.15×10^{-3} (**)	<i>SMAD9, ID1, SMAD7, SMAD6, GREM2</i>
GO:0042981~regulation of apoptosis	24	2.91×10^{-2} (*)	<i>DEPDC6, KCNMA1, PTPRF, ERBB3, ARHGEF7, SMAD6, MITF, TGFB3, TNFSF12, STK3, CARD10, GCH1, ATP7A, DHRS2, KRT18, TNFSF13B, INS, ALDH1A3, BNIP3L, TGM2, TNFRSF19, BMF, FGD4, ANGPTL4</i>
GO:0051094~positive regulation of developmental process	11	3.71×10^{-2} (*)	<i>TESC, SMAD9, ID2, PTPRF, LYN, INS, PPARG, TGFB3, TNFSF12, JAG1, ANGPTL4</i>
GO:0060393~regulation of pathway-restricted SMAD protein phosphorylation	3	3.97×10^{-2} (*)	<i>SMAD7, SMAD6, TGFB3</i>
GO:0030155~regulation of cell adhesion	7	4.45×10^{-2} (*)	<i>TESC, LAMA4, ARHGAP6, ACVRL1, ERBB3, SMAD7, TGM2</i>
GO:0043009~chordate embryonic development	12	4.87×10^{-2} (*)	<i>C6ORF59, EDNRA, ACVRL1, HAND1, EPAS1, TGFB3, PDGFRB, ROR2, HES7, PTCH1, HOXD1, APBA1</i>
Molecular Function (GO)			
GO:0004629~phospholipase C activity	5	3×10^{-3} (**)	<i>EDNRA, PLCB3, CHRM3, CHRM1, PLCB1</i>
GO:0004725~protein tyrosine phosphatase activity	8	4×10^{-3} (**)	<i>DUSP5, DUSP2, PTPRF, PTPRH, PTPRT, PTPRU, RNGTT, DUSP6</i>
GO:0008081~phosphoric diester hydrolase activity	7	5×10^{-3} (**)	<i>EDNRA, PLCB3, CHRM3, PDE7A, CHRM1, PDE4D, PLCB1</i>
GO:0034713~type I transforming growth factor beta receptor binding	3	7×10^{-3} (**)	<i>SMAD7, SMAD6, TGFB3</i>
GO:0005072~transforming growth factor beta receptor, cytoplasmic mediator activity	3	1.8×10^{-2} (*)	<i>SMAD9, SMAD7, SMAD6</i>
GO:0030695~GTPase regulator activity	15	2.4×10^{-2} (*)	<i>ARHGEF7, EXPH5, DOCK9, RABGAP1L, SLC26A10, DOCK6, ARHGEF10, STARD13, MYRIP, ARHGAP6, SGSM2, SYTL4, CHN2, DOCK10, FGD4</i>
GO:0033549~MAP kinase phosphatase activity	3	2.5×10^{-2} (*)	<i>DUSP5, DUSP2, DUSP6</i>
GO:0004714~transmembrane receptor protein tyrosine kinase activity	5	4×10^{-2} (*)	<i>FGFR2, FGFR3, ERBB3, PDGFRB, ROR2</i>
GO:0005246~calcium channel regulator activity	3	4.1×10^{-2} (*)	<i>NPY, HPCAL4, NPY2R</i>
GO:0005160~transforming growth factor beta receptor binding	3	4.1×10^{-2} (*)	<i>SMAD7, SMAD6, TGFB3</i>

The differentially expressed genes in both cell lines were grouped in categories classified as significantly (*) and very significantly (**) enriched in neurosphere samples. Genes were categorized according to the biological processes they are involved in and to the molecular functions they code for.
doi:10.1371/journal.pone.0113105.t004

The choice of CSC markers is still controversial and the search of specific genes that help to identify it is the real challenge for the characterization and research of new therapeutical targets in neuroblastoma [81].

Regardless the growing evidence in new approaches and in the identification of new therapeutic targets, the treatment for neuroblastoma is still evasive. Nowadays, it includes surgery, radiation and/or chemotherapy depending on the patient's stage and risk stratification of the disease [5]. Only some new compounds are included in the schema as 13-cis-retinoic acid together with anti-GD2 antibodies and interleukin-2, a combination that has increased the progression-free survival [82]. The literature includes an increasing number of new compounds with great potential to be introduced in the treatment. This is the case of drugs that targeted *MYCN* and *ALK* inhibitors that currently are in preclinical evaluation [83]. The evidence of possible targets

involved in the development and regulation of other tumors could be an approach to develop new strategies in neuroblastoma. A good example are the different pathways involved in tumorigenesis and CSC regulation, as Wnt [62,64,67–69], Notch [84], Hh [85–87] and TGF- β [18,88,89]. In this connection, an interesting case are the ion transporters, described as essential for cell proliferation and which appear to have a role in cancer development [90–92]. Evidence is particularly extensive for Ca^{2+} and K^{+} channels [93] and Romania *et al* already described their importance in neuroblastoma [94]. In our analysis, several genes coding for Ca^{2+} and K^{+} channels were altered in CSC-like subpopulation like *KCNMA1*, previously described in prostate cancer [95] and in breast cancer [96,97], and *CACNLG* also altered in gastric cancers, colorectal cancers and acute myeloid leukemia (AML) [98]. Several reports propose that ion transporters have clinical potential not only as therapeutical targets but also as prognosis

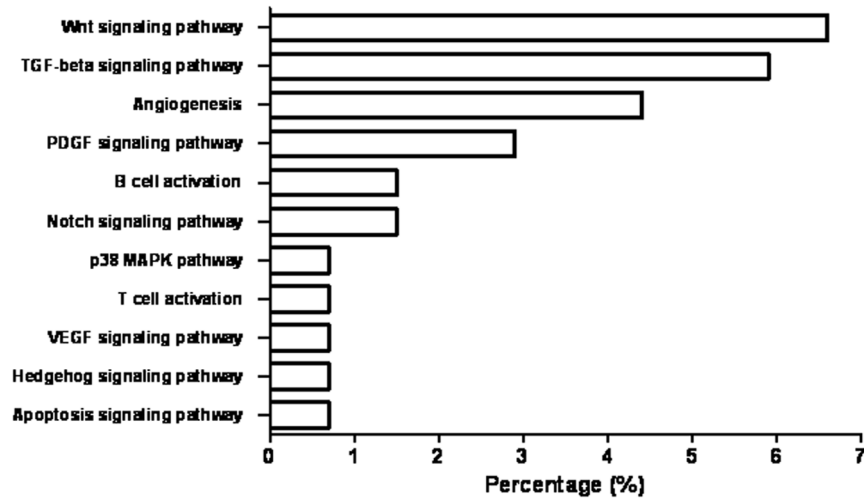


Figure 3. PANTHER classification by signalling pathway. The differentially expressed genes in both SK-N-DZ and SIMA CSC-like cells were classified by PANTHER and graphed. The percentage represents the number of genes altered against total number of genes involved in each pathway.

doi:10.1371/journal.pone.0113105.g003

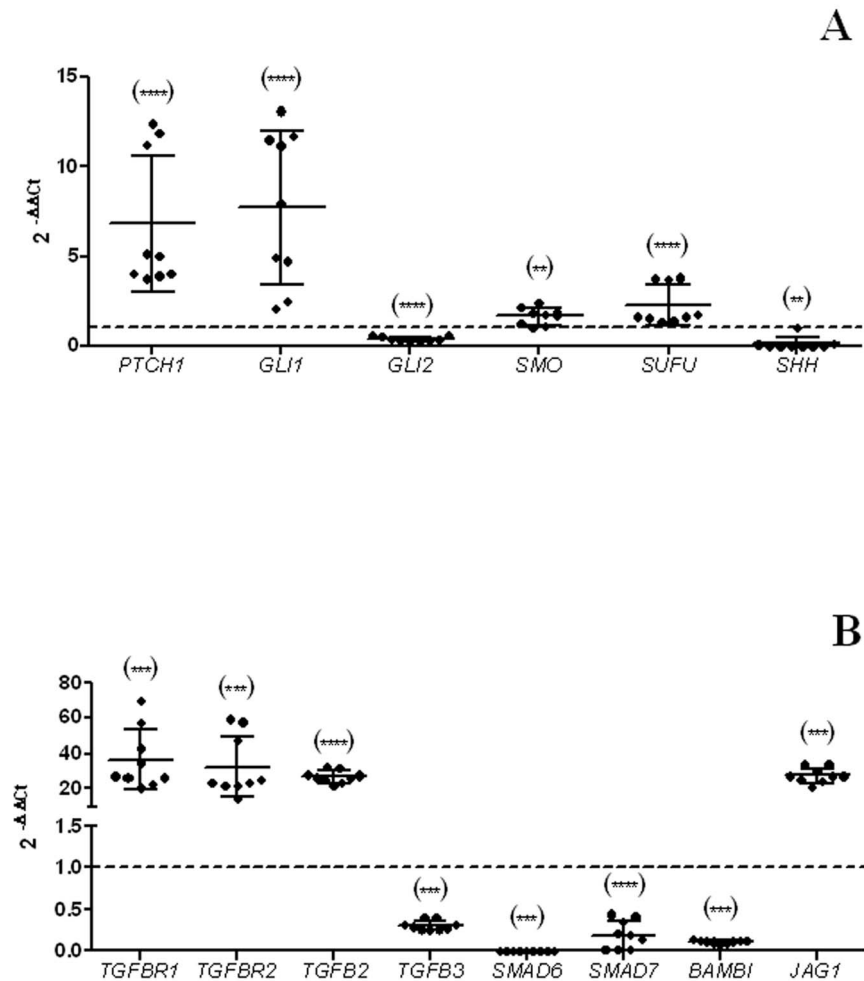


Figure 4. RT-qPCR for Sonic Hedgehog (A) and TGF- β pathways analysis (B) in SIMA CSC-like cells. The graphs represent the $2^{-\Delta\Delta C_t}$ values obtained by RT-qPCR for neurospheres. The dotted line indicates the $2^{-\Delta\Delta C_t}$ control (cell line) value equal to 1. Significance against control: $p < 0.05$ (*); $p < 0.01$ (**); $p < 0.001$ (***) and $p < 0.0001$ (****). Selected genes cover the most relevant components of each pathway. Results confirmed aberrant activation of Hh (A) and TGF- β (B) signalling pathways in CSC-like cells.

doi:10.1371/journal.pone.0113105.g004

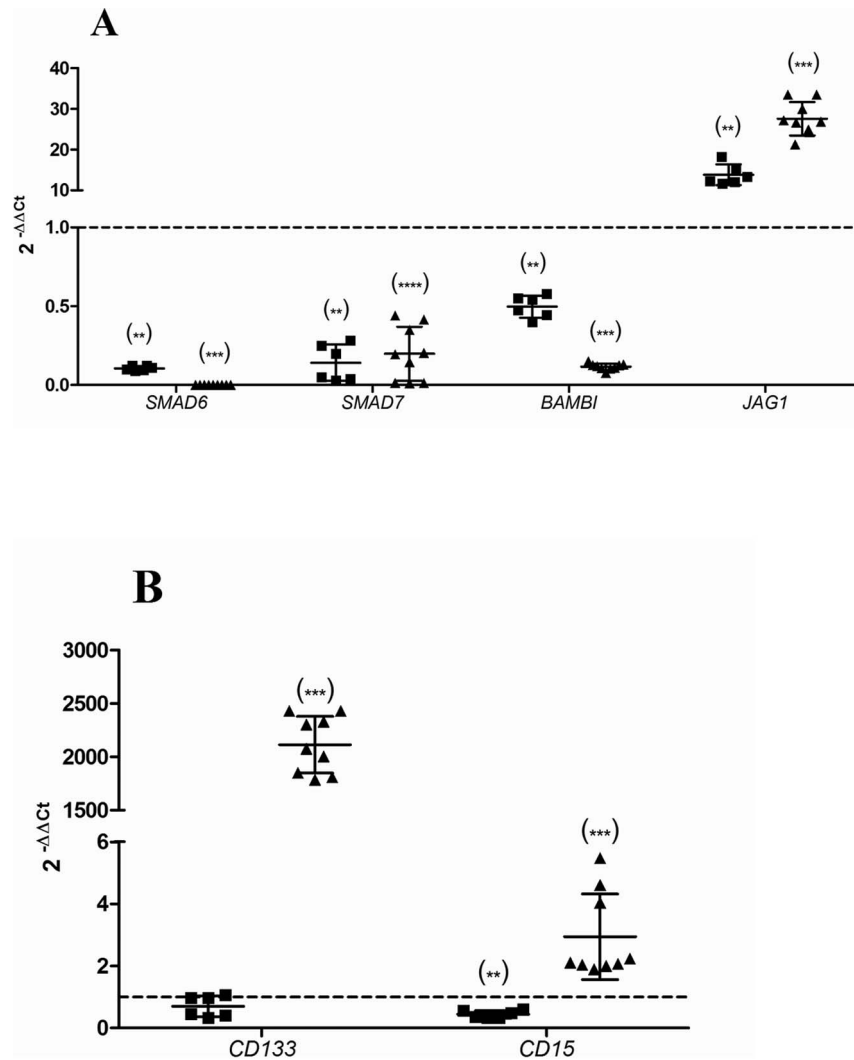


Figure 5. Gene expression by RT-qPCR. The graphs represent the $2^{-\Delta\Delta Ct}$ values obtained by RT-qPCR for neurospheres. The dotted line indicates the $2^{-\Delta\Delta Ct}$ control (cell line) value equal to 1. Significance against control: $p < 0.05$ (*); $p < 0.01$ (**); $p < 0.001$ (***) and $p < 0.0001$ (****). **Corroboration of expression array (A).** Both SK-N-DZ (■) and SIMA (▲) CSC-like cells showed a similar expression profile. **Stem Cell Markers expression (B).** Results confirmed a high overexpression of CSC markers in SIMA cell line after the neurosphere formation assay. doi:10.1371/journal.pone.0113105.g005

markers or to improve actual treatments [99–103], as blocking channel activity seems to impair the growth of some tumors, including neuroblastoma [99,104]. The presence of altered genes of Ca^{2+} and K^{+} channels in neuroblastoma CSC-like subpopulations confirms and opens the possibility to develop new compounds that could act at different levels and subpopulations within neuroblastoma. This is only one example of the importance of redirecting treatments towards more effective CSC molecular therapies to achieve total elimination of the tumor cell population and avoid relapses [40,105].

In conclusion, we found that the expression profile of neuroblastoma CSC-like cells differs significantly from the expression profile in standard neuroblastoma cell lines, which is seen as altered signalling pathways involved in stem cell proliferation pathways as Wnt, Notch, Hh and TGF- β , suggesting a cross talk among them and with other pathways. The CSC markers analysis reveals no correlation between the cell lines, displaying the heterogeneity of neuroblastoma tumors and CSC-

like population but opening the possibility to identify other potential markers. Taking together, these results confirm the importance of different pathways in CSC regulation and the identification of possible candidate targets for molecular CSC therapies in neuroblastoma. The results presented highlight new information for the CSC-like phenotype in neuroblastoma and indicate the importance of redirecting current cancer treatments towards CSC molecular therapies to achieve total elimination of the tumor cell population and improve treatment effectiveness.

Supporting Information

Table S1 Supplementary data. Up and downregulated genes list from the expression array in each cell line. (XLS)

Table S2 Supplementary data. Upregulated genes list shared in both cell lines. (XLS)

Table S3 Supplementary data. Downregulated genes list shared in both cell lines.
(XLS)

Table S4 Supplementary data. Genes list not found in PANTHER classification.
(XLS)

References

- Dhir S, Wheeler K (2010) Neonatal neuroblastoma. *Early Hum Dev* 86: 601–605.
- Cheung NK, Dyer MA (2013) Neuroblastoma: developmental biology, cancer genomics and immunotherapy. *Nat Rev Cancer* 13: 397–411.
- Park JR, Bagatell R, London WB, Maris JM, Cohn SL, et al. (2013) Children's Oncology Group's 2013 blueprint for research: neuroblastoma. *Pediatr Blood Cancer* 60: 985–993.
- Maris JM (2010) Recent advances in neuroblastoma. *N Engl J Med* 362: 2202–2211.
- Davidoff AM (2012) Neuroblastoma. *Semin Pediatr Surg* 21: 2–14.
- Matthay KK, George RE, Yu AL (2012) Promising therapeutic targets in neuroblastoma. *Clin Cancer Res* 18: 2740–2753.
- Ross RA, Spengler BA (2007) Human neuroblastoma stem cells. *Semin Cancer Biol* 17: 241–247.
- Singh SK, Clarke ID, Hide T, Dirks PB (2004) Cancer stem cells in nervous system tumors. *Oncogene* 23: 7267–7273.
- Reya T, Morrison SJ, Clarke MF, Weissman IL (2001) Stem cells, cancer, and cancer stem cells. *Nature* 414: 105–111.
- Alison MR, Lin WR, Lim SM, Nicholson LJ (2012) Cancer stem cells: in the line of fire. *Cancer Treat Rev* 38: 589–598.
- Sumer-Turanligil NC, Cetin EO, Uyanikgil Y (2013) A contemporary review of molecular candidates for the development and treatment of childhood medulloblastoma. *Childs Nerv Syst* 29: 381–388.
- Gong A, Huang S (2012) FoxM1 and Wnt/beta-catenin signaling in glioma stem cells. *Cancer Res* 72: 5658–5662.
- Holland JD, Klaus A, Garratt AN, Birchmeier W (2013) Wnt signaling in stem and cancer stem cells. *Curr Opin Cell Biol* 25: 254–264.
- Faigle R, Song H (2013) Signaling mechanisms regulating adult neural stem cells and neurogenesis. *Biochim Biophys Acta* 1830: 2435–2448.
- Huang FT, Zhuang-Sun YX, Zhuang YY, Wei SL, Tang J, et al. (2012) Inhibition of hedgehog signaling depresses self-renewal of pancreatic cancer stem cells and reverses chemoresistance. *Int J Oncol* 41: 1707–1714.
- Sethi N, Kang Y (2011) Notch signalling in cancer progression and bone metastasis. *Br J Cancer* 105: 1805–1810.
- Shao H, Huang Q, Liu ZJ, Keiran SMS (2012) Chapter Seven - Targeting Notch Signaling for Cancer Therapeutic Intervention. *Advances in Pharmacology: Academic Press*. pp. 191–234.
- Joseph JV, Balasubramanian V, Walenkamp A, Kruyt FA (2013) TGF-beta as a therapeutic target in high grade gliomas - promises and challenges. *Biochem Pharmacol* 85: 478–485.
- Park KS (2011) TGF-beta Family Signaling in Embryonic Stem Cells. *Int J Stem Cells* 4: 18–23.
- Sakaki-Yumoto M, Katsuno Y, Derynck R (2013) TGF-beta family signaling in stem cells. *Biochim Biophys Acta* 1830: 2280–2296.
- Zhou BB, Zhang H, Damelin M, Geles KG, Grindley JC, et al. (2009) Tumour-initiating cells: challenges and opportunities for anticancer drug discovery. *Nat Rev Drug Discov* 8: 806–823.
- Wainwright DA, Nigam P, Thaci B, Dey M, Lesniak MS (2012) Recent developments on immunotherapy for brain cancer. *Expert Opin Emerg Drugs* 17: 181–202.
- Huang da W, Sherman BT, Stephens R, Baseler MW, Lane HC, et al. (2008) DAVID gene ID conversion tool. *Bioinformatics* 24: 428–430.
- Dennis G Jr, Sherman BT, Hosack DA, Yang J, Gao W, et al. (2003) DAVID: Database for Annotation, Visualization, and Integrated Discovery. *Genome Biol* 4: P3.
- Huang da W, Sherman BT, Tan Q, Collins JR, Alvord WG, et al. (2007) The DAVID Gene Functional Classification Tool: a novel biological module-centric algorithm to functionally analyze large gene lists. *Genome Biol* 8: R183.
- Mi H, Dong Q, Muruganujan A, Gaudet P, Lewis S, et al. (2010) PANTHER version 7: improved phylogenetic trees, orthologs and collaboration with the Gene Ontology Consortium. *Nucleic Acids Res* 38: D204–210.
- Mi H, Muruganujan A, Thomas PD (2013) PANTHER in 2013: modeling the evolution of gene function, and other gene attributes, in the context of phylogenetic trees. *Nucleic Acids Res* 41: D377–386.
- Thomas PD, Campbell MJ, Kejariwal A, Mi H, Karlak B, et al. (2003) PANTHER: a library of protein families and subfamilies indexed by function. *Genome Res* 13: 2129–2141.
- Livak KJ, Schmittgen TD (2001) Analysis of relative gene expression data using real-time quantitative PCR and the 2⁻(Delta Delta C(T)) Method. *Methods* 25: 402–408.
- Thomas GM, Frame S, Goedert M, Nathke I, Polakis P, et al. (1999) A GSK3-binding peptide from FRAT1 selectively inhibits the GSK3-catalysed phosphorylation of axin and beta-catenin. *FEBS Lett* 458: 247–251.
- van Amerongen R, Nawijn MC, Lambouij JP, Proost N, Jonkers J, et al. (2010) Frat oncoproteins act at the crossroad of canonical and noncanonical Wnt-signaling pathways. *Oncogene* 29: 93–104.
- Besho Y, Miyoshi G, Sakata R, Kageyama R (2001) Hes7: a bHLH-type repressor gene regulated by Notch and expressed in the presomitic mesoderm. *Genes Cells* 6: 175–185.
- Kochert K, Ullrich K, Kreher S, Aster JC, Kitagawa M, et al. (2011) High-level expression of Mastermind-like 2 contributes to aberrant activation of the NOTCH signaling pathway in human lymphomas. *Oncogene* 30: 1831–1840.
- Yan X, Lin Z, Chen F, Zhao X, Chen H, et al. (2009) Human BAMB1 cooperates with Smad7 to inhibit transforming growth factor-beta signaling. *J Biol Chem* 284: 30097–30104.
- Zavadil J, Cermak L, Soto-Nieves N, Bottinger EP (2004) Integration of TGF-beta/Smad and Jagged1/Notch signalling in epithelial-to-mesenchymal transition. *EMBO J* 23: 1155–1165.
- Speleman F, De Preter K, Vandesoempele J (2011) Neuroblastoma genetics and phenotype: a tale of heterogeneity. *Semin Cancer Biol* 21: 238–244.
- Capasso M, Diskin SJ (2010) Genetics and genomics of neuroblastoma. *Cancer Treat Res* 155: 65–84.
- Ohira M, Nakagawara A (2010) Global genomic and RNA profiles for novel risk stratification of neuroblastoma. *Cancer Sci* 101: 2295–2301.
- Villamon E, Berbegall AP, Piqueras M, Tadeo I, Castel V, et al. (2013) Genetic instability and intratumoral heterogeneity in neuroblastoma with MYCN amplification plus 11q deletion. *PLoS One* 8: e53740.
- Schatton T, Frank NY, Frank MH (2009) Identification and targeting of cancer stem cells. *Bioessays* 31: 1038–1049.
- Kuiper RP, Ligtenberg MJ, Hoogerbrugge N, Geurts van Kessel A (2010) Germline copy number variation and cancer risk. *Curr Opin Genet Dev* 20: 282–289.
- Dear PH (2009) Copy-number variation: the end of the human genome? *Trends Biotechnol* 27: 448–454.
- Fanciulli M, Petretto E, Aitman TJ (2010) Gene copy number variation and common human disease. *Clin Genet* 77: 201–213.
- Ghavifekr Fakhr M, Farshdousti Hagh M, Shانهbandi D, Baradaran B (2013) DNA Methylation Pattern as Important Epigenetic Criterion in Cancer. *Genet Res Int* 2013: 317569.
- Nejman D, Straussman R, Steinfeld I, Ruvolo M, Roberts D, et al. (2014) Molecular rules governing de novo methylation in cancer. *Cancer Res* 74: 1475–1483.
- Jones PA, Baylin SB (2007) The epigenomics of cancer. *Cell* 128: 683–692.
- Liu Y, Cope L, Sun W, Wang Y, Prasad N, et al. (2013) DNA copy number variations characterize benign and malignant thyroid tumors. *J Clin Endocrinol Metab* 98: E558–566.
- Kim KI, Kim TK, Kim IW, Ahn KS, Yoon SS, et al. (2012) Copy number variations in normal karyotype acute myeloid leukaemia and their association with treatment response. *Basic Clin Pharmacol Toxicol* 111: 317–324.
- Jones PA (2014) At the tipping point for epigenetic therapies in cancer. *J Clin Invest* 124: 14–16.
- Sigalotti L, Fratta E, Coral S, Maio M (2013) Epigenetic drugs as immunomodulators for combination therapies in solid tumors. *Pharmacol Ther* 142: 339–350.
- Montenegro MF, Sanchez-Del-Campo L, Fernandez-Perez MP, Saez-Ayala M, Cabezas-Herrera J, et al. (2014) Targeting the epigenetic machinery of cancer cells. *Oncogene*, doi: 101038/onc2013605.
- George RE, Lahti JM, Adamson PC, Zhu K, Finkelstein D, et al. (2010) Phase I study of decitabine with doxorubicin and cyclophosphamide in children with neuroblastoma and other solid tumors: a Children's Oncology Group study. *Pediatr Blood Cancer* 55: 629–638.
- Stallings RL, Foley NH, Bryan K, Buckley PG, Bray I (2010) Therapeutic targeting of miRNAs in neuroblastoma. *Expert Opin Ther Targets* 14: 951–962.
- Goff LA, Davila J, Swerdel MR, Moore JC, Cohen RI, et al. (2009) Ago2 immunoprecipitation identifies predicted microRNAs in human embryonic stem cells and neural precursors. *PLoS One* 4: e7192.
- Jima DD, Zhang J, Jacobs C, Richards KL, Dunphy CH, et al. (2010) Deep sequencing of the small RNA transcriptome of normal and malignant human B cells identifies hundreds of novel microRNAs. *Blood* 116: e118–127.
- Witten D, Tibshirani R, Gu SG, Fire A, Lui WO (2010) Ultra-high throughput sequencing-based small RNA discovery and discrete statistical biomarker

Author Contributions

Conceived and designed the experiments: GGO AB JSC. Performed the experiments: RO GGO SM SL NP JG GD. Analyzed the data: GGO BM JAR JSC. Contributed reagents/materials/analysis tools: AB BM JAR JSC. Wrote the paper: RO GGO JSC.

- analysis in a collection of cervical tumours and matched controls. *BMC Biol* 8: 58.
57. Coulon A, Flahaut M, Muhlethaler-Mottet A, Meier R, Liberman J, et al. (2011) Functional sphere profiling reveals the complexity of neuroblastoma tumor-initiating cell model. *Neoplasia* 13: 991–1004.
 58. Wezel F, Pearson J, Kirkwood LA, Southgate J (2013) Differential expression of Oct4 variants and pseudogenes in normal urothelium and urothelial cancer. *Am J Pathol* 183: 1128–1136.
 59. de Resende MF, Chinen LT, Vieira S, Jampietro J, da Fonseca FP, et al. (2013) Prognostication of OCT4 isoform expression in prostate cancer. *Tumour Biol* 34: 2665–2673.
 60. Wang YD, Cai N, Wu XL, Cao HZ, Xie LL, et al. (2013) OCT4 promotes tumorigenesis and inhibits apoptosis of cervical cancer cells by miR-125b/BAK1 pathway. *Cell Death Dis* 4: e760.
 61. Ezeh UI, Turek PJ, Reijo RA, Clark AT (2005) Human embryonic stem cell genes OCT4, NANOG, STELLAR, and GDF3 are expressed in both seminoma and breast carcinoma. *Cancer* 104: 2255–2265.
 62. Lu Y, Zhu H, Shan H, Lu J, Chang X, et al. (2013) Knockdown of Oct4 and Nanog expression inhibits the stemness of pancreatic cancer cells. *Cancer Lett* 340: 113–123.
 63. Tantin D (2013) Oct transcription factors in development and stem cells: insights and mechanisms. *Development* 140: 2857–2866.
 64. Yang S, Zheng J, Ma Y, Zhu H, Xu T, et al. (2012) Oct4 and Sox2 are overexpressed in human neuroblastoma and inhibited by chemotherapy. *Oncol Rep* 28: 186–192.
 65. Jerabek S, Merino F, Scholer HR, Cojocaru V (2013) OCT4: Dynamic DNA binding pioneers stem cell pluripotency. *Biochim Biophys Acta* 1839: 138–154.
 66. Faunes F, Hayward P, Descalzo SM, Chatterjee SS, Balayo T, et al. (2013) A membrane-associated beta-catenin/Oct4 complex correlates with ground-state pluripotency in mouse embryonic stem cells. *Development* 140: 1171–1183.
 67. Xin YH, Bian BS, Yang XJ, Cui W, Cui HJ, et al. (2013) POU5F1 enhances the invasiveness of cancer stem-like cells in lung adenocarcinoma by upregulation of MMP-2 expression. *PLoS One* 8: e83373.
 68. Yang L, Zheng J, Xu T, Xiao X (2013) Downregulation of OCT4 promotes differentiation and inhibits growth of BE (2)-C human neuroblastoma I-type cells. *Oncol Rep* 29: 2191–2196.
 69. Shi J, Shi W, Ni L, Xu X, Su X, et al. (2013) OCT4 is epigenetically regulated by DNA hypomethylation of promoter and exon in primary gliomas. *Oncol Rep* 30: 201–206.
 70. Bailey JM, Leach SD (2012) Signaling pathways mediating epithelial-mesenchymal crosstalk in pancreatic cancer: Hedgehog, Notch and TGFbeta. In: Grippio PJ, Munshi HG, editors. *Pancreatic Cancer and Tumor Microenvironment: Transworld Research Network, Trivandrum, India*.
 71. Bertrand FE, Angus CW, Paris WJ, Sigounas G (2012) Developmental pathways in colon cancer: crosstalk between WNT, BMP, Hedgehog and Notch. *Cell Cycle* 11: 4344–4351.
 72. Wu WK, Wang XJ, Cheng AS, Luo MX, Ng SS, et al. (2013) Dysregulation and crosstalk of cellular signaling pathways in colon carcinogenesis. *Crit Rev Oncol Hematol* 86: 251–277.
 73. Puro B (2012) Notch inhibition as a promising new approach to cancer therapy. *Adv Exp Med Biol* 727: 305–319.
 74. Buttitta L, Mo R, Hui CC, Fan CM (2003) Interplays of Gli2 and Gli3 and their requirement in mediating Shh-dependent sclerotome induction. *Development* 130: 6233–6243.
 75. McDermott A, Gustafsson M, Elsam T, Hui CC, Emerson CP Jr, et al. (2005) Gli2 and Gli3 have redundant and context-dependent function in skeletal muscle formation. *Development* 132: 345–357.
 76. Nguyen V, Chokas AL, Stecca B, Ruiz i Altaba A (2005) Cooperative requirement of the Gli proteins in neurogenesis. *Development* 132: 3267–3279.
 77. Guo X, Wang XF (2009) Signaling cross-talk between TGF-beta/BMP and other pathways. *Cell Res* 19: 71–88.
 78. Kurpinski K, Lam H, Chu J, Wang A, Kim A, et al. (2010) Transforming growth factor-beta and notch signaling mediate stem cell differentiation into smooth muscle cells. *Stem Cells* 28: 734–742.
 79. Wan F, Zhang S, Xie R, Gao B, Campos B, et al. (2010) The utility and limitations of neurosphere assay, CD133 immunophenotyping and side population assay in glioma stem cell research. *Brain Pathol* 20: 877–889.
 80. Jiang Y, Boije M, Westermarck B, Uhrbom L (2011) PDGF-B Can sustain self-renewal and tumorigenicity of experimental glioma-derived cancer-initiating cells by preventing oligodendrocyte differentiation. *Neoplasia* 13: 492–503.
 81. Courmoyer S, Nyalendo C, Addioui A, Belounis A, Beauvoyer M, et al. (2012) Genotype analysis of tumor-initiating cells expressing CD133 in neuroblastoma. *Genes Chromosomes Cancer* 51: 792–804.
 82. Yu AL, Gilman AL, Ozkaynak MF, London WB, Kreissman SG, et al. (2010) Anti-GD2 antibody with GM-CSF, interleukin-2, and isotretinoin for neuroblastoma. *N Engl J Med* 363: 1324–1334.
 83. Barone G, Anderson J, Pearson AD, Petrie K, Chesler L (2013) New strategies in neuroblastoma: Therapeutic targeting of MYCN and ALK. *Clin Cancer Res* 19: 5814–5821.
 84. Takebe N, Nguyen D, Yang SX (2013) Targeting Notch signaling pathway in cancer: Clinical development advances and challenges. *Pharmacol Ther* 141: 140–149.
 85. Amakye D, Jagani Z, Dorsch M (2013) Unraveling the therapeutic potential of the Hedgehog pathway in cancer. *Nat Med* 19: 1410–1422.
 86. Michaud NR, Wang Y, McEachern KA, Jordan JJ, Mazzola AM, et al. (2014) Novel Neutralizing Hedgehog Antibody MEDI-5304 Exhibits Antitumor Activity by Inhibiting Paracrine Hedgehog Signaling. *Mol Cancer Ther* 13: 386–398.
 87. Xie J, Bartels CM, Barton SW, Gu D (2013) Targeting hedgehog signaling in cancer: research and clinical developments. *Oncotargets Ther* 6: 1425–1435.
 88. Liu Z, Bandyopadhyay A, Nichols RW, Wang L, Hincin AP, et al. (2012) Blockade of Autocrine TGF-beta Signaling Inhibits Stem Cell Phenotype, Survival, and Metastasis of Murine Breast Cancer Cells. *J Stem Cell Res Ther* 2: 1–8.
 89. Wakefield LM, Hill CS (2013) Beyond TGFbeta: roles of other TGFbeta superfamily members in cancer. *Nat Rev Cancer* 13: 328–341.
 90. Schwab A, Stock C (2014) Ion channels and transporters in tumour cell migration and invasion. *Philos Trans R Soc Lond B Biol Sci* 369: 20130102.
 91. Hoffmann EK, Lambert IH (2014) Ion channels and transporters in the development of drug resistance in cancer cells. *Philos Trans R Soc Lond B - Biol Sci* 369: 20130109.
 92. Becchetti A, Munaron L, Arcangeli A (2013) The role of ion channels and transporters in cell proliferation and cancer. *Front Physiol* 4: 312.
 93. Arcangeli A, Becchetti A (2010) New Trends in Cancer Therapy: Targeting Ion Channels and Transporters. *Pharmaceuticals* 3: 1202–1224.
 94. Romania P, Castellano A, Surace C, Citti A, De Ioris MA, et al. (2013) High-resolution array CGH profiling identifies Na/K transporting ATPase interacting 2 (NKAIN2) as a predisposing candidate gene in neuroblastoma. *PLoS One* 8: e78481.
 95. Kunzelmann K (2005) Ion channels and cancer. *J Membr Biol* 205: 159–173.
 96. Khaitan D, Sankpal UT, Weksler B, Meister EA, Romero IA, et al. (2009) Role of KCNMA1 gene in breast cancer invasion and metastasis to brain. *BMC Cancer* 9: 258.
 97. Oeggerli M, Tian Y, Ruiz C, Wijker B, Sauter G, et al. (2012) Role of KCNMA1 in breast cancer. *PLoS One* 7: e41664.
 98. Arcangeli A, Crociani O, Lastraioli E, Masi A, Pillozzi S, et al. (2009) Targeting ion channels in cancer: a novel frontier in antineoplastic therapy. *Curr Med Chem* 16: 66–93.
 99. Pardo LA, Stuhmer W (2014) The roles of K(+) channels in cancer. *Nat Rev Cancer* 14: 39–48.
 100. Ningaraj NS, Sankpal UT, Khaitan D, Meister EA, Vats TS (2009) Modulation of KCa channels increases anticancer drug delivery to brain tumors and prolongs survival in xenograft model. *Cancer Biol Ther* 8: 1924–1933.
 101. Lang F, Stourmaras C (2014) Ion channels in cancer: future perspectives and clinical potential. *Philos Trans R Soc Lond B Biol Sci* 369: 20130108.
 102. Azimi I, Roberts-Thomson SJ, Monteith GR (2014) Calcium influx pathways in breast cancer: opportunities for pharmacological intervention. *Br J Pharmacol* 171: 945–960.
 103. Kondratskiy A, Yassine M, Kondratska K, Skryma R, Slomianny C, et al. (2013) Calcium-permeable ion channels in control of autophagy and cancer. *Front Physiol* 4: 272.
 104. Weaver AK, Liu X, Sontheimer H (2004) Role for calcium-activated potassium channels (BK) in growth control of human malignant glioma cells. *J Neurosci Res* 78: 224–234.
 105. Rahman R, Heath R, Grundy R (2009) Cellular immortality in brain tumours: an integration of the cancer stem cell paradigm. *Biochim Biophys Acta* 1792: 280–288.